

Design of a high-speed 20,000 TEU nuclear container vessel

Leurs Zeno



Thesis for the degree of MSc in Marine Technology in the specialization of *ship design*

Design of a 20,000 TEU high-speed nuclear container vessel

By

Z.G.M Leurs

Performed at

C-Job Naval Architects

This thesis (MT.23/24.002.M) is classified as confidential in accordance with the general conditions for projects performed by the TU Delft.

24-10-23

Company supervisor
Responsible supervisor: ir. N. de Vries
E-mail: n.devries@c-job.com

Thesis exam committee
Chair/Responsible Professor: ir. K. Visser
Staff Member: ir. J. Gelling
Staff Member: Dr. ir. J.F.J. Pruyn
External faculty member: Dr. J. A. Annema
Company Member: ir. N. de Vries

Author Details
Studynumber: 5379946
Author contact e-mail: zeno.leurs@gmail.com

Preface

With this thesis I end my seven years as a student which started in the Maritime Academy of Antwerp and ended at the Marine Technology department of the TU Delft. Where from I leave as a proud engineer to enter the maritime industry.

This work covers the design of a high-speed 20,000 TEU nuclear container vessel. This in order to obtain a master degree in Marine Technology with a specialization in ship design. The subject was chosen due to my own great interest in the energy transition and its wide variability for different ship types. Nuclear propulsion showed great potential with like for like replacement in earlier research [71] but this thesis investigates the changes in design parameters for complete new builds where the initial focus lies upon container vessels. In addition I wanted to step outside my comfort zone and choose a subject that was unconventional, in the hope to make it more accessible for future research. A goal, which in my opinion is reached throughout this work.

The road to the finish line of this thesis was not without diversions or bumps but it made me see concepts within the maritime industry and my own personal life more clear. Wherefore I am deeply grateful to my supervisors, family, girlfriend and friends.

First of all I would like to thank my daily company supervisor Niels De Vries from C-job Naval Architects who was always ready to clear my view or inspire me with simple but impact-full quotes. His vision on the project was of enormous help and brought me where I am today. Secondly I want to thank my daily TU Delft supervisor Jaap Gelling who kept me on the right track and always came with to the point advice. Thirdly I would like to thank my second TU Delft supervisor Klaas Visser who's feedback and remarks throughout the process were of great help. This extends to all my colleagues at C-job who helped me throughout the process of my thesis.

On a more personal level I would also like to thank my family, girlfriend and friends. Who never gave up on me even if it looked like there was no coming back. Without their support I couldn't have brought this journey to a good end.

I wish you a pleasant reading time.

*Leurs Zeno
Delft, October 2023*

Abstract

This thesis delves into the intricate process of formulating an answer to the pivotal research question:

“What are the design characteristics of an economic high speed nuclear container vessel?”

The report systematically unfolds in six chapters, primarily focusing on a comprehensive literature study.

The exploration begins with an in-depth analysis of various nuclear reactors, emphasizing aspects such as load following, capital costs, fuel expenses, operational and maintenance costs, and decommissioning expenditures. Key challenges in implementing these reactors within ship designs are scrutinized, including considerations of safety, location, and refueling intervals.

Subsequently, the study investigates the intricate relationship between vessel speed and economic factors such as income, operational costs, and freight rates in liner shipping. Operational costs, especially fuel expenses, are found to significantly impact speed-dependent factors.

Concurrently, the impact of speed on hull shape and propulsors is evaluated, revealing a proportional increase in wave-making resistance at higher speeds and necessitating a reevaluation of power estimation methodologies.

The literature study is concluded with an assessment of three types of propulsors, where conventional propellers emerge as the preferred choice due to their efficiency, power range, and scalability.

The research then starts with the economic speed determination process, vital in shaping the vessel's design. This involves constructing a resistance curve based on a volume-scaled high-speed model vessel and factoring in components like CAPEX, OPEX, voyage costs, and freight rates. The study highlights the significant influence of freight rates on speed for all cases and underscores the viability of nuclear-powered vessels in achieving higher economic speeds due to lower fuel costs, especially over extended service lives.

With these foundational insights, the design process is initiated, emphasizing the optimal balance between speed, capacity, and real-world constraints. A scaled-down version of the nuclear concept vessel is developed, demonstrating a decrease in resistance while adhering to stability criteria. The resulting nuclear vessel design showcases a streamlined hull shape, minimal general arrangement alterations, and enhanced stability, with a notable preference for a three-propeller layout to optimize performance.

In conclusion, this study presents a concept design for a 20,000 TEU nuclear container vessel that achieves an increased economic speed, leading to design refinements in hull shape and propulsors. The research underscores the viability of nuclear propulsion in enhancing the efficiency of container shipping, providing valuable insights for future innovations in maritime transportation.

Summary

This thesis report covers the process of formulating an answer to the main research question:

“What are the design characteristics of an economic high speed nuclear container vessel?”

As the detailed potential of generation IV nuclear propulsion for complete new builds is unknown. This report is divided into six chapters where the first four cover the literature study that aims to find all input parameters in order to determine an economic speed for a nuclear driven container ship and the possible impact on the hull shape and propulsors. The fifth and sixth cover the determination of this economic speed and its impact on the hull shape, general arrangement, stability and propulsor configuration compared to conventional designs.

Nuclear reactors

First, a thorough examination of the characteristics of the GEN IV, (V)HTR and MSR for load following, capital, fuel, O&M, and decommissioning costs. Revealed that, higher power levels were found to reduce relative capital costs, fuel costs were also seen to be considerably lower than for MDO. Additionally, a method for estimating reactor shielding based on power was validated. Potential challenges in implementing the reactor within a ship design were researched based on factors such as location, safety, and refuelling. Notably, the major difference with a conventional ship design was the long refuelling interval and compartmentalization of the reactor room to facilitate removal during salvage operation in the case of ship wreckage.

Relation speed & income

Secondly, a detailed investigation into what the key factors are that contribute to income and are depended on speed in liner shipping was carried out. Taking capital costs into regard, only the main engine depended on speed. Operational costs, specifically O&M and fuel costs, were as well influenced by speed. For nuclear-powered ships, other operational costs depending on speed, excluding fuel, were not included. Voyage costs were identified higher for the nuclear case whereas freight rates showed a proportional relationship with container ship average speed and were also seen to be volatile.

Relation speed & hull shape

Thirdly, to evaluate differences in design characteristics based on speed for conventional MDO container vessels, two high-speed vessels were compared with conventional-speed vessels. The deadweight to displacement, B/D, and B/T ratio did not differ from the conventional ones. Ratios that showed differences included an increased L/B ratio and decreased block coefficient, both explained by the proportional increase in wave-making resistance at higher froude numbers. Consequently, the installed power per TEU also significantly increased, indicating that estimating power based on conventional slow-speed container ships was not ideal. Instead, the identified reference vessels were preferred for this purpose.

Relation speed & propulsors

Lastly as part of the literature, three propulsor types for potential use in the propulsion line were evaluated, considering factors such as general application, effective speed domain, power range, parallel application and scalability. Out of these, conventional propellers were seen to be most fit between a speed range of 0-33 knots. Water jets could be implemented starting at speeds of 30 knots on wards however conventional propellers remained to be the preferred choice from an efficiency, power range and scalability point of view. High speed propellers were disregarded because they only become effective from 50 knots on wards and have difficulties in scaling up with respect to radiated noise and loss of thrust.

Based on the above mentioned findings the research phase was started.

Economic speed determination

The first design characteristic that was evaluated was the design speed. This is done via an economic speed model evaluated on two routes, between Rotterdam and Shanghai using the Suez canal and between Rotterdam and New York. As input the speed depended components of CAPEX, OPEX, voyage costs and freight rates were used. In order to couple these to speed, a resistance curve was constructed based on a volume scaled high speed model vessel. This was done using Froude scaling which insured the wave making resistance would not be underestimated up until the calculated design speed of 38.18 knots for the concept vessel case. Three different cases were studied, namely, a conventional MGO case with a service life of 25 years and two nuclear cases with respective service lives of 25 and 50 years. A first sensitivity analysis revealed that the freight rate had a big influence on speed for all cases and the fuel cost solely for the MGO case. Furthermore, the reactor CAPEX was seen to have a less substantial role, that degraded over increased service life. For both nuclear cases an increase in economic speed was seen compared to the conventional MGO case, due to the significantly lower fuel cost. In addition the 50-year nuclear case showed a speed increase when compared to the 25-year case due to the decrease of annual cost for the reactor capex. Besides that, a shorter route showed a logical increase in economic speed for all cases as the revenue stayed constant but the effective costs went down. The obtained findings indicated that a nuclear-powered container vessel, featuring a cargo capacity of 20,000 TEU, was initially capable of achieving an economic speed of 30 knots with a projected service life of 50 years.

Design process

Next the design process was entered. For the original design there was little to gain with a view on resistance, despite variations in dimensions and block coefficient keeping a constant displacement. While the initial design focused on minimizing the resistance, its unconventional LOA and T raised concerns. With a required capacity of 20,000 TEU, similar capacity could be achieved in shorter, wider vessels. This led to a re-evaluation of volume, weight, and application of real-world constraints on the main dimensions. Calculations indicated an excess of 4,590 TEU's, 26% overshoot in displacement and over-dimensioned LOA and T compared to real-world constraints. This led to a scaled down version of the nuclear concept vessel. Notably, the scaled down nuclear concept vessel corrected for carrying capacity showed a 2% decrease in resistance when compared to the initial design. This showed the dominant role of frictional resistance as the Froude number was equal to 0.25 indicating that the wave making resistance is of less importance in the found speed domain.

The resulting nuclear concept vessel was evaluated on four design characteristics namely hull shape, general arrangement, stability, and propulsor configuration. The hull shape featured a low C_b of 0.63 due to a high design speed, chosen to decrease resistance. General arrangement changes were minimal compared to conventional designs. The reactor compartment was however positioned to minimize risk of radioactive spill. This is seen by the positioning and compartmentalization. Stability assessment revealed that there were only two necessary load cases due to limited nuclear fuel requirements. Aside of that all intact stability criteria were met without any challenge. Propulsor analysis favoured a three-propeller layout over a two-propeller lay-out, exhibiting better performance in various criteria. The chosen configuration demonstrated a 11% reduction in installed power compared to the two-propeller lay-out, mainly explained by the reduction in thrust loading coefficient.

In conclusion a concept design of a 20,000 TEU nuclear container ship showed an increase in economic speed which gave way to a smaller C_b and an increase of propulsors, whereas the influence on general arrangement and stability were seen to remain limited.

Contents

Preface	i
Abstract	ii
Summary	iii
List of Figures	xi
List of Tables	xiii
Nomenclature	xiv
Introduction	1
1 Nuclear reactors	2
1.1 Basic reactor concepts	2
1.1.1 Small Modular Reactors (SMRs)	4
1.1.2 Generation IV reactors	4
1.1.3 Thorium as nuclear fuel	4
1.2 Initial filtering	6
1.3 Molten Salt Reactor	7
1.3.1 History & development	7
1.3.2 Basic principles	8
1.3.3 Fuel characteristics	8
1.3.4 Safety	8
1.3.5 Technology Readiness Level (TRL)	9
1.3.6 Power generation	9
1.4 Very High Temperature Reactor	10
1.4.1 Introduction and development	10
1.4.2 Basic principles	10
1.4.3 Fuel characteristics	10
1.4.4 Safety	11
1.4.5 Technology Readiness Level (TRL)	12
1.4.6 Power Generation	12
1.5 Load following	12
1.5.1 Reactor poisoning	12
1.5.2 Molten salt reactor	14
1.5.3 Very high temperature reactor	15
1.5.4 Conclusion load-following	15
1.6 Cost description	17
1.6.1 Capital costs	17
1.6.2 O&M costs	21
1.6.3 Fuel costs	21
1.6.4 Decommissioning costs	25
1.7 Sizing & weight estimation	26
1.7.1 Reactor vessel	26
1.7.2 Shielding	26
1.8 Additional technical points for the implementation of a reactor in a ship design	29
1.8.1 Location	29
1.8.2 Safety	29
1.8.3 Refuelling facilities	30
1.9 Summary of discussed reactor technologies	30

1.10 Chapter conclusion	33
2 Relation speed & income	34
2.1 Opex & Capex: cost of ownership	34
2.1.1 Capital cost	34
2.1.2 Operational cost	35
2.2 Route selection	38
2.2.1 Rotterdam to Shanghai	38
2.2.2 Rotterdam to New York	39
2.3 Revenue	39
2.4 Chapter conclusion	43
3 Relation speed & hull shape	44
3.1 High-speed container ships	44
3.1.1 FastShip concept	44
3.1.2 Sea-land class container ships	45
3.1.3 Maersk B-class	46
3.2 Relation with conventional container ships	47
3.2.1 Deadweight vs Displacement	48
3.2.2 Main particulars	48
3.2.3 Cb vs speed	50
3.2.4 TEU vs Installed power	51
3.3 Chapter conclusion	52
4 Relation speed & propulsors	53
4.1 Conventional submerged propellers	53
4.1.1 General application	53
4.1.2 Effective speed domain	54
4.1.3 Power range	55
4.1.4 Parallel application	55
4.2 Waterjets	57
4.2.1 General application	57
4.2.2 Effective speed domain	57
4.2.3 Power range	59
4.2.4 Parallel application	59
4.2.5 Marine application	60
4.3 High speed propellers	61
4.3.1 General application	61
4.3.2 Effective speed domain	61
4.3.3 Power range	62
4.3.4 Parallel application	62
4.4 Comparison of propulsors	62
4.5 Chapter Conclusion	64
5 Economic speed determination	65
5.1 Definition of concept vessel	65
5.1.1 Model ship selection	65
5.1.2 Resistance prediction method selection	66
5.1.3 Resistance calculation of 20,000 TEU concept ship	73
5.2 Definition of economic speed model	74
5.2.1 Cases	74
5.2.2 CAPEX	74
5.2.3 OPEX	75
5.2.4 Voyage costs	75
5.2.5 Freight rate	75
5.3 Sensitivity analysis	76
5.3.1 Selection of initial design speed	81
5.4 Chapter conclusion	82

6	Impact of speed on design	83
6.1	Design variations of the 20.000 TEU nuclear concept vessel to decrease resistance . . .	83
6.2	Volume check of concept design	85
6.2.1	Sizing of machinery room	85
6.2.2	Accommodation sizing	94
6.2.3	TEU sizing	94
6.2.4	Conclusion volume check of concept design	96
6.2.5	Weight assessment of initial nuclear container vessel	97
6.3	Check of main dimensions with real-world constraints	100
6.3.1	Scaling down of nuclear concept vessel	101
6.4	General arrangement 1st iteration	101
6.5	Stability 1st iteration	106
6.5.1	Departure/arrival fully loaded condition	106
6.5.2	Departure/arrival ballast condition	108
6.6	Propulsors 1st iteration	110
6.6.1	Final propeller design choice	114
6.7	General arrangement second iteration	116
6.8	Final comparison with diesel equivalent vessel	119
6.9	Chapter conclusion	121
7	Conclusion	122
8	Recommendations	124
	References	127
	Appendices	135
A	Nuclear reactors	136
A.1	Nuclear fuel costs	136
A.1.1	Fuel costs	136
A.1.2	Fuel cost calculation	136
A.1.3	Sizing & weight estimation	137
B	Relation speed & income	138
B.1	Capital cost	138
B.2	Machinery cost	140
B.3	Operational costs	140
B.3.1	Freight rates	140
C	Propulsion line	144
C.1	Waterjets	144
D	Optimal speed determination	145
D.1	Initial resistance estimation	145
E	Optimal speed model	146
E.1	Analytical speed model	146
E.2	Optimal speed model plots	148
E.2.1	Rotterdam - New York	148
F	Volume check	150
F.1	Turbine cross-section calculation	150
F.2	Midship cross-section	150
F.3	Weight assessment	151
G	Stability 1st iteration	152
G.1	Center of gravity calculation	152
G.1.1	Loaded Condition	152
G.1.2	Ballast Condition	154
G.1.3	Lightship	154
G.1.4	Deadweight	156

- G.1.5 Wind silhouette 157
- G.1.6 Ballast tank configuration 157
- H Propulsors 1st iteration 158**
- H.1 Open water diagrams 158
 - H.1.1 Two propeller lay-out 158
 - H.1.2 Three propeller lay-out 159
- I General arrangement second iteration 160**
- I.1 Machinery room 160

List of Figures

1.1	Basic reactor components [71]	2
1.2	Comparison uranium fuel-cycle and thorium fuel-cycle[64]	5
1.3	Speed vs deadweight container vessels	6
1.4	Diagram of Molten Salt Reactor	7
1.5	Diagram of Very High Temperature Reactor	10
1.6	Pebble bed reactor design and prismatic reactor design	11
1.7	Xenon deadtime - 20% excess reactivity [140]	12
1.8	Xenon response to reactor power change [138]	13
1.9	Xenon response to reactor shutdown [138]	14
1.10	Load following of a MSR [34]	15
1.11	Typical profile operations [132]	16
1.12	Capital cost breakdown [14]	17
1.13	Capital cost breakdown for different production cases [174]	18
1.14	Specific capital cost for different degrees of modularisation [96]	19
1.15	Capital cost trend line A	20
1.16	Capital cost trend lines with uncertainty band (25%)	20
1.17	Uranium Price probability until 2050 [89]	22
1.18	Comparison U3O8 vs SWU price based on [42] & [143]	23
1.19	Decommissioning procedure NS Mutsu [8]	25
1.20	Weight-power relation [74]	26
1.21	Penetrating power of different radiations [150]	27
1.22	Reactor Shielding weight estimation based on [71] [9] [127] [186] [66] [93]	28
1.23	Reactor + shielding radius estimation based on [71] [93]	29
2.1	Annual operating cost for different container sizes [125]	35
2.2	HSFO 380 vs. Container Average speed [133]	37
2.3	Bunker costs over the past 10 years [161]	37
2.4	Spot freight rates 2020-2022 [54]	40
2.5	Changes in transported volume from 2019-2022 [54]	41
2.6	Freightos Baltic Index vs Container average speed [133]	41
2.7	Freight rates spot and contract 2019-2021 [24]	42
3.1	FastShip Profile and Hull Shape [176]	45
3.2	Sea-land and Mclean lead ship [20]	45
3.3	Maersk Boston [102]	46
3.4	Deadweight vs Displacement (0-4000 TEU)[176][135] [183][72]	48
3.5	Length vs breadth (0-4000 TEU)[176][135] [183] [72]	48
3.6	Resistance components with increasing speed[172]	49
3.7	Deadweight vs L/B (0-20,000 TEU) [176][135] [183][72]	49
3.8	Froude number vs Midship section [176][135] [183][72]	50
3.9	Froude number vs Cb[176][135] [183][72]	50
3.10	TEU vs Pb (0-4000 TEU)[176][135] [183][72]	51
4.1	Max power per ship propulsor through time [59]	53
4.2	Effect on open water efficiency for single or twin screw (By courtesy of MARIN)	56
4.3	USS Gerald Ford propulsor layout [111]	56
4.4	USS Gerald Ford propulsor lay-ou [38]	57
4.5	Propulsive efficiencies/coefficients	58
4.6	Waterjet power ranges [179]	59

4.7	Freedom class LCS waterjet system [3]	60
4.8	Voith linear jet integration [27]	60
4.9	High speed propeller layout [168]	61
5.1	Comparison of resistance prediction methods for Maersk B	72
5.2	Used efficiencies in power curve	73
5.3	Sensitivity plot Rotterdam-Shanghai Nuclear 50-year	76
5.4	Sensitivity plot Rotterdam-Shanghai Nuclear 25-year	77
5.5	Sensitivity plot Rotterdam-Shanghai Diesel 25-year	77
5.6	Cost breakdown nuclear (50y) scenario B	78
5.7	Cost breakdown nuclear (25y) scenario B	79
5.8	Cost breakdown diesel (25y) scenario B	80
6.1	Design spiral for the 20.000 TEU nuclear concept vessel	83
6.2	L/B and B/T variations with corresponding resistance at 30 knots	84
6.3	C_b variations with corresponding resistance at 30 knots	84
6.4	Schematic representation of the full propulsion layout that is used to make the volume and weight estimation of the machinery room taken from K. Houtkoop [71]	85
6.5	Open brayton cycle turbine with heat rejection capabilities taken from K. Houtkoop [71]	88
6.6	Operating profile nuclear concept vessel Rotterdam - Shanghai trip	89
6.7	Peak shaving role of batteries	90
6.8	Electrical grid possibilities	91
6.9	Close-up of machinery room for redundant lay-out with cubic VHTR	93
6.10	Top view of machinery room for redundant lay-out with cubic VHTR	94
6.11	Container margins above and below deck [70]	95
6.12	Cross-section midship	95
6.13	Side-view	96
6.14	Isometric view	97
6.15	Lightship weight prediction based on significant ship 2004-2020 and [72].	99
6.16	Machinery room 1st iteration	102
6.17	Machinery room 1st iteration (top view)	103
6.18	Cross-section midship 1st iteration	104
6.19	Side-view 1st iteration	104
6.20	Top view 1st iteration	105
6.21	Isometric view 1st iteration	105
6.22	GZ-curve departure/arrival condition fully loaded	107
6.23	GZ-curve departure/arrival condition ballast	109
6.24	Propulsion chain efficiency - two propellers	113
6.25	Propulsion chain efficiency - three propellers	114
6.26	Propeller efficiency outline	115
6.27	Propeller stern view	116
6.28	Machinery room system diagram based on [71] with own additions	117
6.29	Machinery room three propeller lay-out close-up	117
6.30	Machinery room three propeller lay-out top view	118
6.31	Machinery room three propeller lay-out Isometric view	118
6.32	Main differences with conventional diesel container ships	119
A.1	SWU cost and uranium cost [42] & [143]	136
A.2	Full nuclear fuel cost calculation for 5% enriched Uranium	137
A.3	Trend lines constructed with data from [74]	137
B.1	Total capital cost and cost per TEU for increasing vessel size [125]	138
B.2	Construction cost per TEU for increasing vessel size [117]	139
B.3	Construction cost per TEU 2005-2017 [117]	139
B.4	Power cost relation for a conventional container ship	140
B.5	FBX 11 - Route	140
B.6	FBX 11 - Freight rate	141

B.7	FBX 12 - Route	141
B.8	FBX 12 - Freight rate	141
B.9	FBX 21 - Route	142
B.10	FBX 21 - Freight rate	142
B.11	FBX 22 - Route	143
B.12	FBX 22 - Freight rate	143
C.1	Interaction efficiencies vs froude number for monohull and catamaran[163]	144
D.1	Froude scaling exercise	145
E.1	Optimal speed model with only varying speed	147
E.2	Sensitivity plot Rotterdam-New York Nuclear 50 years	148
E.3	Sensitivity plot Rotterdam-New York Nuclear 25 years	148
E.4	Sensitivity plot Rotterdam-New York Diesel 25 years	149
F.1	Turbine duct cross-section calculation	150
F.2	Midship cross-section HMM Algeciras	150
F.3	Deadweight breakdown	151
G.1	Container arrangement; red = empty (2 ton), green = full (9 ton)	153
G.2	Steel structure center of gravity calculation	154
G.3	Machinery room center of gravity calculation	154
G.4	Cargo deadweight center of gravity calculation	156
G.5	Wind silhouette loaded condition	157
G.6	Wind silhouette ballast condition	157
G.7	Ballast tank configuration	157
H.1	Open water diagram propeller	158
H.2	Open water diagram center propeller	159
H.3	Open water diagram wing propellers	159

List of Tables

1.1	Load following characteristics	16
1.2	Capital cost per kW (efficiencies marked with '*' are estimates based on [156] because the used thermal efficiency was not found in the publication)	19
1.3	O&M costs estimates based upon [45],[10],[174]	21
1.4	Prognosis for Uranium cost expressed in \$/kg [89]	22
1.5	Estimated fuel cost Uranium 5% enrichment - general [\$/kg]	24
1.6	Estimated fuel cost Uranium 20% enrichment - general [\$/kg]	24
1.7	Decommissioning cost upper & lower limit based upon [120][152][126] [19]	26
1.8	Comparison of selected reactor technologies based upon previously discussed sections. Rows denoted with * depend on the power of the selected reactor thus a reference to the figure or table to be used is given. Based on [71] and own additions from previous sections	30
1.9	Advantages and disadvantages of discussed reactor types from a marine application perspective based on [71] and own additions from previous sections	31
2.1	Machinery cost factors from [175]	35
2.2	Voyage cost Rotterdam-Shanghai	39
2.3	Voyage cost Rotterdam-New York	39
3.1	Fast containerships [87] [176] (*) top speed = service speed	44
3.2	Vessel characteristics FastShip [176]	45
3.3	Vessel characteristics SL-7 [20]	46
3.4	Vessel characteristics Maersk B-series [160] [87] (*) top speed	47
4.1	Comparison FPP and CPP based on [39][106][59][60]	54
4.2	Comparison of propulsors (*) 75% is only for high froude numbers around 0.6	62
5.1	Comparison of high-speed model vessels [135][183]	65
5.2	Initial main dimensions of 20,000 TEU nuclear concept vessel (*) based on froude number	66
5.3	Limitations of Holtrop & Mennen prediction method [142]	67
5.4	Limitations of Van Oortmerssen prediction method [107]	68
5.5	Limitations of Marwood & Bailey prediction method (*) length-displacement ratio [108]	68
5.6	Limitations of MARIN fast displacement hulls [86]	68
5.7	Limitations of Compton prediction method [4]	69
5.8	Limitations of Fung prediction method [4]	69
5.9	Main parameters Maersk B [4] [183] [160] (*) estimated by MAXSURF	70
5.10	Comparison table of discussed methods with model vessel Maersk B (*) $M = Lwl/\nabla^{1/3}$	70
5.11	Difference in resistance at design speed Maersk B	72
5.12	Holtrop & Mennen Input 20,000 TEU concept vessel (*) estimated with Maxsurf	73
5.13	Capital costs	74
5.14	Operational costs	75
5.15	Voyage cost Rotterdam-Shanghai	75
5.16	Voyage cost Rotterdam-New York [122] [145] [170]	75
5.17	Freight rates nuclear concept vessel	75
5.18	Impact of different variables on the economic speed (Rotterdam - Shanghai)	77
5.19	Impact of different variables on the economic speed (Rotterdam - New York)	78
5.20	Definition of scenario's in economic speed plots	78
5.21	Cost breakdown nuclear concept ship scenario A, B & C (50-year)	79
5.22	Cost breakdown nuclear concept ship scenario A, B & C (25-year)	79
5.23	Cost breakdown diesel reference ship scenario A, B & C	80

5.24	Economic speeds for different scenario's, used propulsion line and lifetime for the route from Rotterdam to Shanghai	80
5.25	Economic speeds for different scenario's, used propulsion line and lifetime for the route from Rotterdam to New York	81
6.1	Volume per MW _{th} calculation values from [71]	87
6.2	Derived properties for battery package from [57][5]	90
6.3	Emergency engine properties[103]	91
6.4	Volume and weight of machinery room components (207 MW _e) (*) including converters, busbars and rectifiers	92
6.5	Nuclear container vessel characteristics after volume check	96
6.6	Deadweight calculation nuclear concept vessel in fully loaded condition	98
6.7	Lightship weight calculation nuclear concept vessel	99
6.8	Real-world constraints in main dimensions (*) over 400 m vessels need permission to cross suez canal (**) additionally cross-sectional area not more as 1,006 m ²	100
6.9	Comparison of reference vessels with final constraints	100
6.10	Nuclear container vessel characteristics after real-world constraints	102
6.11	Loading conditions IMO intact stability code	106
6.12	Loading conditions nuclear concept ship	106
6.13	Point of gravity determination of nuclear concept vessel loaded condition	106
6.14	Intact stability check departure/arrival condition fully loaded	106
6.15	Point of gravity determination of nuclear concept vessel ballast condition	108
6.16	Intact stability check departure/arrival condition ballast	108
6.17	Thrust deduction and wake factor estimation [175][124]	111
6.18	Min Ae/Ao calculation for lay-out with two propellers	111
6.19	Min Ae/Ao calculation for lay-out with three propellers	111
6.20	Tip speed evaluation using the wageningen B5-90 series in Propcalc	112
6.21	Tip speed evaluation using the wageningen B5-75 series in Propcalc	112
6.22	Maximum delivered power evaluation	113
6.23	Main characteristics of propellers	114
6.24	Electric motors	116
G.1	Point of gravity determination of lightship	152
G.2	Point of gravity determination of deadweight	153
G.3	Deadweight ballast condition	154
I.1	Volume and weight of machinery room components three propeller lay-out (*) including converters, busbars and rectifiers (210 MW _e)	160

Nomenclature

Abbreviations

Abbreviation	Definition
AC	Alternating Current
CAPEX	Capital costs
CPP	Controllable Pitch Propeller
DC	Direct Current
DWT	Deadweight
ESD	Energy Saving Device
FEU	Forty feet equivalent unit
FOAK	First-of-a-kind
FPP	Fixed Pitch Propeller
GFR	Gas-cooled fast reactor
GHG	Green House Gas
GT	Gross Tonnage
GWd/tHM	Giga Watt days per ton heavy material
H&M	Holtrop & Mennen
IMO	International Maritime Organisation
ISO	International Organization for Standardization
L-MOM	Longitudinal Moment
LCG	Longitudinal Center of Gravity
LCS	Littoral Combat Ships
LCB	Longitudinal Center of Buoyancy
LNG	Liquefied Natural Gas
LOA	Length over-all
LPP	Length between perpendiculars
LSW	Lightship weight
LWR	Light Water Reactor
LWI	Length waterline
LMTD	Logarithmic Mean Temperature Difference
M&A	Management and administration
M&B	Marwood & Bailey
MFDH	MARIN systematic series fast displacement hulls
MW _e	Megawatt electric
MW _{th}	Megawatt thermal
MSR	Molten Salt Reactor
MSRE	Molten Salt Reactor Experiment
MSFR	Molten Salt Fast Reactor
NRC	Nuclear Regulatory Commission
NREL	National Renewable Energy Laboratory
NT	Net Tonnage
NOAK	N th -of-a-kind
ORNL	Oak Ridge National Laboratory
O&M	Operation and Maintenance
OPEX	Operational costs
PWR	Pressurized Water Reactor
R&M	Repair and maintenance
RPM	Rotations Per Minute

Abbreviation	Definition
RPS	Rotations Per Second
SCNT	Suez Canal Net Tonnage
SCWR	Super-Critical-Water-cooled-reactor
SMR	Small Modular Reactor
SPMG	Semiplaning monohull-geometry
SFR	Sodium-cooled Fast reactor
SOLAS	Safety Of Life At Sea
Sv	Sievert
SWU	Seperative Working Unit
TCG	Transverse Center of Gravity
TEU	Twenty feet equivalent unit
Th	Thorium
TRL	Technology Readiness Level
ULCV	Ultra Large Container Vessel
VCG	Vertical Center of Gravity
VHTR	Very High Temperature Reactor
V.MOM	Vertical Moment
WED	Wake Equalizing Duct
WNA	World Nuclear Association
Xe	Xenon

Symbols

Symbol	Definition	Unit
A_e/A_o	Minimum blade area ratio	[-]
B	Width	[m]
C_b	Block coefficient	[-]
C_m	Midship coefficient	[-]
C_p	Prismatic coefficient	[-]
C_{stern}	Stern shape coefficient	[-]
C_{wp}	Waterplane coefficient	[-]
D	Depth	[m]
D	Diameter	[m]
GM	Metacentric Height	[m]
J	Advance Ratio	[-]
K_t	Thrust coefficient	[-]
P	Power	[MW] or [kW]
p_o	Atmospheric pressure	[Pa]
p_v	Vapour pressure	[Pa]
R	Resistance	[-]
T	Draught	[m]
T	Thrust	[kN]
t	Thrust deduction factor	[-]
V	Velocity	[m/s] or [knots]
V_a	Speed of advance	[m/s] or [knots]
W	Wake factor	[-]
Z	Number of propeller blades	[-]
$\frac{P}{D}$	Pitch over diameter ratio	[-]
k	Keller factor	[-]
n	Propeller rotational speed	[rev/sec]
η	Efficiency	[-]
ρ	Density	[kg/m ³]

Introduction

Introduction

Globally, shipping is one of the largest industries that is roughly responsible for 3% of Green house Gas (GHG) emissions [128]. By 2050 the annual total GHG emissions from international shipping should be at 50% when compared to 2008. In order to reach this goal new power and propulsion methods have to be considered [62]. Earlier research carried out by K.Houtkoop has shown the initial potential of next generation nuclear power with like for like replacement.

However, the further detailed potential of generation IV nuclear propulsion for complete new builds is unknown.

Therefore, the goal of this thesis is exploring this uncertainty by creating a new design with the initial focus being on container vessels because of their relative high speed due to being volume based ships (low C_b), their large installed power and relative constant operating power, which is beneficial for nuclear power generation [71]. For this study a container ship size of 20,000 TEU is selected. By incorporating a larger cargo capacity, it is expected that the additional revenue generated will facilitate the repayment of expenses within a shorter timeframe. This design choice is based on previous studies that have demonstrated the high capital costs associated with nuclear energy [71].

As part of this the design speed will be redetermined since nuclear fuel cost is relatively low when compared to its diesel counterpart which can be of interest for container vessels because of their time sensitive cargo. Once the optimum speed is determined its impact is reviewed on the aspects of hull shape, general arrangement, stability and propulsor configuration.

Structure of report

Main research question:

"What are the design characteristics of an economic high speed nuclear container vessel?"

In order to answer this research question it is needed to analyse the question on different levels and thereby forming sub questions.

Literature section:

1. **What are the properties of the nuclear reactor?**
2. **What are the factors that contribute to income in liner shipping and are they depended on speed?**
3. **Where lies the relation between speed, main particulars, C_b and deadweight?**
4. **Which propulsors are fit for which speed intervals using the existing power plant?**

Research section:

5. **Where does the economic speed for a high-speed nuclear container vessel lie?**
6. **How does this economic speed impact the design and how is it distinguished from a conventional design?**

1

Nuclear reactors

Chapter introduction

This chapter is dedicated to answer the sub literature question:
"What are the properties of the modern nuclear reactor?"

This chapter is dedicated to give a short introduction into reactor technology and its current state. Furthermore two most promising reactor technologies will be discussed in more detail because of their outstanding qualities. In order to have an effective ship design the cost and sizing of such reactors is vital thus these are discussed in more detail along with some additional technical aspects that are deemed important for a design process. These can than be later used as input for determining a new design speed and consequent ship design.

1.1. Basic reactor concepts

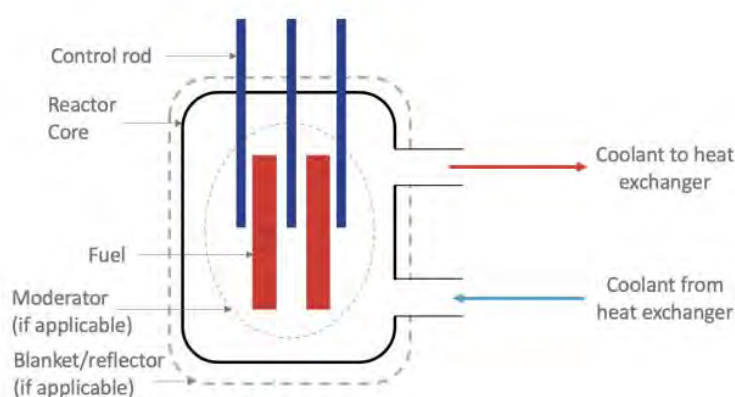


Figure 1.1: Basic reactor components [71]

Use of nuclear energy in the commercial shipping industry is still in its infancy. This section is dedicated to give an introduction to basic reactor concepts to increase the comprehensibility of the report. There are many types of reactors in use and being developed. What they have in common is the production of thermal energy which can be used directly or converted into mechanical energy with the use of a turbine and subsequently into electricity when coupled to a generator [150]. In December 1942 the first man-made self-sustaining chain reaction was obtained since then a lot of reactor design were constructed but they all share the basic components depicted on figure 1.1 [156]

The center of every reactor is called the **active core** here the fission reaction is sustained in order to deliver the needed energy. This core contains **fissile fuel** that delivers the necessary neutrons to

keep the nuclear reaction running [156]. Most commonly this fissile fuel is in a solid state and can be one of the following isotopes ^{233}U , ^{235}U , ^{239}Pu and ^{241}Pu . The only natural occurring isotope that can undergo fission is ^{235}U all other isotopes are made in the reactor vessel itself after neutron absorption and a decay process. Uranium is the most commonly used fuel inside a reactor but only 0.72% is ^{235}U which is essential to start the fission reaction. The remaining 99.275% is fertile material ^{238}U which can transform into the fissile material ^{239}Pu but this needs a neutron and decay process which takes around 2.35 days. ^{233}U is a fissile material that originates from the thorium cycle which is further addressed in 1.1.3. The 0.72% of ^{235}U is not enough to keep a chain reaction going, therefore Uranium is enriched to around 3-5% to be usable in conventional land based reactors. This process is called enrichment and produces a byproduct called "tails", also called "low level waste". These tails are considered "low level waste" because most ^{235}U is removed thus the radioactivity is limited but must not be disregarded. Aside the production of tails enrichment has another downside namely the work that is needed to full fill the enrichment process. This amount of work is expressed in Separative Working Units (SWU) and increases for increased enrichment levels [150].

In MSR the fuel can be in liquid state. To start a reactor with new fuel a neutron source needs to be present to start the fission reaction or decay process. This can be beryllium mixed with polonium, radium or other α -emitters. These α -particles release neutrons during the decay process from beryllium to carbon-12. When a reactor is shutdown and restarted this may not be needed because enough neutrons could be present when the control rods are removed which are discussed later [15].

The **moderator** is where the two main reactor types are split being thermal and fast reactors. Thermal reactors always make use of a moderator in order to slow down neutrons originating from fission to increase the probability of additional fissions. The material is usually graphite or heavy water which are superior over light-water because of their low neutron absorption. Neutrons in thermal reactors typically have an energy around 0.025 eV after being slowed down by the moderator. In a fast reactor a moderator is usually not present and neutrons are classified with an energy around 2 MeV. The neutron environment inside the reactor is the measure for reactivity and is most commonly expressed with the effective multiplication factor k_{eff} . This gives the relation between neutrons present in the current cycle and the previous one as depicted below[156]:

$$k_{\text{eff}} = \frac{\text{no. neutrons at some point in the cycle}}{\text{no. neutrons at the same point in the previous cycle}} \quad (1.1)$$

For a critical reactor this multiplication factor should be equal to 1. This means that an equal amount of neutrons is being absorbed and created due to the fission process. When $k > 1$ the reactor is called supercritical and when $k < 1$ it is called subcritical. The reactivity is expressed by ρ (ρ), making use of k_{eff} :

$$\rho = \frac{k_{\text{eff}} - 1}{k_{\text{eff}}} \quad (1.2)$$

Reactivity is **controlled** by passive and active safety measures. Passive safety measures are also called inherent safety measures because they are due to chemical properties of substances inside the reactor. This is typically due to the negative temperature coefficient of the coolant which is addressed more in detail per reactor type in the following sections. Active safety is most commonly addressed by the use of neutron **absorbers** which can be mixed together with the moderator in the form of boron, cadmium, hafnium or gadolinium. This absorber can also be present in the form of control rods which are cylindrical tubes of a few metres long. By adjusting the level these rods are submerged in the reactor vessel the reactivity can be actively controlled [150].

The main purpose of a reactor is to deliver energy in the form of heat as discussed before. This heat is transported by a **coolant** which can take many forms depending on the reactor type examples are water, heavy-water, liquid sodium, helium gas, carbon dioxide, liquid lead or molten salt in the case of MSR. For a VHTR this is usually helium gas. This coolant transfers the thermal energy from the core to a separate steam or gas cycle to drive a steam or gas turbine respectively. By the help of this process the thermal reactor energy is transformed into mechanical and electrical energy [156].

A **reflector/blanket** surrounds the reactor core in order to decrease the amount of neutrons leaking out of the reactor the material used can be water, graphite or beryllium with the latter being the most effective due to its small atomic mass when compared to the first two. By using beryllium for a given reactor power the reactor volume and weight can be greatly decreased. This type of reflector/moderator is often used in space applications but could also be used on board of ships [165]. In turn the reactor core and reflector are surrounded by a **steel vessel** which is designed to protect the reactor from its surroundings and vice versa in case of melt-down due to insufficient cooling for example.

To protect workers and electrical equipment from radiation a **biological shield** is surrounding the steel vessel. Usually this shield consists out of concrete, water, lead or boron. The shielding typically protects workers and equipment against γ - and neutron-radiation, depending on the energy level β -radiation can also be included. Extra shielding outside the primary loop, being the reactor and first heat exchanger, is possible. An example of this case is the MSR because here the fuel and coolant can be mixed together [49].

Three pillars in current reactor technology are the Small Modular Reactors (SMRs), GEN IV and the use of thorium as nuclear fertile fuel. These are shortly addressed in the following sections to get familiar with the concepts.

1.1.1. Small Modular Reactors (SMRs)

SMRs are defined as reactors with an electrical power not above 300 MW_e where the focus lies primarily on innovation and modularization. Most of the designs that fall under SMRs also adopt advanced and even inherent safety features. They also offer lower initial capital investment because of the Nth-Of-A-Kind (NOAK) concept that normally is not adopted in land-based reactors, here a First-Of-A-Kind (FOAK) is more conventional [48]. Because of their smaller power output they can be implemented in unique industrial or marine applications. It is also stated that some SMRs will be designed for extended periods without refuelling which is of particular interest for marine applications. They are subdivided into following categories[74]:

- Water cooled small modular reactors
- High temperature gas cooled reactors
- Fast neutron spectrum reactors (sodium-, gas- and lead-cooled)
- Molten salt reactors
- Micro reactors (up to 10 MW_e)

1.1.2. Generation IV reactors

Generation IV reactors are the next generation of nuclear reactors that focus on innovative designs. The fundamental goals are identified by the international forum [52] as :

- Sustainability
- Safety & reliability
- Economics
- Proliferation resistance and physical protection

The reactor designs that fall within this description are the Very High Temperature Reactor (VHTR), Sodium-cooled Fast Reactor (SFR), Super Critical-Water-cooled-Reactor (SCWR), Gas-cooled Fast Reactor (GFR), Lead-cooled Fast Reactor (LFR) and the Molten Salt Reactor (MSR) [52].

1.1.3. Thorium as nuclear fuel

Thorium is used as a fertile product and produces the fissile material U_{233} after decay which is then used for the production of fission products, neutrons and kinetic energy which translates in heat as discussed before. Aside this thorium has several benefits when compared with the uranium fuel cycle as discussed below:

1. Thorium is widely available and needs no enrichment like uranium. This leads to the fact that theoretically every gram of thorium can be converted to energy. Also its abundance can solve the

current lack of energy resources. As proof for this statement 6,335,000 ton is given as a world estimate of thorium resources [181]. When less than 1 ton of thorium can produce 1 GW for a whole year [64] [164].

- The nuclear waste produced by the thorium cycle has much shorter half-lives which results in far less long-term toxicity. This is because of the minor actinides that are formed in the thorium fuel cycle which follows from the lower mass number of ^{232}Th compared to ^{235}U or ^{238}U . As a result the waste stream is almost actinide-free which means that the radioactivity levels are acceptable within 300 years opposed to the thousand of years in uranium fuel cycle [164]. In addition the amount of waste produced is also significantly less. As the thorium fuel cycle can use the full amount of mass instead of only a small portion when compared to the uranium fuel cycle as depicted on figure 1.2. This is mainly because the chemical enrichment procedure is not needed for thorium [64].

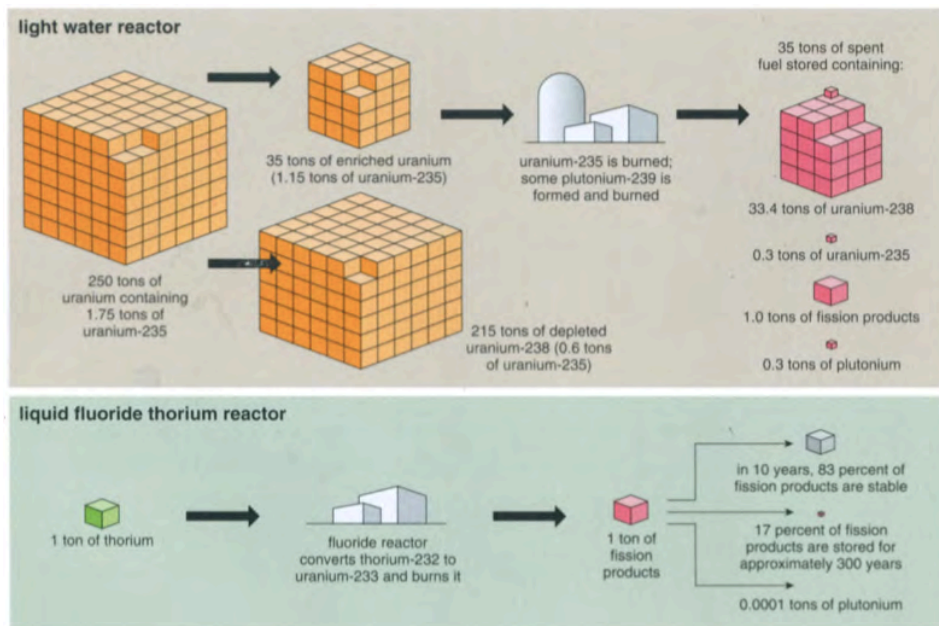


Figure 1.2: Comparison uranium fuel-cycle and thorium fuel-cycle[64]

- High proliferation resistance. This is due to the formation of ^{232}U in fertile isotope ^{233}U . ^{232}U has a relatively short half-life of 73.6 years because it burns itself out at a rapid pace producing decay products that transmit high-energy gamma radiation. This radiations are easily detectable and very harm full to personnel and electronics. Therefore it is not easily converted into nuclear weaponry [64].

When using thorium as a fuel it needs to be reminded that thorium is a fertile material thus it needs two neutrons to from a fissile material to be able to start the thorium fuel cycle going from ^{232}Th to ^{233}U . For this purpose a starter fuel is needed. Possibilities here are ^{235}U , ^{239}Pu and ^{233}U . ^{233}U would be the ideal solution because this way you can make a closed thorium fuel cycle but there are still a lot of technical difficulties to overcome [109].

1.2. Initial filtering

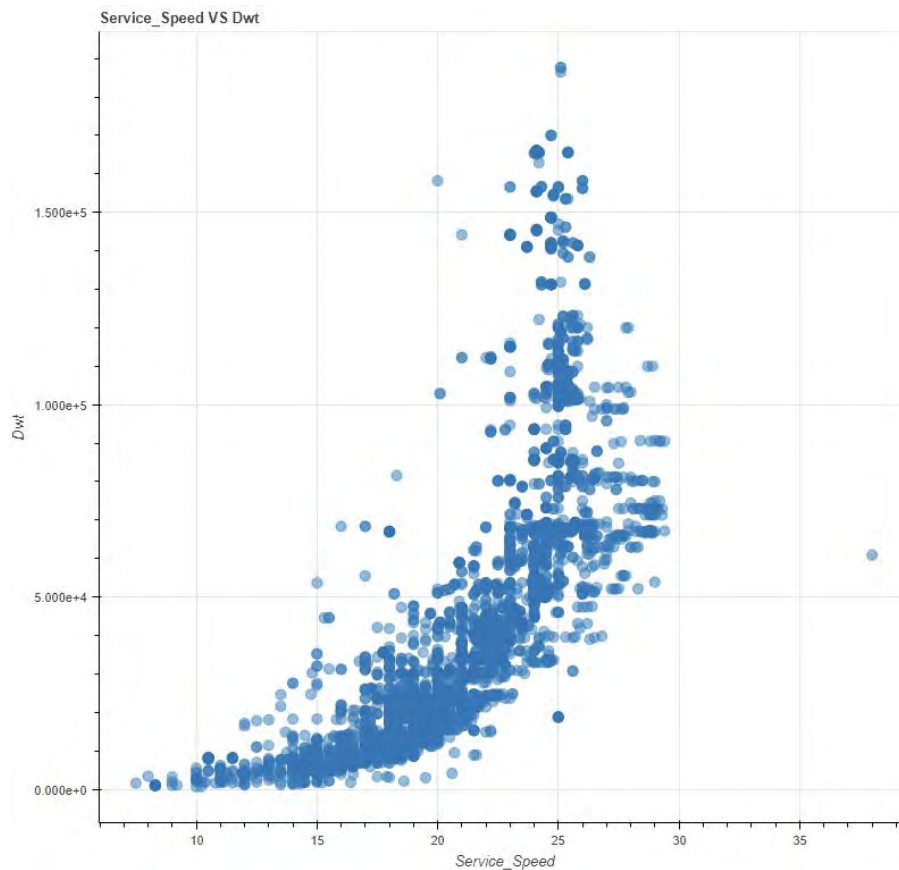


Figure 1.3: Speed vs deadweight container vessels

To narrow down the scope on reactor types an initial estimate of a conventional diesel propelled container vessel is made. A starting TEU capacity of 20,000 TEU is assumed which is defined as a Ultra Large Container Vessel (ULCV) with an initial design speed of 22 knots [104][100]. Based on this a minimal installed power (brake power) of 60 MW is needed for propulsion alone. Next to propulsion power there is also additional power needed for auxiliary machinery, reefer containers and hotel facilities. This is estimated as 21.8 % of the installed power for propulsion based upon a database of reference container vessels [72]. This leads to a total brake power of 72 MW [12]. Reactors are however expressed in thermal megawatt or MW_{th} with an efficiency of approximately 33%. If the previously 72 MW is expressed as megawatt electric this leads to a total of 218 MW_{th} [150].

This shows that the Small Modular Reactors (SMRs) should be studied as they can deliver an electric power up to 300 MW_e with the exception of micro modular reactors which have a typical output of 10 MW_e . Remaining are the water cooled reactors, high temperature gas cooled reactors, fast reactors (liquid-metal, sodium and gas-cooled) and the molten salt reactor [74]. These SMRs were extensively compared on basic principles, fuel use, power generation, safety, TLR and marine application in a previous study [71]. Out of this comparison two reactor types were selected to be most suitable for marine application namely the MSR and the VHTR. Reasons for this selection were high burn-up which indicates a higher fuel efficiency, inherent safety features and increased proliferation resistance which both increase the safety side of reactor operation. Further elaboration on these properties will be given in the following sections.

1.3.2. Basic principles

The working principle of MSR can be subdivided into two main categories based upon the implementation of the molten salt. First the molten salt can be used as a coolant with a solid fuel whereby the working principle heavily resembles the VHTR which will be discussed later. Secondly the molten salt can be mixed with fuel or fissile/fertile material which will be the focus of this section. This subcategory can then be divided according to the reactor's neutron spectrum [52]. In Europe most research & development is done into fast spectrum an example is the thorium Molten Salt Fast Reactor (MSFR) in France, capable of delivering 1400 MW_e [154]. Fast spectrum reactors are also mainly breeder reactors because of their high energy neutrons having a conversion ratio between 1.1-1.3 which means they produce more fissile material than they consume. In the thermal case a moderator will also be present based upon a variety of MSRs found in [75] this will be either heavy water or graphite. This kind is mainly a converter type which have a conversion ratio around 0.5-0.6 which means the amount of fissile material consumed is larger than produced. In both categories a fluid fuel is used where the fuel is mixed with a molten salt often being chloride or fluoride. Because of the liquid state the fuel salt mixture has a dual purpose. It produces the heat (fuel property) and delivers the heat to the power plant as can also be observed on Figure 1.4 [166].

1.3.3. Fuel characteristics

There are a couple of possibilities when considering the fuel use inside a MSR. The uranium fuel cycle is one option that is most commonly used nowadays. The full implementation of the thorium fuel cycle is also possible because of the favourable neutron environment that is needed for thorium because of the need of 2 neutrons to start the conversion to ²³³U. This is established by chemically processing the salt in the primary loop as depicted on figure 1.4. That is why the MSR can have a continuous thorium cycle.

As for the fuel cycle itself a closed one can be established which will increase the fuel efficiency greatly when comparing it with the open fuel cycle. When opting for a closed fuel cycle the spent fuel is reprocessed and partly reused, for this an on site reprocessing facility is needed [95]. For a MSR it is even possible to have a once-through fuelling cycle of 30 years this is proposed in a study by ORNL back in 1980 [49].

The burn-up expressed in GWd/tHM is a measure for the fuel cycle efficiency [150], the higher the value the more fuel is converted into energy over time. When consulting a study that covers a range of SMR[74] theoretical burn-up values were given starting from 100 to over 900. This values can be attributed to the reprocessing plant which removes fission products thereby making a higher burn-up possible [15]. Increasing the burn-up and reprocessing has a positive effect on the fuel cycle efficiency as it will produce more energy and less waste products. In addition the thorium fuel cycle can be used to increase this efficiency even more as depicted in figure 1.2.

1.3.4. Safety

As multiple advantages from an operational point of view were discussed before, on a safety level the MSR also stands out. Inherent safety or passive safety is stated as the dream of every reactor designer. This means that a reactor is able to remain critically stable or shutdown by itself when any malfunction occurs. For the MSR there are multiple properties that lead to a satisfactory result on this account [46].

First the previously discussed negative temperature coefficient plays an important role. The fuel salt mixture itself can thermally expand with increased temperature which will leave less fuel inside the reactor core [46]. This will thus reduce reactivity for increasing temperature. The graphite moderator in the case of thermal spectrum reactors will heat up which lead to an increase of fission rate which in turn increases the reactivity for higher temperatures this is however of small influence. The combination of these two factors leads to an overall strong negative temperature coefficient [110].

Secondly only a low pressure vessel is needed because the salts runs at high temperatures and atmospheric pressure, which saves space. In addition there is no use of water or sodium, which means there is no risk of a steam or hydrogen explosion [95].

Thirdly on the account of passive safety, MSR have a freeze plug installed at the bottom of the core. This

plug is kept below the freezing point of the salt by use of a fan. If the temperature inside the core rises to the melting point of the salt the plug will melt and the fuel salt mixture is led to an exterior basin where it is cooled down, this feature is only possible for liquid fuels [46]. Active safety systems like control rods can work in combination with the passive discussed above.

The fuel salt mixture also has a disadvantage when considering safety. This is because the fuel salt mixture is moving through all loops of the plant as can be observed from figure 1.4. Therefore all these parts need to be shielded to protect personnel from radiation, in addition this will also lead to maintenance difficulties [71]. This could be partly mitigated by using another coolant like helium in the secondary loop.

Another disadvantage is the corrosive nature of molten salt which leads to material degradation. Selection of the correct material inside a reactor is therefore a big challenge. Tritium production from the molten salt is a challenge as well. This forms when lithium is present in the salt, this substance is radioactive and has the possibility to permeate through the reactor vessel [84]. A study on the control of tritium already gives four possible solutions to tackle the problem. One of the proposed solutions is adding Li or Be to the salt in order to reduce to permeation of tritium [73].

Lastly a higher proliferation resistance is obtained due to an increased burn-up. This way the fuel use is more efficient and less nuclear waste is generated that could possibly be used for weaponry. An extra increase in proliferation resistance could be obtained by the use of thorium because of the production of ^{232}U as discussed in 1.1.3 [71].

1.3.5. Technology Readiness Level (TRL)

In a publication by the gen IV international forum the MSR is currently addressed with a TRL of 4 which means the technology is validated in lab [52]. Technical feasibility in the long term still needs to be evaluated especially the corrosive effect of the molten salt on the surrounding materials. Safety licensing and proliferation risks also need additional efforts but as stated before with the use of thorium the proliferation risk will already go down. Some MSR designs are offered by start-up companies but full commercial deployment is seen around 2030 [76]. The world nuclear association states however that the US department of energy has a collaboration with the China academy of sciences with a start-up budget of \$350 million. Here the commercial deployment of the TMSR is also planned in the 2030s [15]. Together with the aforementioned MoltexFLEX from the UK and CMSR of Seaborg a TRL between 4-6 can be assumed.

1.3.6. Power generation

The amount of power a MSR can produce varies from the design, in [74] a range starting from 100 MW_{th} going to 750 MW_{th} is stated. This includes MSR in the thermal and fast neutron spectrum. The outlet temperature in the proposed designs varies from 590-750 °C which can be considered relatively high compared to other reactor designs [74]. This high temperature will have an increasing effect on the carnot efficiency and thus also on the electrical efficiency in a later stage [137]. Due to the high temperature of the fuel-salt mixture the pressure can remain at ambient level thus a MSR will not need a high-pressure vessel [187]. Hereby the risk of significant break or loss of coolant is lowered. As was discussed before.

1.4. Very High Temperature Reactor

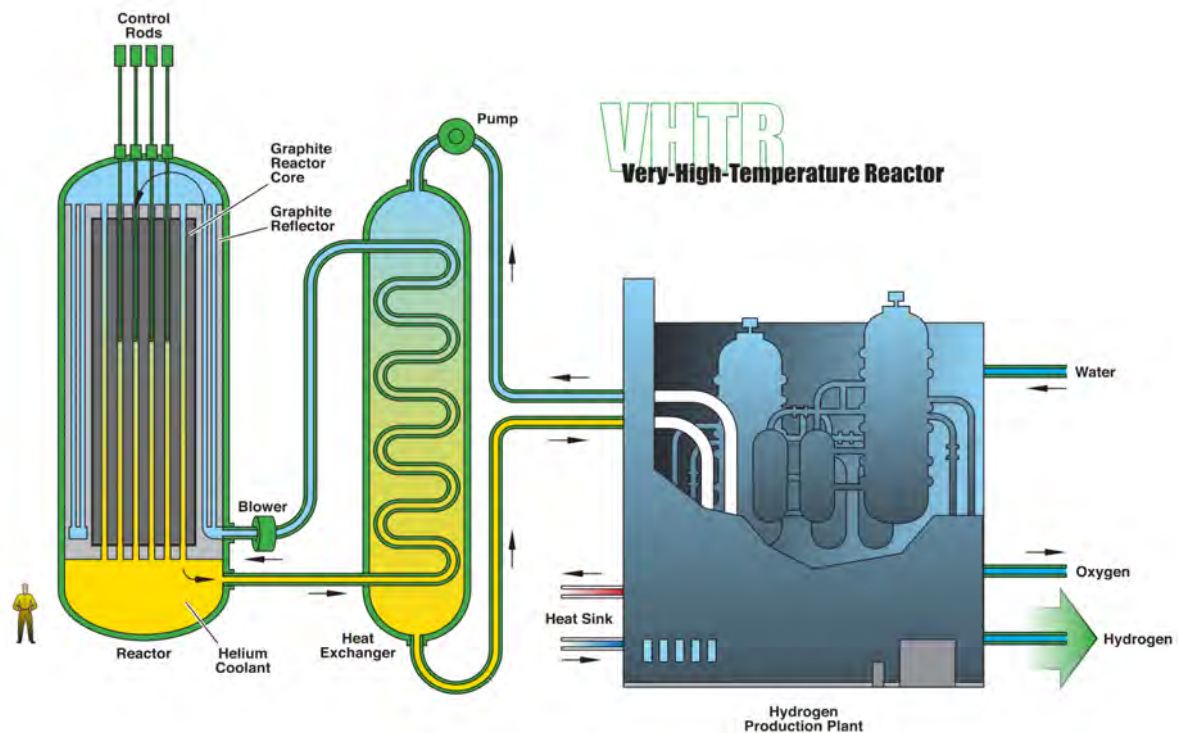


Figure 1.5: Diagram of Very High Temperature Reactor

1.4.1. Introduction and development

Same as for the MSR the VHTR or high-temperature gas-cooled reactor (HTGR) are part of the generation IV reactors. The current development of the HTGR which is also called the VHTR has been ongoing for over 50 years. Multiple developments are taking place and several designs are even being built. From 1963 until present several test HTGR were built in the UK, Germany, Japan and China. Prototypes of HTGR were also built in the USA, Germany and China [136]. China managed to develop the first HTGR which achieved criticality on the 12th of september 2021, after 23 days of the first fuel loading. This HTGR is a part of a reactor plant consisting out of two small reactors that are designed to drive a single 210 MW_e turbine [182]. HTGR are especially attractive for cogeneration because of their high outlet temperatures as depicted on 1.5 which can be used for hydrogen production for example. The Gen IV International Forum (GIF) endorsed six nuclear system concepts in 2001 where the VHTR was part of. GIF stated that the VHTR was deployable the soonest and very suitable for the generation of electricity apart from hydrogen production and other industrial application [136].

1.4.2. Basic principles

The HTGR and VHTR work via the same principle where two different reactor design types are the main difference. These are the prismatic and pebble bed design which are both being used in current designs. The difference will be discussed in the next paragraph. Both of them are thermal reactors thus using a moderator which is mostly graphite [136]. As a coolant helium is the favoured choice because it has the combination of being radiologically inert or neutron transparent and having a high thermal conductivity which is especially favourable above 550 °C. This means compared to molten salt its does not become irradiated because of its inert properties [53].

1.4.3. Fuel characteristics

The uranium and thorium fuel cycle are both possible to a certain extent. The thorium fuel cycle is limited in the aspect that it can only breed thorium and a continuous thorium cycle is not possible. This is however possible for a MSR as discussed before. Test and prototype reactors have been proven to

run on the breeding thorium cycle examples are the AVR that ran in Germany until 1988 or the FSV in the USA that ran until 1989 [136]. Two concepts of fuel element shape are used for the HTGR/VHTR these are pebble bed and prismatic. On figure 1.6 a comparison between the two reactor designs is given. The pebble bed type has a 60mm diameter of which 50mm is filled with kernels of UO_2 about 10,000 pieces of TRISO particles or kernels are present here. Inside a pebble bed core there can be a total of 27,000 fuel pebbles which is the case for the HTR-10 core for example. The other option is a prismatic block of 796mm x 360mm where 13,500 TRISO particles are compressed in a fuel rod and placed in one of the 210 holes[141]. The advantage of using pebbles instead of the prismatic configuration is the option to refuel online which means no shutdown is needed for refuelling[74].

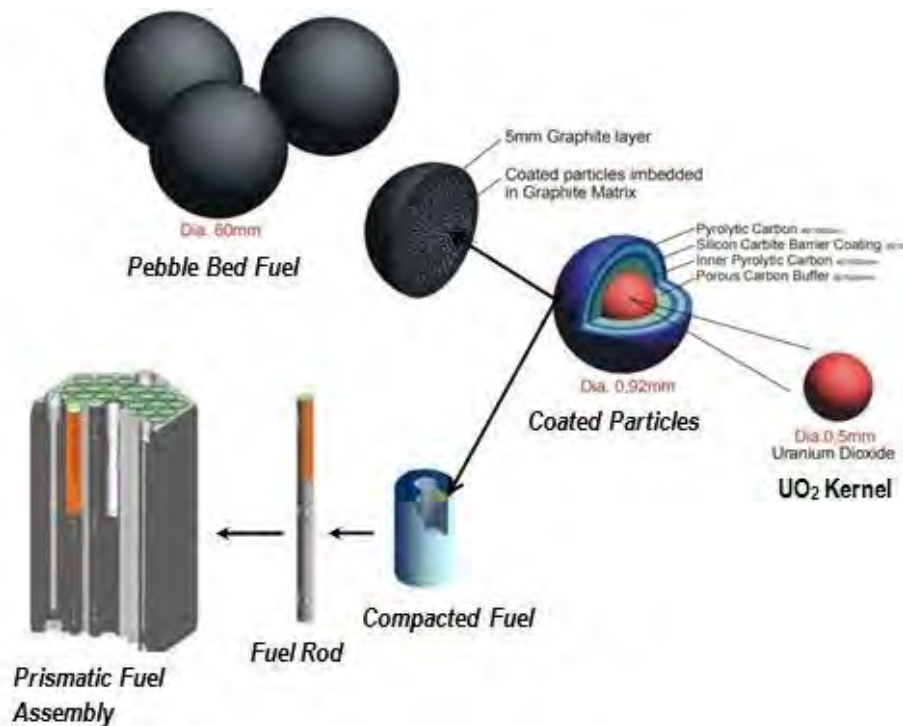


Figure 1.6: Pebble bed reactor design and prismatic reactor design

Both the outer layer of the pebbles as the prismatic fuel block are made of graphite in order to function as a moderator. Reactors that are currently being operated have a burn-up between 80-90 GWd/tHM [74]. Targets for the coming decade are between 150 to 200 GWd/tHM. Theoretically the burn-ups can be even higher but this depends on the fuel properties. Compared to the MSR theoretical burn-ups the ones from the VHTR of HTGR are considerably lower which aside of the already mentioned reason concerning reprocessing can also be attributed due to the fact that with MSRs the fuel is not encapsulated in pebbles or rods [71]. The fuel cycle that is used the most for these types of reactors is currently the open fuel cycle so without reprocessing, other fuel cycles are possible. For the prismatic reactor design this is between 1-2 years for the pebble based reactor design this can be continuous [136].

1.4.4. Safety

The VHTR and HTGR have good passive safety features being a negative temperature coefficient and a low power density in the core. The low power density together with the large volume of graphite inside the core limit the rise of temperature that can occur during an accident [136]. This is due to the graphite having a large thermal inertia that is capable of absorbing heat [33]. Combining this with the negative temperature coefficient the reactor will shutdown in case of an excessive rise of temperature [136].

In addition active safety features are also implemented in both reactor designs. Most commonly used are control rods. For the pebble based reactor an additional safety concern can arise when considering seismic ruptures. This can lead to an increase in reactivity due to increase of pebble density and

increase of the distance to the control rods. Therefore this has to be assessed and proven to have no large influence [33]. This can be of considerable importance when used on board of a vessel but can be considered in the reactor design.

The proliferation risk for HTGR or VHTR is lowered firstly due to the properties of the fuel itself. Low enriched uranium is most commonly used which means a lot of reprocessing is needed for a very small amount of weapon usable uranium. This is combined with the difficulty to reprocess the highly irradiated graphite that encapsulates all fuel kernels. Finally the large burn-up values when compared to PWRs decrease the amount of waste material which in turn increases the proliferation resistance. When thorium would be used instead of uranium this resistance will increase even further [115].

1.4.5. Technology Readiness Level (TRL)

The TRL is where the HTGR and VHTR diverge the most. Most test reactors and prototype reactors are of the HTGR type so these are in a TRL of around 7-8 because full commercial deployment is not yet reality [136] [52]. When looking at technology roadmaps from the GEN IV international forum full demonstration of the VHTR is planned around 2030 and is currently in the performance phase which means prototypes are being optimised. This corresponds to a TRL of around 6-7 which is lower than the HTGR [52]. Reasons for this lower TRL could be the higher operating temperatures that pose a challenge to materials and the still developing HTGR as they are closely related [71].

1.4.6. Power Generation

Output temperatures vary from over 950 °C to around 750 °C. The latter is identified with HTGR and are more common because of their higher TRL as discussed before, the former is associated with the VHTR design [74]. The high operating temperature has a resulting higher electrical efficiency that was also identified with the MSR. Thermal power output for land-based reactor of this design over the last 50 years range from 10 MW_{th} to values of 842 MW_{th} [136]. Application that fall under de SMR definition start with a thermal power of 10 MW. Despite the high output temperature the reactor design still needs a pressurised reactor vessel because of the use of helium. Contrary to the MSR the fuel and coolant are not mixed together [74].

1.5. Load following

1.5.1. Reactor poisoning

Before discussing the possible load following characteristics of the MSR and the VHTR it is important to understand which factors could limit their load range. One of the most important factors is reactor poisoning which is the building up of the fission products ¹³⁵Xe and ¹⁴⁹Sm. These are caused by the decay of fission products Iodine and tellurium. Xe and Sm both have a large neutron cross-section which means they will absorb a large amount of neutrons and thereby less neutrons remain to obtain a fission reaction [156]. This can result in Xenon dead time whereby the reactor can not be started up again because of a too low level in reactivity as displayed on figure 1.7 for a reactor with 20% excess reactivity [140].

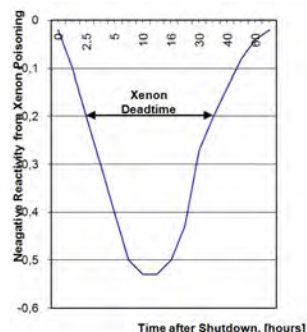


Figure 1.7: Xenon deadtime - 20% excess reactivity [140]

To better comprehend this phenomena two cases will be discussed namely how these fission products

build up for power changes and how they behave for a reactor shutdown. Because Sm has a relatively small neutron cross-section compared to Xe, these cases will be discussed for Xe alone. Nevertheless in a full reactor analysis, Sm build-up should also be taken into account [40].

1.5.1.1 Xenon response to reactor power change

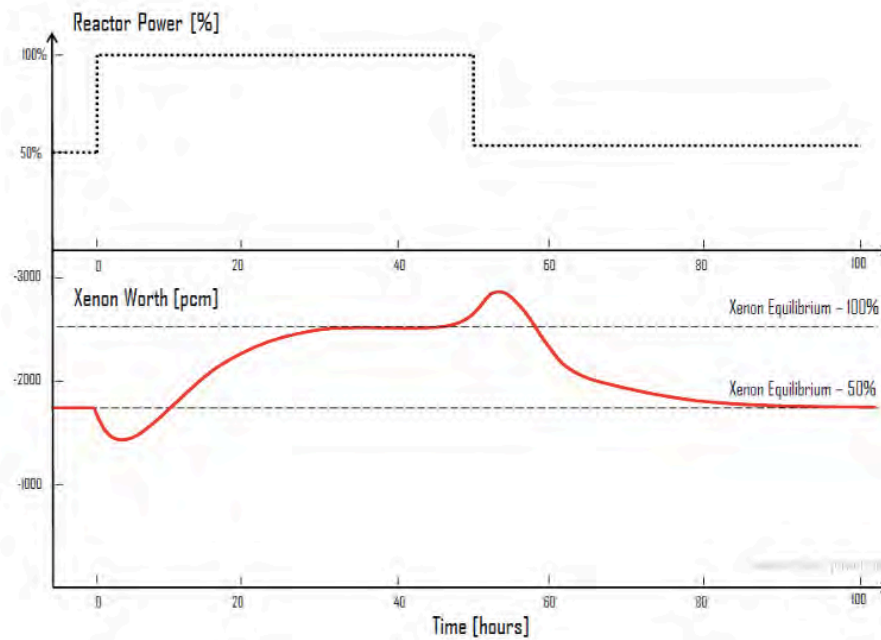


Figure 1.8: Xenon response to reactor power change [138]

On figure 1.8 the concentration of Xe is shown for a varying power level between 50% - 100%. When a reactor is operating for a certain period of time the Xe level will reach an equilibrium this is because the same amount Xe is being burned by neutron absorption and created by decay of Iodine. If the reactor power or neutron flux is then increased the Xe level will first decrease because more Xe is being burned than created due to the increased reactivity [40]. Afterwards a delayed increase is seen that takes time due to Xe being a decay product of Iodine which has a half-life of 6,6 hours so xenon is not instantly formed. The xenon equilibrium is satisfied again after a certain period of time which depends on reactor type and power interval[138]. Changing power levels does not pose a high danger to reactor operation with regard to xenon concentration. As long as the reactor keeps running at an established lower load limit the xenon equilibrium will be reached. This can pose a problem when the reactor core is near his end life if almost all fuel is depleted [40].

To summarize changing the reactor power can be done with regard to xenon production but time is needed to reach a Xe equilibrium level. This is one of the reasons why most land-based reactors can only scale down or up two times a day [121].

1.5.1.2 Xenon response to reactor shutdown

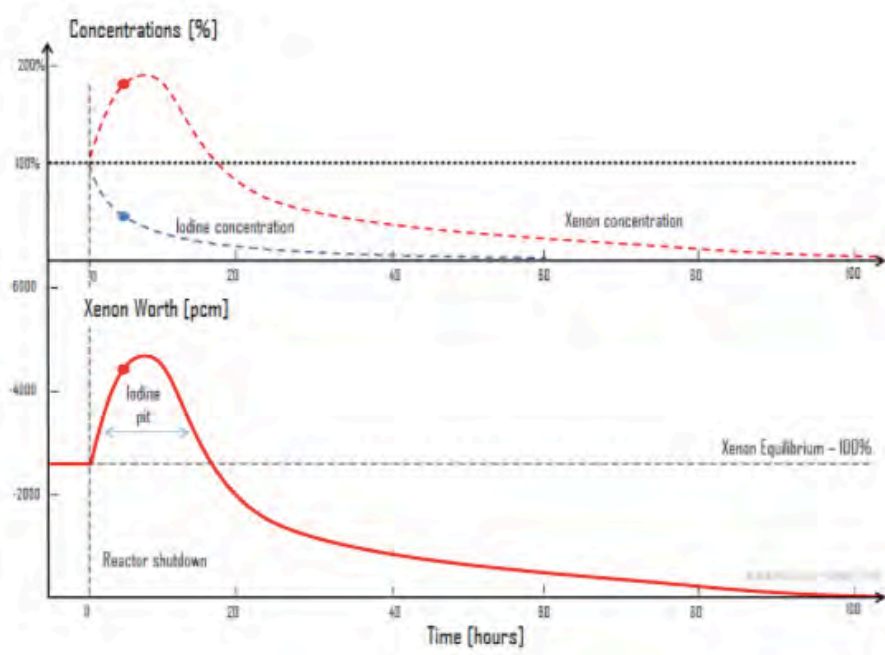


Figure 1.9: Xenon response to reactor shutdown [138]

Most reactors are more sensitive to Xe production when the reactor is suddenly shutdown. The two main factors deciding the severity of the Xe build up are the current power level and the rate at which the shutdown is performed [40]. As can be seen on figure 1.9 the Xe concentration first goes up because the neutron flux/power level is equal to zero so the Xe is not burned away anymore by neutron absorption. The only process that lowers the Xe concentration is decay but the iodine that is present in the core after shutdown will still decay in Xe which explains the increase in Xe concentration [138]. This is due to xenon having a longer half life than iodine. The large increase in Xe concentration and resulting negative reactivity can have as a result that the reactor is not able to start up again for a longer period of time. This can be mitigated by slowly shutting down the reactor instead of momentarily this gives time to burn to xenon that is still present inside the reactor [40].

1.5.2. Molten salt reactor

MSR have a good theoretical quality regarding load-following this is due to the strong negative temperature coefficient of the molten salt as discussed in the safety section. When extra power is needed from the MSR the reactivity will increase because of a drop in temperature from the molten salt inside the reactor core. If the power demand drops the temperature of the molten salt will rise which will decrease the reactivity and thus decreases the nominal power [26]. This is explained by the influence of the negative temperature coefficient. The temperature of the molten salt will reach a stable state after increase or decrease because an increase or decrease in reactivity has an adverse effect on the molten salt core temperature as can be seen on figure 1.10. The temperature of the coolant can be controlled by controlling the pumping speed of the molten salt [34].

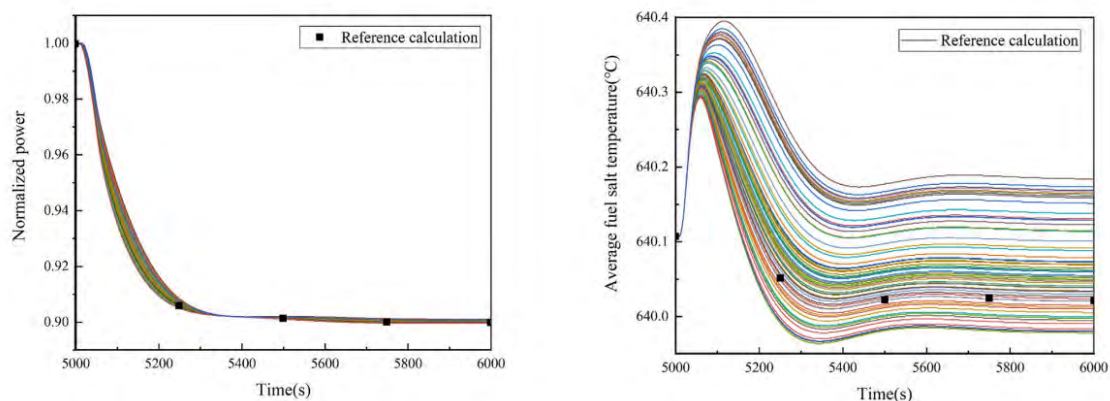


Figure 1.10: Load following of a MSR [34]

An increase in the fuel salt temperature results in a decrease of nominal power of the reactor as indicated above with uncertainty band. Where the nominal power of the complete plant is taken into account and a load response of about 5%/min is obtained [34]. In theory the load-following capabilities of the MSR are even better when only the response of the fuel salt is taken into account and no other components of the plant. A. Laureau et al. researched this case for a MSR with a nominal power of 3 GW and came to an increase of power from 1.5 GW to 3 GW in only 5 seconds. To be able to convert this increase in load variability to a complete nuclear plant an assessment of all components must be carried out which is not possible with the current TRL of the MSR [94].

The xenon poisoning as discussed before is mitigated by the MSR because of its ability to dissolve ^{135}Xe . This is done by two principles, in a MSR with moderator there exists a porous gas space inside the graphite together with circulating voids in the fuel salt itself where Xe is free to alloy. The two prescribed principles can be named as graphite and bubble migration respectively [139].

As mentioned earlier it is a big challenge to find the correct core material for a MSR because of the corrosive nature of the salt. Combining this challenge with frequent heat/temperature changes would cause swelling/shrinking of the core material and thus posing more material challenges that are not yet solved at present [2]. For example temperature transients in the graphite moderator can result in cracking which lowers the thermal conductivity and thereby the effectiveness of the moderator [40]. This should be considered when the load cycles are selected.

As the improved load following capability of the MSR is only theoretical it is best to rely on operating reactor designs which will be discussed in 1.5.4.

1.5.3. Very high temperature reactor

For the VHTR load following is more of a challenge because the fuel remains solid inside the reactor core which results in the build up of xenon and possible danger of reactor poisoning which was discussed before. Also not much studies have been conducted for the load-following of high or very high temperature gas cooled reactors as concluded by [184]. Research that was conducted on this topic identified a theoretical load following capability between 40% - 100% along with a 5%/min ramp-up speed. Therefore the load following capability of these types of reactors can best be identified with operational reactors which will be addressed in the following section.

1.5.4. Conclusion load-following

As stated earlier the practical load-following capability of the MSR and VHTR is not developed well enough to make strong assumptions on their possible better capabilities than conventional nuclear power plants. This is largely due to their lower TRL which are stated in dedicated sections. Therefore operating and existing nuclear reactors are taken as a conservative estimate especially for the MSR case because of its lower TRL.

A case can be made for SMRs as they have a smaller thermal power output than large nuclear reactors

based on land. Therefore their power control could be easier and less safety risks could be involved [47]. A recent study (2020) investigated the technical potential of PWR to preform profile operation and load following. Where profile operation is seen as periodic load changes to create a profile which varies across the day. This is typically two times over a 24h period, three typical profiles are depicted on figure 1.11.

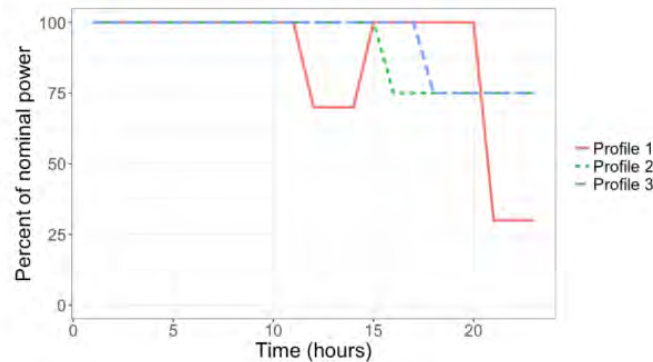


Figure 1.11: Typical profile operations [132]

The amount of power range is a function of time as it depends on the fuel cycle. During the first 65% of the fuel cycle a controllable output between 25% - 100% is feasible. After this the range is reduced to 25% - 80%. This is the case for PWR because boron concentrations inside the primary coolant, which act as a chemical reactivity controller, run low [47]. The ramp-up rate is defined per power interval ranging from 10%/min at 80-100%/min to 2%/min for 20-100%/min. Where a minimal power output of 20-30% is depicted [132]. The same value is found in a study concerning the power generation in Germany by Pressurised Water Reactors (PWRs). There the load following down to 50 % can be conducted at a rate of 5%/min and even 10%/min when limited to 80% of the maximal produced power. The same study states that a KWU-type of PWR where the operating manual is not publicly accessible can even have load changes over a 80% range, as a result the load response is decreased to 3%/min [88].

Thus for now a load variability of 2-5%/min is assumed as this is a safe estimate when regarding other reactor designs. As for the minimal reactor load 50% would be a conservative estimate. Taking the previous mentioned examples of PWRs into account a more wide operating range of 80% of the nominal load is established which means the load can change between 20% and 100%. A daily change of two times per day is assumed for the reactor point of view. Further load variability can be obtained by the use of heat rejection capabilities or batteries. This rather restricted load variability can be linked with a rather constant operating profile of current container vessels but also bulk carriers or tankers can be seen as possible candidates. To obtain sufficient depth in the design proces container ships are the main focus but analogies to other ship designs are possible. Findings concerning the load following and ramp-up rate are summarized below.

Feature	Value
Min Load	20%
Max Load	100%
Ramp-up/down rate	3-5%/min
Number of cycles in 24h	2
Burn-up rate	90 GWd/tHM

Table 1.1: Load following characteristics

1.6. Cost description

Because most literature combine cost estimations for SMR a combined cost description for the MSR and VHTR will be made. When comparing conventional reactors with MSR they will be cheaper to build according to the molten salt reactor market report 2022-2032. They state a MSR will be around half the cost per megawatt when compared to a super-advanced light water reactor. This report offers an extensive review of MSR technologies, applications and acquainted costs but is not publicly available. This shows however that there is a large interest in the technology in different industries where the shipping industry is not left out.

In the following the cost of a nuclear reactor will be divided into four groups namely capital or overnight cost, operation and maintenance cost (O&M), fuel cost and decommissioning costs. In order to have a better representative a lower and upper bound where applicable will be used. In order to use the acquired data all costs will be expressed in \$/kW.

1.6.1. Capital costs

Capital cost of a nuclear power plant is one of the largest when compared to other energy sources like coal-fired or gas plants. They include cost of site preparation, construction, manufacture, commissioning and financing the plant [14]. Capital costs are subdivided by the World Nuclear Association which is recently updated (august 2022) in following percentages where the site development and civil works can be disregarded in a marine application because these are not applicable.

Design, architecture, engineering and licensing	5%
Project engineering, procurement and construction management	7%
Construction and installation works:	
Nuclear island	28%
Conventional island	15%
Balance of plant	18%
Site development and civil works	20%
Transportation	2%
Commissioning and first fuel loading	5%
Total	100%

Figure 1.12: Capital cost breakdown [14]

A study on the economic evaluation of small modular reactors compared large reactors (above 300 MW_{th}) with SMR on a basis of four cases. These cases were modelled to comprehend the impact of going from a FOAK as is the case for large reactors to a NOAK which is applicable for SMR. A breakdown of the total capital cost per case is given on figure 1.13. For case 1 all costs of a large reactor were scaled down on a power basis to be applicable for SMR. Going from case 1 to case 4 discount rates were applied in order to account for the modular design. In this study capital costs were subdivided in direct, indirect, owners & contingency and factory costs [174]. Within the direct cost are mainly all reactor and balance of plant costs, indirect cost cover engineering for example, owners & contingency include management costs and costs that are not known and factory costs are costs for building the factory that produces the reactors. Except for owners & contingency costs these can all be related to the subdivision on 1.12 [14]. An overview of the different cases is given on figure 1.13 where the capital expenses are expressed per kW_e. The factory costs could be neglected in this report because the SMR would be bought after already been manufactured but they don't seem to play a significant role in the total capital expense. From figure 1.13 an initial upper bound of \$9,000/kW_e can be derived this is for the FOAK case where the costs of the SMR are scaled with a large reactor. A lower limit of \$4,550/kW_e for a NOAK is read from the graph below. In this case cost reduction were applied with respect to case 1, these consisted out of the following contributions[174]:

- Case 2
 - Direct costs (15%)
 - Indirect costs (50%)

- Case 3
 - Indirect costs (40%)
 - Contingency & owner's costs (40%)
- Case 4
 - Direct costs (20%)
 - indirect costs (50%)
 - Contingency & owner's costs (50%)

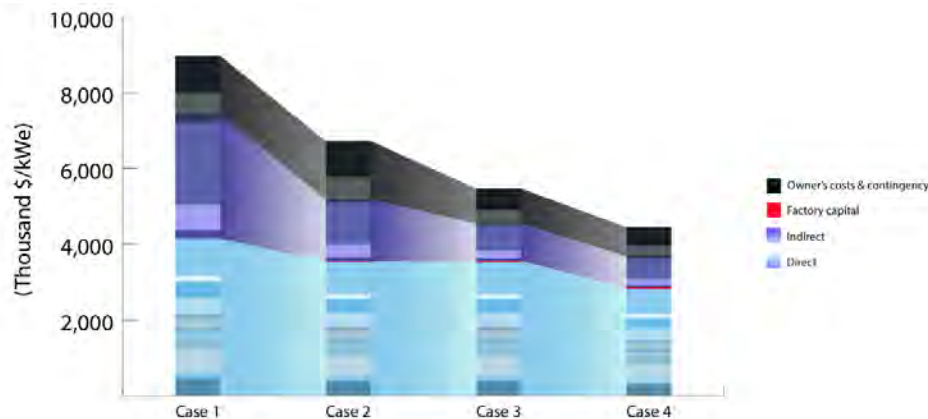


Figure 1.13: Capital cost breakdown for different production cases [174]

This study shows the possible cost reduction for SMR and gives a good estimate of the capital expenses [174]. Apart from cost reduction a smaller reactor design can also increase costs. A lower power density in the case of the VHTR can increase the cost per MW or specialized processing of the fuel in the case of molten salt [45]. This has however the benefit of enhancing the neutron life quality which makes the theoretical application of a full thorium cycle possible [2]. The increase in cost for smaller power generation is shown in a cost-benefit study for remote mining in the Canadian North where a MSR of 6.7 MW_e is used for electricity generation and a capital cost is estimated at \$14,925/kW_e which is a big increase when compared with the previous study. This power application is too small for the required installed power estimated in section 1.2 but is given to show the increase in cost for smaller power applications.

The concept of NOAK for SMR was also used in a study where 12 different companies participated with all different advanced reactor concepts but not limited to SMR. Here an upper limit of \$5,855/kW_e and lower limit of \$2,053/kW_e was established for the capital cost. Here the capital costs consisted out of direct, indirect, financing, supplementary, pre-construction and owner's costs [45]. So they are a good comparison with the previously found material. In addition a study from 2021 carried out by the department of nuclear science and engineering USA did a similar research compared to [174]. Here a detailed bottom-up approach was carried out to compare the capital expenses of two large PWR with two SMR designs. The PWR's had an output of 1,144 MW_e and 1,400 MW_e. The SMRs consisted out of a multi-module model of 12x57 MW_e separate SMRs and a SMR of 160 MW_e. For the PWR's a capital cost of respectively \$4,238/kW_e and \$5,337/kW_e was found with a similar definition of capital costs as defined above. The main difference between these two values is the extra investment of passive and active safety systems respectively. The SMRs had an average capital cost of \$4,059/kW_e for a multi-module plant of 685 MW_e [158]. Another study evaluated the economic viability of light water small modular reactors developed by Nuscale. They developed the first and only SMR that received design approval from the Nuclear Regulatory Commission (NRC). The studied power plant consisted out of 12 SMRs with an individual 60 MW_e output giving a total of 720 MW_e. As an estimation the total capital cost for the whole power plant was divided by the number of SMRs and the power output which gave a total of \$3,610/kW_e [25]. Another example for SMR with the focus on LWR is given by C.A. Lloyd et

al. here the reduction in capital cost is examined by applying several degrees of modularisation where the maximum degree of modularisation obtains a almost 50% decrease in capital cost per kW_e as is observed on figure 1.14. The final value found for a SMR of 300 MW_e is $\$5,720/\text{kW}_e$ here 66% of the site costs are moved to a factory here it is also seen that for smaller power application the specific capital cost increases as depicted on figure 1.14 [96].

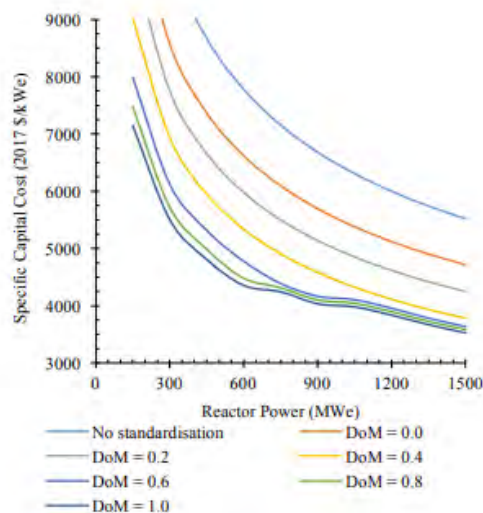


Figure 1.14: Specific capital cost for different degrees of modularisation [96]

A final reviewed study did a techno-economic analysis of a 45 MW_e PWR where the capital cost that only apply to the vendor are estimated by 16 experts in the nuclear industry. Almost all experts explained that the smaller the power output of a SMR becomes the greater the overnight costs will due to the increased cost of the pressure vessel and comparable components. 11 experts gave a median cost between $\$2,000/\text{kW}_e$ and $\$9,200/\text{kW}_e$ the remaining 5 experts argued that the capital costs lied even higher for such small power applications. The values they stated had a lower limit of $\$9,200/\text{kW}$ and a upper limit of $\$25,500/\text{kW}_e$ [7]. The argument that for smaller power output SMR become more expensive in specific capital expense is also an argument to opt for a container vessel because of their large installed power.

To be able to compare different reactor concepts on the aspect of capital cost it is needed to convert $\$/\text{kW}_e$ to $\$/\text{kW}_{th}$ with the use of the thermal efficiency as depicted in table 1.2 below for the studied sources.

Source	$\$/\text{kW}_e$	thermal efficiency [%]	$\$/\text{kW}_{th}$	SMR type	Power [MW_e]
11 experts [7]	2,000-9,200	28.1	7,117-32,740	PWR	45
5 experts [7]	9,200-25,500	28.1	32,740-90,747	PWR	45
[158]	5,230	31.3	16,708	PWR	160
[174]	4,790	31.5	15,205	PWR	225
[45]	2,053-5,855	32.1	6,396-18,240	divers	<300 MW_e
[96]	5,720	33.0*	17,333	PWR	300
[96]	5,000	33.0*	15,152	PWR	400
[96]	4,500	33.0*	13,636	PWR	500
[96]	4,225	33.0*	12,803	PWR	600
[158]	4,059	31.3	12,968	PWR	685
[25]	3,611	33*	10,941	PWR	720

Table 1.2: Capital cost per kW (efficiencies marked with '*' are estimates based on [156] because the used thermal efficiency was not found in the publication)

As can be seen from the table above almost all reactors are of the PWR type. This is because of their

higher TRL and very limited data concerning the specific capital cost of the MSR or VHTR. Its assumed to be a fair estimation to take these capital expenses as an initial estimate. If further detailed cost breakdown would become available it should be updated. For the gathered material in table 1.2 the reduction of 20% of site development and civil works is not taken into account that is included in the capital cost of a reactor as depicted in figure 1.12. This 20% can be taken as an additional cost for the extra components needed in a marine propulsion drive train like shaft an propeller expenses.

Plotting the values of table 1.2 gave the scatter plot on figure 1.15a. The power starts at 45 MW because this is seen as a minimal power level for the considered application. For smaller power levels development of the U-battery which is a HTGR can be considered with an electric output of 4 MW_e. Their estimate for the capital cost lies between \$16,500/kW_e and 28,750\$/kW_e. It can be seen that the data point for 45 MW_e with a specific capital cost of 25,500 \$/kW_e lies far outside the range of the other data points along with the lower limit for the 45 MW_e equal to \$2,000/kW_e. In order to make a reasonable estimated trend line for the capital expenses these data points are disregarded because the former is deemed to be too pessimistic and the latter to be too optimistic based upon the gathered literature. Therefore the more conservative 9,200 \$/kW_e is selected for lower powers. Using these plotted data points a fluent trend line is constructed with formula $y = 7326.7e^{-0.001x}$ as can be seen on figure 1.15b.

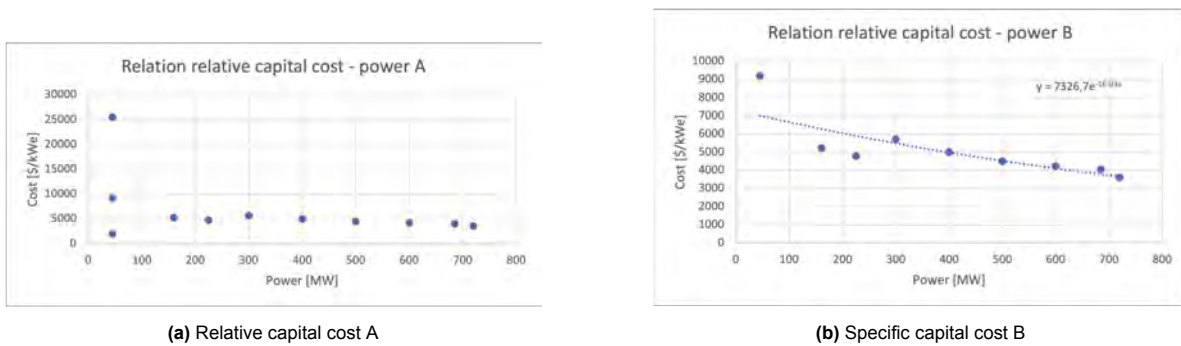


Figure 1.15: Capital cost trend line A

The trend line on figure 1.15b is taken as the median for the relative cost estimation, because of the large variation in relative cost for lower powers around 45 MW_e an uncertainty band of 25% at the upper and lower side is taken. This percentage is conventionally used in cost estimations [13]. Hereafter it is possible to construct trend lines for the absolute cost with the same uncertainty band. The end result is seen on figure 1.16 where the orange trend line is the median. The previously mentioned relative capital cost for the smaller power application of the Ubattery confirms the formed trend line in that way that for smaller powers the relative capital cost will rise [22]. This point is not plotted in the trend lines below because the power output is considered to small. For vessels with smaller output powers this reactor type could be considered.

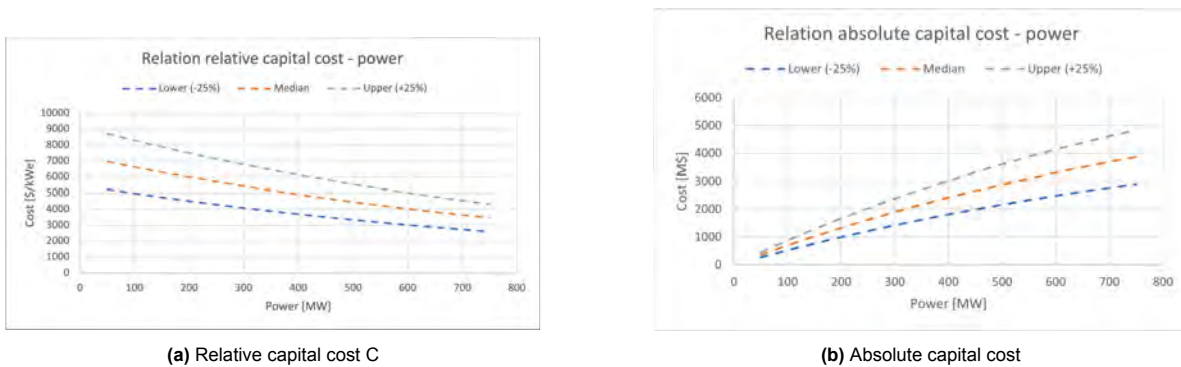


Figure 1.16: Capital cost trend lines with uncertainty band (25%)

Because of the wide range of the capital cost and the still uncertain influence on the economic speed. A range from 3000-9000 \$/kW is assumed to be used for further study. This to determine the exact influence of the reactor capital cost and take into account the high uncertainty that still remains.

1.6.2. O&M costs

Operating and maintenance costs are the costs to maintain and operate a nuclear power plant. They consists of all non-fuel costs which are for example plant staffing, purchased services, replaceable materials and equipment. Further these can be divided into fixed and variable costs where fixed (plant staffing) are considered the biggest. These will be considered as extra costs for maintaining the reactor plant by specialists [113].

A first estimate for the O&M is given by [45] where 12 different companies participated with all different advanced reactor concepts but not limited to SMR as discussed for the capital costs. Here the O&M for conventional nuclear was estimated at a minimum of \$14/MWh, an average of \$23/MWh and a maximum of \$30/MWh a subdivision between fixed and variable costs is not given [45]. A study on the cost and performance characteristics of new generating technologies by the US depicts a variable O&M cost of \$3.14/MWh and a fixed cost of \$99.43/kW-year this is for a SMR of 600 MW. The National Renewable Energy Laboratory (NREL) made a prediction of the fixed an variable O&M costs for a SMR of 600 MW up until 2050 where they respectively are kept constant to \$114/kW-year and \$3.6/MWh. This was also based on the same annual energy report used by the US but with an approximate 20% increase in fixed costs to account for inflation [10]. The same study that looked at four different scenarios to compare FOAK with NOAK as discussed before also did an estimation on the O&M costs, in this case there was again no subdivision between fixed and variable costs. Their data is based on Boldan and Sabharwal (2014) and came to a total of \$18/MWh which include maintenance of power plants, employees salaries and insurance [174]. If we look at the example of the US study the fixed an variable O&M costs are respectively 78.3% and 21.7%. This relation can be used on the other data found resulting in the table 1.3. The total estimate is calculated by taking the average of all values found. Both the max and min value of [45] are taken into account because in this study multiple modular reactors are taken into account so it is beneficial to not disregard them.

Source	Fixed O&M [\$/kW-year]	Variable O&M [\$/MWh]
MIN[45]	96.01	3.04
AVG[45]	157.77	4.991
MAX[45]	205.77	6.51
[10]	99.43	3.14
[10]	114	2.84
[174]	123.42	3.91
Total average estimate	132.73	4.07

Table 1.3: O&M costs estimates based upon [45],[10],[174]

1.6.3. Fuel costs

To determine the total fuel cost three central pillars are needed. The raw material price, the amount of fuel required and the cost that comes with the enrichment process [71]. The amount of fuel required depends mainly on the layout of the propulsion line and operational profile these will be discussed in the research section. In this section an overview of the fuel cost from mining up until disposal of nuclear waste will be given in order to have a total price per kg enriched Uranium. As a comparison the price for thorium will also be evaluated.

The World Nuclear Association (WNA) divides the front end fuel cycle costs into four categories namely the uranium cost, the conversion cost, the enrichment cost and the fuel fabrication cost. These are respectively accountable for 51%, 7%, 24% and 18%. Therefore the uranium cost expressed in \$/kg and the enrichment cost expressed in \$/SWU will be examined in further detail. The conversion and fuel fabrication costs are assumed to be \$16/kg (kg mined) and \$300/kg (kg end product) respectively as depicted by the WNA. The back end fuel cycle consists out of the encapsulation and disposal of spent fuel or nuclear waste, for this an estimate from literature of \$405 per kg of enriched uranium is used

[14] [171].

1.6.3.1 Cost Uranium U₃O₈

Uranium is defined as a heavy material which has been responsible for concentrated energy production for over 60 years. Uranium ore is mined in an open-pit or underground, after being mined it is pulverized and treated to extract the usable uranium. Uranium is different than other commodities like gold, nickel or copper because there is no formal exchange to trade uranium. In fact this is done by direct negotiation between buyers and sellers. Therefore the fuel can be sold under the spot market price and this is typically done for one delivery or a long-term contract that can range between 2-10 years[185]. This long-term contracts represent about 90% of the uranium trade while only 10% accounts for the spot market. Another distinct feature is the independence uranium has over other commodity markets like oil or coal as stated by Kryzia etal. [89].

The price of uranium went down in May 2011 due to the Fukushima nuclear plant meltdown and stayed low until 2021. Here a nine-year high of \$48/pound was observed in September. This was due to a uranium holding company called Sprott's acquisition of Uranium Participation Corporation who purchased 400,000 pounds of uranium to found a new trust. Along with the political instability in Kazakhstan around that time there was an upward trend in uranium prices [69]. At the end of 2021 the price had stabilized around \$45/pound but around the middle of April it hit \$64.5/pound as a consequence of the Ukraine war. At the time of writing¹ the price of uranium has eased to \$48.15/pound [42]. Kryzia etal. also did a prediction of uranium prices based on probable demand and supply of uranium in the future. Their expected values are summarized in table 1.4 an figure 1.17 with a probability distribution.

Year	2020	2025	2030	2035	2040	2045	2050
Expected value	91	90	91	97	108	118	130

Table 1.4: Prognosis for Uranium cost expressed in \$/kg [89]

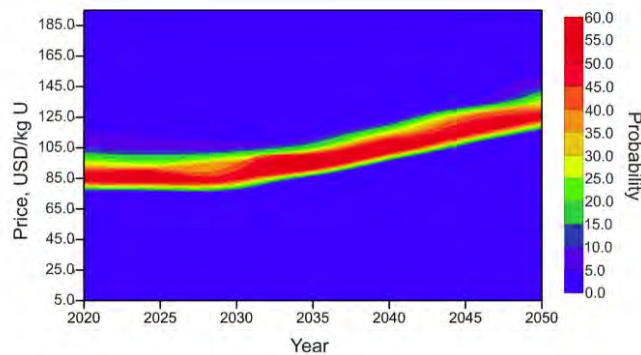


Figure 1.17: Uranium Price probability until 2050 [89]

A current spot price of \$106.15/kg is found which lies within the probability band of the showed study. Nevertheless the uncertainty spread is only 5% according to Kryzia etal. [42]. This is due to the model not taking into account extreme short-term fluctuations as this is very hard to predict. Other studies like the one of Wallet investor's predicts \$91/kg by December 2023 and \$97.41/kg in August 2025 which lie well within the probability band proposed by Kryzia etal. [185]. Therefore it is assumed the expected values of Kryzia etal. can be used as a median for the uranium cost in \$/kg. This raw uranium cost must be multiplied with the feed factor that indicates the amount of raw uranium needed to produce one kg of enriched uranium. This way the total cost of raw uranium can be determined.

¹December 2022

1.6.3.2 Enrichment cost

As discussed before enrichment is necessary to produce an effective nuclear fuel that can be used inside a reactor core to start a fission reaction and produce the needed energy. In order to do this the percentage of ^{235}U must be increased relative to the ^{238}U content. This is done via the enrichment process whereby natural uranium is converted into its gaseous form uranium hexafluoride. The gasification is done because of the different chemical and physical properties of ^{235}U and ^{238}U which are easily manipulated in gaseous form [156]. Three methods for this enrichment process exist namely gaseous diffusion, gas centrifuge and laser isotope separation. Today enrichment by the use of a centrifuge is most commonly used because it is more energy efficient and compact as gaseous diffusion. Laser isotope separation is predicted to be even more energy efficient but is still in development. Using the centrifugal method the uranium hexafluoride is brought into an evacuated cylinder which is rotated at a speed around 60,000 rpm, the more heavy ^{238}U particles are collected near the outer walls. The ^{235}U is collected near the central axis where it is drawn off [44].

The enrichment cost is expressed in SWU which displays the amount of work needed to enrich uranium to a certain level and depends on the enrichment level itself and the feed factor of raw uranium. An example calculation of the SWU factor for 1 kg of enriched uranium is elaborated in appendix A.1.2 based on Tsoufanidas et al. [169]. The cost per SWU is not a constant one but varies similarly to the uranium cost per kg. Elaboration on this trend can be found in appendix A.1.1. Using the data from appendix A.1.1 the cost of SWU and Uranium is compared from the Fukushima incident up until present day which can be observed on figure 1.18 from this it can be seen that both values follow the same trend. Therefore it is assumed that the price per SWU is to follow the same trend as the price per kg uranium for the foreseeable future as depicted on figure 1.17 which shows an increasing price.

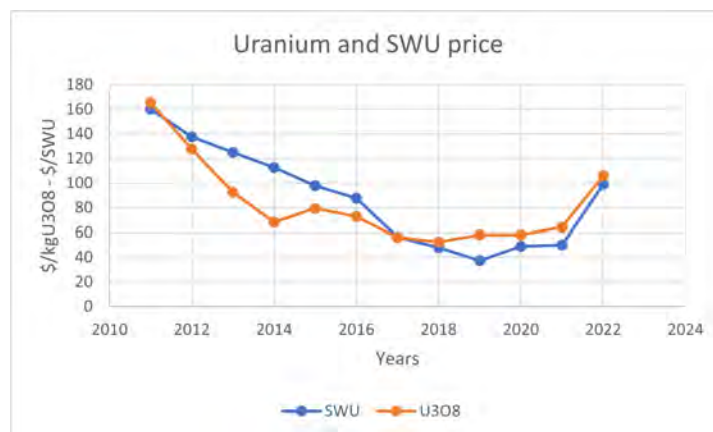


Figure 1.18: Comparison U3O8 vs SWU price based on [42] & [143]

1.6.3.3 Fuel cost estimation

Using the gathered information it is now possible to make an estimation of the fuel cost up until 2050 with the assumption that conversion and fuel fabrication cost stay constant as stated before. For the SWU an initial median value of 80 \$/SWU is chosen as this is the estimated average from figure A.1a. For the upper and lower limit a bandwidth of 50% is chosen as this was the same for the capital cost. The cost of Uranium is taken from table 1.4 with the same uncertainty band as discussed above. The fuel cost is then calculated for intervals of five years by following the study of Kryzia et al. by giving an upper, median and lower limit cost [89]. The full calculation can be found in appendix A.1.2. The result is seen in tables 1.5 & 1.6 which are expressed in \$/kg enriched uranium. These values are calculated for 5% and 20% enrichment because normal power reactors operating today have a maximum level of enrichment of 5% but especially for smaller and modular reactor designs a higher enrichment is becoming of interest. This can be up to 20% for advanced power reactors fuels that could be used in the MSR or VHTR [15]. In addition the cost for spent fuel is also added.

Year	2020	2025	2030	2035	2040	2045	2050
Upper limit	2,809	2,786	2,809	2,946	3,174	3,403	3,698
Median	2,418	2,400	2,418	2,528	2,711	2,893	3,130
Lower limit	2,027	2,014	2,027	2,110	2,247	2,384	2,561

Table 1.5: Estimated fuel cost Uranium 5% enrichment - general [\$/kg]

Year	2020	2025	2030	2035	2040	2045	2050
Upper limit	10,307	10,202	10,307	10,951	11,988	13,045	14,426
Median	8,511	8,426	8,511	9,018	9,856	10,701	11,401
Lower limit	6,714	6,651	6,714	7,095	7,723	8,357	9,186

Table 1.6: Estimated fuel cost Uranium 20% enrichment - general [\$/kg]

To put the above values in perspective with a two-stroke marine diesel variant the specific fuel consumption is used in optimal working points. For conventional marine diesel engines this value lies around 170 g/kWh. If the same value is calculated for a nuclear propulsion with turbine assuming an efficiency of 33% and a conservative burn-up value of 90 Gwd/tHM a specific fuel consumption of 0.0014 g/kWh is found. Assuming a full electric lay-out is chosen which leaves the option open for the use of battery power and offers a less complex gearbox arrangement as described by [71]. The efficiencies of the shaft (0.99), gearbox (0.99), electromotor (0.97), frequency converter (0.99) and switchboard (0.97) should be taken into account. For the diesel variant only a shaft efficiency needs to be taken into account because of a direct drive set-up. Both variants are thus compared up until the shaft. For the nuclear option this results in \$0.0144/kWh (20% enrichment upper limit 2020) and for the marine diesel option using the current IFO 380 price of \$888/t this results in \$0.157/kWh. This shows a factor 10 difference in fuel costs where for the nuclear option the higher limit is taken.

1.6.3.4 Comparison thorium

As discussed before thorium is a viable replacement for the uranium fuel cycle because of its abundant character, high proliferation resistance and production of minor actinides which reduces the time period of harmful radioactivity to around 300 years instead of thousand of years for the uranium fuel cycle [64]. According to a study of ORNL from 1965 the amount of thorium that was known in those days was capable of delivering 200 million kW for over 40 years with a burn-up of 30 GWd/tHM. This was a greater deliverer of electricity than the electrical industry of the US in that time period.

As previously stated Thorium does not need to be enriched like Uranium but since Thorium is a fertile material it still needs fissile material to start the chain reaction. This can be done through the use of kickstarter fuel in the form of fissile material. The Copenhagen atomics waste burner uses spent nuclear fuel for this purpose in the form of $F^7LiThPu$ [162]. The cost of Thorium as raw material is at the time of writing² \$30/kg [35]. The enrichment cost will be equal to zero and as an assumption the conversion and fuel fabrication cost can be regarded equal to the ones of uranium. When only these factors are taken into account a total thorium fuel cost of \$346/kg is found which is an immense reduction when compared to the values in tables 1.5 and 1.6. A less optimistic approach is followed by the national nuclear laboratory in the UK. For a once-through thorium cycle the thorium will only deliver a fraction of the uranium needed to sustain the chain reaction to convert ^{232}Th to ^{233}U . Therefore the left-over uranium will need to be enriched to a very high level so that compared to the enrichment cost of the uranium fuel cycle cost savings will be small. When a closed fuel cycle is considered where the ^{233}U is recycled by a reprocessing plant the costs of the initial uranium ore and enrichment could be overcome. However a large investment in the thorium reprocessing and fuel fabrication plant will be needed. This is seen as to be not economically beneficial over the uranium fuel cycle by the national nuclear laboratory [63]. A comparison between the uranium and thorium fuel cycle was also carried out by the IAEA where it was concluded that for the once-through cycle the fuel costs indeed increase significantly because of the sub criticality of Thorium which is disadvantageous for the burn-up and the required enrichment level of the fissile starter fuel but not for the fuel cost [78].

²December 2022

Taking the considerations found in literature two ways can be taken. The optimistic one which is also taken by Copenhagen atomics wasteburner were thorium is seen as a much cheaper fuel when compared to uranium. This would be closely related to the calculated value of \$346/kg. Aside this a conservative approach can be taken to assume that the cost of thorium is equal to the enriched uranium price. In both cases thorium still possesses beneficial properties over uranium in terms of abundance, radioactive waste production and proliferation resistance as discussed in section 1.1.3.

1.6.4. Decommissioning costs

Decommissioning costs include planning of the decommissioning up until the actual removal of the complete plant and waste materials. Earlier nuclear power plants were designed to operate for around 30 years, now more advanced reactor designs including the SMR are being designed for an operating life between 40 to 75 years. Nevertheless at the end of these years the reactor needs to be decommissioned, cleaned up and demolished. The International Atomic Energy Agency defines three options for decommissioning namely immediate dismantling, safe enclosure or entombment [180]. Decommissioning is a process that takes time, worldwide over 200 commercial, experimental or prototype and 500 research reactors are taken out of operation but only 25 are fully dismantled [180].

The OECD nuclear energy agency published a survey in 2016 regarding the shutdown of nuclear power plants ranging from power output of 12 MW_e to 1,410 MW_e. They estimated the decommission cost of a 1,100 MW_e between \$460/kW_e and \$730/kW_e. A smaller nuclear power plant around 500 MW_e was estimated between \$1,070/kW_e and \$1,220/kW_e for a full decommission [120]. Another study from 1990 did a survey of decommissioning costs for smaller nuclear power plants ranging from 72 MW_e to 250 MW_e. The average cost per kW_e also depended on the country where the decommissioning took place, a lower limit for the USA was established at 114 \$/kW_e and an upper limit for the UK at 254 \$/kW_e [19].

Ships like the NS savannah, Mutsu and Otto Han were also dismantled along with numerous submarines. The decommissioning cost for the NS savannah was estimated at \$77 million expressed in 2008 dollars. This included the waste removal activity dependent costs, period dependent costs and collateral and special item costs. Noteworthy is that over 30% of the decommissioning cost was attributed to waste removal [152]. For the NS Savannah this resulted in a decommissioning cost per MW_e of \$3.15 million or \$3153/kW_e. For the decommissioning of submarines a report intended to reduce these cost was published in 1992. The decommissioning process of a submarine consist out of three stage namely inactivating and defueling the submarine, removing and disposing of the empty reactor compartment and recycling of the submarine hull. These stages could also be identified for a surface ship, for the NS Mutsu the decommissioning procedure is depicted below, all stages that were discussed for a submarine reappear in this procedure [8].

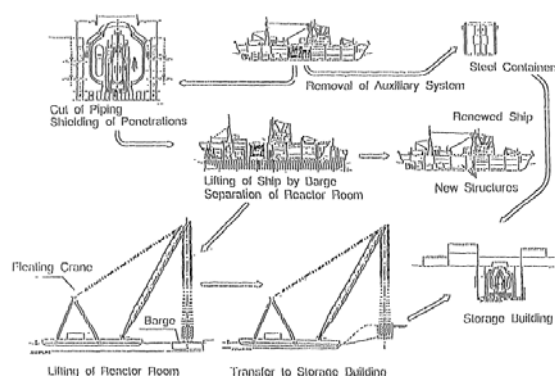


Figure 1.19: Decommissioning procedure NS Mutsu [8]

The cost of decommissioning for submarines varied a lot depending on the shipyard. A minimal cost of \$12 million and a max of \$21.4 million was established. The main differences are reported to be due to the way each shipyard categorizes and reports its inactivation work requirements. If a thermal power

of 150 MW is assumed which is an average power output for naval submarines and a thermal efficiency of 33%, a lower limit of 242\$/kW_e and an upper limit of 432\$/kW_e are established [126].

Source	Lower limit [\$/kW _e]	Upper limit [\$/kW _e]
[120]	1,070	1,220
[19]	114	254
[152]	/	3,153
[126]	242	432
Total average estimate	475	1,265

Table 1.7: Decommissioning cost upper & lower limit based upon [120][152][126] [19]

These decommissioning costs are mainly based upon PWRs. This is because SMRs are of a new technological generation, thus decommissioning has not yet happened for these technologies. That is why an estimate is made with the sources available.

1.7. Sizing & weight estimation

1.7.1. Reactor vessel

To be able to have a generic estimate on the reactor size and weight, a study from 2020 about the advances in SMRs was used. The study covers all SMRs concepts that were discussed before. The weight, height, and diameter of all SMRs were gathered and plotted over an increasing power level. SMRs that lied outside the general trend were removed in a similar manner as was done for the capital cost section. This was done to obtain a more stable and constant trend. First, the relation between power and weight was established, which can be observed on figure 1.20. This is deemed to be the most important characteristic of the reactor vessel because it is contained within the shielding, thus the volume is of not much importance. More information about trendlines that relate reactor density and the diameter to height ratio to reactor power are added in the appendix A.1.3.1 [74].

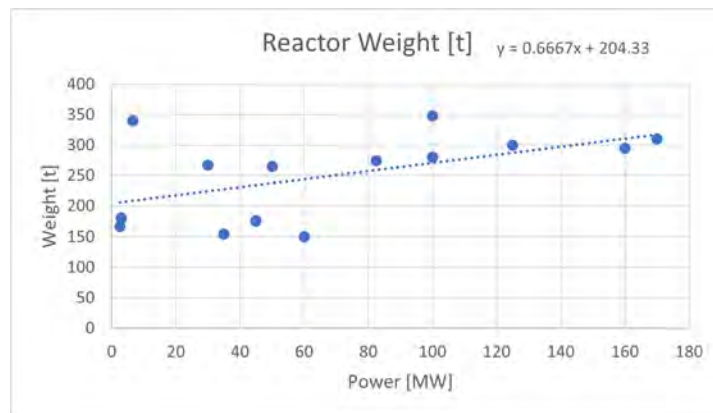


Figure 1.20: Weight-power relation [74]

Using the above trendline, it is now possible to find the weight of the reactor vessel when only given a power input, which can be used in the design stage of the vessel [74].

1.7.2. Shielding

Shielding is vital to protect the crew from radiation. When considering shielding, two radiation types are important, namely gamma and neutron radiation. Aside from these two radiation types, there are also beta and alpha radiation, but these are charged particles which collide with molecules and atoms inside the material, due to which they lose their energy and have a very low penetration depth. Gamma radiations, or photons, are absorbed by atoms instead of being slowed down; that is also why the term attenuation length is used instead of penetration depth for gamma radiation. Neutrons have an electric charge equal to zero, which leads to a very weak interaction with matter; neutrons will therefore have

a relatively large penetration depth [150]. On figure 1.21 it can be seen how the different radiation types are stopped by materials. As can be seen lead is very good to stop gamma-radiation but is very poor in stopping neutrons. Therefore shielding is always a combination of materials as also proposed by [71]. Therefore shielding is usually split into two parts namely the primary and secondary shielding. The primary shielding is located on the reactor which protects against radiation from the reactor, primary coolant system, radioactive waste disposal system and installations that are in close contact with these systems. The secondary shielding is surrounding the reactor containment vessel and nearby bulkheads. Shielding for auxiliary equipment can be categorized as secondary shielding as well [127].

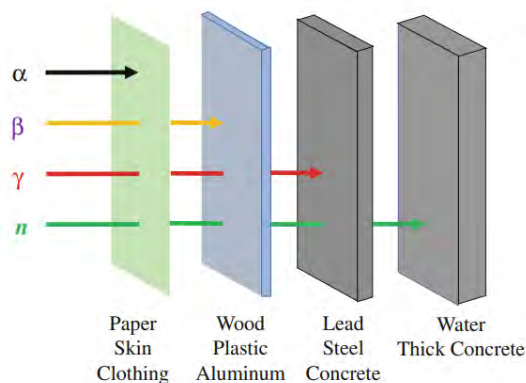


Figure 1.21: Penetrating power of different radiations [150]

In order to make an estimation for the weight of the reactor shielding different publications on marine applications are researched. This is done because the weight of shielding is considerable as will become clear from literature. The first application is the general cargo vessel NS Savannah. This was the first nuclear-powered commercial vessel. It was in service between 1962 and 1972. The NS Savannah was fitted with a PWR that had a thermal capacity of 74 MW_{th}. The primary shield was a shield tank surrounding the reactor vessel which was filled with water in order to protect the secondary shield against excessive neutrons radiation. The secondary shield was a combination of concrete and lead with polyethylene. The layer with lead and polyethylene was primarily to protect against gamma radiation. The combined weight of both the primary and secondary shielding was approximately 2,000 ton [9]. The second nuclear ship found in literature is a Japanese general cargo vessel called Mutsu and sailed between 1972 and 1996. It was taken out of use because of a radiation accident. The reactor had a thermal capacity of 36 MW. The combined weight of all shielding was estimated at 2,260 ton. The consistency of the shielding is similar to the NS Savannah [127]. In 1994 an advanced marine reactor design was established called the Marine Reactor X (MRX). This was done in order to minimize the weight and space properties of the reactor shielding. The reactor itself was an integral PWR which means the steam generator was installed inside the pressure vessel. The weight of the reactor plant and volume of the containment vessel was calculated to be respectively 50% and 70% of the previously mentioned NS Mutsu despite it having a thermal power of 100 MW_{th}. This gives an estimated weight of shielding equal to 1,130 ton [186]. In 2007 a concept design for a 800 TEU container feeder was made as a master thesis. A 40 MW_{th} HTGR was chosen to be most applicable to this design. The total weight of the shielding was calculated to be 1,370 ton. The calculation was done using Sabine 3 which is normally only designed for PWR's or boiling water reactors but with a simplification in design materials it was seemed fit for HTR as well [83]. Hirdaris et al. carried out a study on the concept design of a Suezmax tanker that is powered by a SMR of 70 MW_{th} where room inside the containment vessel is made to fit another 70 MW_{th}. One module of 70 MW consists out of two SMR of 35 MW_{th}. For both configurations the weight of the shielding remained identical because of the design and was equal to 3374.3 ton [66]. As last component K.Houtkoop made a function that gives the relation between reactor power and shielding weight. Herefore he used the analytical "removal-attenuation" method for neutron shielding and the "point kernel method" for gamma shielding which are found in [93]. The method consisted of determining a distance measured from the core in order to have a maximum radiation concentration of 1mSV/year at the edge of the outer shielding, which is the radiation threshold for external personnel on

a nuclear power plant. When this distance was calculated it was used to make a spherical volume so that the radiation was stopped equally at all sides. Next the densities of the corresponding materials were used to determine the mass of the shielding. To make the shielding module easier to handle a cubical box was made around the sphere with sides equal to two times the radius of the sphere. As materials a combination of water or concrete with lead was considered respectively for neutron and gamma radiation. From a comparison with other available data from literature it was made clear the concrete with lead option was most sensible [71]. To check the method used by K.Houtkoop two data points were added. First the design of the Ubattery with a power of 10 MW_{th} was used. The neutronflux, thermal power en reactor volume was given after contact with the company and was respectively equal to $1.83 \cdot 10^{18}$ neutrons/cm², 10 MW_{th} and 13,289 m³. Secondly another data point was added from a study concerning nuclear propulsion of high-performance cargo vessels or Fast ships which also carried out an extensive economical comparison between conventional and nuclear propulsion. Two HTR were installed with a combined power of 257 MW_e were a specific weight of 11kg/kW was established [176].

All found results are plotted on figure 1.22 and it can be seen that the weight for the Ubattery and Fastship lies in the vicinity of the curve fit established by K.Houtkoop. The formed trend line with polynomial depicted in the right corner of figure 1.22 can be used to make an estimate on the weight of the reactor shielding. The major outliers in the figure can be identified as the 1994 MRX and the Suezmax tanker with one reactor. This can be explained by the MRX being especially developed to decrease space and weight of the reactor shielding. The excessive weight of the Suezmax tanker is due to the extra space left for a second reactor which has the same total weight as described before. Thus the general trend line can be seen as a conservative estimate. As is also described by K. Houtkoop where the polynomial displayed on figure 1.22 is the higher upper limit of his estimation to take into account extra material surrounding the reactor previously described as being encapsulated by the primary shielding.

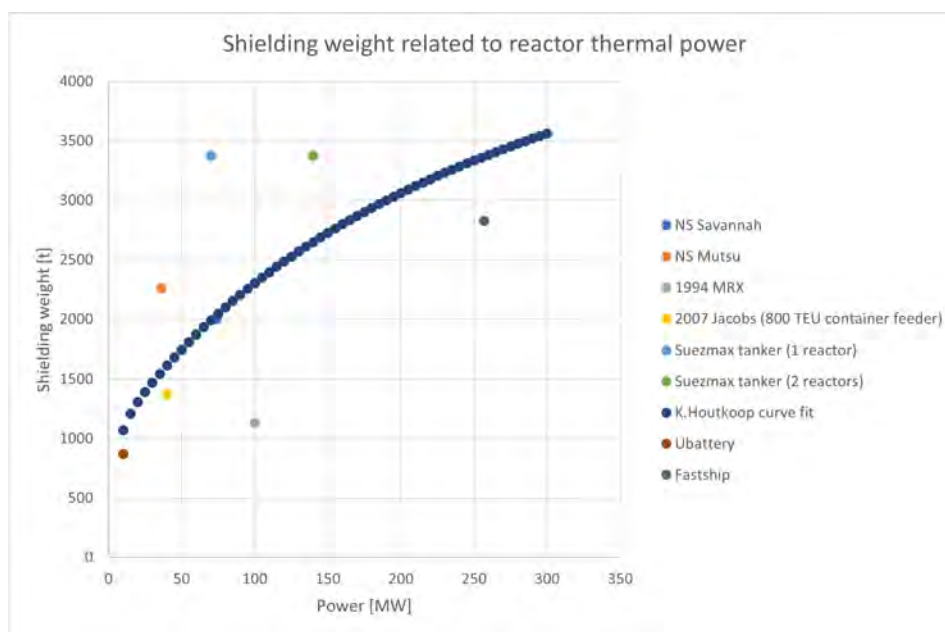


Figure 1.22: Reactor Shielding weight estimation based on [71] [9] [127] [186] [66] [93] [176]

The radius of the reactor core plus shielding in function of thermal power can be seen on figure 1.23. The graph is made using the same method as described by [71] where the layer for neutron shielding consists out of concrete and the layer for photon shielding out of lead. Using the depicted radius the volume of the reactor and shielding can be calculated in a later stage of the design. Where the shielding will encapsulate the reactor so the volume of the reactor itself is not of high interest [93].

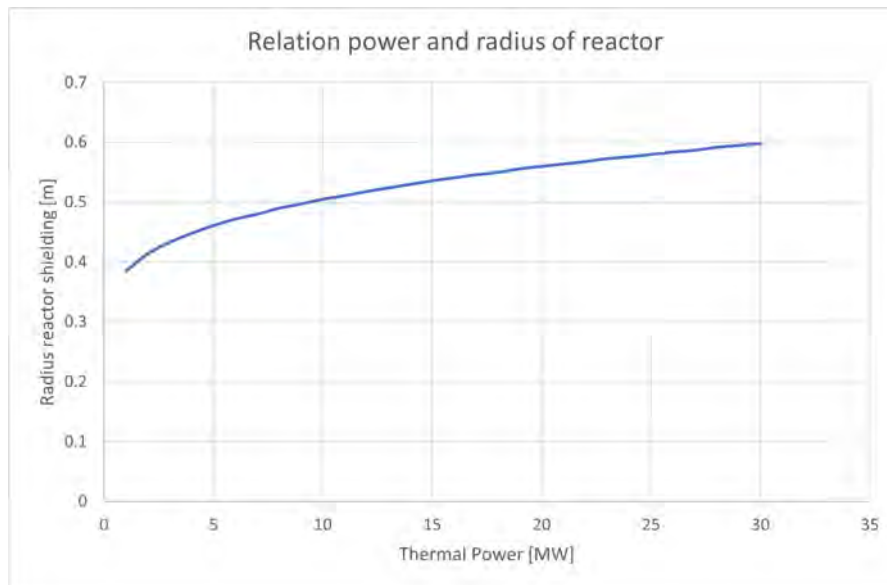


Figure 1.23: Reactor + shielding radius estimation based on [71] [93]

1.8. Additional technical points for the implementation of a reactor in a ship design

Apart from the shielding there are some additional technical points concerning the reactor design and implementation in a ship design. These can be identified as location, safety and refuelling facilities.

1.8.1. Location

Looking at historic applications the reactor compartment was placed in the centreline of the ship, as low as possible and relatively close to the accommodation this is seen on the earlier discussed Savannah, Mutsu and FastShip concept [176]. This is beneficial from a stability and collision perspective. Stability wise because of the considerable shielding weight as calculated before and collision wise because of a least possible risk of collision damage. From a motions perspective this is also beneficial because of its central position which makes it less susceptible to rolling motions. On the NS Savannah and Mutsu the reactor is also placed near half the ship length to decrease pitch motions [127]. The upper part of the reactor is also seen to be free for the possibility of maintenance and refuelling if historical designs as the Savannah and Mutsu are observed [9]. The midship position in case of a container vessel would lead to a large decrease in cargo capacity thus is not deemed ideal for that case. The exact location needs to be determined in the design process.

1.8.2. Safety

Safety in this section is meant as the safe operation of the reactor on board disregarding the passive and active safety features discussed earlier. Especially the release of radioactive material into the marine environment which got more attention due to the Fukushima Daiichi incident [150]. These are already addressed in the International Maritime Organisation (IMO) rules dating from 1981. Here it is stated the reactor compartment should be compartmentalized by fitting bulkheads or cofferdams extending from the double bottom up until the bulkhead deck. Apart from lowering the risk of release this also contributes to collision and fire safety. The compartmentalization is also important in the aspect of salvage operation as it is stated that the reactor compartment must be designed in such a way that it facilitates removal in case of a ship wreck [80]. Thus this should be taken into account in the design process. The study by Jacobs handled the topic of salvaging and stated the easiest way to handle it was indeed compartmentalization so that the reactor compartment can be cut free without endangering the radioactive material [83]. Measures against the possibility of terrorism or piracy should also be taken into but this would require a full risk assessment of the vessel design which falls outside the scope of this report.

As the rules and examples from literature are mainly based on PWR they are also important for advanced reactor concepts as the MSR or VHTR. Thus they provide a good basis for the protection of crew and environment against radioactive material.

1.8.3. Refuelling facilities

Refuelling of a nuclear powered ship diverges considerably from a conventional design. The minimum refuelling interval for the discussed reactors is 1-2 years but for practical consideration the reactor design can be constructed in such a way the refuelling coincides with the dry docking period as proposed by a study from the university of London. The main hazard lies in handling the spent fuel which poses significant radiological and health issues. For pressurized water reactors this is done via extra shielding and a controlled water bath to transfer the fuel from ship to a storage facility [29]. The process of refuelling and extended maintenance for a PWR after a period of 5 years can take up to one month according to the IAEA [77]. A concept design of a high-speed trans-pacific nuclear container-ship of 9,200 TEU with PWR opted for the possibility of an internal refuelling crane but is anticipated to raise additional nuclear safety and security concerns. Thus extending the core lifetime and using a direct refuelling method is favoured for further development. The reactor core for this specific concept was designed to last for 5 years where the same process for refuelling as described above is anticipated. The refuelling duration is estimated to be around 40 days which can be scheduled within the drydocking period. The nuclear refuelling process is estimated at \$2 million for core removal & replacement [151]. These considerations are for a 280 MW_e PWR with for a ship with a design speed of 35 knots and 121,100t displacement, 364m LOA, 42.1m breadth and 13.1m design draft. This type of refuelling is the best compared with a prismatic VHTR because it also makes use of fuel rods like the PWR and is not able to have online refuelling. For the MSR and pebble bed VHTR online refuelling is possible which could lower the refuelling time but increase nuclear safety and security aspects.

1.9. Summary of discussed reactor technologies

An overview of the discussed reactor types and their characteristics is given below. The load following, cost and size sections are added as last. These depend on the power output of the reactor. The fuel costs are not included here because they also depend on the amount of fuel used by the propulsion line and this is not established yet. To have an idea about the fuel cost per kg of enriched uranium see Table 1.5 & 1.6.

Reactor type	MSR	VHTR - Pebble bed		VHTR - Prismatic
Neutron spectrum	thermal/fast	thermal		thermal
Fuel cycle	open/closed	open		open
burn-up [GWd/tHM]	90+	90-200+		90-200+
Fuel Type		U/Pu/Th		
Level of Uranium enrichment	LEU	3-20%		
Sub reactor type	breeder/convertor	breeder(with thorium)/convertor		
Thorium capability	breeding/continuous	breeding		breeding
Refuelling process	online/offline	online		offline
Min refuelling cycle		1.5-2 years		
Max refuelling cycle	continuous/lifetime	continuous		1.5 - 2 years
Safety		active/passive		
theoretical load following	possible	/		/
Load interval		20-80%		
Ramp-up/ramp-down rate		3-5%/min		
Operating temperature	<800°C	<700°C and 700-1000°C+°C for (V)		<700°C and 700-1000°C+ for (V)
Capital cost estimate*		Figure A.3		
Decommission cost estimate*		Table 1.3		
Weight estimate reactor*		Figure 1.20		
Weight estimate shielding*		Figure 1.22		
Volume estimate shielding*		Figure 1.23		

Table 1.8: Comparison of selected reactor technologies based upon previously discussed sections. Rows denoted with * depend on the power of the selected reactor thus a reference to the figure or table to be used is given. Based on [71] and own additions from previous sections

To get a better overview of the discussed reactor types a summary of advantages and disadvantages

for each reactor type is given.

Reactor Type	MSR	VHTR
Advantages	<ul style="list-style-type: none"> • Passive/active safety • High proliferation resistance • Very high burn-up possible which reduces waste production and increases fuel efficiency • Fuel cycle can be both open or closed and refuelling can vary from short to long term • High operating temperature gives higher electrical efficiency • Xenon poisoning is mitigated • Theoretically capable of increased load following (not taking into account the BoP) • Capable of using thorium even in a continuous cycle because of the good neutron environment (re-processing of salt) 	<ul style="list-style-type: none"> • Passive/active safety • High proliferation resistance • High burn-up possible which reduces waste production and increases fuel efficiency • Refuelling can vary from short to continuous depending on the fuel packing. Online refuelling is possible with pebble based • High operating temperature gives higher electrical efficiency especially for the VHTR • Relatively high TRL • Capable of using thorium as a part fuel
Disadvantages	<ul style="list-style-type: none"> • Tritium production when lithium is present in salt • Corrosive nature of salt • Lower TRL • When the coolant fuel mixture leaves the reactor core it is irradiated so extra shielding requirements must be established or use of different coolant 	<ul style="list-style-type: none"> • Susceptible to xenon poisoning • Pebble bed reactor can be susceptible to vessel movements and vibrations which can lead to variations in reactivity • Low power density which is accompanied by a large volume of graphite that will contribute to nuclear waste

Table 1.9: Advantages and disadvantages of discussed reactor types from a marine application perspective based on [71] and own additions from previous sections

From Table 1.8 and 1.9 it can be derived that the MSR and VHTR posses many benefits but there are still technical difficulties to overcome. When these reactor types are compared to the other SMR designs listed earlier in section 1.1.1 they surpass the PWR on a passive safety level, fuelling options and increased electrical efficiency due to higher operating temperatures. These make up for the higher TRL of 8-9 from PWR. The fast neutron spectrum reactors namely sodium-, gas- and lead-cooled have a TRL comparable with the MSR but have individual difficulties regarding their coolant use:

- Sodium has two safety concerns first sodium is flammable when a leak is formed and secondly when reacting with water it can form hydrogen which is also highly flammable.
- A gas cooled fast reactor operates at high pressure thus a pressure vessel is needed and their is the possibility of a high pressure leak.
- A lead cooled reactor specifically forms a problem when lead-bismuth is used. When bismuth

captures a neutron a highly toxic element polonium is formed which leads to extra concerns for refuelling.

As the MSR can serve as a fast reactor as well it is deemed this reactor design has the most favourable design characteristics. Therefore the MSR is selected for a long-term solution and the VHTR for the short term with regards to their difference in TRL [71].

1.10. Chapter conclusion

The two most promising reactor concepts being the VHTR and the MSR were introduced because of their high burn-up, possible use of thorium, high passive safety features and high operating temperatures. With the VHTR being the best option for short term implementation because of its higher TRL. They were discussed into more detail on the aspects of load following, capital costs, fuel costs, O&M costs and decommissioning costs. Most interesting was the decrease of relative capital cost for increasing power levels which is also seen with conventional energy sources. The nuclear fuel cost was also seen to be a factor 10 cheaper as the conventional MDO fuel where for the nuclear fuel high enriched uranium was used as comparison. This coincided with the trend surrounding nuclear energy being high capital costs but low operational costs.

Additionally a method for determining the reactor shielding weight and volume was found in literature. The shielding consisted out of a combination of lead and concrete proposed by [71]. This proposal was validated by two additional pebble bed High temperature reactors being the Ubattery and a reactor concept that was fit onto a 1400 TEU fast container ship. In addition possible technical difficulties in the implementation of the reactor inside a ship design were identified on the basis of location, safety and refuelling. With the major difference for a conventional ship design being the long refuelling interval and compartmentalization of the reactor room.

Uncertainties that still remain are the total cost and size of the reactor for a new ship design as this is depended on the economic speed of the nuclear driven container vessel. All the inputs from the nuclear aspect that seemed necessary as input for the economic speed determination have been defined. Possible impacts on the ship design are to be studied later.

2

Relation speed & income

Chapter introduction

This chapter is dedicated to answer the sub literature question:

”What are the factors that contribute to income in liner shipping and are they depended of speed?”

Stopford classifies shipping costs in three main categories namely the capital costs, operating cost and the fuel cost. Where the latter is included in the operating costs for this report. These are also applicable to conventional liner shipping [159]. This chapter is dedicated to do the same in order to find the factors in liner shipping that contribute to income and are depended on speed. Where income is defined as the revenue minus the considered costs. Where applicable the comparison with a nuclear variant will be made if not already covered in Chapter 1.

These are investigated to discover which factors need to be taken into account for the economic speed determination and to carry out a similar exercise for a diesel reference case.

2.1. Opex & Capex: cost of ownership

2.1.1. Capital cost

The capital cost that is of most interest to this report is the one of the main engine because this is a substantial change in capital cost compared to a nuclear variant and is logically depended on speed. As the cargo capacity is equal to 20,000 TEU a total value for the capital of \$8,000/TEU is found. This however covers all capital cost also the ones that are not depended on speed therefore this value is not further used. For a more extensive overview of the total capital cost per TEU appendix B.1 can be consulted [117].

A value used in practice is equal to \$350/kW for the capital cost of a diesel engine. This value should however be checked with other sources in literature. A publication from professor Manuel Ventura researcher at the university of Lisbon is used for this purpose. He proposes following two equations for the calculations of machinery cost which are based on current statistics an apply to oil tankers, bulk carriers, container carriers and general cargo [175].

$$C_m = k_1 \times P_{MCR}^{k_2} \quad (2.1)$$

$$C_m = 1.6 \times \left(\frac{P_b}{100}\right)^{0.82} \times m_M + CF_m \quad (2.2a)$$

$$CF_m = Hh_m \times m_M \quad (2.2b)$$

$$Hh_m = 1600 \times \left(\frac{P_b}{100}\right)^{0.6} \times k \quad (2.2c)$$

Both equations could be used but equation 2.2a includes the cost of the shaft line and propeller thus this would be an overestimation of the machinery cost. Equation 2.1 only includes the cost of the installed engine and gives parameters according to the type of engine as can be seen in table 2.1 [175].

	k_1	k_2
Diesel (2 stroke)	19.877	0.620
Diesel (4 stroke)	12.507	0.647
2 x Diesel (2 stroke)	14.141	0.65
Steam Turbine	38.48	0.54

Table 2.1: Machinery cost factors from [175]

When using the equation 2.1 the P_{MCR} should be expressed in brake horsepower (hp) thus the relation $1 \text{ kW} = 1.341 \text{ hp}$ can be used. The used equation is compared to a unit cost of $\$350/\text{kW}$ and it is seen that for higher powers around 60 MW they converge thus this is deemed satisfactory for the intended purpose. A plot can be found in appendix B.2.

2.1.2. Operational cost

According to an OECD study in 2015 the operating costs excluding fuel costs for container vessels are split into manning, insurance, stores, spares, lubricating oils, repairs & maintenance (R&M), dry docking and management & administration (M&A) [125]. The same division is followed by Stopford and Murray [159][117]. A graphical representation is given below on figure 2.1 for increasing vessel sizes.

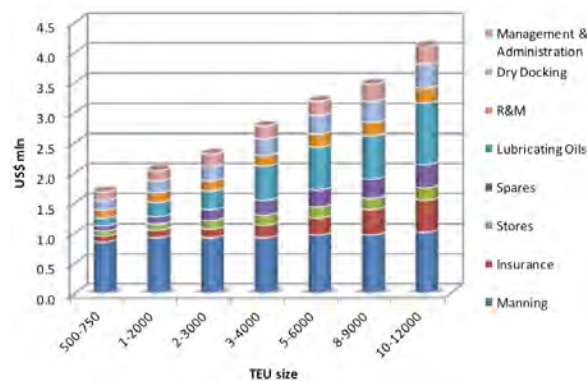


Figure 2.1: Annual operating cost for different container sizes [125]

It can be seen that all costs increase almost linearly except for the stores and manning costs. OECD estimated that for a modern 19,000 TEU vessel the operating cost per annum would be $\$5.2$ million. This is based upon the graph above, which is constructed with the use of Drewry Maritime research data and the own elaborations of the OECD.

The main cost factors that will increase with speed are identified as the lubricating oil and repair & maintenance cost that can be combined as operation & maintenance cost (O&M), as also done for the nuclear reactor in chapter 1. The same principle is used in a study carried out by the university of Hamburg [112]. The rest of the vessel running costs are seen as constant for changing speed thus will have no effect in determining an economic speed. These will be disregarded for further analysis.

2.1.2.1 Operation & maintenance cost

The O&M cost include all costs to keep the engine running properly and are subdivided in consumables and maintenance where fuel costs are excluded. Consumables include the consumption of lubricating oil but also take into account the use of coolant and emissions control catalysts and reagents for example. Maintenance includes the labor and material cost for scheduled and unscheduled repairs. A tech-

nical report from Electric Power Research Institute (EPRI) estimates the maintenance cost for diesel engines to range from 0.01 to \$0.02/kWh and the operation cost which includes the use of lubrication oil and use of urea¹ is estimated as \$0.0058/kWh. The combined O&M is estimated as \$0.015/kWh for a 2 MW internal combustion engine [65]. In another source that is also used for the operation and maintenance cost of the nuclear reactor described in chapter 1 a similar cost is given for a 21 MW internal combustion engine. The O&M cost is split here in a variable and fixed cost respectively equal to \$36.81/kW-year and \$5.96/MWh. If these are expressed in the same units as described above a total of \$0.0105/kWh is found [10]. Combining these two sources an estimation for the total O&M cost can be made by taking the average between the two.

2.1.2.2 Nuclear variant

For a nuclear propelled ship lubrication oil is not obsolete but in comparison with a diesel engine deemed negligible. The operation & maintenance costs were already covered in chapter 1. The rest of the operational cost consist out of management & administration, dry docking, spares, stores, insurance and manning. No reason in literature is found to increase the cost of spares or stores for a nuclear propelled ship. In the study of the university of London that was mentioned in the previous chapter a comparison between operational costs for a nuclear and conventional container ship of 9,200 TEU is made. Management & administration and dry docking were kept constant, manning costs were increased by 38% due to special training in reactor operation and engineering as also mentioned by the IMO regulation A.491(XII) [80]. The insurance is expressed as 1% of the capital cost of the nuclear vessel for H&M together with \$350,000 for the P&I insurance per year. The conventional vessel is insured for a value of \$1 million/year. This results in an increase of 87% for the total insurance of the nuclear vessel per year [151]. Another publication that was previously discussed concerning a nuclear FastShip of 1,432 TEU also states a difference in operational costs. The only noteworthy difference lies again in manning and insurance. Where a relative increase of 10% for manning cost is seen. The insurance only increases with 4%. The remaining operational costs were kept constant [176]. In both publications the largest difference in operational costs was seen in the fuel consumption respectively a decrease of 74% per year for the publication of the London university were a fuel cost of \$455/ton was assumed and a reduction of 86% per year for the FastShip nuclear concept, here no value of the fuel cost was given [176][151].

The manning cost will not increase with increasing speed as the crew would get monthly payments regardless of how fast the vessel is sailing and an extra cost factor for nuclear specialist on board of the vessel is already covered by the nuclear O&M. The variations of insurance costs in literature are observed to be very large thus no conclusion can be drawn here. Therefore this cost post is not taken into account for the current study.

2.1.2.3 Fuel/bunker cost

The fuel or bunker cost is the third category of cost that is analyzed. Its relation with speed is related in a conservative way when using the cube law. A more accurate relation is constructed with a vessel specific resistance curve where the wave making and frictional resistance are taken into account. Using this relation the container speed can be related to fuel cost as is depicted below on figure 2.2 which shows the average container speed (blue) for vessels ranging from 3,000-8,000 TEU in relation to HSFO 380 prices (orange). A somewhat inverse correlation can be observed [133]. The regions where there is no clear inverse relation being Q4-2016 to half Q1-2017 and halfway through Q2-2018 to Q3-2018 show that another variable is of importance being the freight rate that also has a profound effect on the vessels speed which is discussed in section 2.3. An average specific fuel consumption of 170 g/kWh is assumed for further use as this value is widely used in practice.

¹Used to convert dangerous nitrogen oxides into harmless nitrogen gas and water

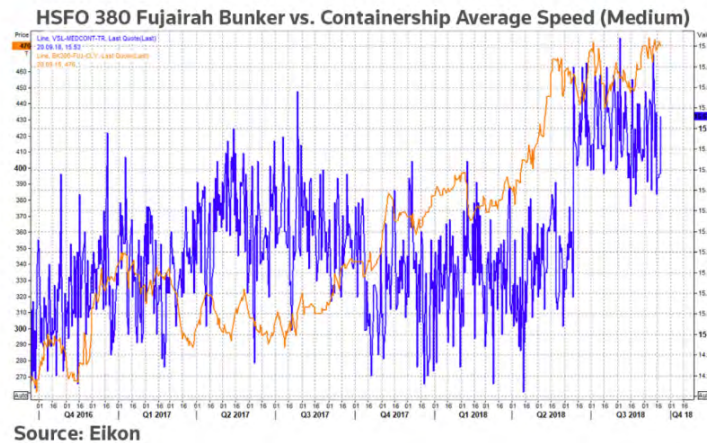


Figure 2.2: HSFO 380 vs. Container Average speed [133]

If the speed and consumption is known the next ingredient that is needed is the price of fuel oil. Throughout time this price is very volatile as it is susceptible to the world economical and political situation as can be seen on figure 2.3 [161].



Figure 2.3: Bunker costs over the past 10 years [161]

It should be noted that before 1 January 2020 IFO 380 was the dominant bunker choice which was followed by VLSFO. The graph above is based upon the price index of 20 leading global bunkering ports. The largest spike seen in the graph is due to the upcoming war between Russia and Ukraine where the Russian oil exports were slowly but surely phased out. If the lowest bunker price is compared with the highest over the last 7.5 years an increase of 679% is seen [161].

Another important factor for diesel propelled ships is the carbon tax which is seen as an additional cost for burning fuel. For every gram of diesel that is burned 3.161 grams of CO₂ are released [43]. This carbon tax was proposed by Japan in May 2022 the idea is to insert a carbon tax of \$56/mt starting from 2025. This tax would then increase every five years to as high as \$637/mt by 2040. Using the previously established relation of amount of grams CO₂ per gram of diesel burned this accounts for at least 3 ton of CO₂ per ton burned fuel. This means per ton of burned fuel an extra \$168 has to be paid from 2025 if the proposal of Japan is adopted [97].

In order to make an estimate on the bunker price a range of possible values is adopted where the carbon tax is included. This way a variation of scenario's can be analyzed. The range adopted for this report is equal to 400-1,000 \$/ton with the used fuel being Marine Diesel Oil (MDO).

2.2. Route selection

Apart from discussing which route is selected to observe the effect of increasing speed on costs, the different voyage costs will also be discussed. For the purpose of this report the voyage costs consist out of port dues, pilotage, tugs and canal dues in case the Suez canal is used. These are discussed with relation to speed because the faster a ship sails from A to B over a defined operating time the more port visits it will make thus these voyages costs will become more frequent. Assuming that port congestion and availability of containers to be shipped are of no issue. For the current analysis it is assumed nuclear powered vessels are allowed to enter the described ports.

2.2.1. Rotterdam to Shanghai

For Rotterdam the port dues are expressed in two rates, the first being in function of Gross Tonnage (GT) and the second on the weight of the amount of containers. These are respectively \$0.255/GT and \$0.510/ton of TEU [147]. For Shanghai a total port due solely in function of the GT was found of \$0.191/GT [167]. In a publication from the Dutch pilotage tariffs it is possible to determine the pilotage fee depending on the draught of the vessel and the inland route taken, for this scenario it will be assumed that loading/discharging will take place at the Maasvlakte II, later alterations are possible. This leads to a pilotage costs of \$7,321 [99]. Container vessels in the order of 20,000 TEU generally need three tugs for assistance while manoeuvring. In the port of Rotterdam the price is \$4,697/tug [147]. For Shanghai the pilotage and tugs costs are not found but assumed to be similar to Rotterdam.

The largest voyage cost in this route consists out of the canal due of the Suez canal which provides a shorter alternative to Shanghai than sailing around Cape Agulhas. The main factor in determining this fee is the Suez Canal Net Tonnage (SCNT). Normally this is calculated by the classification society or the Suez canal port authority. If the SCNT is not available an estimation can be done which is described by Stopford. The gross and net tonnage are added together and divided by two on which 10% is added [159]. As a reference ship the Ever Given was used, this came to a total of approximately \$700,000 which is converted to a value in GT (\$3.195/GT) so that an approximation can be made for other vessels [17].

The assumption can be made that voyage costs for a nuclear powered container vessel will be higher than for a conventional one. For port due tariffs and pilotage nothing is stated concerning nuclear powered vessels but in the port of Rotterdam the consideration of LNG carriers is made. Due to lack of other available information the fees for a LNG driven vessel will be taken into account for the nuclear variant because this can also be considered as an additional risk. For the port dues a fee of 0.330/GT is given, for container handling the fee remains unchanged [147]. The pilotage cost for a LNG carrier is also increased because it has to be picked up sooner which leads to a total cost of \$8,345 [99]. The same fee is assumed for Shanghai.

An article from the the Maritime Executive describes the possible bottlenecks for a nuclear powered vessel with a MSR to pass the Suez canal. The Suez canal authority discourages the passing of nuclear powered vessels with the main reasoning being a possible blockage due to shutdown of the reactor. Exemptions have been made in the past for non-commercial nuclear vessels but only in very rare occasions following from intergovernmental negotiations. Solutions as shutting down the reactor and being towed, being driven by an on board battery or the use of emergency diesel generators are proposed for a commercial vessel [173]. To make an estimation for the Suez canal fee concerning a nuclear driven vessel, an LNG carrier with the dimension of the Ever given is taken with the same reasoning as above. This comes to a total of \$1,026,602.67 which is \$4.686/GT [17]. In table 2.2 the total voyage cost per trip from Rotterdam to Shanghai or vice versa is shown some costs are expressed per GT so that these values can also be used for other vessels with different particulars. The port dues of Rotterdam and Shanghai are added and the pilotage cost and Suez canal dues are doubled. This is done to be able to calculate the voyage cost per trip from A to B.

	Conventional	Nuclear
Port dues	\$0.45/GT + \$0.51/ton of TEU	\$0.66/GT + \$0.51/ton of TEU
Pilotage	2 x \$7,321	2 x \$8,345
Tugs	2 x 3 x \$4,697/tug	2 x 3 x \$4,697/tug
Suez canal dues	2 x \$3.12/GT	2 x \$4.69/GT

Table 2.2: Voyage cost Rotterdam-Shanghai

The distance from Rotterdam to Shanghai using the Suez canal is 10,664 nM. The Suez canal itself has a length of 104.4 nM where the maximal speed for container ships is 8 knots. This leads to an average transit time around 14-15 hours [17]. Aside from the maximal speed limit in the Suez canal a constant speed over the track will be assumed.

2.2.2. Rotterdam to New York

The same voyage costs for Rotterdam will be applied as discussed before. For New York the port dues consist again out of two rates. The first depends on the length of a vessel, for vessels above 275m the rate is \$45.37/m/day which is taken as an estimate because for previous estimates the Ever Given was chosen as an example. The second rate is meant for cargo handling and is equal to \$13.13/TEU [122]. The fee for pilotage on the lower Hudson river depends on the amount of pilot units which is calculated by dividing the product of the LOA, moulded depth and breadth by 10,000 in feet. For larger cargo vessels as the Ever Given this value will lie above 100 thus a standard fee of \$14.02/pilotage unit is maintained [145]. The tug price in the port area of New York is expressed per net registered ton. An average of \$0.552/NT is found which is considerably larger than the found tug cost in Rotterdam. For a vessel with the sizing as the Ever Given this would come to a total of \$54,734 compared to the \$14,091 of Rotterdam when three tugs are used [170].

For the nuclear option the same incremental increase as for Rotterdam is used as no information about LNG carriers or similar vessels is found for New York.

	Conventional	Nuclear
Port dues Rotterdam	\$0.26/GT + \$0.51/ton of TEU	\$0.33/GT + \$0.51/ton of TEU
Port dues New York	\$45.37/m/day + \$13.13/TEU	\$55.68/m/day + \$13.13/TEU
Pilotage Rotterdam	\$14,642	\$16,690
Pilotage New York	\$14.02/pilotage unit	\$15.74/pilotage unit
Tugs Rotterdam	\$4,697/tug	\$4,697/tug
Tugs New York	\$0.55/NT	\$0.55/NT

Table 2.3: Voyage cost Rotterdam-New York

The distance from Rotterdam to New York is equal to 3,360 nM and it will be assumed a constant speed is maintained over this track.

2.3. Revenue

According to Stopford revenue depends on three main categories namely cargo capacity, productivity and freight rates. Cargo capacity is fixed as a design parameter to 20,000 TEU, productivity is partly addressed in 2.2 on the aspect of port time [159]. The focus of this section will lie on making a good estimate on freight rates per TEU/FEU and mapping the relation to speed. This will be done by looking at how freight rates have changed during the passed years and how they will be likely to evolve over the coming months.

On figure 2.4 the volatile character of the spot freight rate price for a FEU can be seen from the start of the corona pandemic until time of writing². The change in freight rate is seen for the four largest trading lanes spread around the world with the main origin in Asia which all follow a similar trend

²January 2023

[54]. The rise in freight rate was a cascade of events all originating from one common source, the coronavirus. Ports lacked their workers because they were sick at home. Containers shipped by land to reach their final destination couldn't cross borders due to public health restrictions which resulted in congestion on land. Similarly crews intended to operate container vessels could not cross the border because of the same rationale and resulted in massive port congestion. These factors were combined with the rest of the world being in full lockdown and increasing the demand of goods to deliver because of their immobility which resulted in a huge demand shift [30]. The end result can be seen on figure 2.4 around October 2021 where the freight rate for one FEU from Asia to the east coast of the US went over \$20,000 which also occurred during the peak season that normally falls within August until end of October. The differences in freight rates over the world trade routes are mainly due to differences in inflation, port congestion and local work forces. Around the peak of freight rate in October until the beginning of 2022 there were a total of 100 vessels waiting to get into the container terminal at the East coast of the US [54].

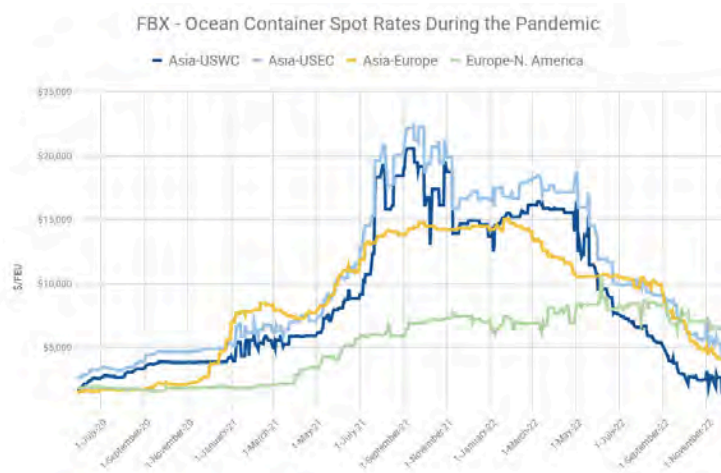


Figure 2.4: Spot freight rates 2020-2022 [54]

Up until may 2022 the freight rates remained extremely high but from that moment on they dropped and kept on decreasing even throughout the peak season of 2022. The route Asia to US West coast has a current price of \$1,400/FEU which is down 90% compared to one year ago. Similarly the freight rate from Asia to the US East coast is 75% lower compared to last year and the same trend is seen for the Asia to Europe trade route. The reason for this decline in freight rates is three folded. First there was the tendency of importers to order big volumes earlier in the year, secondly another shift in demand that started in the summer of 2022 and thirdly inflation. The pull forward of orders was done by importers to mitigate the delays they experienced a year before so the orders that would normally be shipped during the peak season of 2022 were already shipped around spring. The shift in demand consisted out of a decrease in demand plus the tendency of the consumer to buy less electronics compared to lockdown times. These two factors lead to a decrease in transported volume as can be seen on figure 2.5 where the transported volume is expressed in TEU. Nevertheless the levels of transported volume did not plumb below pre-pandemic volumes for the Asia to US route but converged to them. A decrease in transported volume lead to an increase in supply capacity due to less port congestion which was especially seen on the east coast of the US as mentioned before. This lead to decrease in freight rate which is seen on figure 2.4 [54].

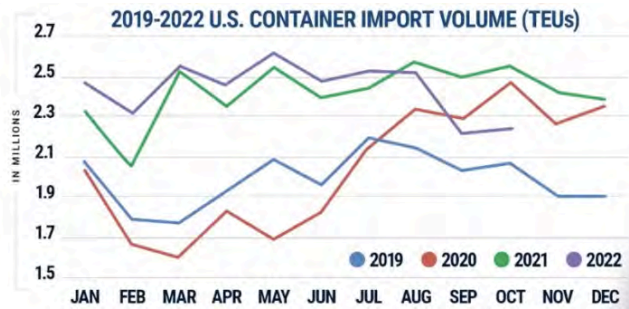


Figure 2.5: Changes in transported volume from 2019-2022 [54]

Freightos [54] predicts that the trade volumes will decrease further on a global level leading to a further decrease in freight rate due to less port congestion. Nevertheless they state that due to inflation, charters and fuel prices will go up, thus carriers will try to keep these rates above their break-even points by making use of capacity management³. This will presumably lead to rates settling above pre-pandemic rates from 2019.

If the freight rate is compared to the container ship average speed a clear correlation can be seen. Increased freight rates lead to ship owners to increase speed in order to get to ports faster. Similarly ship owners will reduce speed if the freight rates decline in order to optimize speed in relation with fuel consumption as discussed earlier. A good example of this trend is given on figure 2.6 where the global Freightos Baltic Index (green) is expressed to container ship average speed (blue).

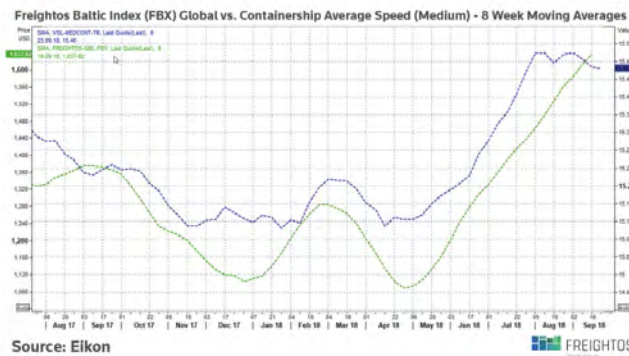


Figure 2.6: Freightos Baltic Index vs Container average speed [133]

³a balance exercise with capacity and services to keep demand and supply evenly, which was already successfully done in 2020

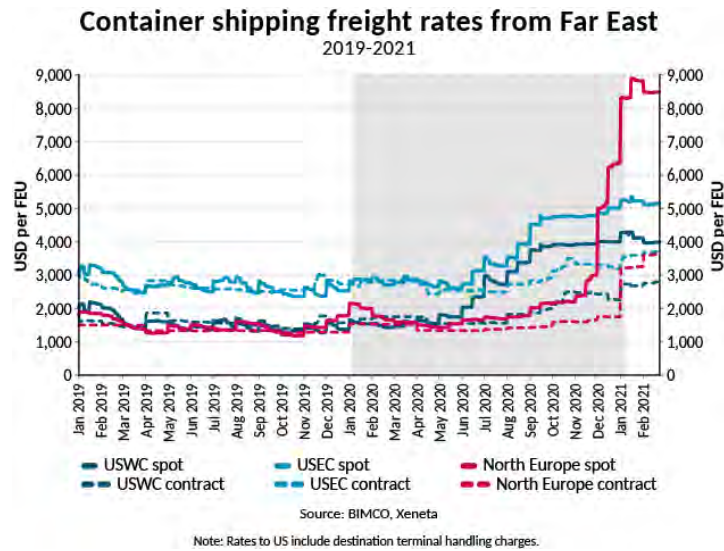


Figure 2.7: Freight rates spot and contract 2019-2021 [24]

All freight prices that are gathered up until now are expressed in FEU this is because an FEU is the standard measure in container shipping.

If the freight rates of the selected routes are studied being between Northern Europe and China/East Asia (FBX11 & FBX12) and between Northern Europe and North America East Coast (FBX21 & FBX22) and average freight rate between 1000 - 3000\$ is found. During the pandemic these values increased above this range and there were also occasions when the freight rates lied below this range as discussed before. Nevertheless, these events do not occur frequently thus these are not taken into account. The specific routes and freight rates studied for determining the freight rate interval are added in appendix B.3.1.

2.4. Chapter conclusion

In this chapter the main factors that contribute to income were analysed as three main categories namely the capital cost, operational cost and freight rates. For these three categories it was evaluated which sub factors were depended on speed. For the capital cost it was found that only the cost of the main engine was depended on speed. For this a value of \$350/kW was used from practice and validated with literature.

The operational costs that contributed to income and were depended on speed are identified as the O&M cost and fuel cost. The O&M cost is subdivided in a fixed and variable component respectively equal to 36.81 \$/kW/year and 10.5 \$/MWh . For a nuclear propelled ship an increase in manning cost was found to be between 10-37%. This due to special training required for the crew to be able to sail the vessel in a safe manner. It is however assumed that the manning cost is not depended on speed as the crew would get paid the same per month regardless of how fast the vessel is sailing. This would thus not change the absolute value of the economic speed. Other operational costs excluding fuel costs were not seen as principally different from the conventional case.

The fuel cost was observed to be volatile throughout time but a somewhat inverse relation between vessels speed and fuel cost was established due to the influence of a second variable being the freight rate. Including the carbon tax a range from \$400-\$1000/ton was established for the fuel cost. The voyage costs are assumed to be higher for the nuclear case and were based upon an LNG reference vessel. The freight rates were seen to be volatile as well but here a clear dominant proportional relation between freight rates and container ship average speed was found. Based on the baltic exchange a freight rate range form \$1000-\$3000/FEU was found for the described routes.

The exact influence of the several cost factors on vessel speed still needs to be determined in an economical model which is reserved for the research section.

All the inputs that seemed needed to determine an economic speed for a nuclear container vessel were gathered along with additional parameters to do the same exercise for a diesel reference case.

3

Relation speed & hull shape

Chapter introduction

This chapter is dedicated to answer the sub literature question:

”Where does the relation between speed, main particulars, C_b and deadweight lie? ”

The goal of this chapter is to see where a high-speed container vessel diverges from the conventional container ship design. Where high-speed is defined as an increase from the conventional. This is carried out by comparing three high-speed container vessels with an existing database of 7872 conventional container ships on the basis of speed, main particulars, C_b and deadweight.

This is done in order to get an insight in how a container vessel with an increased design speed would differ from its conventional counterparts and to select a reference ship as starting point for the intended 20,000 TEU nuclear design. Where the assumption is made that due to the low fuel cost of nuclear fuel an increase in economic speed would appear.

3.1. High-speed container ships

In order to create a feeling of how fast container ships are constructed two designs series and one concept design will be discussed in more detail.

Vessels	Top speed [knots]	TEU capacity [TEU]	Building year
FastShip concept	37.5*	1,432	/
Sea-land 7 class container ships	33*	2,000	1972-1973
Maersk B-class	35-37	4,000-4,200	2006-2008

Table 3.1: Fast containerships [87] [176] (*) top speed = service speed

3.1.1. FastShip concept

The FastShip concept as discussed earlier for its nuclear application is a marine transport system that relies on a fleet of four semiplaning monohulls-geometry (SPMG) thought out in 2002. This was done by Thornycroft, Giles & Co. for FastShip Atlantic Inc. of Virginia with assistance of the MIT Department of Ocean Engineering for hull design and seakeeping simulation and the MIT Center for transportation studies in relation to market aspects. They are intended to travel from Philadelphia to Cherbourg in less than 4 days. This is made possible through a deep V-hull, relatively full waterplane, flare and wide transom as can be observed from figure 3.1. The FastShip’s prime movers consist out of 5 gas turbines that are coupled to five waterjets making an operating speed of 37.5 knots possible. In the conventional concept the fuel cost is significant due to the high speed and can lead to the design becoming unprofitable. This indicates the potential of nuclear propulsion because of a low fuel cost. The main particulars as well as a hull and profile view are depicted below [176].

Features	FastShip
LOA	262 m
B	40 m
D	/
T	10 m
Displacement	30,750 t
Deadweight	+/- 10,000 t
GT	/
TEU capacity	1,432 TEU
Installed power	250 MW in 5 gas turbines
Speed	37.5 kts
C _b	0.29

Table 3.2: Vessel characteristics FastShip [176]

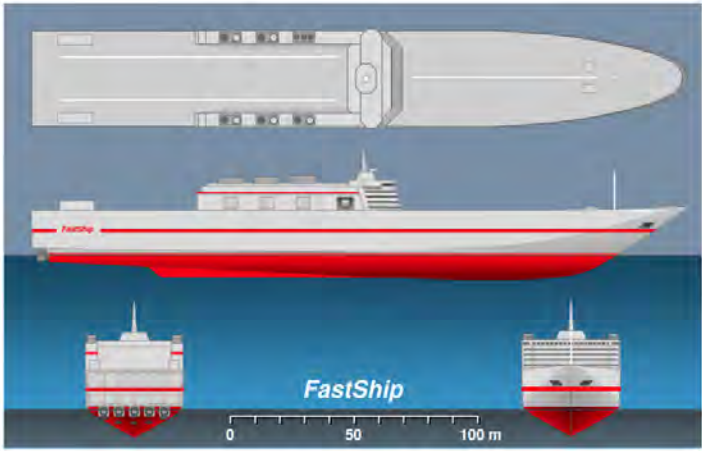


Figure 3.1: FastShip Profile and Hull Shape [176]

This concept design is limited in scalability because of its SPMG. Following the square-cube law the volume and planing area will not scale up in the same manner. This means the dynamic lift will not scale up the same way because this heavily depends on the planing area. Thus using this concept for a 20,000 TEU design will not result in a good concept vessel [56].

3.1.2. Sea-land class container ships



Figure 3.2: Sea-land and Mclean lead ship [20]

In the 1970s container shipping pioneer Malcom McLean and his Sea-land (SL) services made the assumption that speed would become a more important parameter than cargo capacity because of the low fuel oil cost and the lack of emission policy. A total of eight vessels were ordered at the Rotterdamse Droogdok Maatschappij (RDM) and a shipyard in Germany. The SL-7 series were designed to carry around 2,000 TEU which was a normal carrying capacity at that time. The design speed of 33 knots is what set them apart where a typical 26 knots was more conventional. This was achieved using two Foster-Wheeler boilers operating at 60 bar and 510 °C that provided steam to two GE MST-19 steam turbines that delivered a total of 120,000 shp which equals 89.52 MW [20]. These SL-7 series were capable of sailing from the US East Coast to Europe in 6 days and to the Persian Gulf in just 18 days.

Nevertheless, the **high fuel consumption** of the SL-7 series combined with the increase in fuel price due to the 1973 oil embargo resulted in high life cycle costs which endangered their commercial viability. In addition their **seakeeping** posed a problem to meet advertised transit speeds as the sea conditions of the Atlantic ocean would regularly slow down the SL-7 from 30 to 22 knots [135]. For the scope of this project the seakeeping will not be taken into account but should be accounted for in further research. In 1982 all eight container ships were sold to the US navy, here they became Fast Sealift Ships for the transportation of tanks, large-wheeled vehicles and helicopters. An overview of the main particulars is given below [20].

Features	SL-7
LOA	288.4 m
LBPP	268.4 m
B	32.16 m
D	19.510 m
T	9.144 m
Cb	0.5395
Displacement	43,618 t
Deadweight	29,829 t
GT	41.127
TEU capacity	1,968 TEU
Installed power	89.52 MW
Speed	33 kts

Table 3.3: Vessel characteristics SL-7 [20]

3.1.3. Maersk B-class



Figure 3.3: Maersk Boston [102]

The Maersk B-series were designed for rapid transportation of goods between the US West coast and China in a series of seven sister ships. These vessels were built on the core assumption that container shipping was booming between 2001 and 2008 due to the trade growth accelerated by China's

accession to the World Trade Organisation. This resulted in container lines, including Maersk to invest in vessels speed. The economic crisis in 2008 together with a doubling of the **fuel price** in 2010 and an **oversupply of container vessels** resulted in the lay-up of the Maersk B-class. Slow speed was no option for these series because of their narrow yacht-like hull that were only efficient at higher speeds [183].

Nevertheless they were innovative in design with a more streamlined hull and significantly smaller displacement compared to vessels of equal TEU. The installed engine was a Sulzer Wartsila 12RT-flex96C with an output power of 68.4 MW making them capable of sailing a service speed of 28.2 knots and top speed between 35-37 knots. This would equal the power of vessels twice their size sailing at 25 knots. The combination of the slender hull and large installed power resulted in a shift of the accommodation and machine room island towards the fore ship. Which is not seen in conventional panamax vessels. They were also fitted with fin stabilisers in order to prevent excessive rolling of the slender hull.

Maersk did not publish much information about these vessel series but through an interview with Hans Huisman more specific information was gathered and summarized below [160]. For further comparison the service speed of 29.2 knots will be used.

Features	Maersk B-series
LOA	293.83 m
LBPP	278.2 m
B	32.18 m
D	21.4 m
T	12.2 m
Cb	0.59
Displacement	65,700 t
Deadweight	53,634 t
GT	48,788
TEU capacity	4,000 TEU
Installed power	68.64 MW
Speed	29.2/35-37* knots

Table 3.4: Vessel characteristics Maersk B-series [160] [87] (*) top speed

As a side note on the B-class vessels it must be reminded that these series were designed as panamax vessels which restricted their width to 32.3 m. This leads to a disproportionate L/B ratio of 8.7 which is beneficial for higher speeds because of the reduction in wave making and viscous pressure drag resistance but increases the wetted area significantly and thereby the frictional resistance [81]. This is addressed in more detail when comparing these series with conventional container ships.

3.2. Relation with conventional container ships

A database constructed by C-Job naval architects containing 7,872 container ships was used to construct trend lines for conventional speed container ships. This was done in order to see where the container ships that were designed for higher speeds diverge from the conventional speed container ship design [72]. The FastShip concept is plotted in the trend lines for completeness but not discussed because of its SPMG not being fit for the intended design as discussed earlier.

3.2.1. Deadweight vs Displacement

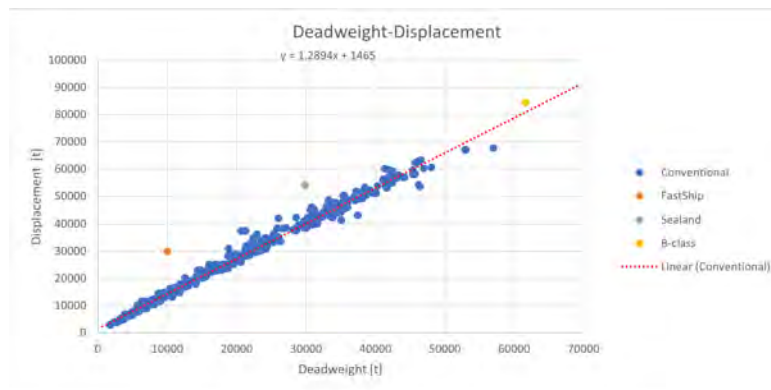


Figure 3.4: Deadweight vs Displacement (0-4000 TEU)[176][135] [183][72]

The Sealand series deadweight to displacement ratio is equal to 0.68 which is 9% lower than the conventional container vessels as seen on figure 3.4. If figure 3.2 is observed where one of the SL-7 series is displayed this can be explained by the sub optimal container distribution on board of these vessels. The container tiers above deck are limited to three which for conventional container design can be up to 8-9 tiers for special designs [36].

For the B-class vessels a value of 0.816 is found which lies within the trend of the conventional container ships and is plotted on figure 3.4. These container vessels typically had five tiers on deck which explains their better fit with the conventional trend. From this comparison it can be seen that for higher speed the ratio between deadweight and displacement stays rather constant with the exemption of the Sealand series [135] [72].

3.2.2. Main particulars

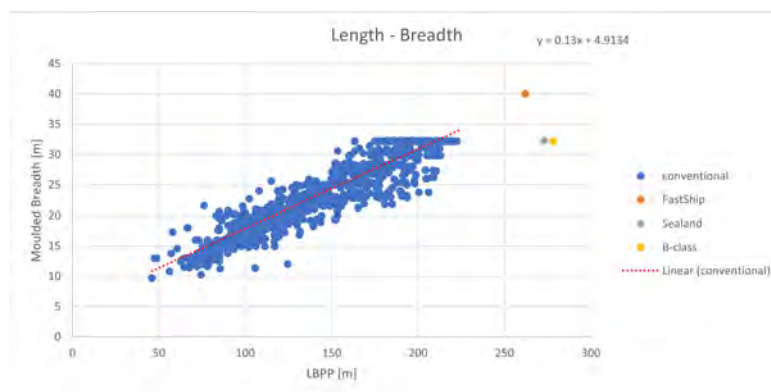


Figure 3.5: Length vs breadth (0-4000 TEU)[176][135] [183] [72]

From figure 3.5 a linear trend between moulded breadth and length between perpendiculars is observed for the conventional container vessels ranging from 0 to 4,000 TEU. For the Sealand and B-class a drop in B/L is seen which is explained by resistance and visually explained on figure 3.6 where the area of interest is indicated on the right side of the red line [72]. For higher speeds the relative contribution of the wave making resistance to the total resistance becomes more dominant. As these ships are designed for higher speeds than conventional speed container ships the B/L ratio becomes lower due to an increase of ships length which reduces the wave making resistance. The effect on the viscous resistance is two fold. The frictional resistance will increase due to an increase in wetted area. The viscous pressure resistance will reduce due to a more slender hull design that reduces the normal component of the viscous resistance.

A lower B/L ratio for higher speeds will thus result in an overall decrease of resistance because of the less dominant role of the frictional resistance in that area [172]. This area being indicated by the red line on figure 3.6. A lower B/L or higher L/B should thus be selected for a high-speed variation as a first estimate when compared to the conventional container ship.

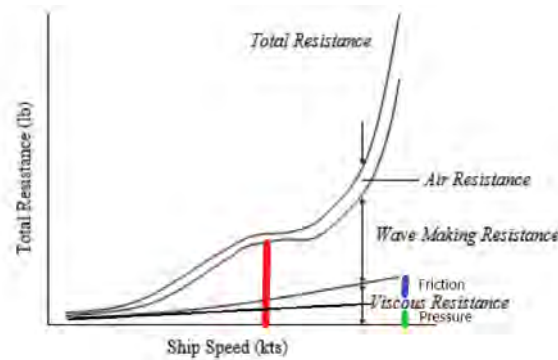


Figure 3.6: Resistance components with increasing speed[172]

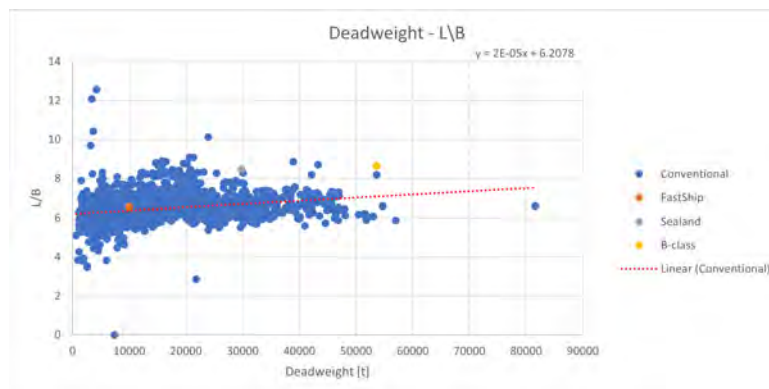
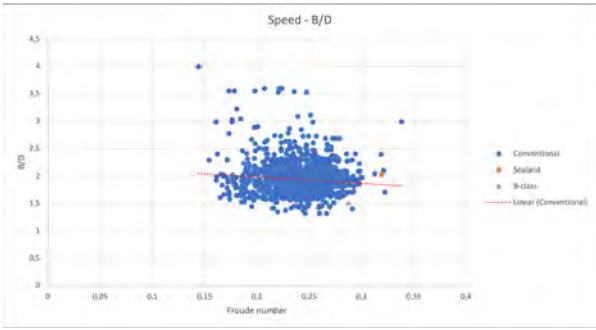


Figure 3.7: Deadweight vs L/B (0-20,000 TEU) [176][135] [183][72]

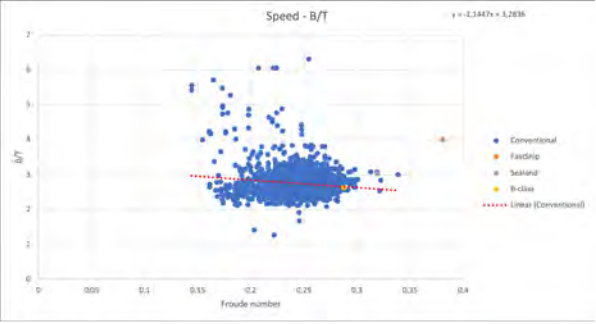
When deadweight is compared to the L/B ratio only a slight increase is seen when deadweight is increased which is explained by the gradual growth of both the length and breadth of container vessels for higher deadweight values to be able to carry more TEU. For the high speed vessels the same trend as in figure 3.5 is seen, namely the increase in the ratio L/B compared to the conventional trend.

The breadth to depth ratio for container vessels is typically 2.0 as is verified by the C-Job database on figure 3.8a and also seen for the Sealand $32.26/15.83 = 2.04$ but seen lower for B-class $32.18/21.4 = 1.5$. This ratio stays rather equal over the froude spectrum.

The same trend can be seen for the B/T ratio which is on average equal to 3. This is explained due to stability considerations as B has a large impact on BM. As is also stated by Watson's design equations. As a first estimate for a high-speed variation the conventional ratio's can be used [101] [72].



(a) Froude number vs B/D (0-4000 TEU)



(b) Froude number vs B/T (0-4000 TEU)

Figure 3.8: Froude number vs Midship section [176][135] [183][72]

3.2.3. Cb vs speed

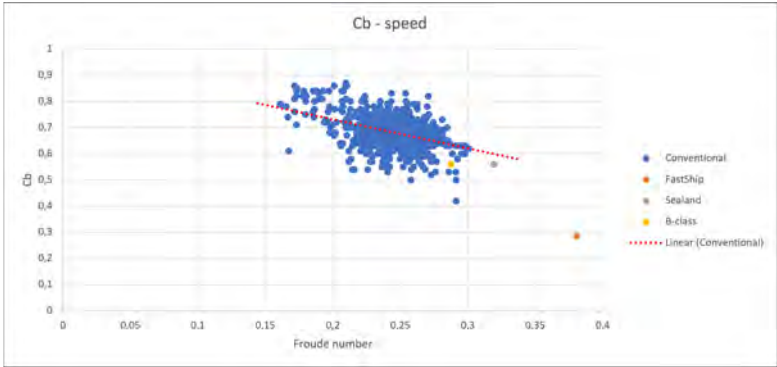


Figure 3.9: Froude number vs Cb[176][135] [183][72]

If C_b is related to froude number a decrease is observed. This is normal because a smaller C_b gives a more slender ship design which is needed for higher froude numbers due to an increase in wave making resistance as discussed before. The same trend for conventional as for the high speed vessels is seen, the block coefficients for Sealand and B-class are given as stipulated in table 3.3 & 3.4 [72].

3.2.4. TEU vs Installed power

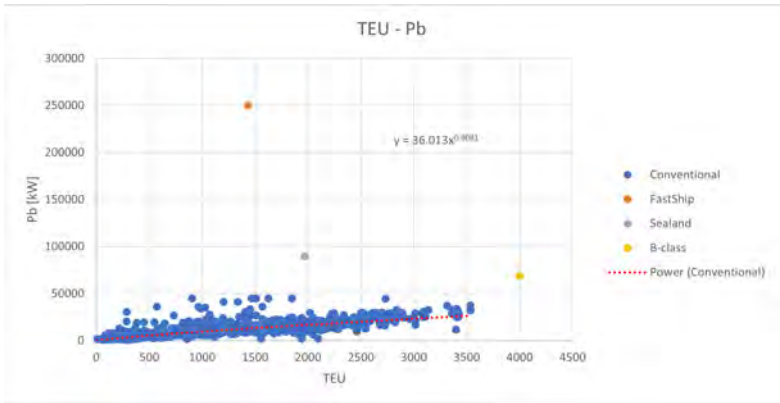


Figure 3.10: TEU vs Pb (0-4000 TEU)[176][135] [183][72]

It can be seen from figure 3.10 that for conventional container ships the power per TEU gradually increases but for the high-speed applications the power per TEU lies significantly higher than the trend. This can be explained by the higher speed which is linked to an increase in total resistance that translates in a higher installed power [72].

Thus in order to make an initial resistance estimation a suitable reference should be selected. This with the view to keep the initial resistance as low as possible and making no underestimation of the wave making resistance.

3.3. Chapter conclusion

In this chapter three vessels with increased operating speeds were introduced of which one concept design was disregarded due to its limitation in scalability but showed the potential of nuclear propulsion at higher speeds. The remaining two vessels were compared with conventional container vessels to evaluate possible differences in design parameters. First of all it was established that for higher speeds the deadweight to displacement, B/D and B/T ratio's remain rather equal when compared to conventional vessels. Secondly the L/B ratio increased and C_b decreased for higher speeds. These two factors are both explained by resistance. An increase in speed will increase the contribution of the wave making resistance which is decreased by increasing L/B ratio and decreasing the block coefficient. A side note was taken that the increase in length contributes to a larger wetted area which increases the frictional resistance to a certain extent but is counteracted by the decrease in wave making and viscous pressure resistance. This should however be evaluated in accordance with the calculated froude number.

A larger variation was seen in the relation between installed power and number of TEU which indicated that the installed power per TEU for speeds above 30 knots is significantly higher than the conventional trend.

The found differences between high-speed container vessels and conventional ones indicate that for ratio's deadweight to displacement, B/D and B/T conventional vessels don't diverge significant for higher speeds. For the ratio L/B , C_b and installed power however, a suitable high-speed reference vessel must be selected in order to enter the first iteration with no underestimation of the wave making resistance. For this the Sealand or Maersk B series can be used. Where the main rationale is to make a first educated guess for the resistance curve in order to couple speed to cost.

4

Relation speed & propulsors

Chapter introduction

This chapter is dedicated to answer the sub literature question:

”Which propulsors are fit for which speed intervals using the existing power plant?”

Using the power plant proposed by K.Houtkoop where the propulsors are driven by electric motors [71] an evaluation is made for which speeds standard propellers, high-speed propellers or waterjets are the best option to implement. This is done to be able to select a propulsor or set of propulsors when the economic speed for the nuclear concept vessel is determined.

4.1. Conventional submerged propellers

4.1.1. General application

Traditionally a ship is propelled by a submerged propeller. In most conventional cases this is applied as a single-screw or twin-screw plant. More than two propellers are sometimes found on naval ships or high speed ferries [106]. Generally propellers are divided into two main categories being a fixed pitch propeller (FPP) and a Controllable pitch propeller (CPP). On figure 4.1 the development of the power output for both propulsor types can be seen up until the year 2000. Waterjets are also included in the graph but will be discussed later. To compare the FPP and CPP in greater detail general characteristics, advantages and disadvantages of both concepts are summarized in table 4.1.

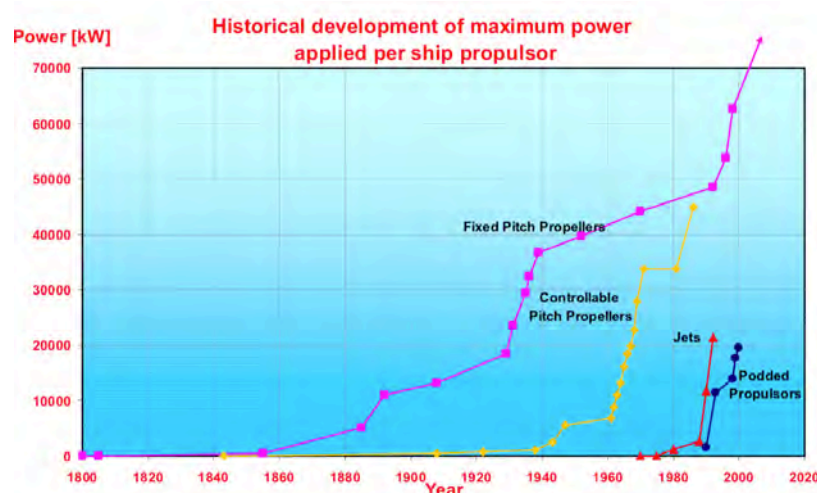


Figure 4.1: Max power per ship propulsor through time [59]

Propeller type	FPP	CPP
General characteristics	<ul style="list-style-type: none"> • Generates thrust dependent on direction of rotation • Main requirements for ships are simplicity and robustness • Used in 90% of container vessels 	<ul style="list-style-type: none"> • Generates thrust depending on the pitch setting • Main requirements for ships are manoeuvrability and dynamic position capabilities
Advantages	<ul style="list-style-type: none"> • Less vulnerable to damage • Lower initial cost • Lower maintenance cost • Higher propulsion efficiency due to smaller hub diameter 	<ul style="list-style-type: none"> • Can propel ship at all speeds without stopping engine • Easy astern operation • Improved efficiency for changing power demands • Easily combined with shaft generator • Easier maintenance if one propeller blade is damaged
Disadvantages	<ul style="list-style-type: none"> • In adverse weather the max RPM can be reached which could endanger propulsion • Limited range of RPM and power for manoeuvring 	<ul style="list-style-type: none"> • System vulnerability due to hydraulic components and sealing rings • High price • Lower propeller efficiency due to hub diameter

Table 4.1: Comparison FPP and CPP based on [39][106][59][60]

Based upon figure 4.1 and table 4.1 it can be concluded that out of the FPP and CPP, the FPP is the best candidate for the project scope. A container ship is known to have a rather constant operating profile and limited manoeuvring characteristics while needing a lot of propulsion force to propel itself. A CPP would not match the mission profile [106] and most electric propulsion lines use FPP because electric motors with variable speed drives are able to provide maximum torque at every speed and also run in reverse [55]. In addition the open water efficiency of a FPP is generally higher.

4.1.2. Effective speed domain

For the effective design of a propeller three key considerations should be accounted for namely: propeller efficiency, cavitation behaviour and pressure pulses. A typical range of propeller efficiency lies between 55 - 75% but in order to maximize this factor cavitation needs to be discussed [38]. Cavitation is a process that comes into existence at the suction side of the propeller where a low pressure region is situated due to the high velocity of the water. If this pressure is lower than the vapour pressure of water, water vapour bubbles are created and as these travel to the pressure side of the propeller they will implode which can have multiple implications. Nevertheless every propeller cavitates during normal operation. Acceptable versions are stable suction side sheet cavitation, tip vortex cavitation and hub vortex cavitation. The kinds of cavitation that should be mitigated are unstable cloud type on the suction side, bubble, blade foot, pressure side and prop-hull vortex cavitation. These version of cavitation can lead to erosion of the propeller, excessive underwater noise radiation and pressure pulses. The creation of the previously mentioned pressure pulses are also a product of cavitation clouds which can lead to inboard vibrations (low frequency) or noise (high frequency) [60]. When designing a propeller, cavitation behaviour and propeller efficiency tend to work against each other as for example an increase in propeller diameter has a positive effect on the efficiency but will decrease the distance between hull and propeller which could lead to excessive pressure pulses. This should be taken into account as for higher vessel speeds cavitation can become uncontrollable. Measure to minimize cavitation are among

others propeller tip unloading, increasing the blade area ratio, a wake adapted design, pressure side rake, increasing the skew or lowering the thrust loading coefficient by implementing a second, third or even fourth propeller [39]. The amount of propellers needed and their minimum blade area ratio to avoid excessive cavitation can be estimated by the Keller criteria which calculates a minimum blade area ratio to avoid excessive cavitation [90].

Energy saving devices (ESDs) could also be used to decrease the formation of cavitation. A possible option is for example the wake equalizing duct (WED). A WED consists of two half ring ducts fitted above the center of the propeller shaft that create a better inflow velocity field which improves cavitation behaviour and also increases the propeller efficiency by approximately 4% [61]. For high-speed application the stern shape of a container vessel will be hydrodynamically optimized thus the inflow velocity field might not be able to be improved as much. Thus the previously stated 4% could be an overestimation.

The effective speed domain of conventional propellers found in literature lies between 0 and 33 knots [38] [16] [116]. This trend can be seen on figure 4.5a, 4.5b and 4.5c. Especially for full displacement vessels, propellers will have a larger efficiency and are therefore conventionally used on them as can be seen from the Sealand series and Maersk B-class which had a service speed of respectively 29.2 and 33 knots. It is however true that propeller designs have to be modified to cope with significant cavitation effects such as erosion and pressure pulses for speeds already above 25 knots. Measures to mitigate this phenomena were already discussed. This rationale is also confirmed by Tom Terwisga who stated that it will always be more efficient to propel a ship with propellers until the ultimate cavitation limit is reached which can be evaluated for a preliminary design with the previously discussed Keller criteria. For propellers at higher speeds alternative propeller design as the Wageningen B-series can also be selected an example of this are the Gawn-burrill series which are modified for faster vessels [60]. This means the propellers are altered in design with a focus on minimizing cavitation effects.

4.1.3. Power range

From figure 4.1 it can be seen that the maximum power per propeller lies around 70 MW which is also seen on the Vessel Emma Maersk which has a single propeller for propulsion and an installed capacity of 80 MW where hotel load is included [72] [60]. Higher ranges are possible if the USS Gerald Ford aircraft carrier is considered which has an installed capacity of 600 MW_e delivered by two PWRs to four shaft lines. Assuming 20% of hotel load this roughly results in a power per propeller of 120 MW [111]. This is however an unconventional case.

4.1.4. Parallel application

If a second, third or even fourth propeller should be implemented or not depends on a number of variables. The first factor is propeller efficiency that is depicted on an open water diagram. If we look at an example where amount of power, speed and diameter are given two scenario's are possible.

1. The propeller diameter can be chosen in such a way that it is heavily loaded and its operating point is situated left of the open water efficiency top. Replacing the propeller by two propellers with the same diameter will result in a shift of operating point towards the efficiency top and result in a significant decrease of load on the propellers. This scenario is depicted by the green lines on figure 4.2
2. The propeller diameter can also be chosen in such a way that the thrust loading is lower and situated near the top of the efficiency curve. If here two propellers are chosen with the same diameter instead of one the efficiency will drop. This scenario is depicted by the yellow lines on figure 4.2. Alternatively in this scenario two propellers with a smaller diameter can be designed in order to increase the open water efficiency.

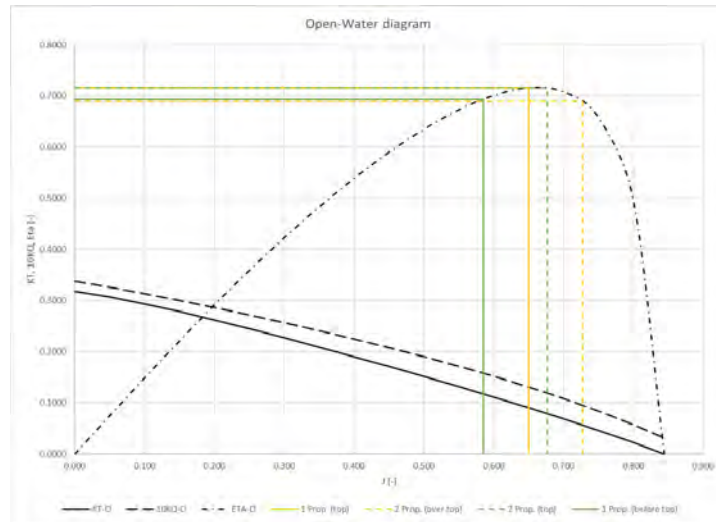


Figure 4.2: Effect on open water efficiency for single or twin screw (By courtesy of MARIN)

The positive effect on the open water efficiency is also shown by a study from Man Solutions where a twin screw application on a 20,000 TEU container vessels sailing 22 knots resulted in a 6-8% increase of efficiency due to the lower thrust loading and lower wake factor due to positioning of the propellers [104]. Another important reason to switch to multiple propellers is the available space at the stern of the vessel. Theoretically a propeller can be as large as needed but this is mainly restricted by the propeller hull clearance and subsequent pressure pulses. Thus if one propeller can not deliver the required thrust by itself at a certain limit diameter, two or even three propellers can be opted for. With the implementation of multiple propellers alteration in the ship design such as additional skegs or exposed shaft lines come into play together with additional costs. A tool to determine the amount of propellers in function of cavitation limits is the Keller criteria as discussed before which can be used in a preliminary design stage only. An example where multiple propellers are used on a full displacement vessel is the USS Gerald Ford aircraft carrier which is equipped with four shaft lines and can reach speeds above 30 knots [111]. This shows the described theory in practice and is depicted on figure 4.3.



Figure 4.3: USS Gerald Ford propulsor layout [111]

4.2. Waterjets

4.2.1. General application

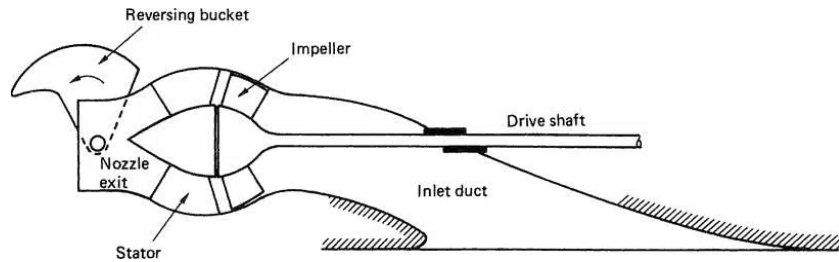


Figure 4.4: USS Gerald Ford propulsor lay-ou [38]

Waterjets have a broad range of applications from small sport boats to large megayachts, high-speed ferries or naval ships which can be classified as light displacement ships. They differ in working principle compared to conventional propellers as they try to maximize the velocity difference between in- and outlet rather than minimizing it and focus on pressure differences [38]. The working principle is depicted on figure 4.4. The impeller draws in seawater through an inlet which is usually a flat bottom. The water is accelerated by the impeller and pushed through the nozzle. The nozzle converts the high water flow into a waterjet which is used for propulsion [39]. This acceleration of the water can also be seen as a change in momentum which creates thrust resulting in propulsion [38]. Essentially a waterjet can be seen as a pump which is placed in a very short pipe. If a pump is compared to a propeller they do not show the same limits. An efficiency of 90% or more are plausible figures for pumps which lies in contrast with the previously discussed propeller efficiency. However the overall efficiency of the waterjet consists out of more parameters that are discussed in the next section.

The conventional application is limited to semi-displacement hulls, planing hulls, fast catamarans and surface effect ships. All of these ships have the distinct feature of a very shallow draft and low payload which is not seen with conventional container vessels [116]. Examples of bigger scale use are the Freedom-class littoral combat ships (LCS) that are propelled by 4 Rolls-Royce/komewa 153SII/153BII waterjets connected to 2 Rolls-Royce MT30 36 MW gas turbines. The ship has a semiplaning steel monohull and can achieve 47 knots. The Independence-class LCS are also propelled by 4 waterjets but have a trimaran hull design [3].

4.2.2. Effective speed domain

For the effective speed domain of waterjets the overall propulsive efficiency of a waterjet should be analyzed which is given by:

$$\eta = \eta_0 \times \eta_{INT} = \eta_I \times \eta_{JS} \times \eta_{INT} \quad (4.1)$$

Where η_0 can be compared with the open water efficiency of a propeller and consists out of the ideal efficiency η_I and the system jet efficiency η_{JS} . η_{INT} is the interaction efficiency and can be related to the combination of the hull efficiency and relative rotative efficiency of a propeller. η_I depends on the thrust coefficient (see appendix C.1), η_{JS} accounts for the internal pump losses and is stated to be between 0.9-0.95. η_{INT} depends on the hull shape more specifically the L/B ratio. This efficiency is highly sensitive in the hump region (froude number around 0.4) as depicted in appendix C.1 [163].

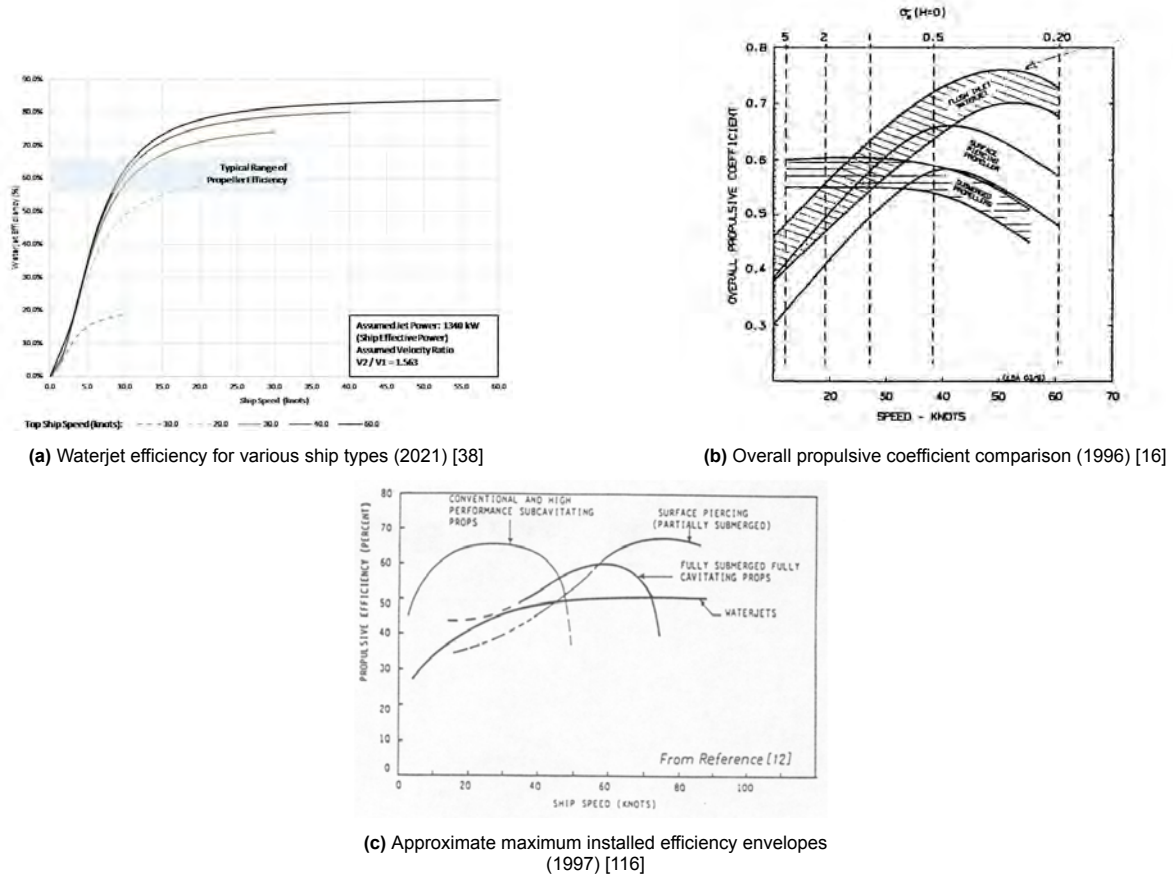


Figure 4.5: Propulsive efficiencies/coefficients

On figure 4.5 the waterjet efficiency (4.5a), overall propulsive coefficient (4.5b) and propulsive efficiency (4.5c) are depicted for waterjets. The waterjet efficiency depicted on figure 4.5a is plotted for six vessels with a different design speeds. The vessel sailing 30 knots surpasses the efficiency domain of conventional propellers [38]. On figure 4.5b the overall propulsive coefficient is depicted for waterjets, submerged propellers and surface piercing propellers. Here it is also observed that the waterjets are best used from 30 knots on wards [16]. On figure 4.5c the propulsive efficiency is plotted and here the optimal efficiency for waterjets is reached around 50 knots. Nevertheless, the point where conventional propellers decay in propulsive efficiency and waterjets still increase lies around 30 knots [116]. Despite the differences in absolute values of efficiencies or coefficients the same trend is seen in all three sources namely the 30 knots transition point where waterjets become interesting from an efficiency point of view.

The differences in absolute value could be due to the use of different formula. Other possible reasons were identified as:

- Differences in thrust loading coefficient which influences the ideal efficiency.
- Differences in inlet performance of the waterjet which can reduce the best overall efficiency to 59% [134]. This can be identified with the hull interaction efficiency which is further discussed in appendix C.1.
- Higher jet system efficiency due to new developments and differences in years of the publications.

Waterjets are seen to deal better with cavitation limits as seen on figure 4.5a & 4.5c this is explained by the impeller design partly but the major factor is the outlet nozzle of the waterjet that can be manipulated for higher speeds to mitigate cavitation effects in the pump housing. Nevertheless the effect of cavitation can still reduce the efficiency as seen on figure 4.5b where it goes down at approximately 50 knots. This

could be explained by the impeller design or faulty operation of the nozzle but no direct reason is given in the publication [16].

In conclusion it can be derived from figure 4.5a, 4.5b and 4.5c that the effective speed range for waterjets starts around 30 knots below this region their efficiency goes down sharply. This is explained by their inability to create enough momentum with limited water flow rates [38]. Their optimum efficiency within their speed range, ranges from 45% to 75% if the found literature is used. Where figure 4.5a is not used as an optimal efficiency as it is deemed too optimistic. The 75% upper boundary can be identified for high froude numbers starting from 0.6. This was evaluated in collaboration with T. Terwisga.

4.2.3. Power range

Wärtsilä currently provides the widest spectrum of waterjet power ranges. The ranges that are available at time of writing¹ are depicted on figure 4.6.



Figure 4.6: Waterjet power ranges [179]

Out of the anonymous interview with Kongsberg their largest waterjet came apparent to be the Rolls-Royce Kamewa VLWJ235 waterjet of 27 MW that was fitted on board of a Japanese passenger ferry with a LOA of 140m. It was stated that these Kamewa series were intended to extend their power level towards 50 MW per unit. These units are not yet available but they confirm the trend depicted on figure 4.1. A scaling exercise could thus be possible to obtain higher power levels of waterjets but a limit on cavitation is still present as the vapour pressure remains constant. As a guideline for waterjet scaling the parametric study of T. Terwisga could be used [163].

4.2.4. Parallel application

Waterjets are often used in parallel application. The most common combinations were explained by an associate of Kongsberg. They vary from a single waterjet to a maximum of four. Where from three waterjets onwards, one of the waterjets acts as a booster and can no longer be used to steer. The four waterjet application has two boosters instead of one. A study on the analysis of waterjet-hull interaction and its impact on the propulsion performance of a four-waterjet-propelled ship stated that the inner waterjets were more efficient than the outer waterjets due to the inflow of the water but this is also said to be highly influenced by the hull shape [58]. After a discussion with Wärtsilä, Marin and Dyckstra naval architects it is found that the main rationale for the amount of waterjets is the amount of available space in the transom.

¹February 2023

4.2.5. Marine application



Figure 4.7: Freedom class LCS waterjet system [3]

The application of waterjets on a larger scale is seen with the Littoral combat ships (LCS) as discussed before and seen on figure 4.7. Here two waterjets are used as boosters (inner) and two for manoeuvring (outer). After an anonymous interview with Kongsberg some additional design parameters for the implementation of a waterjet became apparent. First it was stated that for waterjets mass is a very important factor that can also be seen in the conventional use of waterjets for light displacement vessels. Secondly the waterjet outlet needs to be halfly submerged with regard to efficiency which implicates that the vessel needs to be correctly ballasted throughout operation. Thirdly waterjet propulsion on bigger ships is often not selected because of the influence of fouling that can greatly reduce speed and thereby the performance of the waterjet. For smaller ships this is easily mitigated because they can be lifted out of the water easily, for bigger ships divers or dry docking would be necessary which can be expensive. To integrate a conventional waterjet system requires a complex pumping arrangement that will result in a loss of displacement at the aft of the vessel. Waterjet propulsion systems are also seen as significantly heavier than the conventional propeller power plant. As a comparison one propeller of the USS Gerald Ford aircraft carrier weighs around 30 ton with a power per shaft of 120 MW. The biggest booster type waterjet of wärtsila capable of delivering 35 MW has a weight of 34 ton [179].

4.2.5.1 Voith linear jet

A possible solution to the displacement problem is the use of a new waterjet concept named the voith linear jet. It combines the working principle of a waterjet with the lay-out of a propeller as it is fully integrated in the hull as seen on figure 4.8 and does not require a complex pumping system as with conventional waterjet systems [27].



Figure 4.8: Voith linear jet integration [27]

4.3. High speed propellers

4.3.1. General application



Figure 4.9: High speed propeller layout [168]

High speed propellers in this report are considered as supercavitating propellers and surface piercing propellers. These kind of propulsors are generally used on small high speed craft and some naval applications as seen on figure 4.9.

4.3.1.1 Supercavitating propellers

As discussed before cavitation has a big influence on the operation of conventional propellers. Especially when ship speeds increase to values above 30 knots. In these cases the velocities along the propeller blade are so high that considerable cavitation is unavoidable. A possible solution to this problem is than to prolong the formed cavity so that it collapses far downstream from the propeller trailing edge. This principle is used with supercavitating propellers. The shape of the propeller blade is different from the conventional one as it is triangular shaped with a straight edge hereby the cavities that detach from the blade are often twice or three times the chordlength [90].

4.3.1.2 Surface Piercing propellers

A derivative of the supercavitating propeller is the surface piercing propeller where the propeller shaft is just above the free surface and the propeller itself is partly submerged. The leading edge is often skewed in order to minimize the impact force on the water when entering and exiting. The trailing edge is straight as well and the blade sections are similar to the ones of supercavitating propellers [90]. The difference with a supercavitating propeller is that the pressure in the cavity is not equal to the vapour pressure but the atmospheric pressure. This leads to a larger blade area ratio to produce the same thrust when compared to supercavitating propellers.

4.3.2. Effective speed domain

From figure 4.5c it is apparent that super cavitating propellers seem to become efficient at speed ranges above 50 knots [116]. This is because they only become efficient for very low propeller loadings where the thrust loading coefficient needs to be lower as 0.1. This poses a problem at lower speeds where the thrust loadings are higher [90].

The range for surface piercing propellers is comparable with supercavitating propellers. They do have additional losses due to the entering and leaving of the blade into the water [90]. Nevertheless it is possible that their efficiency is higher as seen on figure 4.5c [116]. Optimal efficiencies from 50 knots on wards varies between 60-65% for both discussed high speed propellers.

4.3.3. Power range

The power range found in literature is only applicable to small high-speed craft and ranges from 0-4 MW [146]. After consultation of T. Terwisga it became clear that scaling up the power level is possible but this would produce a significant amount of radiated noise when compared to conventional propellers which would not make these propulsors fit for large scale applications. As propeller noise is considered as one of the main contributors to commercial shipping noise especially under cavitating conditions which are applicable for both high speed propellers because of their cavitating nature [23].

In addition the scaling up exercise could lead to additional loss of thrust because the pressure on the suction side would not fall below the vapour or atmospheric pressure on such a large scale.

4.3.4. Parallel application

For parallel application a similar reasoning as for conventional propellers can be used. Thus depending on the chosen diameter and thrust loading two, three even four propellers can be opted for.

Surface piercing propellers are always used in twin screw arrangement with opposite turning direction because they produce a significant amount of side thrust when operated [90].

4.4. Comparison of propulsors

In table 4.2 an overview of the discussed criteria of each propulsor type is given.

	Conventional propellers	Waterjets	High speed propellers
General application	Small to large craft	Small to large craft	Small craft
Effective speed domain	0 - 33 knots	30 - ... knots	50 - ... knots
Optimum propulsive efficiency	55 - 75%	45 - 75%*	60 - 65%
Power Range	0-120 MW	0-50 MW	0-4 MW
Parallel application	YES	YES	YES
Scalability	YES	Limited	Limited

Table 4.2: Comparison of propulsors (*) 75% is only for high froude numbers around 0.6

For general application the conventional propeller is used most widely on large scale full displacement vessels with multiple examples in the industry such as the previously mentioned USS Ford Gerald. Second are the waterjets which are conventionally seen on luxurious yachts or small naval vessels. Examples of bigger scale use are the Freedom-class LCS and the independence-class LCS. The found applications do share the tendency to be light displacement vessels such as the semi-planing hull of the Freedom LCS or the trimaran of the Independence LCS as this is beneficial for the waterjet performance. The general application of high speed propellers is limited to small high speed craft in the commercial and naval sector.

The widest effective speed domain ranges from 0 to 33 knots and belongs to the conventional propellers where the end speed is based upon the practical example of the sealand vessels with propulsive efficiencies ranging between 55-75%. Hereafter conventional propellers have to cope with extensive cavitation effects such as pressure pulses and erosion which can also lead to thrust breakdown and a consequent loss in efficiency. Waterjets become interesting from 30 knots onward and not earlier due to the need of being able to create enough momentum with respect to water speed. Propulsive efficiencies found in literature range from 45-75%. Where the upper limit of 75% is only possible for Froude numbers around 0.6. However if there is the option to choose between a propeller or waterjet the propeller will always be more efficient taking into account cavitation limits of propellers. This is explained by the bigger diameter that is available for propellers when compared to the impeller diameter of waterjets which has a significant effect on the ideal efficiency. A possible option would be a hybrid propulsion line when the cavitation limit of propellers is reached as seen on the Ecstasy of Feadship were both propeller and waterjet are used in parallel [51]. High speed propellers only become interesting from 50 knots onwards due to their inability to cope with high thrust loadings. Their efficiency ranges from 60-65%.

The power range has a clear winner in larger scale application being the conventional propeller that was also fit in fourfold on the USS Gerald Ford where an estimation of 120 MW per propeller was

made. Waterjets come in second with the Kamewa series that were intended to extend their power level until 50 MW. Further scaling up of the power level would be possible keeping in mind a cavitation limit that is depicted in parametric models [163]. The high speed propellers were only found for relatively low power levels. Further scaling up of these propellers would be possible but could lead to excessive radiated noise due to the cavitating nature of both propellers and consequent loss of thrust because the pressure level at the suction side of these propellers could not be brought lower than the vapour/atmospheric pressure.

Parallel application is possible for all propulsors types where for surface piercing propellers a contra-rotating twin screw arrangement is essential to counter the produced side thrust. Reasons for parallel application were identified as a means to lower the thrust loading coefficient and spacial considerations in terms of hull clearance with respect to propellers or available space in the transom when waterjets are used.

For waterjets in particular some differing aspects on marine implementation were found when compared to conventional propellers. First waterjets their outlet needs to be halfly submerged in order to function properly. Secondly fouling on the vessel hull can result in a large loss of hull interaction efficiency which can only be removed by divers or when in dry dock. Thirdly the weight/power ratio of a waterjet was found to be 0.97 t/MW compared to 0.25 t/MW for a conventional propeller excluding the shaft for both applications. Lastly the installation of a conventional waterjet system results in significant loss of displacement aft of the vessel. As a solution to the draft and displacement problem the voith linear jet was introduced as a new concept.

4.5. Chapter Conclusion

In this chapter three main groups of propulsors were analyzed on the basis of general application, effective speed domain, power range and parallel application. These were conventional propellers, waterjets and high speed propellers.

Out of this comparison came that for the range from 0 - 33 knots conventional propellers are the best option. Their main constraints are excessive cavitation effects that can result in pressure pulses, erosion and thrust breakdown.

Waterjets are mainly used from 30 knots on wards due to their inability to produce enough momentum at lower water speeds. It is however found that when conventional propellers are still an option they should be selected because they will result in a higher propulsive efficiency due to higher available diameters but hybrid solutions could also be possible when necessary. Scaling up of waterjets beyond the stated power level could result in cavitation problems. Additionally, effect of hull fouling, specific operating draft, loss of aft displacement and substantial weight should be taken into account when implementing waterjets.

From 50 knots on wards high speed propellers can be used, this is because they can only handle low thrust loadings ($C_t < 0.1$). Scaling these propellers up to the required power level could result in a high production of radiated noise and loss of thrust which makes them unsuitable for the intended design.

This way a preliminary framework is constructed for the selection of propulsors based upon vessel speed.

5

Economic speed determination

Chapter introduction

This chapter is dedicated to answer the sub-research question:

”Where does the economic speed for a high-speed nuclear container vessel lie?”

In this chapter the first step of the first iteration is made for the 20,000 TEU nuclear container vessel starting from model vessel Maersk B due to speed and spatial considerations. The most suitable resistance prediction method is selected after an in-depth comparison with the Maersk B as starting point. This input is used in the speed model to determine an initial realistic design speed to be used for further design variations in order to improve resistance and take into account real life constraints on main dimensions.

5.1. Definition of concept vessel

5.1.1. Model ship selection

As discussed in chapter 3 when the speed is nearing hull speed the wave making resistance becomes dominant. For this reason two high-speed container vessel were discussed being the Sealand and Maersk B series. This in order to select the best model ship for the 20,000 TEU concept vessel for higher speeds. Main data of both vessels is displayed in table 5.1 for comparison.

	Sealand	Maersk B
Installed Power	90 MW	69 MW
Design speed	33 knots	29.2 knots
Prime mover	Boilers with steam turbines	Diesel engine
Building year	1970	2006
Main dimensions (LPP,B,T)	272.8/32.26/10.61 m	278.2/32.18/12.2 m
TEU capacity	2,000 TEU	4,000 TEU
Froude number	0.32	0.29

Table 5.1: Comparison of high-speed model vessels [135][183]

Out of the two model vessels the Maersk B is chosen because of several considerations. First more effective use of space when the amount of containers is considered. Secondly, the Maersk B is equipped with a diesel engine which has a higher power density than boilers coupled to steam turbines which is used on board of the Sealand. This is also true for a nuclear prime mover as a volume saving of 67% was stated in previous study which makes Maersk B the preferred choice [71]. This was however in a like for like replacement scenario.

Starting from the Maersk B a scaling factor is determined based on TEU size as depicted in the following formula:

$$\lambda_L = \left(\frac{20,000}{4,000} \right)^{\frac{1}{3}} \quad (5.1)$$

This factor is used to determine the initial concept design of the 20,000 TEU container vessel in terms of length between perpendiculars (LPP), width (B) and draft (T). Using the scaled LPP which is deemed equal to the length of the waterline (LWL) the Froude number of the Maersk B and nuclear concept vessel is kept constant which leads to a design speed of 38.18 knots for the concept design. By keeping the Froude number constant the resistance prediction will be accurate up until the calculated design speed. Where no underestimation of the wave making resistance is made. It should be noted that the design speed will be re-evaluated by the economic speed model in section 5.3.

The initial main particulars of the concept vessel are depicted in table 5.2. It should be stated that this gives a good initial starting point for the design but as the Maersk B was a panamax vessel its width might not be optimized for resistance. This design consideration is further addressed in section 6.1, as well as real-world constraints.

Scale factor	1.71
LOA	502.44 m
LPP = LWL	475.72 m
B	55.03 m
T	20.86 m
Displacement	328,500 t
C_b	0.59
Design speed*	38.18 kts
Froude number	0.29

Table 5.2: Initial main dimensions of 20,000 TEU nuclear concept vessel (*) based on froude number

5.1.2. Resistance prediction method selection

In order to make a good estimate of the resistance several prediction methods are discussed. To evaluate which prediction method would be most suitable to use for the Maersk B and in extension the 20,000 TEU nuclear concept vessel several prediction methods are compared on the basis of speed application, restrictions in main dimensions and hull form. Out of this comparison the most suited prediction method will become apparent. As the reference ship is a displacement type hull a selection for the resistance predictions of this type of hull is made. These include but are not limited to Holtrop & Mennen, Van Oortmerssen, Fung and Compton. In addition the prediction method of Marwood & Bailey and the MARIN fast displacement hull series are also discussed as its application concerns high speed displacement hulls.

For completeness the three main factors where the total resistance consists of are depicted below:

$$R_{total} = R_F + R_V + R_W \quad (5.2)$$

where:

- R_F = frictional resistance
- R_V = viscous pressure resistance
- R_W = wave making resistance

In the discussed resistance methods all three of these components are included but may appear in different format. For each method the total resistance is expressed in the sub-components that the method takes into account. The extra resistance components outside the three discussed above may differ per method as explained in the following paragraphs.

5.1.2.1 Holtrop & Mennen (H&M)

To estimate the resistance of displacement type ships Holtrop and Mennen is considered to be one of the most used and well known prediction methods. The total resistance prediction consists out of following factors:

$$R_{total} = R_W + R_V + R_{Cor} + R_{App} + R_{Air} \quad (5.3)$$

Where R_W is the wave making and breaking resistance which is caused by the generation of free surface waves and includes the bulb and transom components. In other resistance prediction methods R_w is included in the residuary resistance R_R together with the viscous pressure resistance, spray and eddy making resistance. Holtrop & Mennen formulates this differently and has no record of including spray and eddy making resistance. R_V is the viscous resistance meaning both frictional and pressure resistance. It takes shape by means of a form factor k where $R_V = (1+k)R_F$ with R_F being the frictional resistance. Holtrop & Mennen calculates R_F independently using the ITTC' 57 ship-model correlation line or the Schoenherr friction line [4]. That correlates the Reynold number to a dimensionless frictional resistance factor of a flat plate, the form factor k then accounts for the 3D shape of the vessel. R_{Cor} is the model-ship correlation resistance [68]. It accounts for an increase in resistance between model and ship due to hull roughness and inaccuracies of the model test techniques and subsequent extrapolation methods. It is stated that this margin can account for about 10% of the calculated total resistance [67]. R_{APP} is the appendage resistance and R_{air} is the air resistance for the above-water hull and superstructure.

The prediction method is based on a regression analysis of 147 ship models and 82 trial measurements of 46 new ships. This includes a vast range of vessels namely tankers, bulk carriers, general cargo, fishing vessels, tugs, container ships, frigates and others. This is what gives it its wide applicability. According to Lothar Birk, author of fundamentals of ship hydrodynamics, Holtrop & Mennen is the only method that uses the ITTC form factor k which improves the accuracy of the speed-power predictions on the basis of model tests. As this form factor takes into account the effect of a three-dimensional hull form on the frictional resistance [129]. The applicability of Holtrop varies for different ship types but an extended overview is found in [142] and depicted in Table 5.3 [67].

Ship Type	Max Fn	C_p	L/B	B/T
Tankers, bulk carriers	0.24	0.73-0.85	5.1-7.1	2.4-3.2
Trawlers, tugs	0.38	0.55-0.65	3.9-6.3	2.1-3.0
Container ships, destroyers	0.45	0.55-0.67	6.0-9.5	3.0-4.0
Cargo liners	0.30	0.56-0.75	5.3-8.0	2.4-4.0
RoRo Ships, Car ferries	0.35	0.55-0.67	5.3-8.0	3.2-4.0

Table 5.3: Limitations of Holtrop & Mennen prediction method [142]

5.1.2.2 Van Oortmerssen (V.O.)

Van Oortmerssen is based upon a regression analysis of 93 models of tugs and trawlers. Where the total resistance consist out of the following components:

$$R_{total} = R_R + R_F + R_{Cor} + R_{App} + R_{Air} \quad (5.4)$$

As can be seen from the equation above Van Oortmerssen does not calculate the wave making resistance separately as it is included in R_R as well as the viscous pressure resistance. It also makes no use of a form factor but only calculates the frictional resistance using the ITTC'57 friction line [4]. The full publication of Van Oortmerssen is not found publicly available but its limitations are found in an online PIAS manual and depicted below.

Ship Type	Max Fn	C _p	L/B	B/T
Trawlers & tugs	0.5	0.5-0.73	3.0-6.5	1.9-4.0

Table 5.4: Limitations of Van Oortmerssen prediction method [107]

In addition this method has a limitation in volume of 3000 m³ and a max length between perpendiculars of 80 m [107].

5.1.2.3 Marwood & Bailey (M&B)

Marwood & Bailey is based upon the results of systematic series test of fast round bilge displacement type model hulls. Vessels that are covered in this prediction method are patrol vessels, launches, work and river boats and destroyer type vessels like corvettes or frigates. These series of tests were carried out to widen the applicability range of these types of vessels on the basis of length-displacement ratio. It covers both frictional and residual resistance as stated in formula below:

$$R_{total} = R_R + R_F \quad (5.5)$$

Where the R_R includes wave making, breaking, spray, eddy making and viscous pressure resistance. R_F includes the frictional resistance calculated using the ITTC'57 friction line. Nevertheless, no form factor is used and R_{Cor} , R_{Air} or R_{App} are also not included. The input values for this resistance method are limited to length and width of the waterline and corresponding displacement. Its limitations are depicted below [108].

Ship Type	Fn	M*	L/B	B/T
Work boats, naval - and patrol vessels	0.3-1.1	4.5-8.5	3.8-7.5	1.9-11

Table 5.5: Limitations of Marwood & Bailey prediction method (*) length-displacement ratio [108]

5.1.2.4 MARIN systematic series fast displacement hulls (MFDH)

The MARIN systematic series is build around a parent model by varying the L/B, B/T and block coefficient. This resulted in 33 hull forms that were build and tested in calm water up to a maximum speed of Froude number 1.14. 24 of these hull forms were also tested in head waves which is contrary to most systematic series as these are mainly carried out in calm water. A regression analysis has also been carried out to allow interpolation between the obtained results. The components of the total resistance are depicted in following formula:

$$R_{total} = R_W + R_F + R_{App} + R_{Air} \quad (5.6)$$

Where again no use is made of the form factor or computation of the R_{Cor} . The viscous pressure resistance in this case is included in the wave making resistance R_W . The limitations of the prediction method in main parameters are depicted below [86].

Ship Type	Max Fn	C _b	L/B	B/T
Frigates	1.14	0.35-0.55	4-12	2.5-5.5

Table 5.6: Limitations of MARIN fast displacement hulls [86]

5.1.2.5 Compton

Compton is a resistance prediction algorithm designed for coastal patrol, training or recreational powerboat type hull forms that have a transom stern and operate in the displacement or semi-planing regimes [4]. Its resistance components are depicted in the formula below:

$$R_{total} = R_R + R_F + R_{Cor} + R_{App} + R_{Air} \quad (5.7)$$

As can be seen from the equation above Compton does not calculate the wave making resistance separately as it is included in R_R as well as the viscous pressure resistance. It also makes no use of a form factor but only calculates the frictional resistance using the ITTC'57 friction line [4]. Its limitations are stated below.

Ship Type	F_n	C_p	L/B	B/T
Coastal patrol- & powerboats	0.1-0.6	/	4-5.3	/

Table 5.7: Limitations of Compton prediction method [4]

5.1.2.6 Fung

Fung is a resistance prediction algorithm and applicable for displacement ships with transom stern hull forms. This prediction method is mainly used instead of Compton when the vessel gets to big. The regression analysis used for this algorithm is based upon 739 models test carried out at the David Taylor model basin [4]. Its resistance components are depicted in the formula below:

$$R_{total} = R_R + R_F + R_{Cor} + R_{App} + R_{Air} \quad (5.8)$$

As can be seen from the equation above Fung does not calculate the wave making resistance separately as it is included in R_R as well as the viscous pressure resistance. It also makes no use of a form factor but calculates the frictional resistance using the ITTC'57 friction line [4]. Its limitations are stated below.

Ship Type	F_n	C_p	L/B	B/T	C_{wp}
Transom stern displacement ships (TSDS)	0.13-0.91	0.53-0.77	2.52-17.94	1.70-10.21	0.66-0.84

Table 5.8: Limitations of Fung prediction method [4]

5.1.2.7 Pre-selection of resistance prediction methods

Making use of the main parameters for the model vessel Maersk B depicted in table 5.9 a pre-selection of the resistance prediction methods can be made.

Feature	Maersk B
Lwl = LPP	278.2 m
B	32.18 m
T	12.2 m
Δ	65,700 t
C_b	0.6
C_p^*	0.59
C_{wp}^*	0.8
Shiptype	Containership

Table 5.9: Main parameters Maersk B [4] [183] [160] (*) estimated by MAXSURF

Feature	Maersk B	H&M	V.O.	M&B	MFDH	Compton	Fung
F_n	0.3	0-0.45	0-0.5	0.3-1.1	1.14	0.1-0.6	0.15-0.91
L/B	8.97	3.9-9.5	3.0-6.5	3.8-7.5	4-12	4-5.3	2.52-17.94
B/T	2.64	2.1-4.0	1.9-4.0	1.9-11	2.5-5.5	/	1.70-10.20
M^*	4.52	/	/	4.47-8.5	/	/	/
C_b	0.6	/	/	/	0.35-0.55	/	/
C_p	0.59	0.55-0.85	0.5-0.73	/	/	/	0.53-0.78
C_{wp}	0.8	/	/	/	/	/	0.66-0.84
Shiptype	Containership	Various	Trawlers/Tugs	Naval	Naval	Power boats	TSDS

Table 5.10: Comparison table of discussed methods with model vessel Maersk B (*) $M = Lwl/\nabla^{1/3}$

Out of the comparison table above three resistance prediction methods are disregarded being V.O., MFDH and Compton. V.O.'s reach for L/B ratio's only goes until 6.5 plus the maximal waterline length of these systematic series is 80 m. In addition the series is based upon trawlers and tugs so not deemed fit as a prediction method. MFDH is based upon frigates which also explains its low reach regarding C_b . The possibility to use MFDH is not publicly available but was requested at DAMEN and carried out by an anonymous employee. Out of this prediction came that the Maersk B had a too large displacement. The program was only able to predict the resistance at half the displacement. Thus also not identified as suitable prediction method. Lastly Compton has the lowest reach of all prediction methods regarding L/B ratio which is explained by its applicability to power boats and recreational craft.

The three resistance prediction methods that remain and are further investigated are H&M, M&B and Fung. This is because of their wide applicability and close matching with the model vessel Maersk B. The L/B reach of M&B lies outside the one of the Maersk B but it must be kept in mind that the Maersk B was a panamax vessel thus its width might not be optimized for resistance but to fit the panama canal. Therefore Marwood & Bailey is also kept as a possible resistance prediction method as it still has an upper bound for L/B of 7.5 which is high compared to V.O. and Compton.

5.1.2.8 Final selection of resistance prediction method

To select the best possible resistance prediction method two different approaches are compared to the outcome of the different resistance prediction methods. First a propeller calculation is carried out using Propcalc with as input:

- $D_{\text{propeller}} = 8.55 \text{ m}$
- $\eta_{\text{shaft}} = 0.99$
- $P_b = 68,640 \text{ kW}$

- Propeller rpm = 105 (estimated)¹
- Thrust deduction factor (t) = 0.15 [28]
- Wake factor (w) = 0.2 [28]
- Design speed = 29.2 knots
- B4-70 (estimated)

Out of this calculation a total resistance of 3,130 kN resulted with an open water efficiency of 65% at the design speed. Secondly a propulsion chain calculation was made starting from the installed power of 68,640 kW assuming the same efficiencies as described above plus a relative rotative efficiency of 1.0. Using equation 5.9 this resulted in a resistance of 3,124 kN.

$$R = \frac{P_{Effective}}{V_s} = \frac{P_b \times \eta_{a_h} \times \eta_{a_r} \times \eta_{a_o} \times \eta_{a_{shaft}}}{V_s} \quad (5.9)$$

It is seen that the outcome of the two approaches lie very close to each other. As can also be seen on figure 5.1 by the red star and blue triangle.

For H&M two different calculations were made one with the main input parameters of the Maersk B as depicted in table 5.9 where assumptions were made for following factors:

- Temperature Seawater = 20°C
- 1/2 entrance angle bowshape = 10.2°
- Sternshape = Pram + gondola
- $A_{Rudder} = 100\text{m}^2$
- $A_{Bilgekeels} = 200\text{m}^2$
- Diameter of bowthruster = 4m
- Longitudinal Center of Buoyancy (LCB) = -1,1%
- $C_{wp} = 0.827$
- $C_m = 0.954$

The other calculation was carried out with a hull form out of Maxsurf. It was made with the input of the main dimensions of the Maersk B and ultimately had 2% more displacement. The same hull form is used for Fung. In order to use M&B within its boundary conditions the width of the Maersk B is increased by 15.3% the remaining input parameters were the length between perpendiculars and the displacement in ton taken from table 5.9. The final comparison is made on figure 5.1.

¹To keep the tip speed in a realistic range

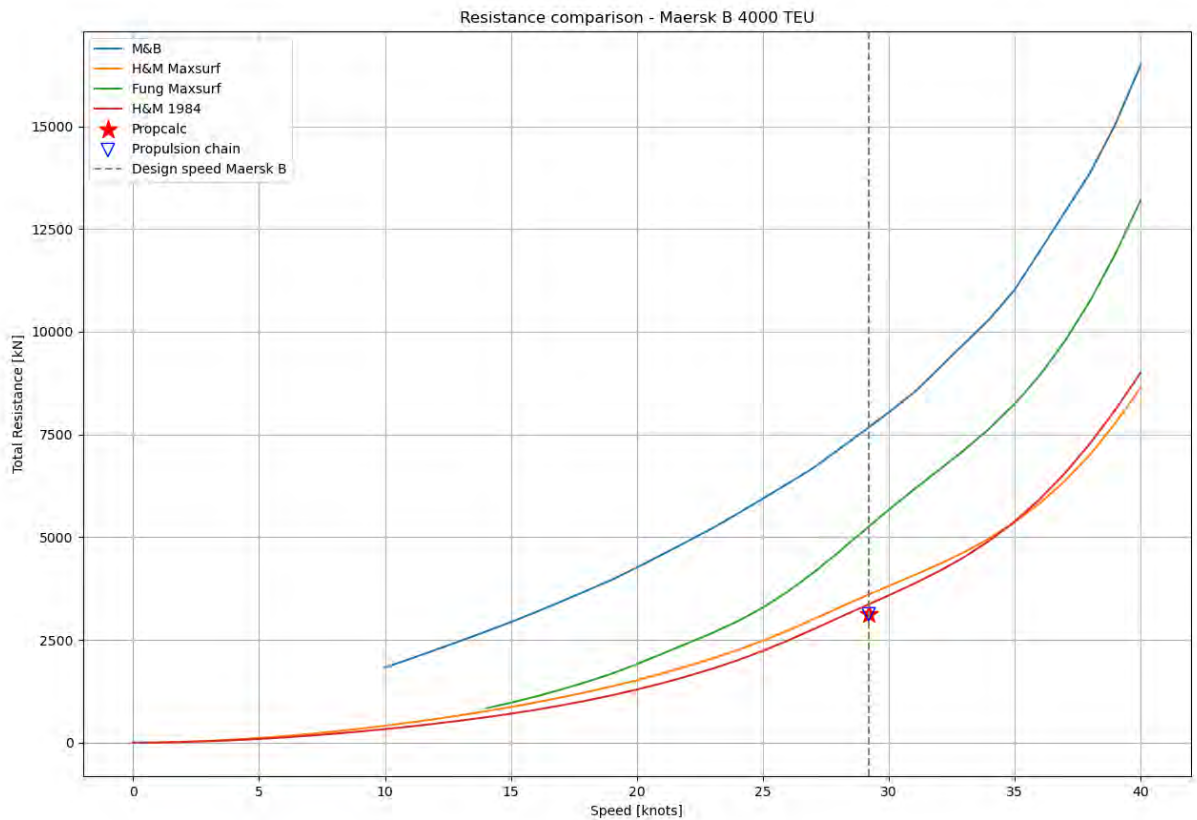


Figure 5.1: Comparison of resistance prediction methods for Maersk B

From 0-20 knots it is observed that both the estimations of H&M and Fung lie close to the initial estimation curve of the resistance. M&B diverges from the beginning, this can be explained by the increased width of the vessel but also due to the difference in used reference hulls thereby M&B is disregarded as resistance prediction method for further use. From 20 knots on wards Fung starts to diverge from the initial estimate but also from the two predictions by H&M. For further validation of the remaining resistance prediction methods the resistance at 29.2 knots is compared as this is the design speed of the Maersk B and gives the most accurate image of reality. The resistances at this speed are depicted in table 5.11 for the different methods.

Method	Resistance [kN]	Speed [kts]	Difference from initial estimate [%]
M&B 15.3% increase in width	7580.61	29.2	143
Fung Maxsurf	5,152.10		65
H&M 1984	3,164.42		6
H&M Maxsurf	3,551.30		14
Initial estimate	3,124.20		-

Table 5.11: Difference in resistance at design speed Maersk B

Here it is seen that both M&B and Fung diverge out of proportion so thereby Fung is also disregarded as resistance prediction method. The reason for this can lie in the use of different reference ships for the algorithm than the Maersk B. The two calculations carried out by H&M diverge respectively 6% and 14%. After the design speed of 29.2 knots it is observed that both H&M calculations increase significantly. This is explained by the increase in wave making resistance around this speed with Froude

number 0.3.

In conclusion H&M is selected for the resistance prediction of the 20,000 TEU nuclear concept vessel. As this prediction method gives a good indication of the resistance at the design speed of the model vessel Maersk B and predicts the wave making resistance at higher speeds in a good way.

As validation of the use of Holtrop & Mennen a second reference vessel is used of the Maersk Y-class with a design speed of 25.8 knots a TEU capacity of 10,000 TEU and an installed power of 68,640 kW. Assuming the same efficiencies as in equation 5.9, a total resistance of 3,536 kN is calculated. When this vessel with LPP 334m, B 45.6 m, T 13.0 m and a displacement at T of 127,568 t is filled in into Holtrop & Mennen where the factors that are estimated by Maxsurf in table 5.12 are assumed the same a total resistance of 3,670 kN is found. This gives a difference of 3% with the previously calculated value. Hereby the selection of Holtrop & Mennen as resistance prediction method is further validated.

5.1.3. Resistance calculation of 20,000 TEU concept ship

Using Holtrop & Mennen with input stipulated in table 5.12 the initial resistance curve for the 20,000 TEU nuclear concept ship is established.

Feature	Value
Scale factor	1.71
LOA	502.44 m
LPP = LWL	475.72 m
B	55.03 m
T	20.86 m
Displacement	328500 t
C_b	0.59
LCB	-1.1%*
Area bulb	7% $B \times T^*$
Center height bulb	45% T^*
Transom area	6% $B \times T^*$
C_{stern}	25
C_m	0.95*
C_p	0.61*
C_{wp}	0.83*
1/2 bow entrance angle	10.2*

Table 5.12: Holtrop & Mennen Input 20,000 TEU concept vessel (*) estimated with Maxsurf

To use this resistance curve in the speed model that is covered in section 5.2 the resistance has to be transformed to installed power for both the diesel reference and nuclear concept vessel. For the hull, relative rotative and open water efficiency the same values are used as depicted in section 5.1.2.8. The rest of the efficiencies differs per propulsion chain as depicted in figure 5.2. For the diesel reference ship only the shaft efficiency is used as large container vessels are usually fitted with two-stroke engine and thus do not need a gearbox. The propulsion line of the nuclear concept vessel is taken from K. Houtkoop with corresponding efficiencies [71].

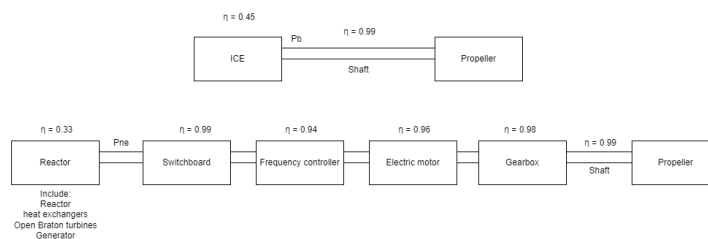


Figure 5.2: Used efficiencies in power curve

This gives following equations for the power curve where X should be substituted with speed in knots. These equations are formed from the Holtrop & Mennen resistance calculation and power is expressed in MW.

$$P_{ne(nuclear)} = 0.0148X^3 - 0.3275X^2 + 3.6448X - 7.2576 \quad (5.10)$$

$$P_{b(diesel)} = 0.0130X^3 - 0.2867X^2 + 3.1911X - 6.3541 \quad (5.11)$$

5.2. Definition of economic speed model

The economic speed model is created for the diesel reference vessel and the nuclear concept vessel. The diesel reference ship is included to make a comparison with reality to see where the limits of the model lie. The following routes are considered:

- Shanghai - Rotterdam
- New York - Rotterdam

On this routes following assumptions are made:

- No port congestions
- Port restrictions not considered in model (will be adjusted in chapter 6)
- No port or Suez canal restrictions for the nuclear vessel
- Freight rate (range) is based on the average of both directions
- One trip = back and forth from port to port
- 3 days per port for loading/unloading [32]
- 15 hours to pass the Suez canal at a max speed of 8 knots [17]

5.2.1. Cases

For the speed model three different cases are evaluated. Two for the nuclear concept vessel with variation in service life between 25 and 50 years. One for the diesel reference case with a service life of 25 years. All three cases are evaluated over the two depicted routes.

The included costs and freight rates are summarized in the tables below both for the nuclear and diesel version which are based upon literature as discussed in previous chapters 1 and 2. The previously determined power-speed curve is used to link the capital and operational costs to increasing speed.

5.2.2. CAPEX

	Nuclear [\$/kW]	Diesel [\$/kW_e]
Reactor unit/ICE	3000-9000	350
Switchboard + frequency controller [177]	500	/
Electromotor [177]	250	/
Gearbox [177]	100	100

Table 5.13: Capital costs

The reactor unit includes the cost for the reactor, heat exchangers, turbines and generators as depicted on figure 5.2 and discussed in section 1.6.1. In addition it also includes the decommissioning cost of the reactor. Due to the large variation in reactor unit capital cost this is kept as a variable to evaluate the impact on the economic speed as also discussed in chapter 1 section 1.6.1.

5.2.3. OPEX

	Nuclear	Diesel
O&M fixed [\$/kW_e/year]	132.73	36.81
O&M variable [\$/MWh]	4.07	10.5
Fuel cost [\$/kg]	2642 \$/kg	400-1000
Specific fuel consumption [g/kWh]	0.0014	170

Table 5.14: Operational costs

The fuel cost for nuclear is taken for 5% enriched uranium and based upon the average of table 1.5 from chapter 1 as the value per kilogram is rather constant. Where the cost for handling and storing the nuclear waste is also included as discussed in chapter 1. As the nuclear fuel cost was seen as of not much significance in previous studies [71] on the total cost this value is kept constant. Further studies could consider the cost for 20% enriched uranium or thorium but they are not expected to be of much influence. The nuclear specific fuel consumption is calculated for the lower value of the burn-up being 90 GWd/tHM were this value is converted to g/kWh by making use of a thermal efficiency of 33%. This value is independent of the used fuel being uranium or thorium. For the diesel reference case the fuel cost is varied as this is a volatile factor as seen in chapter 2, the carbon tax is also included in this price. The used fuel is Marine Diesel Oil (MDO). The specific fuel consumption is assumed to be 170 g/kWh.

5.2.4. Voyage costs

	Nuclear	Diesel
Port dues	\$0.66/GT + \$0.51/ton of TEU	\$0.45/GT + \$0.51/tonnes of TEU
Pilotage	2 x \$8,345	2 x \$7,321
Tugs	2 x 3 x \$4,697/tug	2 x 3 x \$4,697/tug
Suez canal dues	2 x \$4.69/GT	2 x \$3.12/GT

Table 5.15: Voyage cost Rotterdam-Shanghai

	Nuclear	Diesel
Port dues Rotterdam	0.330/GT + 0.510/ton of TEU	0.255/GT + 0.510/tonnes of TEU
Port dues New York	\$55.68/m/day + \$13.13/TEU	\$45.37/m/day + \$13.13/TEU
Pilotage Rotterdam	\$8,345	\$7,321
Pilotage New York	\$15.74/pilotage unit	\$14.02/pilotage unit
Tugs Rotterdam	3 x \$4,697/tug	3 x \$4,697/tug
Tugs New York	\$0.552/NT	\$0.552/NT

Table 5.16: Voyage cost Rotterdam-New York [122] [145] [170]

The voyage costs depicted in table 5.15 for Rotterdam to Shanghai and table 5.16 for Rotterdam to New York are already explained in section 2.2.1 and 2.2.2 of chapter 2. They are calculated for a full round trip from port to port as stated before by the definition of one trip.

The distances from Rotterdam to Shanghai and from Rotterdam to New York are respectively 10,664 nM and 3,360 nM. Where the Suez canal is used for the former.

5.2.5. Freight rate

Freight rate	\$/FEU
Far east - North Europe	1000-3000
North America East coast - North Europe	1000-3000

Table 5.17: Freight rates nuclear concept vessel

The freight rate is expressed in \$/FEU thus the cargo capacity of 20,000 TEU is calculated as 10,000 FEU in the model. For the total revenue a load factor of 85% is also included as the vessel is not always fully loaded and also carries empty containers, resulting in 8,500 FEU paid transport [112]. Due to the large variation in freight rates the freight rate is also kept as a variable to see what its impact is on the economic speed.

The full analytical description of the speed model can be found in appendix E.1.

5.3. Sensitivity analysis

A sensitivity analysis is carried out on the speed model by varying the reactor unit cost, freight rate and diesel fuel cost. This in order to see what their influence is on the economic speed determination. The results for the route from Rotterdam to Shanghai for both the nuclear as the diesel case are seen on figure 5.3, 5.4 and 5.5. The speed plots for the route from Rotterdam to New York are added in appendix E.2.

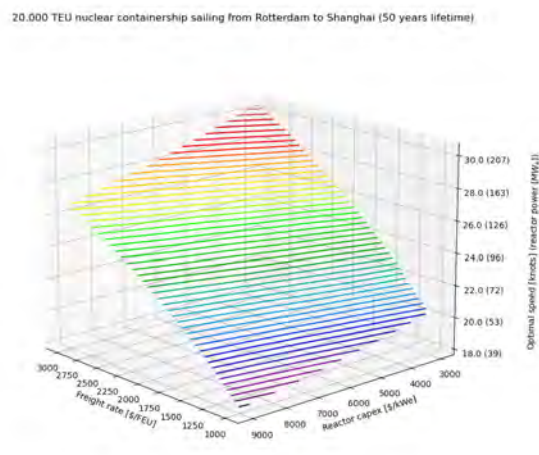


Figure 5.3: Sensitivity plot Rotterdam-Shanghai Nuclear 50-year

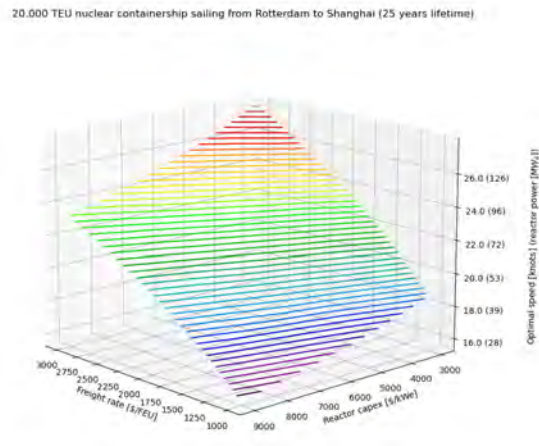


Figure 5.4: Sensitivity plot Rotterdam-Shanghai Nuclear 25-year

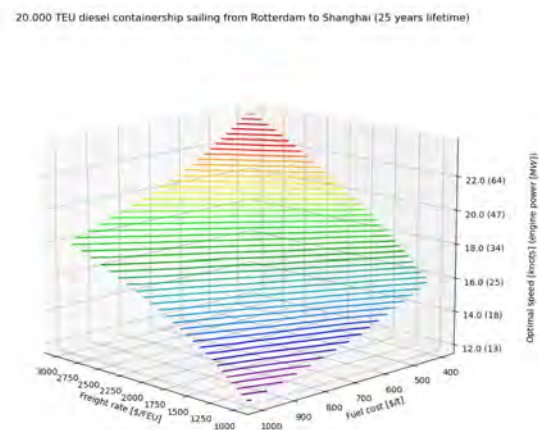


Figure 5.5: Sensitivity plot Rotterdam-Shanghai Diesel 25-year

The freight rate, reactor unit cost and diesel fuel cost all show a clear influence on the economic design speed. In table 5.18 & table 5.19 the sensitivity is depicted on the economic speed determination. Each variable is increased by 50% separately and the effect on the speed is depicted in a percentage. Where the starting value is varied over the range of each variable. For the fixed inputs namely, ICE capex and nuclear fuel cost the values of the previous section are taken as base value. The '+' or '-' depict if its a speed increase or speed decrease. This is done to get a feeling of the impact of each variable.

[%]	Diesel (25y)	Nuclear (25y)	Nuclear (50y)
Freight rate	24 +	22 +	22 +
Reactor/ICE capex	0.4 -	6 -	4 -
Fuel cost	15 -	2 -	2 -

Table 5.18: Impact of different variables on the economic speed (Rotterdam - Shanghai)

[%]	Diesel (25y)	Nuclear (25y)	Nuclear (50y)
Freight rate	20 +	17 +	17 +
Reactor/ICE capex	0.4 -	6 -	4 -
Fuel cost	13 -	1.5 -	1.5 -

Table 5.19: Impact of different variables on the economic speed (Rotterdam - New York)

Biggest influence is observed to be by the freight rate for all cases and diesel fuel cost for the diesel reference case. Reactor capex influence decreases over extended lifetime, this will be discussed in more detail when the the different costs are looked at separately. The nuclear fuel cost is seen to be of very low influence on the economic speed determination thus the previous assumption to keep the fuel cost constant is justified.

To determine the limits of the speed model with respect to reality and to determine an initial bandwidth of design speeds for the nuclear concept vessel a total of three scenario's were created which are depicted below.

Scenario	Definition
A	Highest freight rate - lowest reactor capex/diesel fuel cost
B	Middle freight rate - middle reactor capex/diesel fuel cost
C	Lowest freight rate - highest reactor capex/diesel fuel cost

Table 5.20: Definition of scenario's in economic speed plots

The results for each scenario sailing from Rotterdam to Shanghai are depicted in table 5.24. For this same route the cost breakdowns for the nuclear concept vessel sailing 50 or 25 years and the diesel reference vessel sailing 25 years are depicted in figure 5.6, 5.7 & 5.8 for scenario B to form an idea of their magnitude. Where scenario B is chosen due to its realistic nature. The cost break percentages are summarized in table 5.21, 5.22 & 5.23 per scenario. For the fuel and reactor unit cost the corresponding values for each scenario are taken as stated in table 5.20. The used speeds for these cost breakdowns are depicted in table 5.24.

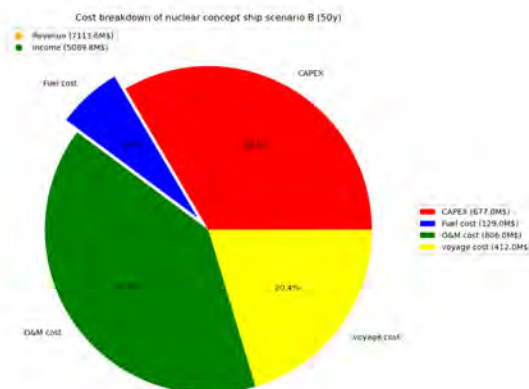


Figure 5.6: Cost breakdown nuclear (50y) scenario B

[%]/[M\$]	Scenario A	Scenario B	Scenario C
CAPEX	24.9/844	33.5/677	35.3/374
Fuel cost	8.0/271	6.4/129	5.0/52
O&M	52.3/1,770	39.8/806	29.6/313
Voyage costs	14.7/498	20.4/412	30.1/318
Revenue [M\$]	12,890	7,114	2,750
Income [M\$]	9,508	5,090	1,693

Table 5.21: Cost breakdown nuclear concept ship scenario A, B & C (50-year)

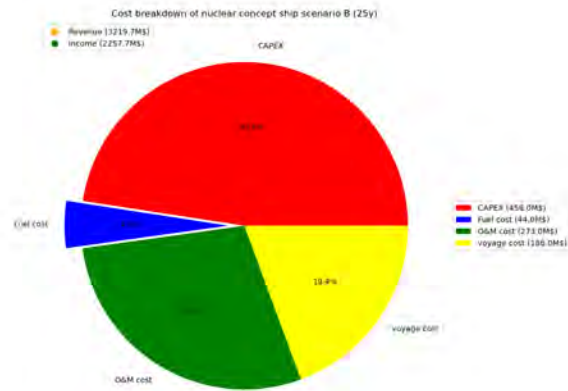


Figure 5.7: Cost breakdown nuclear (25y) scenario B

[%]/[M\$]	Scenario A	Scenario B	Scenario C
CAPEX	38.6/620	47.6/458	49.9/257
Fuel cost	6.3/102	4.6/44	3.5/18
O&M	40.6/652	28.4/273	20.6/108
Voyage costs	14.4/232	19.4/186	26.9/141
Revenue [M\$]	5,999	3,220	1,218
Income [M\$]	4,394	2,258	694

Table 5.22: Cost breakdown nuclear concept ship scenario A, B & C (25-year)

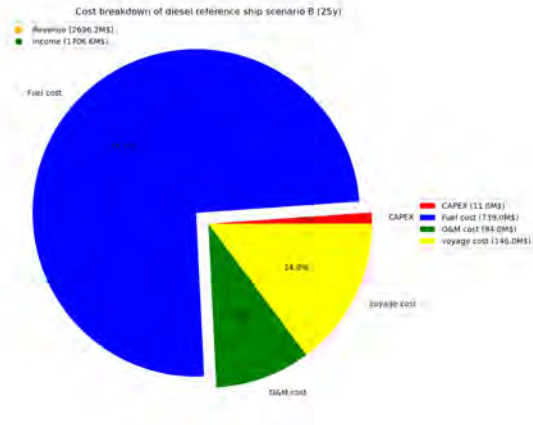


Figure 5.8: Cost breakdown diesel (25y) scenario B

[%]/[M\$]	Scenario A	Scenario B	Scenario C
CAPEX	1.9/30	1.1/11	0.7/4
Fuel cost	69.8/1073	74.7/739	75.6/451
O&M	15.8/243	9.5/94	6.6/39
Voyage costs	12.5/192	14.8/146	17.1/102
Revenue [M\$]	5,298	2,696	941
Income [M\$]	3,762	1,707	344

Table 5.23: Cost breakdown diesel reference ship scenario A, B & C

Scenario (kts)	Diesel (25y)	Nuclear (25y)	Nuclear (50y)
A	24.0'	27.9'	30.5'
B	17.5'	21.5'	24.2'
C	11.7'	15.6'	17.9'

Table 5.24: Economic speeds for different scenario's, used propulsion line and lifetime for the route from Rotterdam to Shanghai

First of all if table 5.24 is observed for the diesel reference ship an economic speed of 17.5 knots for scenario B and 24.0 knots for scenario A is seen. If this is compared with a real life example like the Triple E from Maersk with a TEU capacity of 18,720 TEU a similar division in speed is seen as the triple E has a cruising speed of 16 knots and a top speed of 23 knots [72]. This speed range could be explained by changing market conditions in freight rates and fuel prices as was also seen in chapter 2. As diesel container ships have a large installed power due to the low capex to cope with situations like heavy weather or extra hull fouling but this could also be to change its speed depending on the market conditions. If figure 5.8 & table 5.23 are observed the marginal percentage of the capital cost is seen thus installing an engine with more output power would not make much difference in the total cost.

For the nuclear vessel however due to its large capital cost it would suggest to be more favourable to sail as fast as possible due to the capital cost already been paid and the relatively low contribution of the fuel cost as seen on figure 5.6 & 5.7. However it is also observed the O&M takes a significant portion of the total cost similar to the influence of the capital cost. This is especially true if the operating lifetime is extended to 50 years as seen on figure 5.6 as more running hours are made. In opposition to this, the increased lifetime results in an increase of economic speed as seen in table 5.24 this is explained due to the reactor capital cost being paid over a longer time interval.

In addition when the income of the diesel reference ship is compared to the income of the nuclear ship it is seen that all values for every scenario lay higher for the nuclear cases. The percentual increase of income is 50% on average for the nuclear case with a service life of 25 years when compared to the diesel reference case. This shows that the high capital cost for nuclear propulsion pays off over the long term. It has to be stated that this comparison is a rough indication of reality as only the speed depended cost factors are accounted for. The total cost of ownership should be investigated further to have a more accurate comparison and include cost components such as insurance and dry docking costs for example.

The same exercise was done for the route from Rotterdam to New York excluding the cost breakdown as this is similar to the route from Rotterdam to Shanghai. For the New York route following economic speeds were obtained:

Scenario (kts)	Diesel (25y)	Nuclear (25y)	Nuclear (50y)
A	33.5'	34.5'	37.6'
B	24.8'	27.5'	30.7'
C	17.5'	20.7'	23.6'

Table 5.25: Economic speeds for different scenario's, used propulsion line and lifetime for the route from Rotterdam to New York

Here it is seen that the speeds lie significantly higher. This is explained by a constant freight rate but a reduction in effective costs due to the shorter distance.

Scenario A does not depict a realistic scenario for the diesel reference ship as there are no container ships currently sailing 33.5 knots. If scenario B and C are observed, the same relation as with the route from Rotterdam to Shanghai is seen referring to the optimal and cruising speed of the triple E class. Therefore scenario A is disregarded for the nuclear concept vessel as it does not depict reality.

5.3.1. Selection of initial design speed

Taking above observations into account it is concluded that for the route from Rotterdam to New York scenario A is disregarded due to a too high economic speed for the diesel reference vessel. If scenario B is taken from this route the economic speeds are seen as realistic again when compared to diesel container vessels currently sailing. This scenario also covers all the economic speeds that are calculated for the route from Rotterdam to Shanghai thus correspond to a wide range of possible market conditions.

For the choice between the lifetime of the nuclear concept vessel 50 years is chosen as this is the right economical and sustainable choice. This results in a design speed range between 28 and 30 knots. For the purpose of this report 30 knots is selected.

5.4. Chapter conclusion

In this chapter the economic speed for a nuclear container vessel with a cargo capacity of 20,000 TEU is researched.

First, resistance calculation methods were compared and evaluated with respect to predicting the resistance curve of the Maersk B series as accurate as possible. This resulted in using Holtrop & Mennen. Afterwards this resistance curve was modified for efficiencies in the propulsion line and used in the speed model for the 20,000 TEU nuclear concept vessel. As comparison the same was done for a diesel reference vessel. This was carried out for two routes between Rotterdam and Shanghai and Rotterdam and New York.

A sensitivity analysis of the speed model revealed that the biggest influence on the economic speed is observed to be by the freight rate for all cases and the diesel fuel cost for the diesel reference case. The reactor capex influence showed a less substantial role with a decreasing character over an extended lifetime. The nuclear fuel cost was seen to be of little influence due to its low specific fuel consumption when compared with the diesel variant.

With this knowledge three scenario's were created to obtain a matrix of economic speeds. Here the freight rate, reactor capex and diesel fuel cost were varied from high to medium to low values with an inverse relation between freight rate and reactor capex/diesel fuel cost. Out of this analysis combined with a cost breakdown per scenario the realistic nature of the speed model became apparent as the top and cruising speed of the diesel reference vessel were similar to existing container ships with comparable TEU size. This gave a validation of the speed model. The difference between the diesel and nuclear propelled vessel became clear with the cost breakdown. As the reactor capex was seen to represent between 30-50% of the total lifetime cost which degraded when the lifetime was extended to 50 years. The O&M of the nuclear case was seen to represent 20-50% of the lifetime cost which increased for extended lifetime. The nuclear fuel cost was seen to represent between 4-8% of the total lifetime cost. For the diesel reference vessel the ICE capex lied around 2% and the fuel cost around 70% of the lifetime cost.

The economic speeds found with the speed model of both the 25-year and 50-year service life nuclear options surpass that of the conventional MGO alternative. Additionally, the nuclear option with a 50-year service life displays an increased economic speed in comparison to the nuclear option with a 25-year service life. This is explained by the extended lifetime over which the reactor capex is paid off. Furthermore, higher speeds were observed for the shorter distances which is logical due to consistent freight rates and lower effective costs compared to longer distance cases.

Taking into account the results of the economic speed model it is found that a speed range between 28-30 knots with a service life of 50 years is suitable to investigate nuclear propulsion on board of a 20,000 TEU container vessel further. For the current nuclear concept vessel 30 knots is chosen as a starting point.

6

Impact of speed on design

Chapter introduction

This chapter is dedicated to answer the sub-research question:

”How does this economic speed impact the design and how is it distinguished from a conventional design?”

This is done by entering the design spiral to evaluate the initial nuclear concept vessel in main dimensions and further investigate the impact of the increase in design speed on the conventional container hull and its propulsors. The stability is also addressed to evaluate if the nuclear reactor has an effect on this factor. The subjects that are addressed are stipulated in the flow chart below. Where the actual design spiral is entered from point 4 on wards. At the end of this chapter the comparison with a conventional container ship is made.

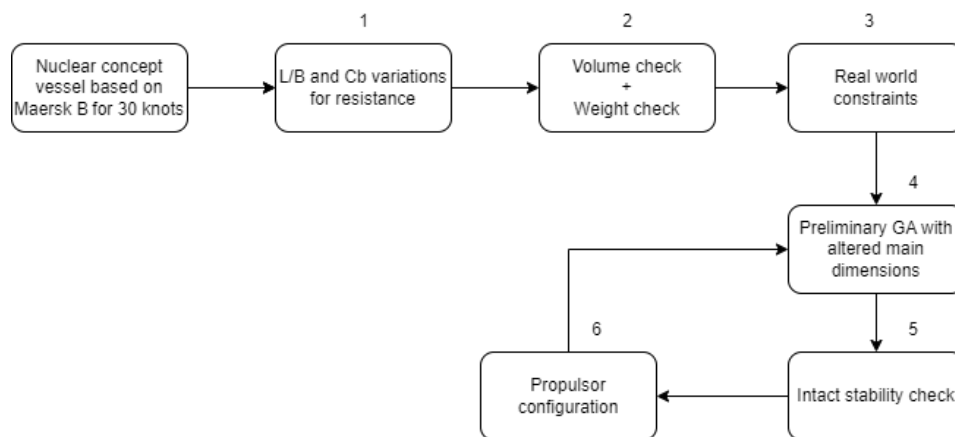


Figure 6.1: Design spiral for the 20,000 TEU nuclear concept vessel

6.1. Design variations of the 20,000 TEU nuclear concept vessel to decrease resistance

Based upon the preliminary conclusion of the design speed the initial L/B and B/T ratio's are varied to find their influence and see if an optimum can be found in resistance. In order to do this Holtrop & Mennen is used with following formulas where the displacement and C_b are kept constant:

$$Lwl = \sqrt[3]{\frac{\nabla}{C_b \times \frac{L^2}{B} \times \frac{B}{T}}} \quad (6.1)$$

$$B = \sqrt[3]{\frac{\nabla}{C_b \times \frac{L}{B}} \times \frac{B}{T}} \quad (6.2)$$

$$T = \sqrt[3]{\frac{\nabla}{C_b \times \frac{L}{B} \times \frac{B^2}{T}}} \quad (6.3)$$

It is observed that the initial L/B and B/T ratio's are already near the optimum regarding the resistance at the predetermined design speed of 30 knots as depicted on figure 6.2. The resistance at 30 knots for the initial ratio's is highlighted in the table with a black square. A further increase in L/B ratio would save 2.2% in resistance but will prolong the vessel more. As the ship is already longer than the longest container ships currently sailing and a further increase results in a marginal benefit the initial L/B ratio is selected. Along with the initial B/T.

		HOLTROP 1984										
B/T	Lw/B	10	9,65	9,3	8,95	8,6	8,25	7,9	7,55	7,2	6,85	6,5
	2,1		7788	7803	7822	7890	8042	8218	8423	8654	8949	9292
2,3		7711	7721	7732	7790	7925	8081	8261	8472	8720	9017	9374
2,5		7669	7672	7678	7727	7849	7988	8149	8336	8556	8817	9129
2,7		7681	7665	7652	7692	7803	7929	8075	8243	8440	8672	8949
2,9		7711	7690	7671	7692	7781	7897	8029	8183	8361	8570	8817
3,1		7757	7730	7705	7721	7800	7892	8007	8147	8310	8500	8724
3,3		7815	7782	7752	7761	7834	7918	8016	8132	8282	8456	8660
3,5		7884	7845	7809	7813	7879	7957	8046	8151	8274	8432	8620

Figure 6.2: L/B and B/T variations with corresponding resistance at 30 knots

Furthermore the block coefficient is varied to see what its influence is on resistance and if an optimum can be found. This is done using the relation between the block coefficient and the mid ship coefficient defined by Jensen (1994). The prismatic coefficient is expressed as the ratio between the block and mid ship coefficient respectively. The initial L/B and B/T as well as the displacement are kept constant which results in figure 6.3.

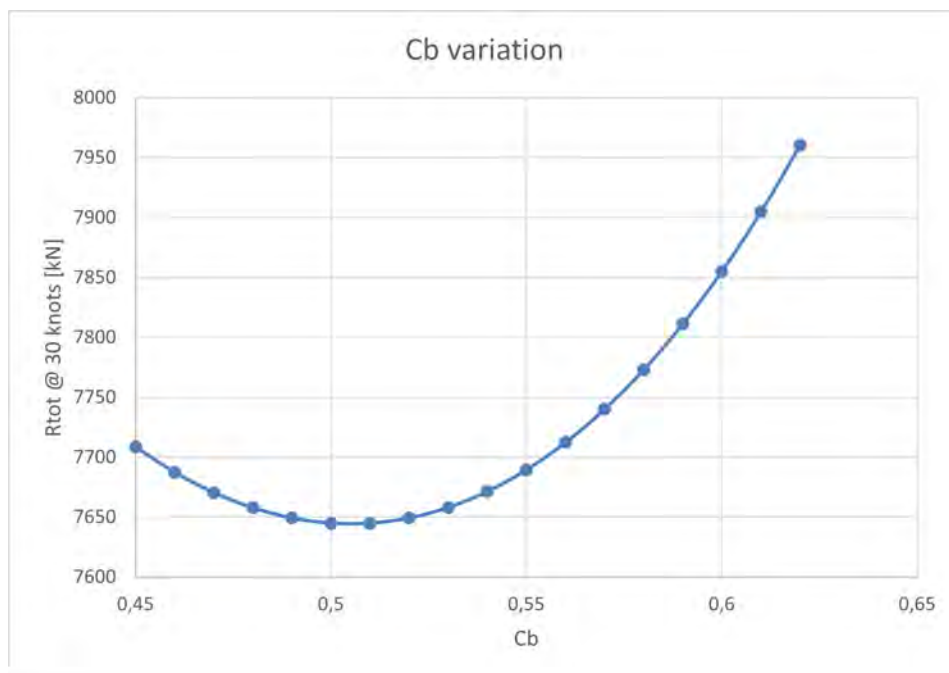


Figure 6.3: C_b variations with corresponding resistance at 30 knots

Here it is observed that the initial block coefficient was already near the optimum of the resistance at a design speed of 30 knots. Further reducing the C_b to as low as 0.52 would translate to a decrease of 1.8% in resistance. Due to the marginal decrease and keeping in mind that the initial C_b of 0.59

is already quite low the block coefficient is kept constant. This is also done to maintain the stability properties of the reference hull.

It should also be noted that the reference vessel Maersk B had a Froude number of 0.29 at a design speed of 29.2 knots. The nuclear concept vessel with a design speed of 30 knots comes to a froude number of 0.23. Despite the considerable difference in froude number the concept vessel is seen to lie near its optimum in resistance as was observed in the variations made above.

6.2. Volume check of concept design

If the dimensions of the concept vessel are observed from the earlier mentioned table 5.12 it can be seen that the vessels main particulars lie well above the ones normally observed for conventional container vessels with similar TEU capacity. For example both the CMA CGM JAQUES and HMM ALGECIRAS with respectively 23,112 and 23,964 TEU on board have a LOA of 399.9m and a draft around 14 to 16m [119]. Therefore the size of the nuclear concept vessel is evaluated to check the actual TEU capacity. This is done by modelling the concept vessel in rhino with as input the main particulars of table 5.12. The main components on board of the ship are estimated in volume and weight being the machinery room, accommodation and TEU number.

6.2.1. Sizing of machinery room

To determine the volume and weight of the machinery room all the components of the propulsion line need to be considered. In order to do this the total installed power of the reactor needs to be calculated first. Using the power curve (5.10) that is used in the economic speed model a total of 207 MW_e is found which corresponds to 627 MW_{th}. This amount of power is used to scale up the used propulsion line of K. Houtkoop which is depicted on figure 6.4. A re-evaluation of the battery system, electrical grid and need of a gearbox is carried out for this concept design as the installed power lies significantly higher than the concepts vessels in the study of K. Houtkoop where the max power was 50 MW_e.

It is assumed that the total installed power covers the sea margin. In rough weather the design speed of 30 knots is not considered realistic due to too excessive vessel's motions. Therefore, no margin is taken into account for heavy weather. However, the sea margin also covers additional resistance due to fouling. For this research it is chosen to not include any margin for fouling. As this is vessel and route specific. The specific influence of rough seas and additional fouling are recommended for further research. The base load consists out of the hotel load equal to 1,820 kW and the balance of plant for keeping the reactor system operable equal to 5.5 kW/MW_{th} [71][155].

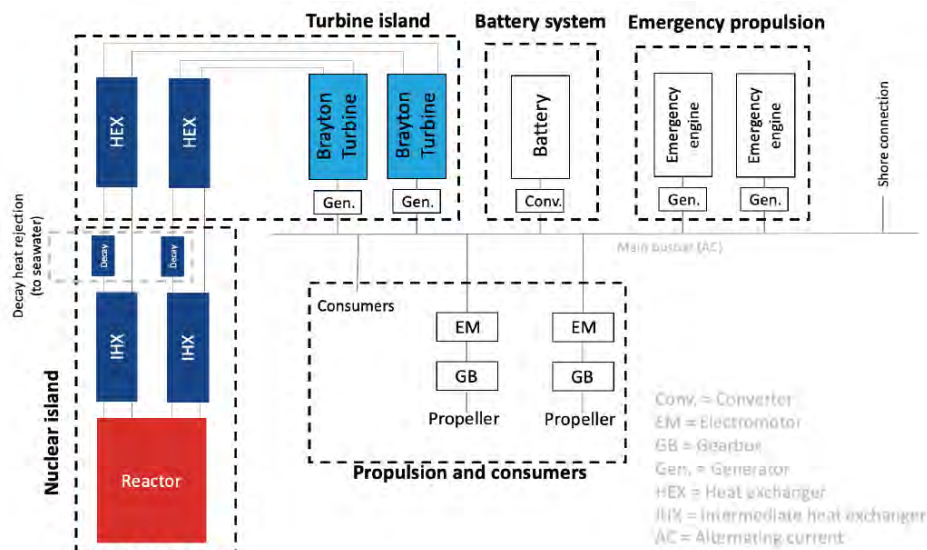


Figure 6.4: Schematic representation of the full propulsion layout that is used to make the volume and weight estimation of the machinery room taken from K. Houtkoop [71]

As can be seen on the figure above the whole propulsion line is doubled to ensure redundancy as well as an emergency propulsion section in case of reactor failure. The reasoning here is that the power generation side being the nuclear and turbine island can deliver full reactor power on both circuits, and the propulsion and consumer side is split in two parts of 50%. So that in this lay-out the two propellers combined would ensure a design speed of 30 knots.

The layout is chosen to be fully electric as this gives way to the implementation of battery power for peak shaving of load demands as well as easy use of emergency genset operation. In addition the possibility of reversed cold ironing can be utilized when the vessel is in port. The amount of propellers is depicted to be two here but this will be evaluated in section 6.6.

For each component depicted in the propulsion line on figure 6.4 the volume and weight estimation will be discussed in the following paragraphs together with a short description or reconsideration.

Reactor

The reactors implemented are the previously discussed generation IV VHTR and MSR that are chosen because of their high burn-up, possible use of thorium, high passive safety features and higher operating temperatures when compared to other SMR designs as previously discussed in chapter 1. The VHTR can be seen as the short term solution due to its higher TRL which is estimated at 10-20 years. The MSR shows great potential for the longer term (20+ years) due to its higher burn-up values which reduces the amount of fuel needed to produce power and its capability of using thorium in a continuous cycle due to its rich neutron environment which is made possible by reprocessing the fuel-coolant mixture. The use of thorium would reduce the amount of tails and long lived nuclear waste [71].

The reactor core weight itself is estimated by the trend line described in section 1.7.1. The reactor volume is not treated separately as it is enclosed in the reactor shielding.

Shielding material is a major contributor of weight and volume in the machinery room as was previously discussed in section 1.7.2. Where several publications were found with a shielding weight easily above 2,000 ton. Therefore the method used by K. Houtkoop is utilized to determine the volume of the reactor shielding. This method takes into account the two major types of radiation namely neutron and gamma radiation. It is based upon an analytical approach for neutron shielding called the "removal-attenuation" calculation and the "point kernel method" to determine the radiation caused by gamma rays which makes use of the halving distance of the shielding material [93]. This method is however based upon a simplified PWR with uranium as fuel but as described by K. Houtkoop the different types of reactors and fuel compositions are expected to be of negligible influence. The alternative would be to run complex simulations with reactor specific designs which lies outside the scope of this report [71][93].

The shielding calculation thus consists out of two steps. The first is to determine the radius of the concrete shielding to block neutron radiation. This radius is varied using the "removal attenuation" method until the radiation level is equal to half of the maximal radiation dose general public can be exposed too over the time span of a year. This value is equal to 0.5 mSv/year. Half of the radiation dose is selected to reserve the other half for gamma radiation. The shielding material for gamma radiation consists out of lead for which the "point kernel method" is used. This to determine the radius of lead needed to have a radiation dose of again 0.5 mSv/year at the outer layer of the shielding being the lead layer. This way the shielding arrangement is meeting the requirements of the Nuclear Ship Code for the safety of nuclear merchant ships. Here different radiation doses are specified for the navigation bridge, accommodation spaces, cargo spaces and ship's sides. The highest dose is stated to be 7.5 μ Sv/h near the ship's bottom at only 10% of the reactor power. This translates to 6.6 mSv/year which lies well above the predetermined 1 mSv/year wherefore the reactor shielding is currently designed [79].

Due to the higher limit in radiation dose external personnel can also come on board as this lies at 1 mSv/year. For the full and detailed shielding calculation the report of K. Houtkoop can be consulted.

From this calculation a total radius of the reactor core plus shielding is found. To determine the weight of the shielding material the outer volumes of both the concrete and lead sphere are determined and multiplied by the density being respectively 2.4 g/cm³ for normal concrete and 11.35 g/cm³ for lead. The calculated value differed +6% with the value calculated using the polynomial of K. Houtkoop and this is deemed to be satisfactory. The reactor itself can be positioned in a spherical form or surrounded by

a cubic box with the sides equal to two times the calculated radius. This would lead to an increase in volume but beneficial for storing purposes.

Heat exchangers

The heat exchangers chosen in the propulsion line are of the helical coil type with counter flow as they are proven to have relatively small volumes per MW_{th} and are widely and conventionally used in the industry. An intermediate heat exchanger is added with regard to safety and segregation. More specifically to avoid radioactive contamination outside the shielding. The volume per MW_{th} is derived by K. Houtkoop making use of the logarithmic mean temperature difference (LMTD), heat transfer coefficient and surface density. As is depicted for both the VHTR and MSR in table 6.1. The difference between reactors is due to the use of different coolants and differences in reactor in and outlet temperatures as described by [71].

Reactor	VHTR	MSR
LMTD_{IHX} [K]	20.6	80.7
LMTD_{HEX} [K]	18.0	101.7
Heat transfer coefficient [W/m²K]	1000	1000
Surface density [m²/m³]	80	80
Volume per MW_{th} IHX	0.61	0.16
Volume per MW_{th} HEX	0.69	0.12

Table 6.1: Volume per MW_{th} calculation values from [71]

The calculation does not consider pressure losses or the possible option to increase the flow of one coolant. This method is intended as a first indication. The medium used in both primary heat exchangers is helium this in order to prevent irradiated molten salt to come into contact with air [71]. In the case of a MSR, helium is heated up in the intermediate heat exchanger by the molten salt. Hereafter helium heats up the compressed air in the primary heat exchanger. By using helium as a medium no neutrons are absorbed as it is neutron transparent. This results in no radioactive contamination.

Decay heat exchangers are also fitted to provide a means to cool down the reactor when no power needs to be generated. Most likely this will occur when a reactor stop takes place. The total amount of decay heat is usually equal to 7% of the total maximum thermal power [156]. For the VHTR and MSR the relative volumes are respectively 0.0020 and 0.0016 m^3/MW_{th} [71].

The weight for the heat exchangers is estimated at 3 ton per m^3 [71].

Open Brayton Turbines

For converting heat into mechanical energy the open Brayton cycle is selected as type of turbine. This turbine is seen to be relatively compact and offers a less complex arrangement when compared to the closed Brayton or Rankine cycle mainly due to the absence of a cooler in between the turbine and compressor. It was also selected because it offered very capable load following performance when using heat rejection [71]. This principle is displayed on figure 6.5.

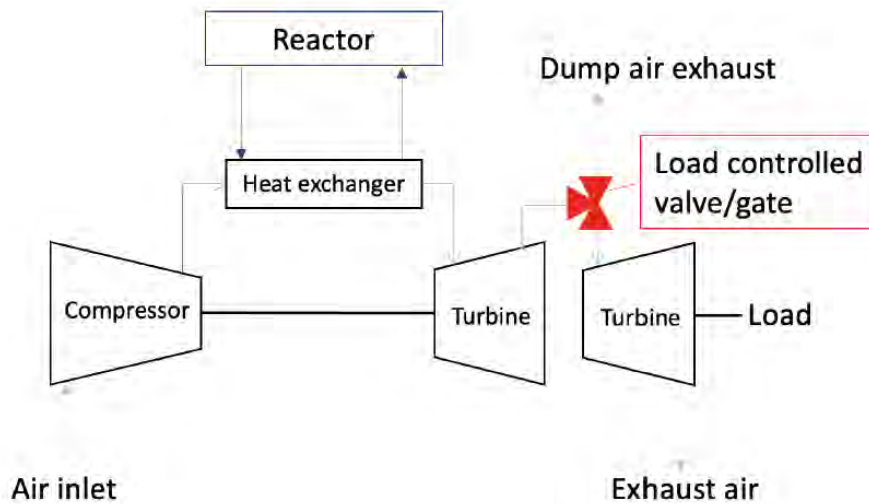


Figure 6.5: Open brayton cycle turbine with heat rejection capabilities taken from K. Houtkoop [71]

A split-shaft design with two turbines is used to enable the heat rejection capability and sustain an optimal compression ratio for the compressor. The first turbine is operated in line with the compressor so that the compressor operation can be sustained, this is also called satisfying the back work of the compressor. Therefore this turbine operates at its most efficient design speed with a fixed RPM. The second turbine is used to deliver the amount of power needed by the vessel for propulsion and auxiliary power where excess power can be rejected by the dumping valve [71]. The second turbine is most commonly operated with a variable RPM to follow the varying load of the vessel [1]. The working medium used in this set-up is air. For further studies supercritical CO₂ in closed loop could be considered as it would take away the dependability of the ambient air where the vessel is sailing but lose the heat rejection capability.

The use of this heat rejection capability can be visualized when looking at the operating profile of the nuclear concept vessel for a single trip between Rotterdam and Shanghai. This situation is depicted on figure 6.6. Where the operating area of the reactor is displayed between the dotted red lines for the lower limit of 20% and the upper limit of 100% as explained in section 1.5.4 of chapter 1. The base load consists out of the hotel load equal to 1,820 kW and the balance of plant for keeping the reactor system operable equal to 5.5 kW/MW_{th} [71][155]. The beginning of the operating profile displays the three days in port followed by the distance sailed from Rotterdam to the entrance of the Suez canal at 30 knots with a reactor ramp-up rate of 5%/min. The drop in reactor load is due to the passing of the Suez canal with a maximum speed of 8 knots here the reactor could operate at 20% of its total load and the surplus in power being 16% can be rejected easily. The same accounts for operating at base load in ports which is displayed again after the ship increases its speed to 30 knots for sailing from the Suez canal to the port of Shanghai.

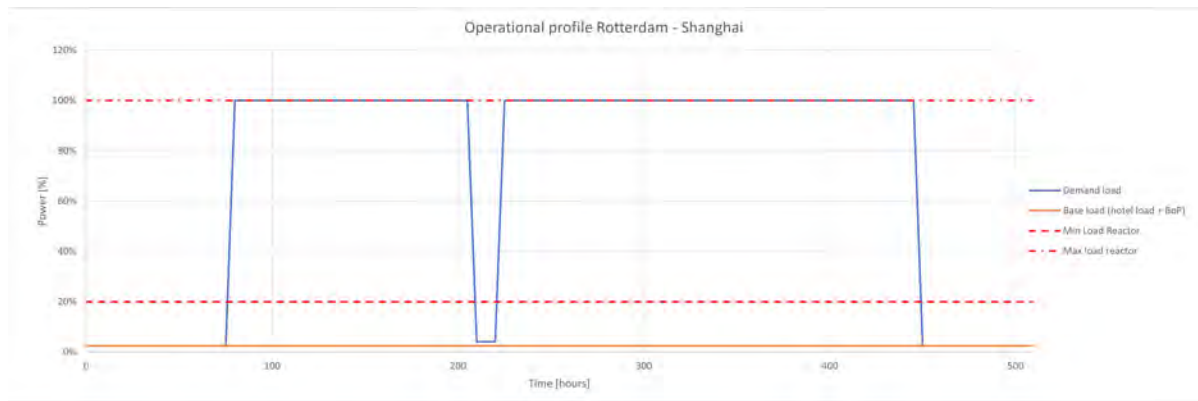


Figure 6.6: Operating profile nuclear concept vessel Rotterdam - Shanghai trip

The size of the open Brayton turbines individually is derived from existing aero-derived marine gas turbines. These are stated to weigh between 1-2 ton/MW_e produced with a corresponding volume of 2-4 m³/MW_e [71].

The ducting cross-section for the air in- and outlet is similarly derived from available marine gas-turbines driven with air. Here the cross-section is expressed per kg/s of air mass flow and equal to 0.063 m²/kg/s [71]. The full calculation of the turbine cross-section can be found in appendix F.1.

Battery system

The battery system is easily implementable due to the full electric lay-out that is selected. Battery systems on large ocean going vessels are mainly used for three different purposes these are summarized below:

- **Spinning reserve:** used as back-up for generators and makes them run more efficiently.
- **Peak shaving/Energy storage:** shave operating peaks in power by providing or storing immediate power and thereby increasing the efficiency of the main power provider.
- **Back-up power:** emergency power role.

A **spinning reserve** is useful when the ship has multiple generators running to ensure redundancy for power production which can have a negative effect on the overall efficiency. The batteries would act as a supplement in power which allows for fewer generators to run and the extra load that could occur is then given by the installed batteries. For the current propulsion line this doesn't seem necessary as all installed generators have their dedicated function and applicability.

For **peak shaving** an example is illustrated on figure 6.7 the peak load is taken as a surplus of 7.5% with respect to the reactor base load based upon an example in literature [130]. Assuming this load changes rapidly over time, faster than the 5%/min rate the reactor can handle, the use of batteries would be beneficial. As this would make it possible for the reactor and turbines to run at a more constant and efficient operating point which saves fuel. In addition working on constant load also has the benefit of decreasing mechanical wear and tear.

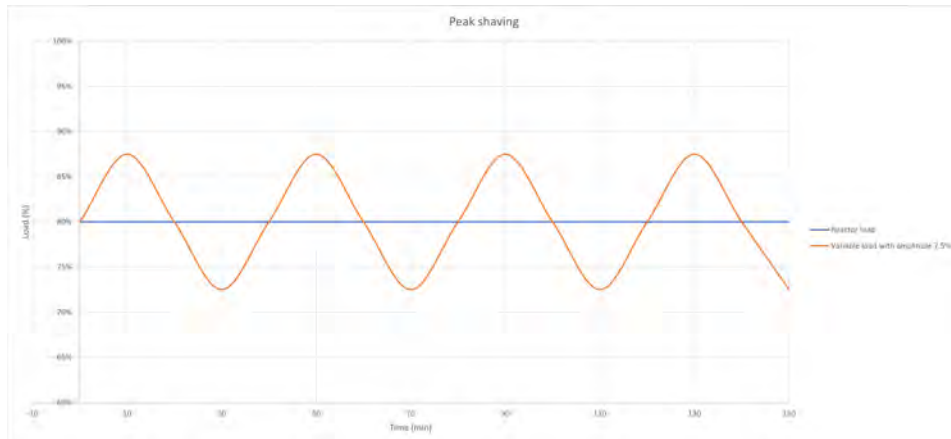


Figure 6.7: Peak shaving role of batteries

The battery system could also be used to **store energy** from the propulsion system. This would be done by storing the excess of power that is not needed for propulsion in the battery pack.

As **back-up power**, batteries are not considered because of size and weight constraints. For this purpose an emergency genset driven by internal combustion engines is a better choice [41].

In conclusion the battery system is thus implemented as a means for peak shaving and energy storage to enhance the overall efficiency of the propulsion line and decrease mechanical wear and tear of the turbine and reactor components. The exact volume and weight of this system is explained later.

The amount of energy a battery can provide over its lifetime is mainly governed by its depth-of-discharge which indicates the amount of power in percentage you can use from the battery before it needs to be recharged. The higher this percentage the more energy you can use of the battery. The depth-of-discharge will diminish over a battery's life time. This expressed by the end of lifetime capacity (E.L.C.) which gives the percentage of the battery that can still be charged at the end of its lifetime which indicates a decay of the depth-of-discharge. Most battery manufactures will recommend to replace or recycle the battery at this point but the battery may still be operable. This should be decided on a case by case basis. The E.L.C. is used as an energy margin as well. Lastly the C-rate of batteries is important to consider as this indicates how fast a battery can charge and discharge with respect to its nominal power. Based upon commercially available batteries the following properties are summarized in table 6.2.

Property	Value
Density [m ³ /MWh _e]	53.67
Weight [t/MWh _e]	30
Depth of discharge	100%
Cycle efficiency	97.8%
E.L.C.	70%
C-rate	1

Table 6.2: Derived properties for battery package from [57][5]

Using figure 6.7 and table 6.2 it is possible to calculate the total installed battery power where the 7.5% is upheld for the percentage of transient loading. This is done with the formula depicted below where r is the transient load expressed in percentage. With the total power needed and a usage interval of 20 minutes it is then possible to determine the total weight and volume of the battery pack.

$$P_{battery}[kWh] = \frac{P_{total} \times r}{E.L.C.} \times \frac{20}{60} \quad (6.4)$$

Emergency engine

The emergency engine is fitted in case of reactor failure and is able to generate 15% of the total installed power. With this amount of power the vessel is able to sail half its speed (15 knots) and provide all additional consumers of power. The amount of fuel is calculated such that the emergency engine with generator can sustain the vessel for a period of 7 days. The fuel used is MGO with a density of 0.86 t/m³ [71].

The weight and dimensions are derived from commercially available marine gensets where the electrical efficiency is 96% [103].

Property	Value
Volumetric power density[kW/m³]	93.89
Weight [kW/t]	112.36
Specific fuel consumption [g/kWh]	183

Table 6.3: Emergency engine properties[103]

Generators

The volume and weight of the generators is again based on commercially available information which can then be used to scale up for the used propulsion line. These values are 433 kW/m³ and 233 kW/t. The installed generators have an assumed efficiency of 100%. As there efficiency is already included in the thermal efficiency of the reactor [6].

Switchboard room

When figure 6.4 is observed it is seen that an AC grid is used. Another possibility could be to use a DC grid in the case of variable RPM operation of the power turbine. This would lead to a saving in efficiency as no frequency controller is used. The different lay-outs are shown in figure 6.8 for a single set-up done for simplicity.

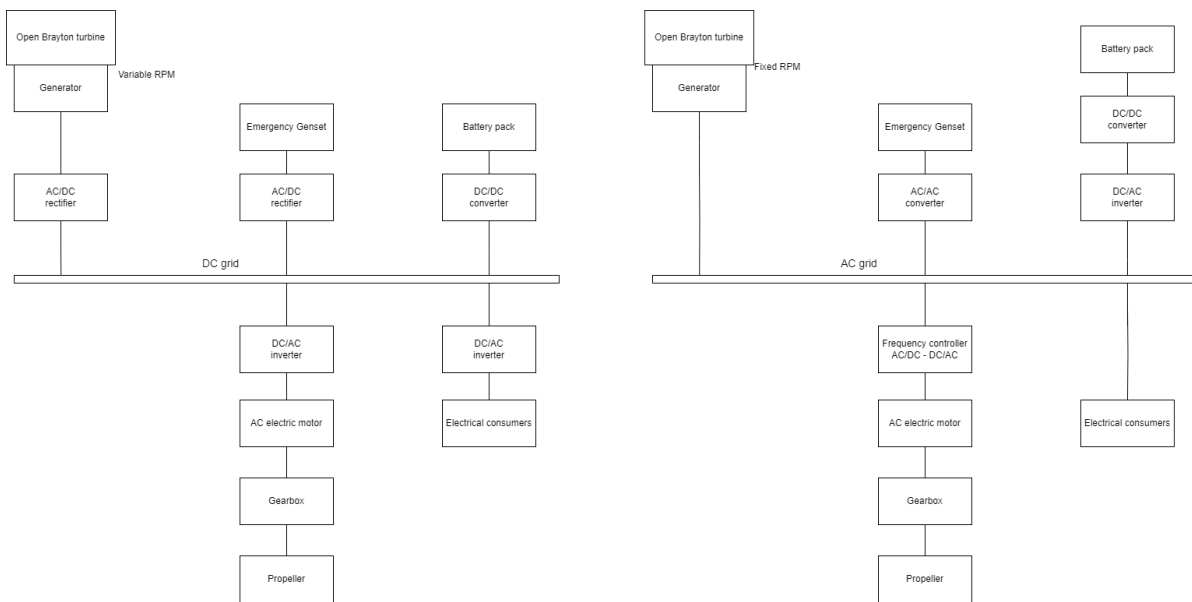


Figure 6.8: Electrical grid possibilities

Starting from the left a DC grid would have an efficiency gain for the battery pack and turbine generator if controlled with variable rpm as only a rectifier is needed for variable rpm operation. Alternatively an AC grid can be combined with a frequency controller to allow for variable rpm operation. This can be discarded as this would result in double loss of efficiency due to use of the frequency controller. If an AC grid is considered a fixed RPM prevents an additional frequency controller or rectifier thus would be more efficient in this operation mode. As seen in 6.2.1 the power turbine is commonly operated with a

variable RPM to follow the load demand of the vessel. Taking this into account a DC grid would be the best choice as this is beneficial for the overall efficiency of the propulsion line and makes the operation of batteries more efficient.

The total volume and weight of all electrical components being rectifiers, converters and busbars is combined in a main switchboard room and estimated based on reference vessels. Here a volume density of 0.02 MW/m³ and a weight density of 0.03 MW/ton are found for offshore vessels with DP3 capability. Considering that the two offshore vessels had installed powers of respectively 5 and 44 MW the relation between volume/weight and installed power can be assumed linear. A cruise vessel with 68 MW installed power had respective values of 0.04 MW/m³ and 0.07 MW/ton. Here the switchboard room is seen to be twice as power dense due to a DP2 capability. For the nuclear concept vessel a DP2 capability is more realistic thus these values are adhered to with the same linear relation. It is assumed that the generated power is divided over two switchboard rooms that are both responsible for 50% of the power conversion to the propulsors and other consumers.

Electromotors

The operating principle of a generator and electromotor is nearly identical so these are scaled in the same manner. The assumed efficiency of the electromotor is 96% [6].

Gearboxes

The gearboxes are derived from commercially available information and are selected as a single in- and output. The values corresponding to the found information are 925 kW/m³ and 511 kW/t [178]. Gearboxes are used because it is expected that the size of the electric motor would be too big for direct drive with low rpm. This means however a marginal decrease in efficiency and a possible new point of failure. The possible point of failure is covered by the redundant set-up of the propulsion line.

6.2.1.1 Total volume and weight of machinery room

Components	Volume [m ³]	weight [t]	amount [redundancy]
Reactor (spheric-cubic)	1,508-2,881	4,481	1
IHX	-		2
<i>VHTR</i>	365	1,096	
<i>MSR</i>	97	292	
Decay heat exchanger	-		2
<i>VHTR</i>	1	4	
<i>MSR</i>	1	3	
HEX	-		2
<i>VHTR</i>	420	1,261	
<i>MSR</i>	73	219	
Open brayton turbines	-		2
<i>Turbines [set of two]</i>	1,206	603	
<i>Funnel in- and outlet</i>	118m ²	-	
Generator	464	863	2
Battery pack	385	215	1
Emergency genset	321	268	2
MGO fuel tank	1,137	978	1
Switchboard room*	2,513	1,436	2
Electromotor	216	401	2
Gearbox	97	176	2
Total_{VHTR} spheric	14,240	17,885	
Total_{VHTR} cubic	15,612	17,885	
Total_{MSR} spheric	13,009	14,193	
Total_{MSR} cubic	14,382	14,193	

Table 6.4: Volume and weight of machinery room components (207 MW_e) (*) including converters, busbars and rectifiers

For the volume check all the upper limits in volume and weight are considered. Which means the cubic VHTR, this to assume worst case scenario. The depicted volumes and weights are for the single layout thus when making the volume/weight estimation the values should be multiplied with the number depicted in the most right column. For the total volume and weight depicted in yellow this is already taken into account. These values are calculated with a total installed power of 207 MW_e.

6.2.1.2 Positioning and lay-out of machinery room

The machinery room is placed aft to maximize container carrying capacity midships as the vessels is fullest in that location.

The reactor island was first positioned near deck level for the implementation of a hatchcover that could be used for refuelling purposes. It was also deemed to be the most safe position for possible collisions.

After further evaluation the reactor island was transferred near the tanktop to contribute positively to a lower center of gravity of the vessel as these components are of considerable weight which can be seen from table 6.4. It is not positioned totally on the tanktop because space is needed for the electromotors and gearboxes. Above the reactor, an open space is implemented for the possibility of maintenance and refuelling. As can be seen on figure 6.9 the reactor with shielding and intermediate heat exchangers is completely compartmentalized and positioned in the center line of the vessel. This to prevent the endangerment of any radioactive material in case of a collision or grounding as it is also positioned above tanktop. The compartmentalization is chosen to allow for an easy salvage operation in case of a ship wreck.

The open brayton turbines with primary heat exchangers and generators are moved towards the deck level to allow for easy connection with the in- and outlet of the air ducts.

On figure 6.9 the first machinery lay-out is shown together with a top view on figure 6.10.

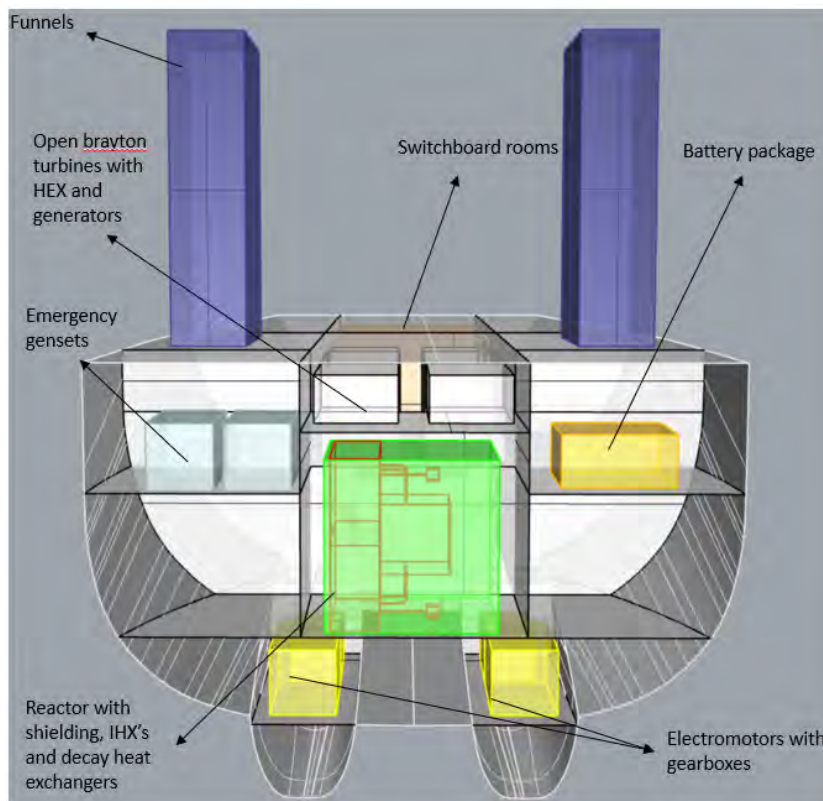


Figure 6.9: Close-up of machinery room for redundant lay-out with cubic VHTR

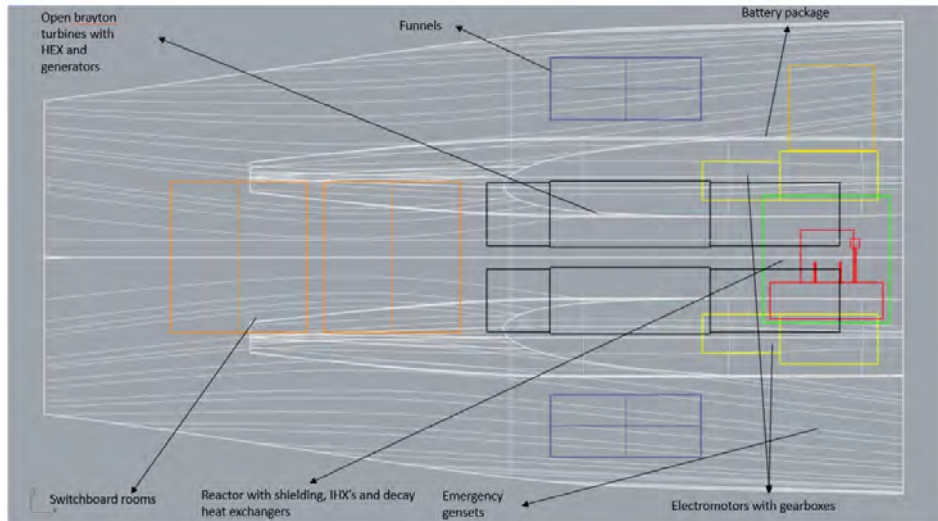


Figure 6.10: Top view of machinery room for redundant lay-out with cubic VHTR

6.2.2. Accommodation sizing

The volume and location of the accommodation is based upon reference vessels with similar TEU capacity like the CMA CGM JAQUES, HMM ALGECIRAS and the HMM OSLO all with TEU capacity's above 20,000 TEU [119]. It is put in the front part of the ship to maximize the carrying capacity as the SOLAS visibility line dictated by the IMO needs to be taken into account. This dictates that the obscured view of the sea surface needs to be less than two ships lengths or 500 m whichever is less. When the accommodation would be placed aft this would lead to a loss of container capacity on deck. It also placed there to distribute the weight longitudinally as the machinery room is place aft.

The length is taken equal to one FEU and the width extending over the breadth of the vessel leaving a passage way for the crew. The number of crew members is assumed to not variate extensively from conventional container ships. It is also stated in the Nuclear-Ship Code for nuclear merchant ships that the crew needs to follow a more stringent training program and is afterwards certified to sail with nuclear propelled ships [79]. It can however be expected that nuclear reactor specialists will need to be present during the operation of the ship for the safe operation of the reactor. Therefore the normal amount of crew members equal to 20 is increased to 25 but this is not deemed to have a significant effect on the sizing of the accommodation [119].

6.2.3. TEU sizing

The width and depth of the vessel were marginally changed to respectively 54.57 m and 35.55 m to accommodate a whole number of containers. The amount of tiers above deck is based upon reference vessels of similar TEU size mentioned in the previous paragraph but will be checked later on in this section. The space in between the top tier of containers and the hatch cover is taken above the minimum of 200 mm to assure enough ventilation space. The vertical clearance at the side of the vessel is taken as 2.1 m to ensure safe and easy passage of the crew. The double hull is taken equal to the width of one TEU as is commonly done in container ships an example of this is shown in appendix F.2 of the HMM Algeciras with a LOA of 399.9 m. This is deemed as a suitable reference because it is expected that the concept vessel will become smaller in the longitudinal direction after the volume check [119]. This way the width of the double hull decreases the large deck openings which contributes to torsional stiffness. Another solution to increase the torsional stiffness is to increase the thickness of the bulkheads in between cargo holds [153]. For the double bottom a formula of classification society Lloyd's register is used which is displayed below:

$$h_{doublebottom} = 28 \times B + 205 \times \sqrt{T} \quad (6.5)$$

The margins taken for twist locks, cell guides and inspection space are displayed on figure 6.11. Where

the longitudinal space between two FEU containers is in total 1.5 m to reserve enough room for lashings rods and inspection by the crew. The weight of a single TEU container is estimated as 14 ton as used before in the speed model for determining the port dues. The center of gravity is fixed on 45% of the height [70].

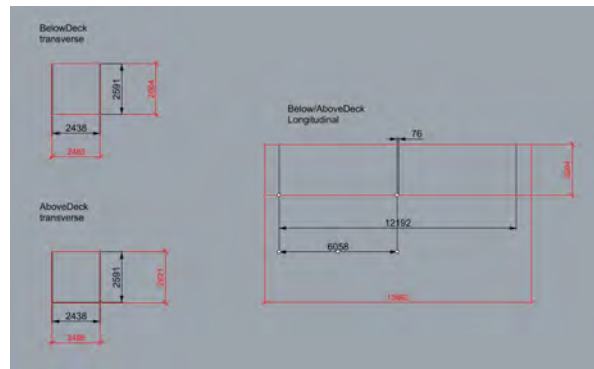


Figure 6.11: Container margins above and below deck [70]

Taking all above considerations into account this resulted in the midship cross-section displayed on figure 6.12. With a preliminary weight of each container the stacking height of the containers can be checked. This value is determined using the stacking load value that is depicted on the convention of safe containers plating of each ISO approved container. It expresses a containers ability to withstand the weight of other containers when stacked without having structural damages. The average value for a standard TEU container lies around 192-216 ton. For the purpose of this report 192 ton is used to stay on the conservative side. If this value is divided by the assumed weight of a TEU equal to 14 ton a total maximum stacking height of 13.7 containers is found. It is observed that the stacking height thus heavily depends on the weight of each individual container. This is also why stacking heights found in literature vary from 6 up until 10 and even higher [98] [36]. The stacking heights on and below deck are respectively 11 and 13 containers high as depicted on figure 6.12. These can thus be found safely for an assumed weight of 14 ton per container. In the container hold fold-out flaps in the cell guides can be used to subdivide the stack and therefore lower the stacking weight for the bottom containers [36]. A further evaluation of the weight per full container is carried out in section 6.2.5.

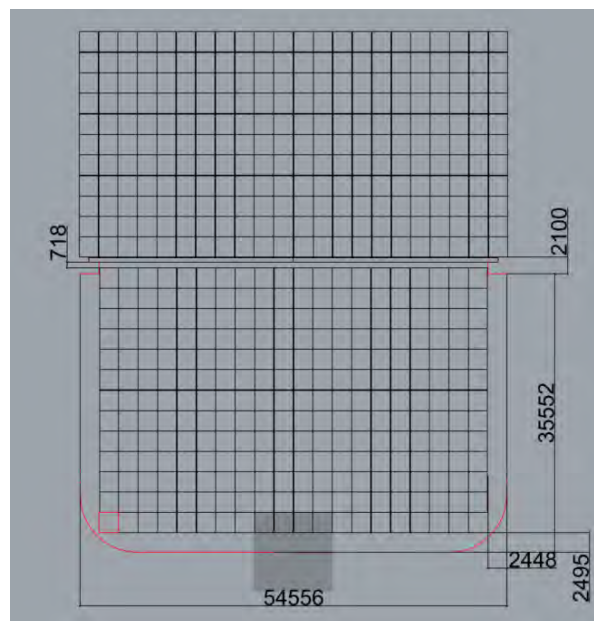


Figure 6.12: Cross-section midship

To have a realistic count of the number of containers that could be fitted in the nuclear concept vessel formed with solely the scaling factor based on TEU size, a double skin of 1.5 m in the forepeak and aftpeak was maintained. A collision bulkhead placed 10 m aft of the forward perpendicular as per SOLAS regulations was also implemented.

6.2.4. Conclusion volume check of concept design

Feature	
LOA	506.78 m
LPP	475.72 m
LWL	486.93 m
B	54.56 m
T	20.86 m
D	35.55 m
Displacement	344,148.9 t
C_b (based on LWL)	0.60
TEU	24,590

Table 6.5: Nuclear container vessel characteristics after volume check

As can be seen from table 6.5 the LOA, LWL and displacement values vary when compared to table 5.12 from previous chapter 5. The increases are respectively 1%, 2% and 5% which is deemed satisfactory for an initial volume check. The total resistance at 30 knots with this ship formed in rhino was calculated again using a grasshopper extension. Here a total of 8795 kN was calculated. This resulted in an increase of 10% in total installed power. Due to the increase in power the reactor volume and weight including its shielding would increase by respectively 7 and 5%. The rest of the propulsion chain its volume and weight are all increased by 13%.

However, for the initial volume estimation this is deemed satisfactory as the main volume that will become bigger is the machinery room and as seen on figure 6.9 and 6.10 enough free space is reserved for possible deviations. From section 6.3.1 on this is taken into account.

Reviewing table 6.5 the increase in TEU capacity equals 4,590 TEU or an increase of 23%. This means that the scaling factor based on TEU volume gives an over dimensioned vessel. It also explains why the initial concept design lies far away from the main dimensions of conventional container ships.

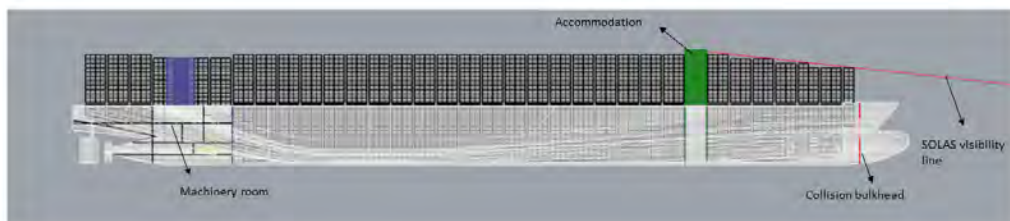


Figure 6.13: Side-view

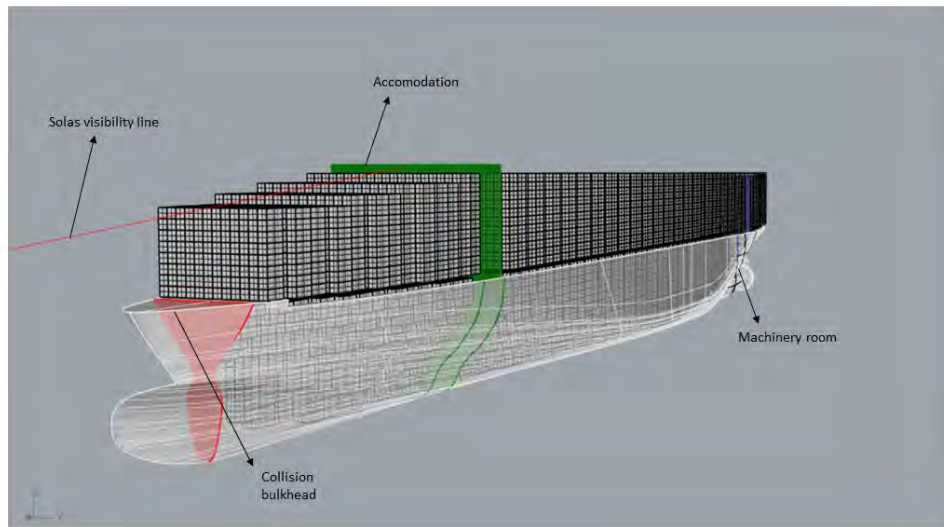


Figure 6.14: Isometric view

From the previously mentioned evaluation it is observed that the nuclear concept vessel that was initially scaled to carry 20,000 TEU can in fact transport 24,590 TEU which is a 23% increase. This increase can be evaluated in the speed model which was discussed in the previous chapter. The increase in cargo capacity translates to an increase in design speed of 2 knots. This considerably increase is due to the large influence of the freight rate as previously addressed.

This observation shows that the initial design speed of 30 knots was even on the conservative side as the vessel that was used for this calculation could in fact carry more containers as initially estimated. Thus leading to a higher revenue over time which translated to a higher increase in design speed. For the further design of the nuclear concept vessel 30 knots will be held as the design speed so keeping this potential increase as design margin.

In conclusion of the volume check it can be stated that scaling with a factor of 1.71 based on TEU size results in a concept vessel that can carry 23% more containers than initially stated. This is a first reason to scale down the initial nuclear concept vessel in main dimensions.

6.2.5. Weight assessment of initial nuclear container vessel

6.2.5.1 Deadweight

Aside of a volume check a weight assessment is carried out in order to compare the displacement with the deadweight (DWT) and lightship weight (LSW). This is to evaluate if the concept vessel is in equilibrium at given draft. The displacement is already calculated by making use of the formed rhino model depicted in the previous paragraph. The deadweight accounts for the cargo weight, ballast weight, bunkers, lube oil, spares, fresh water and crew. To make an estimation for the cargo weight the t/TEU values must be re-evaluated as this value was taken as 14 ton in the speed model but not validated. For this, two references vessels being the MSC Gülsun and the CMA CGM Jacques¹ are taken with a respective TEU capacity of 23,756 and 23,112 TEU [118][119]. To calculate the t/TEU of these vessels all factors except the cargo weight are subtracted from the design deadweight which results in a remaining weight reserved for cargo. This value is divided by the number of TEU and results in cargo-DWT/TEU expressed in t/TEU. These are calculated to be 7.28 and 7.65 t/TEU for a diesel and dual fuel (diesel + LNG) container ship respectively. The same exercise is done for the nuclear concept vessel where

¹Propelled by LNG

the design deadweight is derived from the two references vessel based on a factor expressed in DWT/TEU. This resulted in a cargo-DWT/TEU of 7.95 t/TEU for a carrying capacity of 20,000 TEU which shows that the nuclear concept vessel can carry more ton of cargo when compared to vessels of similar TEU size. This is due to the decrease in needed bunkers as the amount of nuclear fuel needed is very limited. In appendix F.3 the comparison calculation for the references vessels propelled by diesel and LNG .

This is easily demonstrated when the operating profile of figure 6.6 is considered for the duration of five years. This means that the concept vessel will sail 70% of the time at full load (100% of reactor load) and 30% at part load (20% of reactor load). When the total installed power of 207 MW_e is taken into account and the earlier derived specific fuel consumption of 0.0014 g/kWh a total of 9 ton in 5 years is needed. This value is for all nuclear material not only the fissile portion. This can be seen as negligible when the total weight of the emergency propulsion is observed from table 6.4 being equal to 978 t for only a period of seven days at half of the design speed. This also shows the benefit of using nuclear power with respect to autonomy and refuelling period. Which can vary between 18 months and the lifetime of the reactor that can be up to 60 years and more [71].

In order to satisfy the load factor of 85% assumed in the speed model the weight of a full container is taken as 9 ton and the weight of an empty container is taken equal to 2 ton. This gives a total of 7.95 ton per TEU which equals the calculated value derived from real life examples. The weight of a container could be varied for different loading conditions as long as the 7.95 t/TEU value is satisfied as this limits the carrying capacity of the vessel.

The ballast weight is taken as 0 ton because it is assumed the concept vessel does not need ballast in fully loaded condition. Lube oil, spares, fresh water and crew weight are estimated using Ventura's formulas which are based on statistical regression analyses of diesel propelled container ships where the lube oil estimation is done for gas turbines. It is assumed these estimations are also valid for the nuclear concept vessel [175]. A summary of the calculated weights is given below for the nuclear concept vessel.

Feature	
Cargo deadweight	159,000 t
Ballast weight	0 t
Nuclear fuel	9 t
Emergency diesel fuel	978 t
Lube oil	29 t
Spares	456 t
Fresh water	84 t
Crew	10 t
Total design deadweight	160,559 t
Cargo DWT/TEU	7.95 t/TEU

Table 6.6: Deadweight calculation nuclear concept vessel in fully loaded condition

6.2.5.2 Lightship weight

The lightship weight consist out of the structure steel weight of the hull and accommodation, equipment weight on deck and the weight of the machinery room excluding the emergency fuel as this is already included in the deadweight. This was first estimated using estimation formulas by D'Almeida (2009). This estimation method used a formula depending on LOA, B and D. To cross-check this formula references ships from significant ships were used with LOA varying from 250-399.9 m and TEU capacity ranging from 6,000 to 24,000 TEU. The average diversion in lightship weight was +29%. This estimation method was therefore discarded.

A second approach was carried out using the database of C-Job called RefWeb which is previously used in chapter 3. Using the parameters LOA, B and D, a regression model was created to make a prediction of the lightship weight. The main problem with the database of C-Job was the limitation in length which was restricted to 214 m. Therefore the before mentioned reference vessels from significant

ships were added to the regression model which lead to the final regression model depicted on figure 6.15.

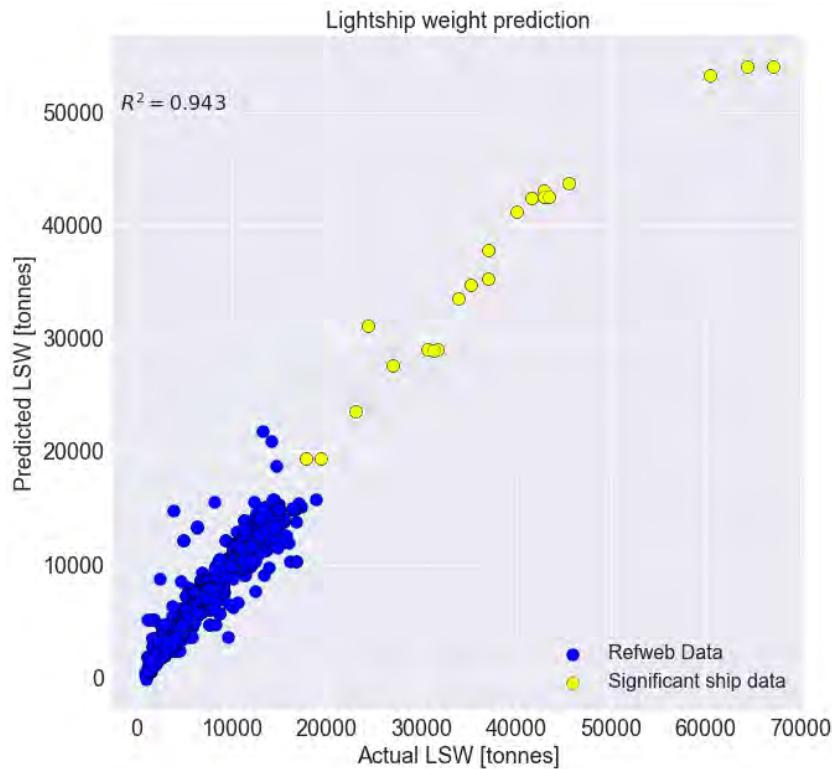


Figure 6.15: Lightship weight prediction based on significant ship 2004-2020 and [72].

Here the RefWeb and significant ships data points are combined where the X-axis represents the actual and the Y-axis the predicted lightship weight. The R^2 is depicted to be 0.943 which gives the indication that the regression function gives a good fit with the used data points. The actual regression function with weighted factors is depicted below.

$$LSW(LOA, B, D) = -81.21 \times LOA + 239.15 \times B + 251.72 \times D + 0.3965 \times LOA^2 \quad (6.6)$$

If this function is used to predict the lightship weight of the references vessel used form significant ships an average diversion of -3% is found. Therefore this method is used for the prediction of the lightship weight of the nuclear concept vessel where the weight of the conventional machinery room is subtracted based upon data of the HMM ALgeciras with a total number of 23,964 TEU [119]. This is done because the lightship weight function only gives a total weight and gives no distinction between hull structure, deck equipment or machinery weight. Afterwards the weight of the nuclear machinery room is added as calculated in table 6.4 for the cubic VHTR as this led to the highest weight as observed in table 6.4. With exclusion from the weight of the emergency fuel as this is part of the deadweight. The result is seen in table 6.7.

Feature	
Lightship weight _{regression model}	82,673 t
Machinery room diesel	-2,955 t
Machinery room nuclear	16,907 t
Total lightship weight	96,625 t

Table 6.7: Lightship weight calculation nuclear concept vessel

6.2.5.3 Total weight assessment

The total calculated deadweight and lightship weight are added together and compared with the scaled displacement from table 6.5. The required displacement is equal to 257,184 ton and the available displacement is equal to a total of 344,149 ton. This results in spare displacement of 86,965 ton (25% difference). If the LWL and B from table 6.5 are kept constant and only the change in draft is observed the difference in displacement would result in a decrease of draft equal to 5 m. This indicates that the concept vessel is also over dimensioned on a weight aspect. Therefore a second reason is given to scale down the nuclear concept vessel based upon a scaling factor of 1.71.

6.3. Check of main dimensions with real-world constraints

The initial main dimensions of the nuclear concept vessel are adhered to real-world constraints in order to see if the design lies within the boundaries to be operable for the proposed sailing routes.

These limitations translate to restrictions in main dimensions for the ports that were selected for the speed model. These being Rotterdam, New York, Shanghai and passage way through Suez. In the table below the restrictions can be observed. For the purpose of this study the restrictions are limited to max LOA, B, design T and air draft.

Port/reference ships	LOA [m]	B [m]	design T [m]	Air draft [m]	Source
Rotterdam	400.00	61.50	22.55	N.A.	[148] [call Port of Rotterdam]
Shanghai	N.A.	N.A.	15.00	N.A.	[131]
New York	N.A.	68.60	15.24	65.53	[123]
Suez canal	400.00*	77.50**	20.11**	68.00	[157][18]
Final limitations	400.00	61.50	15.00	65.63	

Table 6.8: Real-world constraints in main dimensions (*) over 400 m vessels need permission to cross suez canal (**) additionally cross-sectional area not more as 1,006 m²

Limitations in length are mainly due to manoeuvring limitations, the beam limitation comes into play due to the reach of shore based gantry cranes being able to load/unload all containers. Draught limitations are put into place due to the depth of the canals and the air draft due to installed bridges in canals or ports. The port of Rotterdam stated that container vessels with main dimensions surpassing the ones in table 6.8 need to undergo a thorough investigation in sight of the safe navigation inside the port. They did not deny that bigger ships could be possible in the future ².

To further validate the final constraints they are compared with reference ships that carry a similar TEU size. From this it is seen that all three reference vessels lie very close to the found values so therefore these boundary conditions are further validated.

Reference ships	LOA [m]	B [m]	design T [m]	TEU capacity [TEU]	Air Draft[m]	Source
CMA CGM JACQUES SAADÉ	399.90	61.30	14.50	23,112	-	[119]
HMM Algeciras	399.90	61.00	14.50	23,964	-	[119]
HMM Oslo	399.90	61.50	14.50	23,820	-	[119]
Final limitations	399.90	61.50	15.00	20,000	65.63	

Table 6.9: Comparison of reference vessels with final constraints

When the main dimensions of the nuclear concept vessel are observed from table 6.5 it can be seen that both the length and draft lie outside the limitations found in real life. This gives a third and final reason to scale down the nuclear concept vessel. In addition it also gives an indication where the vessel should be increased or decreased in size and gives the margins that go with it.

²This information was gathered after a phone call with the port coordination center of Rotterdam.

6.3.1. Scaling down of nuclear concept vessel

As the volume check, weight assessment and the real world constraints gave three reasons to scale down the nuclear concept vessel this is carried out using the maximal dimensions depicted in table 6.8 and 6.9.

By carrying out the scaling operations the initial nuclear concept vessel main dimensions are altered to 399.90 m, 61.50 m and 15.00 m for respectively the length overall, width and draft.

This sequence of operations yielded a displacement of 219,011 ton, accompanied by a block coefficient of 0.61. A noteworthy observation is the reduction of resistance at a speed of 30 knots by 7.2%³. This phenomenon is explicable by the alteration in displacement and wetted area. As a new Froude number of 0.25 for this new length with 30 knots is observed, which still falls within the regime where frictional resistance predominates. A reduction in wetted area therefore results in a decrease of frictional resistance.

Upon revisiting the weight assessment process described in section 6.2.5, it becomes evident that the modified conceptual vessel falls short in accommodating a carrying capacity of 4.3% in displacement. This discrepancy reinforces the earlier deduction of resistance reduction, as increasing the vessel's carrying capacity to the stipulated 20,000 TEU demands an elevation of the block coefficient (C_b), leading to increased resistance.

To increase the block coefficient, alterations are carried out on the vessel's foreship while keeping the stern shape unaltered, guided by the observation that the LCB lies 5.5% aft of midship. Preserving midship LCB placement results in a lower trim. Thus, the foreship's volume is increased to achieve a minimum 4.3% expansion in carrying capacity.

Through this change, the block coefficient is elevated from 0.61 to 0.63, resulting in a total displacement of 229,403 ton. This represents a modest overshoot of 0.3% when compared with the earlier calculated displacement, a deviation deemed acceptable due to its potential utility in subsequent design phases. These alterations lead to a decrease of resistance equal to 2.2%⁴ when compared to the nuclear concept vessel with a LWL of 486.93 m depicted in table 6.5. This shows again that the frictional resistance is dominant in the selected speed domain.

This results in a total installed power of 222 MW_e⁵. Additionally, the total TEU capacity is re-evaluated, considering a maximum air draft of 65.63 meters necessary for entering the port of New York. The resultant TEU capacity of 20,294 TEU satisfactorily meets the designated criterion of 20,000 TEU. Notably, the DNV rules referring to double hull and double bottom are respected as well. With respective values of 3.463 m and 2.585 m.

6.4. General arrangement 1st iteration

Using the outcome of the down scaling stated in the previous section the design spiral depicted on figure 6.1 is entered by a first iteration on the general arrangement. The result is seen on Figure 6.16, 6.17, 6.18, 6.19, 6.20 & 6.21. These reflect the present configuration adapted to real-world constraints and a decrease in volume and weight. The main particulars are summarized in Table 6.10.

³Difference between 8,795 and 8,164 kN

⁴Difference between 8,795 and 8,600 kN

⁵Taking into account the same values for η_h , η_r , η_o as assumed in section 5.1.2.8 and the propulsion line efficiencies depicted in figure 5.2

Feature	
P_{ne}	222 MW _e
LOA	399.90 m
LBP	373.08 m
LWL	384.46 m
B	61.50 m
T	15.00 m
D	33.00 m
Lightship weight	66,787 t
Design Deadweight	160,849 t
Design Displacement	229,403 t
C_b (based on LWL)	0.63
LCB from APP	182.96 m
TEU capacity	20,294 TEU
Surplus in carrying capacity	664 t

Table 6.10: Nuclear container vessel characteristics after real-world constraints

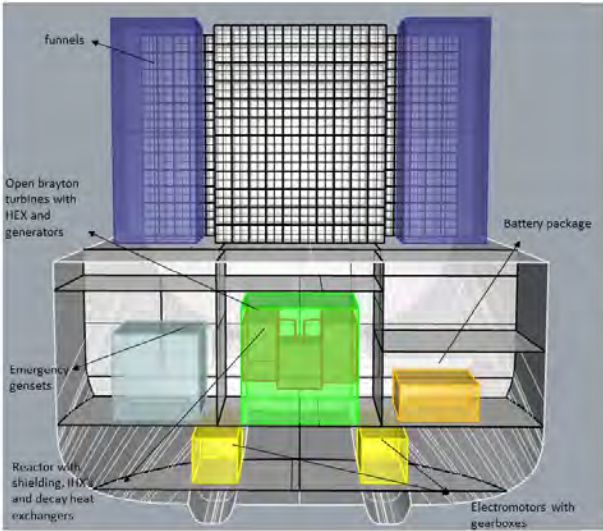


Figure 6.16: Machinery room 1st iteration

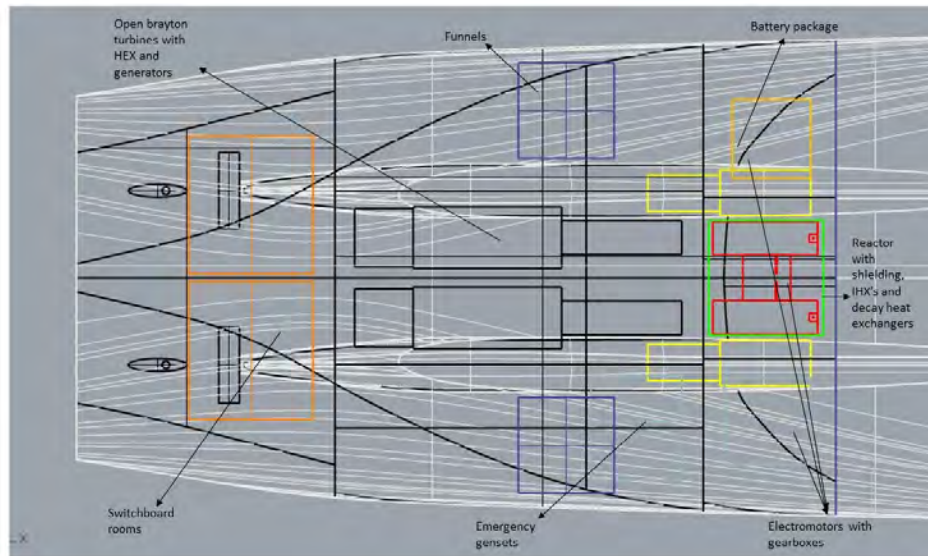


Figure 6.17: Machinery room 1st iteration (top view)

The machinery room is refitted using the new installed power of 222 MW_e using the same method as described in section 6.2.1. Compared to the resistance of the nuclear concept vessel after the volume check a reduction in power equal to 2.2% is calculated. Due to this reduction the reactor volume and weight including its shielding are both decreased by 1%. The rest of the propulsion chain its volume and weight are all decreased by 2%. The percentages are expressed in relation with the machinery components calculated for a total installed power of 227 MW_e which stems from a resistance equal to 8795 kN that was found for the nuclear concept vessel after the volume check in section 6.2.4.

Conforming to contemporary regulations governing nuclear propulsion in maritime commerce, the placement of the reactor compartment adheres to the SOLAS nuclear code, a regulatory framework last revised in 2016. Notably, this code is tailored to pressurized water reactors, although the intrinsic enhanced passive safety attributes of both the VHTR and MSR warrant compliance even within its bounds, serving a cautious approach. Specifically, the SOLAS nuclear code mandates that the reactor compartment be situated longitudinally at a minimum distance of $1.3L^{2/3}$ or 14.5 m from the vessel's side, selecting the lesser of the two, while transversely adhering to a placement of $B/5$ or 11.5 m, again selecting the lesser value [79]. These values are respectively 80.45 m and 22.91 m.

Communication was established with Bureau Veritas to seek insights into potential updates concerning regulations pertaining to nuclear merchant vessels. Regrettably, it was conveyed that there exists no current intention to undertake such revisions within the foreseeable future.

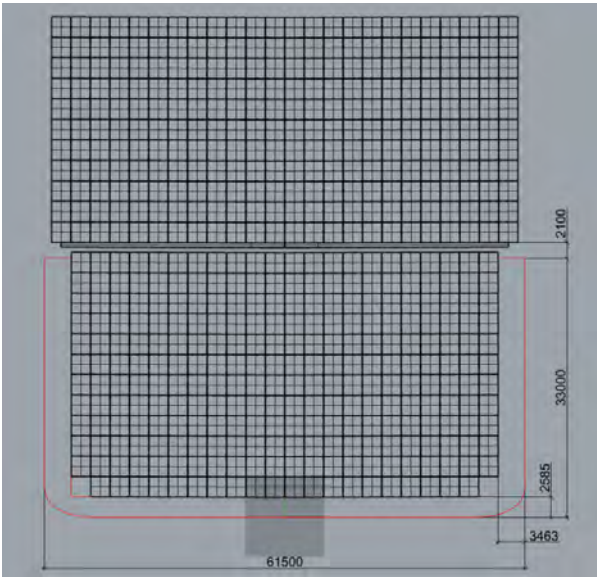


Figure 6.18: Cross-section midship 1st iteration

The number of tiers above and below deck are respectively 11 and 12 which are assumed safe when an average weight per container of 9 ton is assumed. Taking into account a stacking load value of 192 ton as described in section 6.2.3. In addition when the stacking heights are compared with a midship cross-section of the HMM Algeciras depicted in appendix F.2 a similar number of tiers is observed. A more detailed analysis with varying container weights could be carried out but this lies outside the scope of this report.

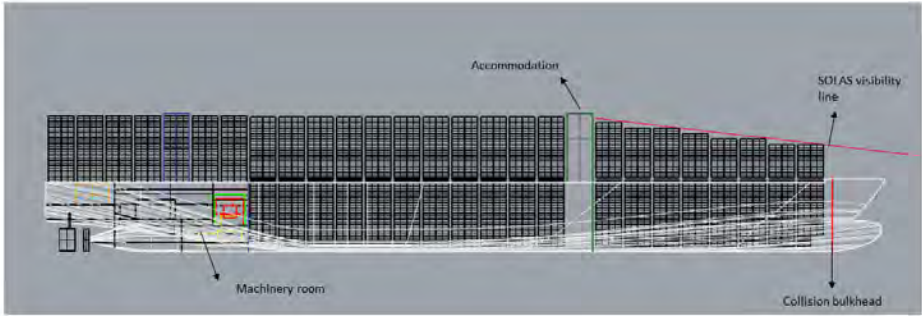


Figure 6.19: Side-view 1st iteration

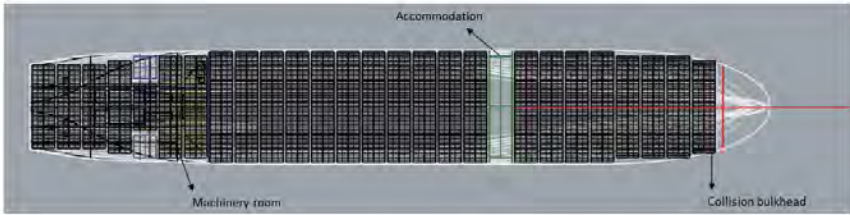


Figure 6.20: Top view 1st iteration

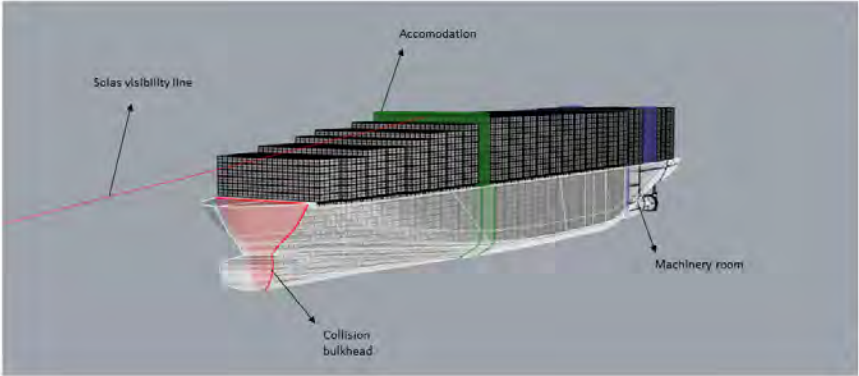


Figure 6.21: Isometric view 1st iteration

6.5. Stability 1st iteration

The next step in the design spiral is evaluating the initial stability. Using the calculated weights and general arrangement it is possible to make a first calculation to evaluate the impact of the increase in design speed and the nuclear propulsion on the stability. The minimum design criteria applicable to all ships depicted by the IMO MSC.267(85) is used. Here four loading conditions are defined and listed in table 6.11. For the nuclear concept vessel however departure and arrival condition are marginally the same condition as the deadweight consists mainly of the cargo deadweight and the fuel weight is very limited⁶. As this was also observed in section 6.2.5. Therefore the scenario's that will be evaluated are departure/arrival in fully loaded and ballast condition where departure and arrival are assumed the same from a weight perspective. As depicted in table 6.12.

Loading condition	Cargo condition	Consumables condition
Departure	fully loaded	100%
Arrival	fully loaded	10%
Departure	no load	100%
Arrival	no load	10%

Table 6.11: Loading conditions IMO intact stability code

Loading condition	Cargo condition	Consumables condition
Departure/Arrival	fully loaded	100%
Departure/Arrival	no load	100%

Table 6.12: Loading conditions nuclear concept ship

6.5.1. Departure/arrival fully loaded condition

To calculate the initial stability of the nuclear concept vessel the position of the center of gravity is determined first. The calculation can be found in appendix G.1.1. The result is depicted in table 6.13.

Component	weight [t]	LCG [m]	TCG [m]	VCG[m]	L-MOM [tm]	T-MOM [tm]	V-MOM [tm]
Lightship	69,370	147.754	-0.103	21.081	10,249,615	-7,113	1,462,405
Deadweight	160,798	190.463	-0.042	31.451	30,626,116	-6,763	5,057,327
Total	230,168	176.403	-0.060	28.566	40,602,225	-13,876	6,575,072

Table 6.13: Point of gravity determination of nuclear concept vessel loaded condition

The calculated center of gravity together with the 3D rhino model is used as input for stability software inside the program Delftship. This makes sure that the intact stability criteria of the IMO can be verified. The required values together with the attained values from Delftship are displayed in table 6.14. The GZ-curve is depicted on figure 6.22.

Feature	Required	Attained
Area 0°- 30°	>0.055 mrad	0.333 mrad
Area 0°- 40°	>0.090 mrad	0.604 mrad
Area 30°- 40°	>0.030 mrad	0.271 mrad
GZ at 30°	>0.200 m	1.609 m
Angle max GZ	>25°	34.3°
Initial GM	>0.15 m	1.924 m
Severe wind and roll criteria	See GZ curve	GZ curve

Table 6.14: Intact stability check departure/arrival condition fully loaded

⁶9 ton for a period of 5 years

In table 6.14 it can be observed that the nuclear concept vessel adheres to all intact stability requirements together with a GM of a good magnitude as this ensures good initial stability and is not too high to cause severe rolling motions.

The aft and fore draft are respectively 17.036 m and 12.465 m which gives a mean draft of 14.751 m. This insures propeller immersion and gives a trim of -4.571 m which translates to a trim angle of -0.7° . The list is calculated to be -1.8° both values are deemed to be satisfactory for the current analysis (see appendix G.1.5).

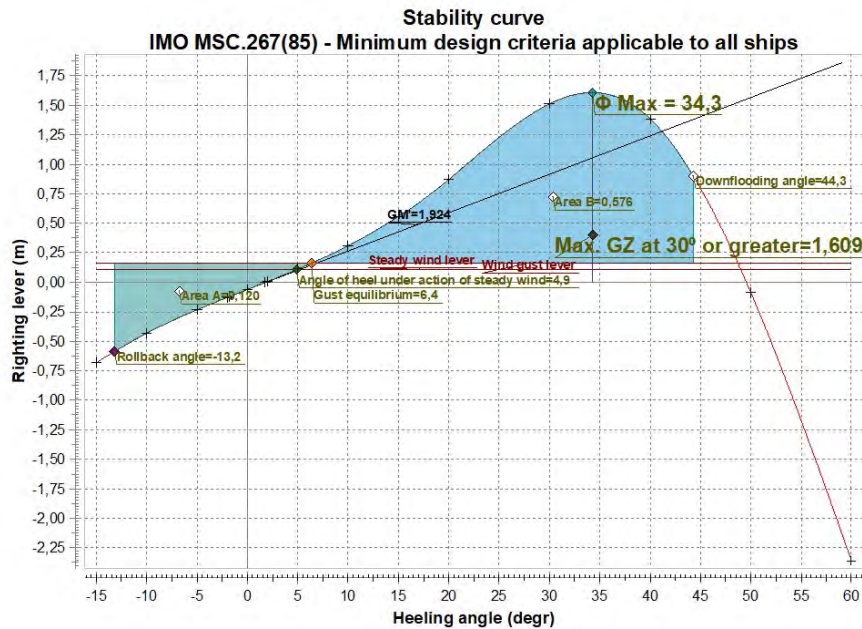


Figure 6.22: GZ-curve departure/arrival condition fully loaded

On figure 6.22 the GZ curve for the fully loaded condition is depicted. In order to comply to the severe wind and roll criteria the vessel is subjected to a sequence of external forces. First a static wind force with a speed of 51.54 knots is exerted on the vessels wind silhouette which can be found in appendix G.1.5. This results in an angle of heel equal to 4.9° portside. Afterwards the vessel is pushed to the starboard side by the influence of waves to an angle of 13.2° . At that point the vessel is subjected to a wind gust from where it rolls back to an angle of heel equal to 6.4° . The area under the GZ curve from the roll back angle up until the gust equilibrium angle is called area A. From the gust equilibrium up until the downflooding angle the area is called B. The ratio A/B must be equal or smaller than 1 for the vessel to overcome the sequence of external forces in a safe manner and return to its equilibrium position. The ratio in this condition is equal to 0.21 thus the vessel is able to overcome these forces safely.

6.5.2. Departure/arrival ballast condition

For the initial stability in ballast condition the followed method for the determination of the center of gravity's location is the same. The only difference is that the cargo deadweight is equal to zero and ballast tanks are used to ensure the vessels stability and propeller immersion. In total five ballast tanks are added, two in the double bottom, two in the double side and one at the forepeak. Their total capacity and location are depicted in appendix G.1.2 along with the other components of the ships deadweight. The lightship is identical to the loaded condition. A graphical lay-out of the ballast tanks is found in appendix G.1.6. It is observed that the total ballast capacity is equal to 44% of the design deadweight depicted in table G.1.4. This lies around 15% higher then that of conventional diesel container ships [119]. This is explained by the absence of large fuel tanks that contribute to the total deadweight of the vessel. It should however be noted that this is calculated for an extreme case where not a single full or empty container is on board. The propeller is also fully immersed in this case but this can be re-evaluated as it is seen in practise that this is not always the case. Therefore this is not taken as a hard design conclusion but can be further investigated in follow-up research.

The final center of gravity location in ballast condition is depicted in table 6.15.

Component	weight [t]	LCG [m]	TCG [m]	VCG[m]	L-MOM [tm]	T-MOM [tm]	V-MOM [tm]
Lightship	69,370	147.754	-0.103	21.081	10,249,615	-7,113	1,462,405
Deadweight	72,195	195.839	-0.093	13.082	14,138,601	-6,763	944,453
Total	141,565	172.276	-0.098	17.002	24,388,216	-13,876	2,406,858

Table 6.15: Point of gravity determination of nuclear concept vessel ballast condition

The calculated center of gravity together with the 3D rhino model is again used as input for stability software inside the program Delftship. Which results in the attained intact stability values depicted in table 6.16.

Feature	Required	Attained
Area 0°- 30°	>0.055 mrad	2.502 mrad
Area 0°- 40°	>0.090 mrad	4.127 mrad
Area 30°- 40°	>0.030 mrad	1.626 mrad
GZ at 30°	>0.200 m	9.949 m
Angle max GZ	>25°	46.3°
Initial GM	>0.15 m	19.441 m
Severe wind and roll criteria	See GZ curve	GZ curve

Table 6.16: Intact stability check departure/arrival condition ballast

From table 6.16 it can be seen that all intact stability criteria are satisfied. The GM value is observed to be 19.441 m which is a rather high value and can lead to excessive short rolling periods at sea. This can cause wear and tear of the deck equipment and discomfort of the crew. It is therefore advised to re-evaluate the stability in ballast condition in further research to address these phenomena. This can be done by placing ballast tanks at higher points above the keel which will increase the vertical position of the center of gravity and therefore lower the GM value. For the purpose of this report the current stability data are assumed to be satisfactory.

The aft and fore draft are respectively 12.740 m and 7.060 m which gives a mean draft of 9.900 m. This insures propeller immersion and gives a trim of -5.680 m which translates to a trim angle of -0.9°. The list is calculated to be -0.3° both values are deemed to be satisfactory for the current analysis (see appendix G.1.5).

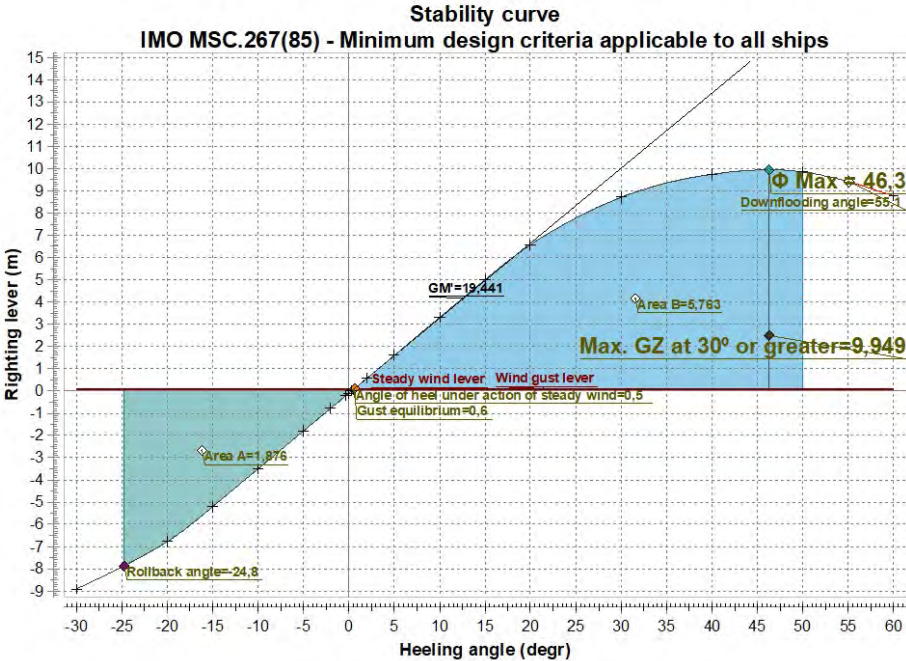


Figure 6.23: GZ-curve departure/arrival condition ballast

From figure 6.23 it is observed that the vessel is also able to withstand the sequence of external forces in ballast condition as the ratio A/B is equal to 0.33.

6.6. Propulsors 1st iteration

The following step in the design spiral is evaluating the propulsors. Starting from a design speed of 30 knots which translates to a froude number of 0.25 the choice of conventional propellers is evident. The propulsive efficiency of waterjets and high speed propellers would lie too low in the calculated speed domain. In addition conventional propellers are widely used on container ship thus would present far less design implications.

Hereafter the comparison is made between using two or more propellers to propel the ship at 30 knots. The two propeller configuration is evaluated together with a three propeller lay-out to investigate the differences. In order to do this in an effective way four design criteria are discussed being the minimum blade area ratio, maximum tip speed, maximum power density and overall efficiency of the propulsion chain.

Auf'm Keller Criteria

First the Auf'm Keller criteria is used to give a rough estimation of the required blade area ratio to prevent cavitation due to excessive thrust loading. The diameter is fixed at 10.5 m in order to comply with hull clearances according to DNV, the number of blades is taken as 5 as commonly used for container ships. The Keller criteria is thereby given by following formula [91]:

$$\frac{A_e}{A_o} = \frac{(1.3 + 0.3Z)T}{(p_o + \rho gh - p_v)D^2} + k \quad (6.7)$$

Where:

- Z = number of blades [-]
- T = thrust per propeller [N]
- p_o = atmospheric pressure = 101,325 [Pa]
- ρgh = hydrostatic pressure with h equal to 9.32 m [Pa]
- p_v = vapour pressure of water = 2,339 [Pa]
- D = diameter of propeller = 0.7T [m] [105] (with T= draft)
- k = keller factor = 0.2 [-]⁷

Using equation 6.7 it is observed that the thrust per propeller is yet to be determined. This can be easily done using following formula:

$$T = \frac{R}{1 - t} \quad (6.8)$$

Where R is the total resistance in newton and t is the dimensionless thrust deduction factor. The thrust deduction factor accounts for an increase in resistance due to the presence of the propeller as it sucks water towards the propeller and therefore increases the resistance on the hull. Together with the dimensionless wake factor, which accounts for the decrease in speed of advance towards the propeller due to the presence of the hull, the thrust deduction forms the hull efficiency.

For the determination of the thrust deduction and wake factor of the three propeller lay-out it is assumed that the center propeller acts as a single screw and the wing propellers act as a double screw.

The wake factor is estimated using Taylor's estimation formulas for early concept design [175]. The thrust deduction factor is estimated using Hekscher estimation formulas assuming exposed propellers shafts with appendages for double screw [124]. The difference between single and double screw is made as the wake factor is expected to decrease due to the propellers being positioned more outwards. The thrust deduction factor is seen to decrease as well for double screw propellers assuming exposed shafts. This can be explained by the reduction in horizontal surface where the propeller exerts a vertical force on. This way less sinkage is observed which results in a reduction of added resistance.

⁷0 for ships with a smooth wake distribution like naval ships and 0.2 for single screw ships. Taken as 0.2 for this case as a safety margin.

	wake factor	thrust deduction factor
Single screw	$w = 0.5C_b - 0.05$	$t = 0.5C_p - 0.12$
Double screw	$w = 0.55C_b - 0.2$	$t = 0.5C_p - 0.18$

Table 6.17: Thrust deduction and wake factor estimation [175][124]

Using the previously determined C_b of 0.63 it is possible to determine the wake and thrust deduction factor for both propeller lay-outs. With a calculated total resistance of 8,600 kN at 30 knots using Holtrop & Mennen it is possible to calculate the min A_e/A_o for both propeller lay-outs⁸. The calculated wake, thrust deduction factor and corresponding thrust per propeller are depicted in table 6.18 for the two propeller lay-out and table 6.19 for the three propeller lay-outs with corresponding minimum A_e/A_o .

	Propeller
t [-]	0.14
w [-]	0.15
T/propeller [kN]	5119
Min A_e/A_o [-]	0.867

Table 6.18: Min A_e/A_o calculation for lay-out with two propellers

	Center propeller	Wing propellers
t [-]	0.20	0.14
w [-]	0.27	0.15
T/propeller [kN]	3583	3413
Min A_e/A_o [-]	0.667	0.644

Table 6.19: Min A_e/A_o calculation for lay-out with three propellers

From table 6.18 it is observed that the required blade area ratio for the two propeller lay-out is rather high but still falls within practical limits [105]. This is explained by the high thrust loading that is divided over two propellers. In table 6.19 it is seen that the minimum A_e/A_o lies significantly lower for both the center and wing propeller which follows from the decrease in thrust loading per propeller.

Maximum tip speed

To further evaluate if the propeller lay-outs can operate without having excess cavitation the tip speed should be evaluated. As the practical limit found in literature for open water propellers lies around 40 - 45 m/s [114][144]. In order to do this the software PropCalc is used where the optimization method with input thrust, ship speed and propeller diameter is chosen. The remaining main input or minimum requirements are previously discussed in table 6.18 & 6.19 for both propeller lay-outs.

Propcalc uses following formula to construct the thrust coefficient curve of the vessel:

$$K_t = \frac{T}{\rho V_a^2 D^2} \times J^2 \quad (6.9)$$

Where:

- K_t = thrust coefficient [-]
- T = thrust per propeller [N]
- V_a = speed of advance = $V(1-w)$ [m/s]
- D = propeller diameter [m]
- J = advance ratio [-]

⁸Resistance for both lay-outs is taken equal here. Thus the difference between a double skeg or single skeg with two exposed shafts is not taken into account

The Wageningen B-series is used in Propcalc to select an initial propeller design. As a first propeller the B5-90 and B5-75 are chosen for respectively the two and three-propeller lay-outs. This is chosen to adhere to the Auf'm Keller criteria. Using the open water diagram of the selected propeller it is possible to plot the K_t ship curve depicted in equation 6.9.

Thereafter the corresponding torque coefficients and open water efficiencies are found for varying pitch over diameter ratio's. This is done to find an optimal open water efficiency and therefore optimal working point of the propeller. When this is carried out it is possible to calculate the rotations per second (RPS) of the propeller. This can be done using the advance ratio that is calculated with following formula:

$$J = \frac{V_a}{nD} \quad (6.10)$$

Where

- n = rotations per second [rev/sec]

The corresponding J values are depicted in table 6.20 & 6.21 along with the calculated RPS and tip speed for respectively the two and three propeller lay-out.

	Propeller
J [-]	0.88
n [rev/s]	1.42
Tip speed [m/s]	46.84

Table 6.20: Tip speed evaluation using the wageningen B5-90 series in Propcalc

	Center propeller	Wing propellers
J [-]	0.90	1.09
n [rev/s]	1.20	1.15
Tip speed [m/s]	39.58	37.93

Table 6.21: Tip speed evaluation using the wageningen B5-75 series in Propcalc

The tip speed in table 6.20 and 6.21 is calculated by translating the RPS using the diameter of the propeller equal to 10.5 m. It is observed that for the two propeller lay-out the tip speed lies outside the found interval of 40-45 m/s indicating that thrust breakdown due to cavitation is likely to occur. For the three propeller lay-out both the center as wing propellers satisfy the tip criteria.

From this observation the three propeller lay-out has a slight benefit over the two propeller lay-out. Which is explained by the decrease of thrust per propeller and thereby the rotational speed in its optimal working point which in turn lowers the tip speed of the propeller.

It is however stated in literature that the geometry of the blade sections have a high influence on the maximal tip speed. An optimised blade section would be able to operate at lower cavitation numbers without any thrust breakdown. This means an increase in possible resultant velocity at the same local pressure which results in a higher possible maximum tip speed.

Therefore a design choice based on tip speed alone can not be made.

Maximum power density

To further evaluate the design choice of a two or three propeller lay-out another physical limit is tested namely the maximum delivered power of an open water propeller expressed in kW/m^2 before several problems can occur in practice. These can vary from vibrations and erosion to thrust breakdown. In literature a limit starting from 600 to 1,000 kW/m^2 is found where the upper limit corresponds with propellers having a good wake distribution. For the purpose of this report an average value of 800 kW/m^2 is used for all propellers. If the disk area is multiplied with the maximum delivered power density a limit of delivered power is found equal to 69.272 MW [144]. This lies in the same order of magnitude

as the power ranges discussed in 4.1.3. It should be noted that this physical limit is a rough indication of reality as it does not take into account blade area ratio or propeller speed that is why this criteria is used in combination with the three other criteria.

Next the delivered power per propeller is calculated for both the two and three propeller lay-out using the calculated values of the hull and open water efficiency. Where the open water efficiency is found through the use of Propcalc, the plotted open water diagrams are added in appendix H.1. The relative rotative efficiency is kept equal to 1.00. This results in the found delivered powers per propeller (P_p) depicted in table 6.22.

	Two propeller lay-out	Three propeller lay-out	
Propeller	Wing	Center	Wing
T [kN]	5119	3583	3413
V_a [m/s]	13.12	11.27	13.12
P_T [MW]	67	40	45
η_o	0.68	0.69	0.72
P_o [MW]	99	58	62
η_r	1.00	1.00	1.00
P_p [MW]	99	58	62

Table 6.22: Maximum delivered power evaluation

It can be seen from table 6.22 that the two propeller lay-out lies well above the physical limitation in power density found in literature. This lay-out would therefore result in problems like excess vibrations, erosion and thrust breakdown. The three propeller lay-out however is seen to adhere to the physical limitation for both the wing and center propellers. This is explained by the division of total thrust over multiple propellers. Hereby a second and more firm reason is found to choose for the three propeller lay-out. To finalize the design choice a comparison in total propulsion chain efficiency is carried out.

Propulsion chain efficiency

On figure 6.24 & 6.25 the total installed electrical reactor power is calculated making use of the revised propulsion chain. This takes into account the change from an AC to a DC grid to enhance overall efficiency of the propulsion line due to the variable RPM operation of the second internal gas turbine. Besides the needed power that the propellers request an additional 3% is reserved for balance of plant and hotel facilities which is stipulated by the other consumers block on figures 6.24 & 6.25. These are based on the same values as described in section 6.2.1. The reactor side is depicted in a simplified view as this lies not in the interest of the current comparison a full lay-out of the reactor side can be found in section 6.2.1 or 6.7.

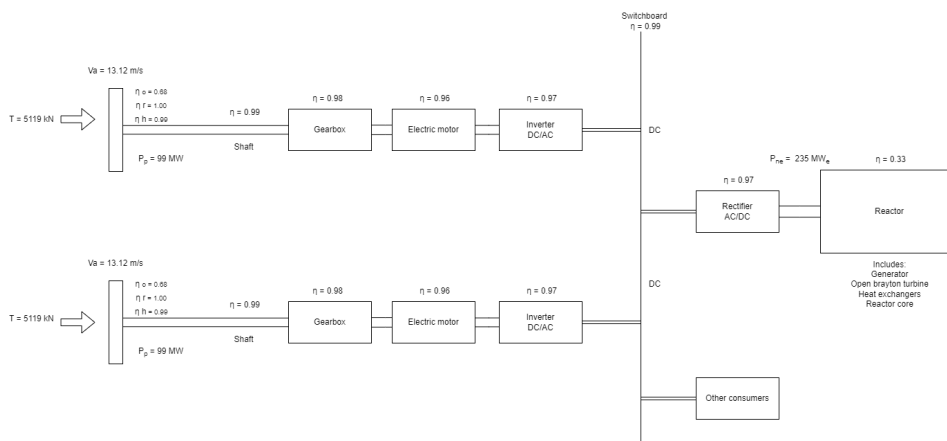


Figure 6.24: Propulsion chain efficiency - two propellers

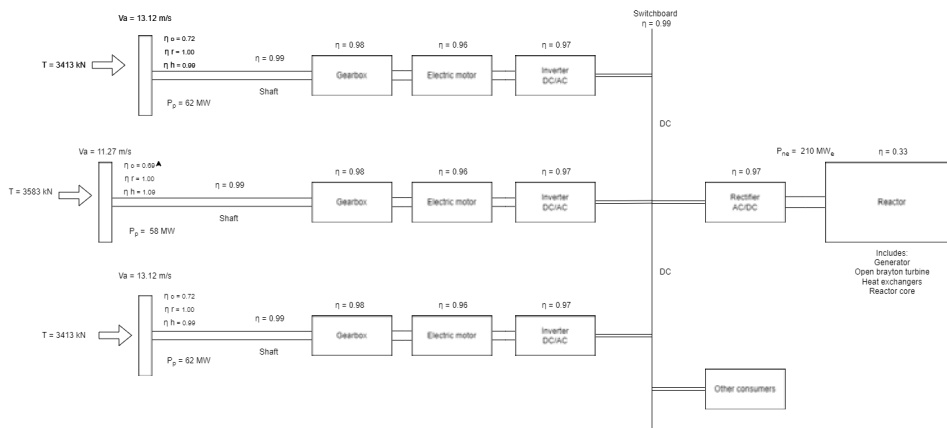


Figure 6.25: Propulsion chain efficiency - three propellers

The two propeller lay-out needs a total installed reactor capacity of 235 MWe this reduces to 210 MWe when three propellers are used. This is explained by the higher open water and hull efficiencies that stem from the division of the total thrust over a larger number of propellers which lowers the thrust loading coefficient and makes the propellers more efficient. This comparison gives a third and final reason to opt for the three propeller lay-out as a significant decrease of 11% in total installed power is seen. Considering the high capital costs of nuclear power this has a strong impact on the design choice.

6.6.1. Final propeller design choice

Based on the comparison between a two and three propeller lay-out considering the Auf'm Keller criteria, tip speed, power density and overall propulsive efficiency it is found that the three propeller lay-out is the best design choice. As the propellers of the triple lay-out adhere to all physical limitations. In addition they save 11% in total installed power due to an increase in open water and hull efficiency that stem from a lower thrust loading coefficient.

If this is compared with the previously installed power of 222 MWe, where a hull and open water efficiency of respectively 1.06 and 0.65 were used, a 5% decrease in installed power is observed.

All the main characteristics of the center and wing propeller for this lay-out are depicted in table 6.23.

	Center propeller	Wing propellers
D [m]	10.5 m	10.5 m
t [-]	0.20	0.16
w [-]	0.27	0.15
T/propeller [kN]	3583	3413
Tip speed [m/s]	39.58	37.92
Ae/Ao [-]	0.75	0.75
Number of blades [-]	5	5
P/D [-]	1.2	1.4
ηo	0.69	0.72
ηh	1.09	0.99
ηr	1.00	1.00

Table 6.23: Main characteristics of propellers

To ensure a better understanding of the internal differences in propulsive efficiencies of the center and wing propellers the efficiencies of all three propellers are depicted on figure 6.26 using the values from table 6.23. Where the hull efficiency is a product of the wake and thrust factor, the open water efficiency is found through the open water diagram of the B5-75 and the relative rotative efficiency is kept at 1.00. Here it is seen that the hull efficiency of the center propeller lies higher than that of

the wing propellers but for the open water efficiency the opposite is true. The explanation lies within the wake factor as this factor lies higher for the center propeller because of its positioning behind the hull. This leads to a higher hull efficiency but a lower open water efficiency. The decrease in open water efficiency is explained by the decrease in speed of advance which leads to a higher thrust loading coefficient. This in turn will lead to a lower open water efficiency. The increase in hull efficiency follows from its definition. The total propulsive efficiency is also depicted on figure 6.26 and it is observed that the center propeller has a significant higher propulsive efficiency than the wing ones because of the high hull efficiency that stems from the increased wake factor as discussed before.

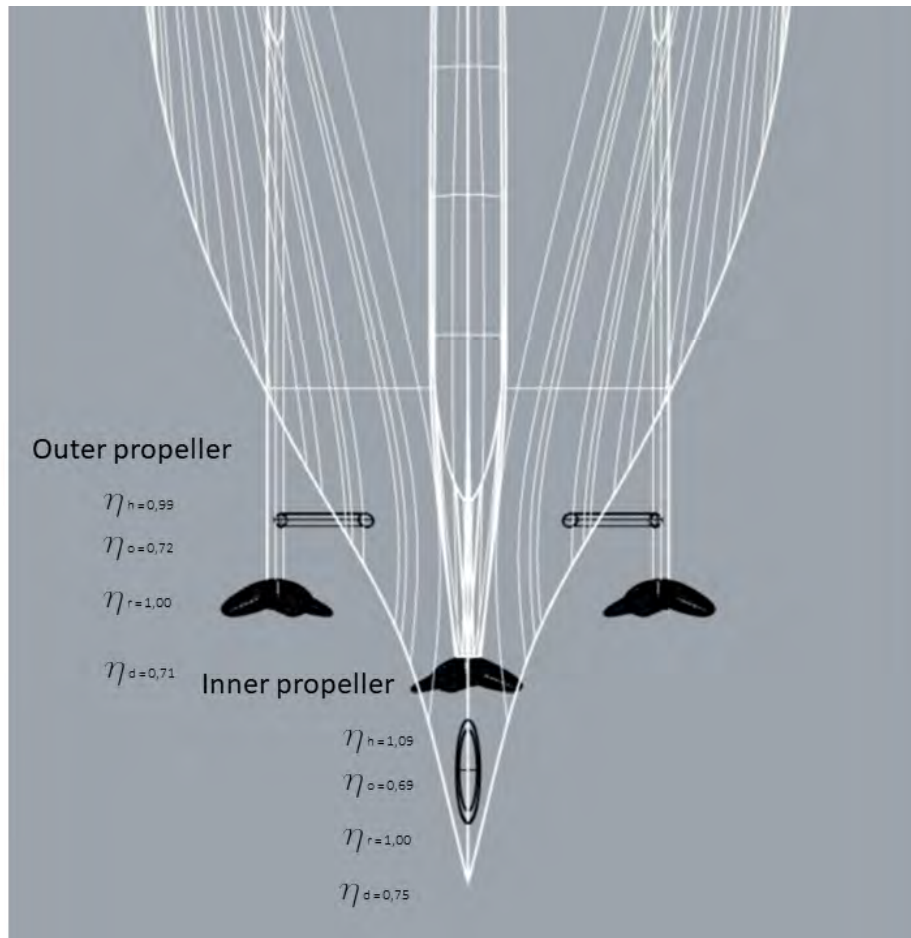


Figure 6.26: Propeller efficiency outline

A graphical view of the propeller lay-out is given on figure 6.27 to enhance the readers understanding and illustrate the differences between the wing and center propellers even better. It can be observed that the wing propellers are both turning outwards this is chosen to decrease rotational losses, as the tip of both propellers produce a swirl directed inwards counteracting the produced wake field. In the next section the general arrangement is re-iterated as the number of propellers increased from two to three.



Figure 6.27: Propeller stern view

6.7. General arrangement second iteration

With the evaluation of the propulsors a last iteration can be made for the general arrangement. Only the machinery room's lay-out will be impacted by the installation of three propellers therefore this aspect is handed solely in this section. In table 6.24 the needed electrical power for each electric motor is depicted making use of the shaft and gearbox efficiency as depicted on figure 6.25.

	Center propeller	Wing propellers
Power output of electric motor [MW]	60	64
Efficiency electric motor	98.8%	98.8%

Table 6.24: Electric motors

The electric motor power output can be considered of a rather high magnitude. Siemens however does develop high-voltage motors up to 70 MW with an efficiency of 98.8%. This means that it would be no problem to install these electric motors as they are already commercially available. When the new found efficiency of 98.8% found in literature a total reactor electrical power of 204 MW_e needs to be installed [11]. This gives a reduction of 2.5% in installed power compared to the old assumed efficiencies of electric motors.

With the newly found electric power outputs the machinery room can be re-evaluated on a volume and mass basis. Where the reactor side is installed as two times 100% from intermediate heat exchanger up until turbine generator as discussed before and the propulsor side is changed to one time 32% for the center propeller and two times 34% for the wing propellers. This ensures enough redundancy in case of a failure within the propulsion chain. The battery power, emergency propulsion systems and switchboard rooms are kept the same as in section 6.2.1. As a general overview the total propulsion line from propeller up until reactor is depicted on figure 6.28

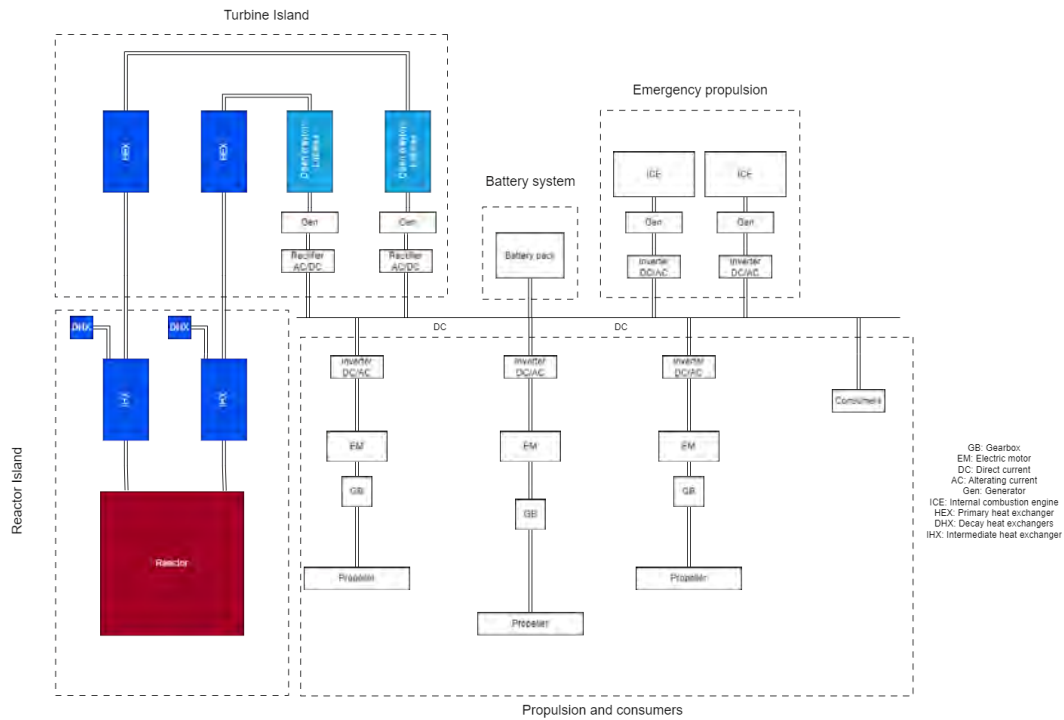


Figure 6.28: Machinery room system diagram based on [71] with own additions

The total masses and volumes of every machinery component can be found in appendix I.1. Due to the decrease in power the mass and volume of the reactor and its shielding respectively decreased by 2 and 4%. Subsequently all other components with the exception of the electric motors and gearboxes decreased 8% in both volume and weight. The overall volume and weight of the electric motors and gearboxes decreased 37% compared to the two propeller lay-out that was previously estimated. The decrease in volume and weight could be further investigated to evaluate the possible increase of cargo capacity or influence on stability but these are expected to be limited. On figure 6.29, 6.30 & 6.31 a graphical representation is given from the machinery room with three propeller lay-out.

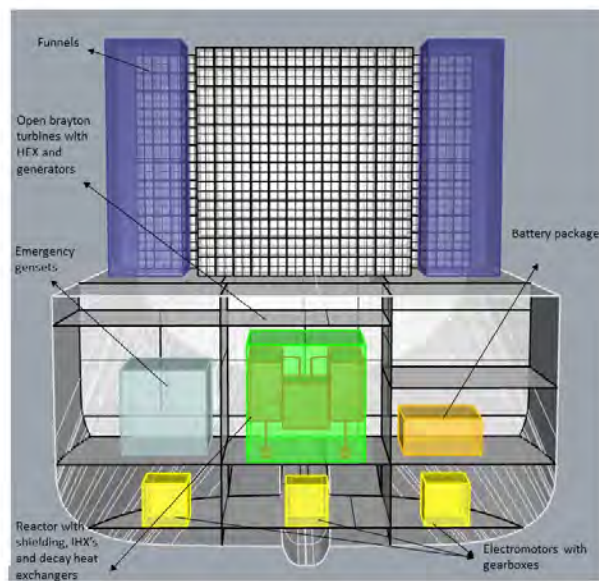


Figure 6.29: Machinery room three propeller lay-out close-up

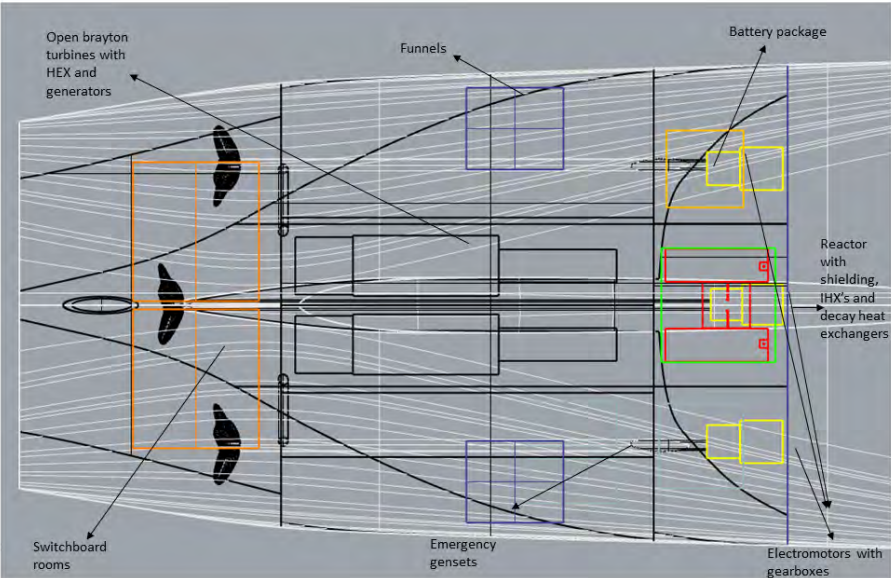


Figure 6.30: Machinery room three propeller lay-out top view

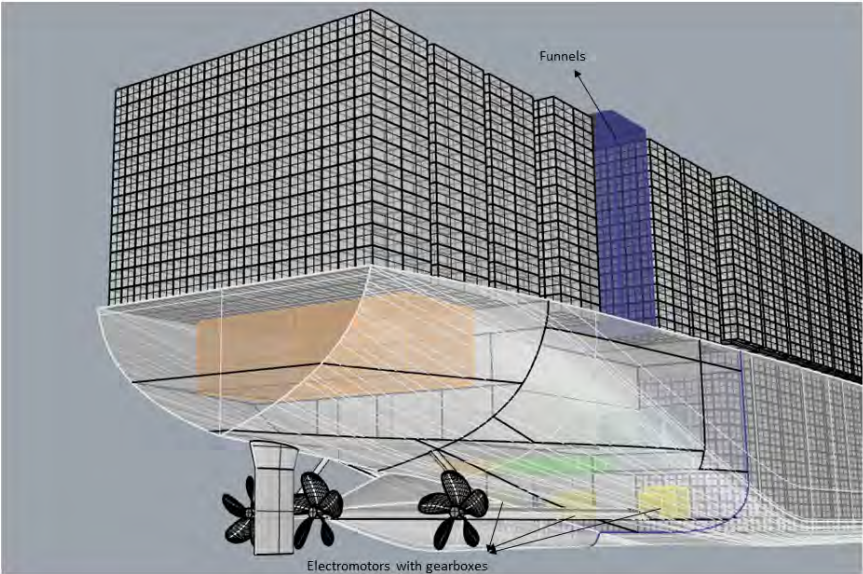


Figure 6.31: Machinery room three propeller lay-out Isometric view

6.8. Final comparison with diesel equivalent vessel

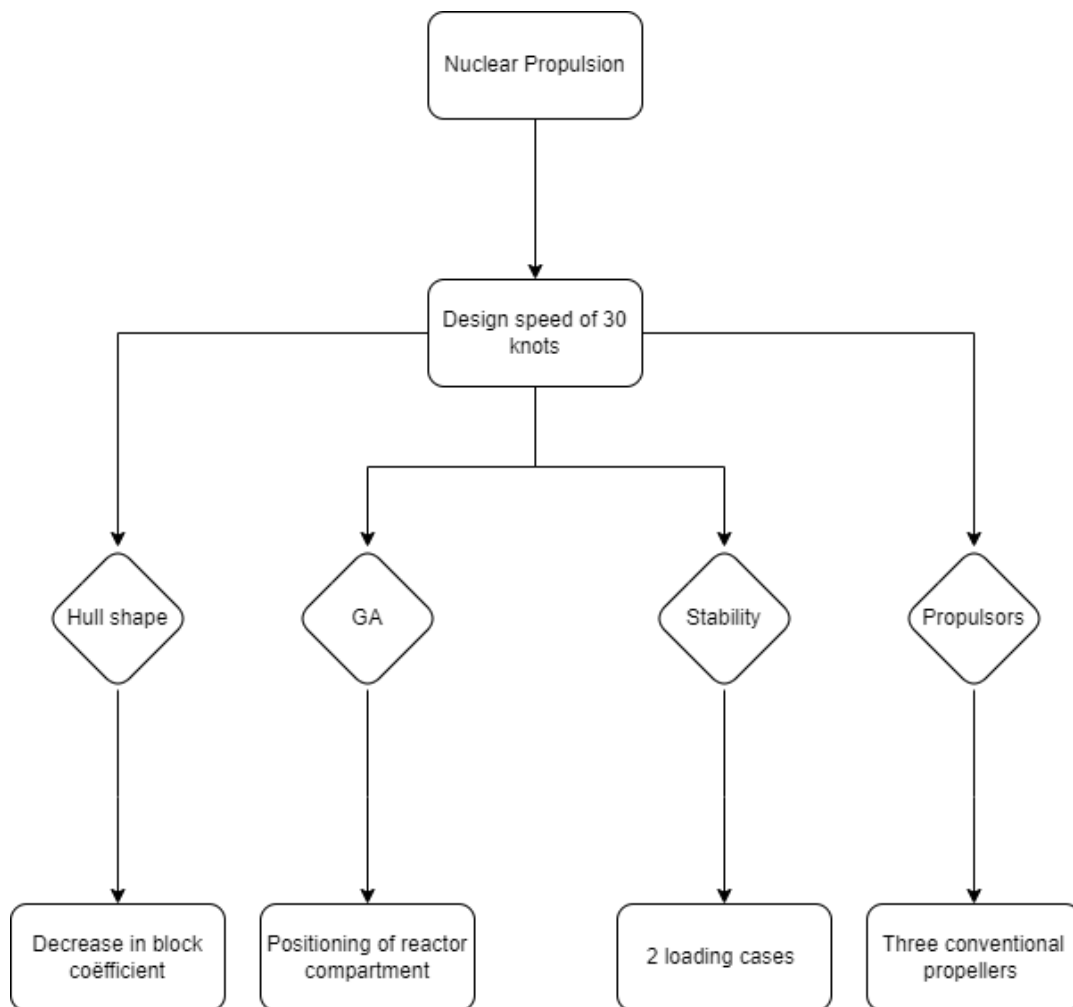


Figure 6.32: Main differences with conventional diesel container ships

Through the utilization of nuclear propulsion, the attainable design speed was elevated to 30 knots for a container vessel featuring a cargo capacity of 20,000 TEU. Subsequently, a conceptual design was formulated to assess its changes on diverse aspects encompassing hull configuration, general arrangement, stability, and propulsor configuration. A brief overview of these design impacts are depicted on figure 6.32 wherein a comparative analysis is drawn with conventional diesel-powered vessels possessing similar cargo capacity such as the Ever Given, CMA CGM JAQUES, and the HMM ALGECIRAS.

The main difference in hull shape was the choice for a lower C_b of 0.63 due to the high design speed. In contrast, the average for conventional vessels lies around 0.70 [119]. The lower C_b is further explained by the model vessel of the design as this was the Maersk B series with a design speed of 29.2 knots and a C_b of 0.56. This resulted in a similar C_b of 0.59 for the first design of the nuclear concept vessel used in the speed model and optimized for resistance as became clear from section 6.1. Later this was refined to 0.61 to adhere to real-world constraints and increased to 0.63 in order to lay at the design draft. The increase in design speed resulted in the choice for a lower C_b .

In general arrangement no design choices out of the ordinary were chosen. As the accommodation was positioned fore to increase cargo capacity and the machinery room aft to ensure propeller immersion and increase propulsive efficiency. The reactor compartment was however positioned to minimize risk of radioactive spill. This is seen by the positioning and compartmentalization.

By assessing the stability of the nuclear concept vessel it became clear that instead of four load cases

described by the IMO only two were needed to be evaluated. Namely the loaded and ballast condition with both being equal for departure and arrival condition. This is explained by the low amount of nuclear fuel needed for a single voyage. The total amount of fuel for an operating period of 5 years is calculated to be 9 ton which incorporates all nuclear fuel not only the fissile portion. For the rest, the significant weight of the nuclear installation had no considerable impact on the stability of the vessel as all intact stability criteria were met without difficulty.

As last the propulsors of the nuclear concept ship were investigated using four criteria namely Auf'm Keller, tip speed, power density and propulsion chain efficiency. The comparison was made between a two and three propeller lay-out. For the first three criteria the three propeller lay-out was seen to have more favourable results. As the required blade ratio was smaller as well as the tip speed. The required power per m^2 was also observed to lay lower. The lower values for the first three criteria result in non-excessive cavitation behaviour which is beneficial for reduced erosion, pressure pulses and has a positive effect on the propeller efficiency as the propeller loses less traction by the absence of vapour-filled cavities. The fourth criteria carried the most weight in the design choice as the overall efficiency lied significantly higher due to the increase in hull and open water efficiency which is mainly explained by the lower thrust loading. As the blade area is increased by 50% due to adding one propeller. The three propeller lay-out had a total saving of 11% in installed power when compared with the two propeller lay-out. Therefore the three propeller lay-out was chosen for this concept design.

6.9. Chapter conclusion

The design process for a nuclear-powered container vessel with a target speed of 30 knots followed a specific approach. Initially based on the volume scaled Maersk B series, variations in L/B, B/T and C_b were explored to optimize resistance. However, the parameters were already near optimal for a constant displacement and remained unchanged.

While the initial design focused on minimizing the resistance, its unconventional LOA and T raised concerns. With a required capacity of 20,000 TEU, similar capacity could be achieved in shorter, wider vessels. This required a reassessment of volume, weight, and application of real-world constraints. Volume assessment considered machinery room, accommodation, and number of TEU. Calculations indicated an excess capacity of 4,590 TEU, justifying scaling down. Weight assessment involving deadweight and lightship weight indicated a 26% overshoot, further justifying scaling down. Real-world constraints posed by ports and canals were considered and an over-dimensioned LOA and T were observed. This led to a scaled down version of the nuclear concept vessel. The revised design showed 7% lower resistance than the original due to decreased wetted area leading to a prompt decrease in frictional resistance. However, carrying capacity fell short by 4.3%, requiring an adjustment to the C_b in order to regain capacity. This resulted in a reduction of resistance by 2% compared to the original scaled version. This showed the dominant role of the frictional resistance at a fronde number of 0.25 and the limited influence of the wave making resistance.

The resulting nuclear concept vessel was evaluated for hull shape, general arrangement, stability, and propulsor configuration, focusing on the speed increase due to nuclear propulsion.

A lower C_b was chosen for the hull shape due to the increase in design speed, influenced by early-stage resistance minimization for higher speeds. General arrangement changes were minimal compared to conventional designs. The reactor compartment was however positioned to minimize risk of radioactive spill. This is seen by the positioning and compartmentalization. Stability assessment revealed that there were only two necessary load cases due to limited nuclear fuel requirements. Aside of that all intact stability criteria were met without any challenge. Propulsor analysis favored a three-propeller layout over a two-propeller layout, exhibiting better performance in various criteria. The chosen configuration demonstrated a 11% reduction in installed power compared to the two-propeller layout. Mainly explained by the reduction in thrust loading coefficient.

7

Conclusion

Nuclear power shows great potential in marine application but its subsequent impact on complete new builds is unknown. Therefore this thesis aims to find an answer to the research question:

“What are the design characteristics of an economic high speed nuclear container vessel?”

This was done by re-evaluating the economic speed, as nuclear reactors are characterized by low fuel costs but high initial capex and its subsequent impact on the ship design. This process involved several design steps, and the main findings are summarized in the following paragraphs.

First a literature study was carried out to gather the required input in order to re-evaluate the economic speed and its impact on the ship design.

Nuclear reactors

A thorough examination of the characteristics of the GEN IV, (V)HTR and MSR for load following, capital, fuel, O&M, and decommissioning costs. Revealed that, higher power levels were found to reduce relative capital costs, fuel costs were also seen to be considerably lower than for MDO. Additionally, a method for estimating reactor shielding based on power was validated. Potential challenges in implementing the reactor within a ship design were researched based on factors such as location, safety, and refuelling. Notably, the major difference with a conventional ship design was the long refuelling interval and compartmentalization of the reactor room.

Relation speed & income

Further on, a detailed investigation into what the key factors are that contribute to income and which are depended on speed in liner shipping was carried out. For the capital costs it was found that only the main engine depended on speed. Operational costs, specifically O&M and fuel costs, were as well influenced by speed. For nuclear-powered ships, other operational costs depending on speed, excluding fuel, were not included. Voyage costs were identified higher for the nuclear case whereas freight rates showed a proportional relationship with container ship average speed and were also seen to be volatile.

Relation speed & hull shape

To evaluate differences in design characteristics based on speed for conventional MDO container vessels, two high-speed vessels were compared with conventional-speed vessels. The deadweight to displacement, B/D, and B/T ratio did not differ from the conventional ones. Ratios that showed differences included an increased L/B ratio and decreased block coefficient, both explained by the proportional increase in wave-making resistance at higher froude numbers. Consequently, the installed power per TEU also significantly increased. These findings indicated that estimating power based on conventional slow-speed container ships was not ideal. Instead, the identified reference vessels were preferred for this purpose.

Relation speed & propulsors

The next step involved evaluating three propulsor types for potential use in the propulsion line, con-

sidering factors such as general application, effective speed domain, power range, parallel application and scalability. Out of these, conventional propellers were seen to be most fit between a speed range of 0-33 knots. Water jets could be implemented starting at speeds of 30 knots onwards however conventional propellers remained to be the preferred choice from an efficiency, power range and scalability point of view. High speed propellers were discarded because they only become effective from 50 knots onwards and have difficulties in scaling up with respect to radiated noise and loss of thrust.

Based on the above mentioned findings the research phase was started.

Economic speed determination

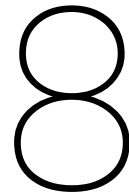
The first design characteristic that was evaluated was the design speed. This is done via an economic speed model evaluated on two routes, between Rotterdam and Shanghai using the Suez canal and between Rotterdam and New York. As input the speed dependent components of CAPEX, OPEX, voyage costs and freight rates were used. In order to couple these to speed, a resistance curve was constructed based on a volume scaled high speed model vessel. This was done using Froude scaling which insured the wave making resistance would not be underestimated up until the calculated design speed of 38.18 knots for the concept vessel case. Three different cases were studied, namely, a conventional MGO case with a service life of 25 years and two nuclear case with respective service lives of 25 and 50 years. A first sensitivity analysis revealed that the freight rate had a big influence on speed for all cases and the fuel cost solely for the MGO case. Furthermore, the reactor CAPEX was seen to have a less substantial role, that degraded over increased service life. For both nuclear cases an increase in economic speed was seen compared to the conventional MGO case, due to the significantly lower fuel cost. In addition the 50-year nuclear case showed a speed increase when compared to the 25-year case due to the decrease of annual cost for the reactor capex. Besides that, a shorter route showed a logical increase in economic speed for all cases as the revenue stayed constant but the effective costs went down. The obtained findings indicated that a nuclear-powered container vessel, featuring a cargo capacity of 20,000 TEU, was initially capable of achieving an economic speed of 30 knots with a projected service life of 50 years.

Design process

Next the design process was entered. For the original design there was little to gain with a view on resistance, despite variations in dimensions and block coefficient keeping a constant displacement. While the initial design focused on minimizing the resistance, its unconventional LOA and T raised concerns. With a required capacity of 20,000 TEU, similar capacity could be achieved in shorter, wider vessels. This led to a re-evaluation of volume, weight, and application of real-world constraints on the main dimensions. Calculations indicated an excess of 4,590 TEU, 26% overshoot in displacement and over-dimensioned LOA and T compared to real-world constraints. This led to a scaled down version of the nuclear concept vessel. Notably, the scaled down nuclear concept vessel corrected for carrying capacity showed a 2% decrease in resistance when compared to the initial design. This showed the dominant role of frictional resistance as the Froude number was equal to 0.25 indicating that the wave making resistance is of less importance in the found speed domain.

The resulting nuclear concept vessel was evaluated on four design characteristics namely hull shape, general arrangement, stability, and propulsor configuration. The hull shape featured a low C_b of 0.63 due to a high design speed, chosen to decrease resistance. General arrangement changes were minimal compared to conventional designs. The reactor compartment was however positioned to minimize risk of radioactive spill. This is seen by the positioning and compartmentalization. Stability assessment revealed that there were only two necessary load cases due to limited nuclear fuel requirements. Aside of that all intact stability criteria were met without any challenge. Propulsor analysis favoured a three propeller lay-out over a two propeller lay-out, exhibiting better performance in various criteria. The chosen configuration demonstrated a 11% reduction in installed power compared to the two propeller layout, mainly explained by the reduction in thrust loading coefficient.

In conclusion a 20,000 TEU nuclear container ship shows an increase in economic speed which gives way to a smaller C_b and an increase of propulsors, whereas the influence on general arrangement and stability are seen to remain limited.



Recommendations

Cost

The used costs in the economic speed model could be further refined to increase the accuracy of the speed determination.

The examined range of costs associated with reactor CAPEX, which encompasses decommissioning expenses in this analysis, remains quite wide and should be further refined to decrease uncertainty in the overall cost of ownership. To achieve this, more detailed input is needed from nuclear power plant developers to assess the initial investment and the associated decommissioning costs at the end of the plant's service life. Moreover, it is essential to account for the impact of inflation on these expenses over extended periods, especially given the 50-year service life examined in this study.

The comprehensive cost of ownership, which is dependent on the speed, has been computed for the nuclear power plant using data applicable to a minimum service life of 50 years, while nuclear reactors can potentially operate for over 60 years. In contrast, the typical service life of a ship is approximately 25 years. Future research should also consider the effects of higher speeds and longer service lives on other ship cost components, such as the steel hull and other non-nuclear plant elements. Although these cost components are expected to be smaller than the nuclear power plant's expenses, their inclusion will enhance the accuracy of the total cost of ownership, which forms the basis for investment decisions and will predict the economic speed more accurately.

The increase in economic speed could potentially lead to an opening of a new market for time sensitive cargo, that lies in between air and conventional slow speed water transport. This is an area that is not covered in this report but could be of potential interest.

Another cost aspect that warrants increased attention is insurance. Currently, the disparity in insurance costs between conventional and nuclear-powered ships is unknown and has not been factored into this study. However, given the sensitive nature of nuclear power, it merits a more thorough examination from an insurance standpoint. Therefore, the respective insurance costs should also be subject to further investigation.

Ship design

On the ship design side of this project further refinements are necessary and recommended.

First of all the shielding weight is based on a spherical PWR design carried out by K.Houtkoop. When a reactor specific calculation could increase the accuracy of the volume and weight determination.

Secondly, the resistance calculation that is carried out used Holtrop & Mennen as this was deemed the best suited method. To increase the accuracy, other methods such as CFD calculations or model tests can be carried out including all appendages. As the effect on resistance of the three propeller configuration is not taken into account for the current study. This would further increase the accuracy of the speed prediction.

Thirdly, in the stability calculation it was seen that a total of 44% ballast capacity of the design dead-weight was needed for propeller immersion in ballast condition. A possible reason for this is the absence of fuel tanks in the case of a nuclear vessel. It could be further researched if this is a hard design consideration for nuclear propulsion. As this is calculated in an extreme condition where no full or empty containers are taken on board and full propeller immersion is assumed to be necessary.

Lastly, the three propeller configuration that is selected for this concept design can also be further investigated. For example the effect of four propellers can be evaluated. As well as the selection of azimuth thrusters instead of wing propellers to increase manoeuvrability and redundancy. The decrease in resistance in this case is questionable as rudders can be designed to recover rotational losses of the propellers. This way they might not increase the total installed power. The use of azimuth thrusters could also improve the wake field at the wing sides due to their hydrodynamic shape which improves the open water efficiency. In addition the Gawn-burrill series could be used instead of the Wageningen B-series as these are intended for high-speed design with a minimization of cavitation.

Marine engineering

As this project focused mainly on the ship design aspect many possible refinements on the marine engineering side remain.

The assumptions made for load following specifically the lower limit of 20% reactor load is based on older reactor designs and can be further investigated. As for this study the range of discussed reactors was limited to the (V)HTR and MSR new developments in reactor designs were not covered. Further research in new/other reactor designs is therefore recommended as the sodium cooled fast reactor is now heavily researched in the naval industry. As fast reactors pertain to have better load following capabilities which is important if a heavily varying load profile is considered. The use of sodium as a coolant does however have safety concerns as sodium is flammable when a leak is formed and when reacting with water it can form hydrogen which is highly flammable.

For the turbine section the open Brayton cycle with air as a medium was selected. As this lead to easier installation and the possibility of heat rejection. For further studies supercritical CO₂ in closed loop could be considered as it would take away the dependability of the ambient air where the vessel is sailing but lose the heat rejection capability.

The systems lay-out is chosen to be fully electric for the purpose of this report. With an installation of 2 x 100% from reactor up until generator to ensure redundancy and enough electrical power to reach the required design speed. This could be re-evaluated if more specific reactor CAPEX comes available. Whereas at the propulsor side 3 x 33% is installed to ensure redundancy in case of component failure. The electric lay-out is chosen due to its simple gearbox arrangement, easy conversion of the battery and emergency propulsion power and possibility for reversed cold ironing. Due to the high installed power following from the increase in design speed it might be interesting to evaluate the impact of turbine direct propulsion in combination with an electric lay-out. For instance the center propeller could be driven directly to increase efficiency of the propulsion chain and the wing propellers could remain fully electric to save the easy implementation of battery, emergency propulsion power and the reverse cold ironing option. This way the best of both system lay-outs could be combined.

Ship operation

In conventional MGO-fueled ships, typically a low initial engine investment cost is seen. It's noticeable that larger engines can be added with relatively minimal extra expenses. This provides the ability to adjust the ship's speed economically in response to factors like freight rates and fuel expenses. However, for nuclear-powered vessels, this flexibility is restricted due to the substantial capital expenditure required for the nuclear reactor. Therefore, it is advisable to conduct a more thorough analysis of all costs associated with nuclear marine propulsion, including capital expenditure, fuel, O&M and other expenses. By gaining a better understanding of these cost components, it becomes possible to more accurately assess the economic risks involved and determine the optimal design speed for a container vessel powered by nuclear energy.

Additionally, in the case of container ships, especially those designed for high speeds, there's a chal-

lenge to consider in terms of adverse weather conditions. In such situations, it may be necessary to temporarily reduce the ship's speed to prevent damage caused by harsh weather conditions at higher speeds. Further research is needed to explore the potential impact of this issue.

Legislation

Legislation with respect to nuclear ship design was briefly addressed in the placement of the reactor and its shielding. Contact was made with classification societies in light of possible developments for GEN IV nuclear reactors as the current legislation is only valid for PWR. The answer turned out to be negative but further investigation in possible changes in this field should be carried out as it is a very important aspect of nuclear power. Especially in view of the public opinion.

Service life

Given that the typical lifespan of a container vessel is approximately 25 years, while a nuclear reactor can operate for more than 60 years, it's worth exploring the possibility of extending the service life of container vessels. Alternatively, one could consider designing the reactor component of the propulsion system in a modular fashion, allowing it to be installed on a new vessel after the initial 25-year period. Both of these options hold promise and merit further in-depth investigation and comparison.

Ship types

For this study the initial focus lied on container vessels because of their relative high speed due to being volume based ships (low Cb), their large installed power and relative constant operating power, which is beneficial for nuclear power generation. An increase in design speed due to lower operational cost also showed to be beneficial due to the time sensitive nature of the cargo.

However other ship types like reefers or cruise vessels should also be considered to further investigate the potential of nuclear propulsion.

References

- [1] MAN Energy Solutions, Jan. 2014. URL: <https://www.youtube.com/watch?v=GF-70yncAVY&t=4s>.
- [2] Oct. 2022. URL: <https://thorizon.com/>.
- [3] /. *Freedom-class littoral combat ship*. Feb. 2023. URL: https://en.wikipedia.org/wiki/Freedom-class_littoral_combat_ship.
- [4] N. A. *MAXSURF resistance - User Manual*. Jan. 2018.
- [5] ABB. *Containerized Energy Storage System*. Jan. 2021.
- [6] ABB. *High voltage engineered induction motors Technical catalog*. Feb. 2023.
- [7] Ahmed Abdulla, Inês Lima Azevedo, and M. Granger Morgan. "Expert assessments of the cost of light water small modular reactors". In: *Proceedings of the National Academy of Sciences* 110.24 (2013), pp. 9686–9691. DOI: 10.1073/pnas.1300195110.
- [8] M. Adachi et al. "The decommissioning plan of the nuclear ship Mutsu". In: *Department of nuclear ship decommissioning* (Sept. 1995), pp. 1–15.
- [9] US department of transportation maritime administration. "NS savannah UPDATED FINAL SAFETY ANALYSIS REPORT". In: *U.S. Department of Transportation Maritime Administration* (Jan. 2017), pp. 1–167.
- [10] US energy information administration. "Cost and Performance Characteristics of New Generating Technologies, Annual Energy Outlook 2022". In: *EIA* (Mar. 2022), pp. 1–4.
- [11] Siemens AG. *The modular concept for a wide range of applications The new SIMOTICS HV HP 2nd Gennbsp; High-voltage motors up to 70 MW*. Jan. 2020.
- [12] ABDALLAH AIJJOU, LHOUSSAIN BAHATTI, and ABDELHADI RAIHANI. "Study on container ship energy consumption". In: *WIT Transactions on Ecology and the Environment* (2019). DOI: 10.2495/esus190031.
- [13] T. P. Anderson. "Cost Estimating Risk and Cost Estimating Uncertainty Guidelines". In: *Calhoun* (Aug. 1997), pp. 339–348.
- [14] World nuclear association. *Economics of nuclear power*. URL: <https://world-nuclear.org/information-library/economic-aspects/economics-of-nuclear-power.aspx>.
- [15] World Nuclear association. *Molten Salt Reactors*. URL: <https://world-nuclear.org/information-library/current-and-future-generation/molten-salt-reactors.aspx>.
- [16] Guest Author. *BEWARE BUYER'S REMORSE: WHY THE COAST GUARD NEEDS TO STEER CLEAR OF THE LCS*. Apr. 1996. URL: <https://cimsec.org/beware-buyers-remorse-why-the-coast-guard-needs-to-steer-clear-of-the-lcs/>.
- [17] Suez Canal Authority. *Tolls calculator*. Jan. 2022. URL: <https://www.suezcanal.gov.eg/English/Navigation/Tolls/Pages/TollsCalculator.aspx>.
- [18] Suez canal Authority. *Canal characteristics*. Jan. 2019. URL: <https://www.suezcanal.gov.eg/English/About/SuezCanal/Pages/CanalCharacteristics.aspx>.
- [19] The World Bank. "Decommissioning of Nuclear Power facilities". In: *Industry and energy department* (Apr. 1990), pp. 1–45.
- [20] John Barnes. Apr. 2021. URL: <https://www.imarest.org/themarineprofessional/on-the-radar/6027-remarkable-speed-record-breaking-ships-from-the-usa>.
- [21] Oak Ridge National Laboratory is managed by UT-Battelle LLC for the US Department of Energy. *Time Warp: Molten salt reactor experiment-Alvin Weinberg's magnum opus: ORNL*. June 2016. URL: <https://www.ornl.gov/blog/ornl-review/time-warp-molten-salt-reactor-experiment-alvin-weinberg-s-magnum-opus>.

- [22] U Battery. *Supporting organisations*. Jan. 2022. URL: <https://www.u-battery.com/>.
- [23] Kostas Belibassakis and Gerasimos Politis. "Generation and propagation of noise from cavitating marine propellers". In: *School of Naval Architecture & Marine Engineering* (May 2019), pp. 1–8.
- [24] BIMCO. *Container shipping: Continued disruption will ensure carrier profitability well into 2021*. Feb. 2021. URL: https://www.bimco.org/news/market_analysis/2021/20210225_container_shipping.
- [25] Geoffrey A. Black, Fatih Aydogan, and Cassandra L. Koerner. "Economic viability of light water small modular nuclear reactors: General methodology and vendor data". In: *Renewable and Sustainable Energy Reviews* 103 (Jan. 2019), pp. 248–258. DOI: 10.1016/j.rser.2018.12.041.
- [26] R.G. Boothroyd. "Integrated molten-salt nuclear reactor systems for base-load power plants". In: *International Journal of Energy Production and Management* 2.1 (2017), pp. 39–51. DOI: 10.2495/eq-v2-n1-39-51.
- [27] Caeses Caeses. *Voith linear jet*. Jan. 2023. URL: <https://www.caeses.com/industries/case-studies/voith-linear-jet/>.
- [28] Ugur Can, Cihad Delen, and Sakir Bal. "Effective wake estimation of KCS hull at full-scale by GEOSIM method based on CFD". In: *Ocean Engineering* 218 (Oct. 2020), p. 108052. DOI: 10.1016/j.oceaneng.2020.108052.
- [29] J S Carlton, R Smart, and V Jenkins. "The nuclear propulsion of merchant ships: Aspects of risk and regulation". In: *Journal of Marine Engineering & Technology* 10.2 (Feb. 2010), pp. 237–247. DOI: 10.1080/20464177.2011.11020247.
- [30] Yan Carrière-Swallow et al. *How soaring shipping costs raise prices around the world*. Mar. 2022. URL: <https://www.imf.org/en/Blogs/Articles/2022/03/28/how-soaring-shipping-costs-raise-prices-around-the-world>.
- [31] Sam Chambers. *Molten Salt Nuclear Power Barge pitched to Indonesia*. Dec. 2022. URL: <https://splash247.com/molten-salt-nuclear-power-bergs-pitched-to-indonesia/>.
- [32] change. *Container pick up from Port: Process & How to save money [2023]*. Jan. 2023. URL: <https://www.container-xchange.com/blog/container-pick-up-from-port/>.
- [33] F. Chen, F. Li, and H. Cougar. "Very High Temperature Reactor (VHTR) Safety Assessment". In: *Gen IV International Forum* 2.1 (June 2018), pp. 1–14.
- [34] Guoyu Chen et al. "Analysis of load-following operation characteristics of liquid fuel molten salt reactor". In: *Progress in Nuclear Energy* 150 (2022), p. 104308. DOI: 10.1016/j.pnucene.2022.104308.
- [35] Kevin Clark. *Is thorium the fuel of the future to revitalize nuclear?* Aug. 2021. URL: <https://www.power-eng.com/nuclear/reactors/is-thorium-the-fuel-of-the-future-to-revitalize-nuclear/#gref>.
- [36] Hermann Coils. Jan. 2023. URL: https://www.containerhandbuch.de/chb_e/stra/index.html?%5C%2Fchb_e%5C%2Fstra%5C%2Fstra_01_03_01_01.html.
- [37] TU Delft. *Fossil free fuels for floating power plants*. Nov. 2022. URL: <https://www.tudelft.nl/en/2022/tnw/fossil-free-fuels-for-floating-power-plants>.
- [38] DMS DMS. *Waterjets: When to use, pros and cons*. Jan. 2021. URL: <https://www.dmsonline.us/waterjets-when-to-use-pros-and-cons/>.
- [39] Klaas van Dokkum. "Propulsion and steering gear". In: *Ship knowledge: Ship design, construction and Operation*. DOKMAR, 2016, pp. 276–297.
- [40] James J. Duderstadt and Louis J. Hamilton. "Fission product poisoning". In: *Nuclear reactor analysis*. John Wiley & Sons, 1976, pp. 590–600.
- [41] ech_{ar}l. *Peak shaving and other ways to use batteries on a vessel*. Mar. 2022. URL: <https://echandia.se/insights/article/peak-shaving-and-other-ways-to-use-batteries-on-a-vessel/>.

- [42] Trading economics. *Uranium2022 data - 1988-2021 historical - 2023 forecast - price - quote - chart*. Dec. 2022. URL: <https://tradingeconomics.com/commodity/uranium>.
- [43] ecoscore. *How to calculate the CO2 emission from the fuel consumption?* Nov. 2022. URL: <https://ecoscore.be/en/info/ecoscore/co2>.
- [44] Energy Education. *Molten salt reactor*. URL: https://energyeducation.ca/encyclopedia/Molten_salt_reactor.
- [45] EIRP. "What will advanced nuclear power plants cost?" In: *EIRP* (Jan. 2016), pp. 1–45.
- [46] Badawy M. Elsheikh. "Safety assessment of molten salt reactors in comparison with light water reactors". In: *Journal of Radiation Research and Applied Sciences* 6.2 (2013), pp. 63–70. DOI: 10.1016/j.jrras.2013.10.008.
- [47] Scholarly community encyclopedia. *Load following of small modular reactors*. Sept. 2022. URL: <https://encyclopedia.pub/entry/26945>.
- [48] Nuclear energy. *Benefits of small modular reactors (smrs)*. Dec. 2020. URL: <https://www.energy.gov/ne/benefits-small-modular-reactors-smrs>.
- [49] J. R. Engel et al. *Conceptual design characteristics of a denatured molten-salt reactor with once-through fueling*. 1980.
- [50] The Maritime Executive. *Modular molten salt nuclear power for maritime propulsion*. May 2021. URL: <https://maritime-executive.com/editorials/modular-molten-salt-nuclear-power-for-maritime-propulsion>.
- [51] Feadship Feadship. *ECSTASEA*. Jan. 2004. URL: <https://www.feadship.nl/fleet/ecstasea>.
- [52] GEN IV international forum. *Technology Roadmap Update for Generation IV Nuclear Energy Systems*. Jan. 2014.
- [53] AP Fraas. "HELIUM AS A REACTOR COOLANT". In: *Progr. in Nuclear Energy, Ser. IV* 4 (1961).
- [54] freightos. *Shipping delays & freight cost increases 2023*. Dec. 2022. URL: <https://www.freightos.com/freight-resources/coronavirus-updates/>.
- [55] R.D. Geertsma et al. "Design and control of hybrid power and propulsion systems for Smart Ships: A review of developments". In: *Applied Energy* 194 (Mar. 2017), pp. 30–54. DOI: 10.1016/j.apenergy.2017.02.060.
- [56] Jaap Gelling. *Horses for courses*. Jan. 2023.
- [57] Cicero Design GmbH. *TS-I HV 80*. URL: <https://www.tesvolt.com/en/products/a-series/ts-i-hv-80.html>.
- [58] Jie Gong et al. "Analysis of waterjet-hull interaction and its impact on the propulsion performance of a four-waterjet-propelled ship". In: *Ocean Engineering* 180 (Apr. 2019), pp. 211–222. DOI: 10.1016/j.oceaneng.2019.04.002.
- [59] Jasper Grevink. *Introduction to CPP applications: The Design Challenge*. Feb. 2023.
- [60] Jasper Grevink. *Introduction to FPP applications: The Design Challenge*. Feb. 2023.
- [61] Jasper Grevink. *Introduction to FPP applications: The Design Challenge*. Feb. 2023.
- [62] The economist group. "Shipping: achieving zero emissions by 2050". In: *Economist Impact* 1.2 (2022), pp. 123–456.
- [63] C. Grove. "Comparison of thorium and uranium fuel cycles". In: *National Nuclear laboratory* (Mar. 2012), pp. 1–31.
- [64] Robert Hargraves and Ralph Moir. "Liquid fluoride thorium reactors". In: *American Scientist* 98.4 (2010), p. 304. DOI: 10.1511/2010.85.304.
- [65] D. Herman. "Installation, Operation, and Maintenance Costs for Distributed Generation Technologies". In: *EPR* (Feb. 2003), pp. 1–92.
- [66] S.E. Hirdaris et al. "Considerations on the potential use of nuclear small modular reactor (SMR) technology for Merchant Marine Propulsion". In: *Ocean Engineering* 79 (2014), pp. 101–130. DOI: 10.1016/j.oceaneng.2013.10.015.

- [67] J. Holtrop. "A STATISTICAL RE-ANALYSIS OF RESISTANCE AND PROPULSION DATA". In: *Marine Technology Monthly* 31.363 (Nov. 1977), pp. 1–6.
- [68] J. Holtrop. "A STATISTICAL RE-ANALYSIS OF RESISTANCE AND PROPULSION DATA". In: *Marine Technology Monthly* 31.363 (Nov. 1984), pp. 1–6.
- [69] J. Holzman. *Sprott Fund transforms uranium spot market*. Oct. 2021. URL: <https://www.spglobal.com/marketintelligence/en/news-insights/latest-news-headlines/sprott-fund-transforms-uranium-spot-market-67100457>.
- [70] Hans Hopman. *Concept ontwerp van een Multipurpose Cargo Vessel*. Jan. 2023.
- [71] K. Houtkoop. "Nuclear reactors for marine propulsion and power generation systems". In: *TU Delft & C-job* 1.1 (2022), pp. 1–169.
- [72] q. Huang et al. "MULTI-SURROGATE ASSISTED EFFICIENT GLOBAL OPTIMIZATION FOR DISCRETE PROBLEMS". In: *Leiden Insititute of Advanced Computer Science* (Dec. 2022), pp. 1–14.
- [73] Y. Huang et al. "Control and monitoring of tritium in molten salt reactor". In: *He Jishu/Nuclear Techniques* 34 (Aug. 2011), pp. 632–636.
- [74] IAEA. *Advances in small modular reactor technology developments: A SUPPLEMENT TO THE IAEA Advanced Reactors Information System (ARIS)*. 2020th ed. IAEA, 2020.
- [75] IAEA. *Advances in small modular reactor technology developments: A SUPPLEMENT TO THE IAEA Advanced Reactors Information System (ARIS)*. IAEA, 2020.
- [76] IAEA. *IAEA Nuclear Energy Series*. Aug. 2021.
- [77] IAEA. *IAEA-TECDOC-1315*. Oct. 2002.
- [78] IAEA. "Thorium fuel cycle — Potential benefits and challenges". In: *IAEA* (May 2005), pp. 1–113.
- [79] IMO. *Nuclear-Ship Code Code of safety for nuclear merchant ships*. Nov. 1981. URL: https://puc.overheid.nl/nsi/doc/PUC_3002_14/1/.
- [80] IMO. *Wwwcdn.imo.org*. Jan. 1981. URL: [https://wwwcdn.imo.org/localresources/en/KnowledgeCentre/IndexofIMOResolutions/AssemblyDocuments/A.491\(12\).pdf](https://wwwcdn.imo.org/localresources/en/KnowledgeCentre/IndexofIMOResolutions/AssemblyDocuments/A.491(12).pdf).
- [81] De Ingenieur. *Groter Panamakanaal in Gebruik genomen*. June 2016. URL: <https://www.deingenieur.nl/artikel/groter-panamakanaal-in-gebruik-genomen>.
- [82] Energy Institute. *Molten salt reactors – a cost-effective nuclear solution to net zero*. Nov. 2022. URL: <https://knowledge.energyinst.org/new-energy-world/article?id=127450>.
- [83] J.G.C.C. Jacobs. "Nuclear Short Sea Shipping". PhD thesis. TU Delft, 2007, pp. 1–131.
- [84] Janis. *Nuclear fission*. 2022. URL: <https://www.nuclear-power.com/nuclear-power/fission/> (visited on 09/19/2022).
- [85] Jan Owen Jansson and Dan Shneerson. *Port Economics*. MIT Press, 1982.
- [86] Geert Kapsenberg. "The MARIN Systematic Series Fast Displacement Hulls". In: *TU Delft* (Nov. 2012), pp. 1–24.
- [87] Savio Koman. *Fastest container and cargo ships in the world*. Mar. 2022. URL: <https://discover.hubpages.com/technology/Fastest-Container-and-Cargo-Ships-in-the-World>.
- [88] Kai Kosowski and Frank Diercks. *Challenges Increase as Generation Portfolio Changes*. Mar. 2021.
- [89] Dominik Kryzia and Lidia Gawlik. "Forecasting the price of uranium based on the costs of uranium deposits exploitation". In: *Gospodarka Surowcami Mineralnymi* 32.3 (2016), pp. 93–110. DOI: 10.1515/gospo-2016-0026.
- [90] G. Kuiper. *Resistance and propulsion 1*. Dec. 2002.
- [91] G. Kuiper. "The wageningen propeller series". In: *The wageningen propellers series* 92–001 (May 1992), pp. 1–91.

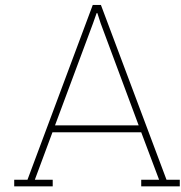
- [92] Samaan Ladkany, William Culbreth, and Nathan Loyd. "Molten salts and applications I: Molten salt history, types, thermodynamic and physical properties, and cost". In: *Journal of Energy and Power Engineering* 12.11 (2018). DOI: 10.17265/1934-8975/2018.11.001.
- [93] John R. Lamarsh and Anthony J. Baratta. *Introduction to nuclear engineering*. Pearson, 2018.
- [94] A. Laureau et al. "COUPLED NEUTRONICS AND THERMAL-HYDRAULICS TRANSIENT CALCULATIONS BASED ON A FISSION MATRIX APPROACH: APPLICATION TO THE MOLTEN SALT FAST REACTOR". In: *American Nuclear Society* (Apr. 2015), pp. 1–12.
- [95] David LeBlanc. "Molten salt reactors: A new beginning for an old idea". In: *Nuclear Engineering and Design* 240.6 (Sept. 2009), pp. 1644–1656. DOI: 10.1016/j.nucengdes.2009.12.033.
- [96] clara A. Lloyd, Anthony R.M. Roulstone, and Campnell Middleton. "THE IMPACT OF MODULARISATION STRATEGIES ON SMALL MODULAR REACTOR COST". In: *University of Cambridge* (Jan. 2018), pp. 1–8.
- [97] Jim Loftis, Ciara Ros, and Tatiana Freeman. *Carbon taxes in the shipping industry-assessing Japan's proposal*. June 2022. URL: <https://news.bloombergtax.com/daily-tax-report-international/carbon-taxes-in-the-shipping-industry-assessing-japans-proposal>.
- [98] Container logistics. *CSC plate: Overview amp; Importance [ultimate 2023 guide] - container xchange*. June 2023. URL: <https://www.container-xchange.com/blog/csc-plate/>.
- [99] Loodswezen. *Pilotage tariffs 2022 region Rotterdam-Rijnmond*. Jan. 2022. URL: <https://www.loodswezen.nl/~media/SiteLoodswezen/Files/Downloads/Tarieven/2022/Pilotage%5C%20Tariffs%5C%202022%5C%20-%5C%20LW%5C%20R-R%5C%20-%5C%201r.ashx>.
- [100] Winterhyr Gas & Diesel Ltd. "Engine selection for very large container vessels". In: *WIN GD* 1.1 (2016), pp. 1–19.
- [101] Watson David G M. "The design equations". In: *Practical ship design*. Elsevier, 2005, pp. 55–79.
- [102] *Maersk Boston (container ship)*. Feb. 2019. URL: https://www.fleetmon.com/vessels/maersk-boston_9313905_29484/#tab-datasheet.
- [103] MAN. *MAN 175D GenSet*. Feb. 2023.
- [104] MAN. "Propulsion trends in container vessels". In: *MAN* 1.1 (2019), pp. 1–30.
- [105] MAN MAN. "Basic principles of ship propulsion". In: *MAN Energy solutions* (Oct. 2018), pp. 1–35. DOI: 5510-0004-04.
- [106] MAN MAN. *Useful technical and organization information for Marine Engineers, superintendent, and Marine spare parts suppliers*. Sept. 2013. URL: http://marengine.com/ufiles/MAN-Basic_Principles_of_Ship_Propulsion.pdf%5C%22.
- [107] Pias Manual. *Overview and applicability of the calculation methods*. Jan. 2019. URL: <http://www.sarc.nl/images/manuals/pias/htmlEN/resist.html>.
- [108] W.J. Marwood and D. Bailey. "DESIGN DATA FOR HIGH-SPEED DISPLACEMENT HULLS OF ROUND-BILGE FORM". In: *National Physical Laboratory* 99 (Feb. 1969), pp. 1–88.
- [109] Daniel Mathers. *The Thorium Fuel cycle*. Nov. 2022.
- [110] L. Mathieu et al. "The thorium molten salt reactor: Moving on from the MSBR". In: *Progress in Nuclear Energy* 48.7 (2006), pp. 664–679. DOI: 10.1016/j.pnucene.2006.07.005.
- [111] Christopher McFadden. *USS Gerald R. Ford: The most advanced carrier of the US cost around \$13.3 billion to build*. June 2022. URL: <https://interestingengineering.com/innovation/uss-gerald-r-ford-advanced-carrier-us>.
- [112] Jasper Meyer, Robert Stahlbock, and Stefan Voß. "Slow steaming in container shipping". In: *2012 45th Hawaii International Conference on System Sciences* (Jan. 2012), pp. 1–10. DOI: 10.1109/hicss.2012.529.
- [113] Benito Mignacca and Giorgio Locatelli. "Economics and finance of molten salt reactors". In: *Progress in Nuclear Energy* 129 (2020), p. 103503. DOI: 10.1016/j.pnucene.2020.103503.
- [114] Leonardo Montoya. URL: <http://www.ricepropulsion.com/TNLS/Cavitation.htm>.

- [115] David Lewis Moses. "Very high-temperature reactor (VHTR) proliferation resistance and physical protection (PR&PP)". In: *Oak Ridge National Laboratory* (2011). DOI: 10.2172/1027406.
- [116] B. Muller. *Small Craft Technology*. Oct. 1997.
- [117] William Murray. "Economies of Scale in Container Ship Costs". In: *United States merchant marine academy* (Mar. 2016), pp. 1–25.
- [118] Royal Institute Naval Architects. *Significant ships of 2019*. Jan. 2019.
- [119] Royal Institute Naval Architects. *Significant ships of 2020*. Jan. 2020.
- [120] NEA. *Costs of decommissioning nuclear power plants*. OECD Publishing, 2016.
- [121] NEA. "Technical and economic aspects of load following with nuclear power plants". In: *Nuclear Development* (Dec. 2021). DOI: 10.1787/29e7df00-en.
- [122] Port of New York. *Tariffs information: Port Authority of New York and New Jersey*. Jan. 2023. URL: <https://www.panynj.gov/port/en/doing-business/tariffs.html>.
- [123] Port Of New York. Jan. 2023. URL: <https://www.panynj.gov/port/en/our-port/container-terminals.html>.
- [124] Lampros Nikolopoulos and Evangelos Boulougouris. "A study on the statistical calibration of the Holtrop and Mennen approximate power prediction method for full hull form, low froude number vessels". In: *Journal of Ship Production and Design* 35.01 (2019), pp. 41–68. DOI: 10.5957/jspd.170034.
- [125] OECD. "The impact of mega-ships". In: *International Transport Forum Policy Papers* (2015), pp. 1–108. DOI: 10.1787/5j1wvzcm3j9v-en.
- [126] United states general accounting office. *Nuclear submarines, Navy efforts to reduce inactivation costs*. United states general accounting office, 1992.
- [127] Hiroshi Ōi and Kazuo Tanigaki. "The ship design of the first nuclear ship in Japan". In: *Nuclear Engineering and Design* 10.2 (1969), pp. 211–219. DOI: 10.1016/0029-5493(69)90040-5.
- [128] Naya Olmer et al. *GREENHOUSE GAS EMISSIONS FROM GLOBAL SHIPPING, 2013–2015*. Oct. 2017.
- [129] P. van Oossanen. "Resistance prediction of small high-speed displacement vessels: State of the ART1". In: *International Shipbuilding Progress* 27.313 (1980), pp. 212–224. DOI: 10.3233/isp-1980-2731301.
- [130] Marcel Ott et al. "The 2-stroke Low-Pressure Dual-Fuel Technology: From Concept to Reality". In: *CIMAC* (June 2016), pp. 1–12.
- [131] Nam Kyu Park and Sang Cheol Suh. "Tendency toward mega containerships and the constraints of Container Terminals". In: *Journal of Marine Science and Engineering* 7.5 (2019), p. 131. DOI: 10.3390/jmse7050131.
- [132] Aiden Peakman, Bruno Merk, and Kevin Hesketh. "The potential of pressurised water reactors to provide flexible response in future electricity grids". In: *Energies* 13.4 (2020), p. 941. DOI: 10.3390/en13040941.
- [133] Refinitiv Perspectives. *Why speed matters in container shipping*. Jan. 2021. URL: <https://www.refinitiv.com/perspectives/future-of-investing-trading/speed-matters-container-shipping/>.
- [134] John Pike. *Military*. Jan. 2000. URL: <https://www.globalsecurity.org/military/systems/ship/systems/waterjet.htm#:~:text=A%20disadvantage%20of%20having%20the,to%20the%20onset%20of%20cavitation..>
- [135] John Pike. *Military*. July 2011. URL: <https://www.globalsecurity.org/military/systems/ship/takr-287.htm>.
- [136] I. L. Piore. *Handbook of generation IV nuclear reactors: A guidebook*. Woodhead Publishing, 2022.

- [137] Nuclear Power. *Thermal efficiency of nuclear power plants*. Feb. 2022. URL: <https://www.nuclear-power.com/nuclear-engineering/thermodynamics/laws-of-thermodynamics/thermal-efficiency/thermal-efficiency-of-nuclear-power-plants/>.
- [138] Nuclear power. *Xenon transients - response to reactor power changes*. Feb. 2022. URL: <https://www.nuclear-power.com/nuclear-power/reactor-physics/reactor-operation/xenon-135/xenon-transients/>.
- [139] Terry J. Price, Ondrej Chvala, and Zack Taylor. "Xenon in molten salt reactors: The effects of solubility, circulating particulate, ionization, and the sensitivity of the circulating void fraction". In: *Nuclear Engineering and Technology* 52.6 (2020), pp. 1131–1136. DOI: 10.1016/j.net.2019.11.026.
- [140] Magdi Ragheb. "Reactor deadtime". In: *Nuclear naval propulsion*. INTECH Open Access Publisher, 2011, pp. 30–31.
- [141] Helmi Fauzi Rahmatullah et al. "Analysis of irradiated pebble bed fuel transfer system in Hot cell 101 radiometallurgy installation". In: *Journal of Physics: Conference Series* 1198.2 (2019), p. 022025. DOI: 10.1088/1742-6596/1198/2/022025.
- [142] Hasan S M Rashidul. "IMPLEMENTATION OF ENERGY EFFICIENCY DESIGN INDEX & ITS IMPACT ON THE DESIGN OF OIL TANKER". In: *ResearchGate* (Mar. 2020), pp. 1–10.
- [143] Nuclear Market Review. "The Market". In: *Nuclear Market Review* (Aug. 2021), pp. 1–8.
- [144] M.X. van Rijsbergen and T.J.C van Terwisga. "ON THE MAXIMUM THRUST DENSITY OF PROPELLERS". In: *International conference on propeller cavitation* (Apr. 2000), pp. 1–24.
- [145] Hudson River Pilots. *Effective July 1, 2023, New Pilotage Base and Surcharge Rate*. Jan. 2023. URL: <https://hudsonriverpilots.com/web/main/rates>.
- [146] Rolla Rolla. *Surface piercing propellers*. Jan. 2023. URL: https://www.rolla-propellers.ch/surface_piercing_propellers_ogg_mp4.html.
- [147] Port of Rotterdam. *Rotterdam port dues*. Jan. 2022. URL: <https://www.portofrotterdam.com/sites/default/files/2021-12/port-tariffs-terms-conditions-2022-port-of-rotterdam.pdf>.
- [148] Port of Rotterdam. *PORT INFORMATION GUIDE*. Jan. 2021.
- [149] Niels van Saase. "The impact of 50,000 TEU vessels on container supply chain". PhD thesis. Erasmus university Rotterdam, 2018, pp. 1–68.
- [150] Enzo De Sanctis, Stefano Monti, and Marco Ripani. *Energy from nuclear fission an introduction*. Springer International Publishing, 2018.
- [151] G. Sawyer et al. "Analysis of high-speed trans-pacific nuclear containership service". In: *Design and operation of Container ships, London, UK* (Jan. 2008), pp. 1–10.
- [152] Sayres and Associates Corporation. "N.S. Savannah". In: *U.S. Department of transportation maritime administration* (Dec. 2008), pp. 1–47.
- [153] Ivo Senjanovic, Nikola Vladimir, and Marko Tomic. "Investigation of torsion, warping and distortion of large container ships". In: *Ocean Systems Engineering* 1.1 (2011), pp. 73–93. DOI: 10.12989/ose.2011.1.1.073.
- [154] Jérôme Serp et al. "The Molten Salt Reactor (MSR) in generation IV: Overview and perspectives". In: *Progress in Nuclear Energy* 77 (2014), pp. 308–319. DOI: 10.1016/j.pnucene.2014.02.014.
- [155] Viknash Shagar, Shantha Jayasinghe, and Hossein Enshaei. "Effect of load changes on hybrid shipboard power systems and energy storage as a potential solution: A Review". In: *Inventions* 2.3 (2017), p. 21. DOI: 10.3390/inventions2030021.
- [156] J. K. Shultis and R. E. Faw. *Fundamentals of nuclear science and engineering*. 3th ed. New York, US: Marcel Dekker, 2002.
- [157] Rick Spilman. *Ever Given — Was Suez-Max Simply Suez Too Much?* Mar. 2021. URL: <https://www.oldsaltblog.com/2021/03/ever-given-was-suez-max-simply-suez-too-much/>.

- [158] William Robb Stewart and Koroush Shirvan. "Capital Cost Estimation for Advanced Nuclear Power Plants". In: *Elsevier* (Nov. 2021). DOI: 10.31219/osf.io/erm3g.
- [159] Martin Stopford. *Maritime economics 3E*. Routledge, 2009.
- [160] Volkswerft Stralsund. *Brooklyn - cargo-vessels-international.at*. Jan. 2023. URL: https://cargo-vessels-international.at/BROOKLYN_IM09313931.pdf.
- [161] Ship amp; Bunker News Team. *Feature: 10 years of Bunker Prices*. June 2022. URL: <https://shipandbunker.com/news/world/366958-feature-10-years-of-bunker-prices>.
- [162] The technology. *Technology*. Jan. 2023. URL: <https://www.copenhagenatomics.com/technology/>.
- [163] Tom Terwisga. *A parametric propulsion prediction method for Waterjet Driven Craft*. Jan. 1997. URL: <https://www.semanticscholar.org/paper/A-parametric-propulsion-prediction-method-for-craft-Terwisga-Tom/087173aee17d8ba839fd5039f12157090c2139ea>.
- [164] THORIUM. *LFTR Overview*. URL: <https://energyfromthorium.com/lftr-overview/>.
- [165] T. A. Tomberlin. In: *Beryllium – A Unique Material In Nuclear Applications* 36 (Nov. 2004), pp. 1–12.
- [166] Nick Touran. *Molten salt reactors*. URL: <https://whatisnuclear.com/msr.html>.
- [167] Ministry of Transport of the People's Republic of China. *Port Charges In China*. Sept. 2019. URL: <https://www.e-ports.com/regulations/dfd5ae8951084a84945ca54cc9cf6c61>.
- [168] Matt Trulio. *High-performance boat propellers: The art of trade-offs*. Apr. 2000. URL: <https://www.boats.com/reviews/propping-for-performance-the-art-of-trade-offs/>.
- [169] Nicholas Tsoulfanidis. "Conversion and enrichment". In: *The Nuclear Fuel Cycle*. American Nuclear Society, 2013, pp. 57–85.
- [170] Moran Tug. *Schedule of rates, terms and conditions effective: March 1, 2022 towage ...* Mar. 2022. URL: https://www.morantug.com/Customer-Content/www/ports-and-operations/RatesPDFs/Moran_NY-NJ_Schedule_of_Rates_Terms_and_Conditions_Mar_1_2022.pdf.
- [171] urengo. *SWU Calculator*. Jan. 2022. URL: <https://www.urengo.com/swu-calculator>.
- [172] USNA USNA. "Chapter 7: Resistance and powering of ships". In: *Resistance and powering of ships*. USNA, 2022, pp. 1–46.
- [173] Harry Valentine. *Could a nuclear-powered cargo ship transit the Suez Canal?* July 2021. URL: <https://maritime-executive.com/editorials/could-a-nuclear-powered-cargo-ship-%20transit-the-suez-%20canal#:~:text=Ports%5C%20and%5C%20Suez%5C%20Canal&text=At%5C%20the%5C%20present%5C%20time%5C%2C%5C%20the,to%5C%20transit%5C%20through%5C%20the%5C%20canal..>
- [174] Benjamin Vogel and Jason C. Quinn. "Economic evaluation of small modular nuclear reactors and the complications of regulatory fee structures". In: *Energy Policy* 104 (2017), pp. 395–403. DOI: 10.1016/j.enpol.2017.01.043.
- [175] Manuel Ventura. *Cost Estimate*. Dec. 2022.
- [176] Julio A. Vergara and Chris B. McKesson. "Marine technology nuclear propulsion in high-performance cargo vessels". In: *Marine Technology and SNAME News* 39.01 (2002), pp. 1–11. DOI: 10.5957/mt1.2002.39.1.1.
- [177] Niels De Vries. "Safe and effective application of ammonia as a marine fuel". PhD thesis. TU Delft, 2019, pp. 1–100.
- [178] Wärtsilä. *WÄRTSILÄ & nbsp; SOLUTIONS & nbsp; FOR MARINE & nbsp; AND OIL & nbsp; GAS & nbsp; MARKETS*. Jan. 2019.
- [179] W wärtsilä. *Midsized waterjets product guide - wärtsilä*. Jan. 2020. URL: <https://www.wartsila.com/docs/default-source/product-files/gears-propulsors/waterjets/product-guide-o-p-midsized-waterjet.pdf>.
- [180] WNA. *Decommissioning Nuclear Facilities*. 2022. URL: <https://www.world-nuclear.org/information-library/nuclear-fuel-cycle/nuclear-wastes/decommissioning-nuclear-facilities.aspx>.

- [181] WNA. *Thorium as a fuel*. Nov. 2020. URL: <https://world-nuclear.org/>.
- [182] WNN. *China's HTR-PM reactor achieves first criticality*. Sept. 2021. URL: <https://www.world-nuclear-news.org/Articles/Chinas-HTR-PM-reactor-achieves-first-criticality>.
- [183] Robert Wright. *World's fastest container ships mothballed*. Feb. 2010. URL: <https://www.ft.com/content/65e522dc-1fce-11df-8deb-00144feab49a>.
- [184] Shifa Wu et al. "A load following control strategy for Chinese modular high-temperature gas-cooled reactor HTR-PM". In: *Energy* 263 (Jan. 2022), p. 125459. DOI: 10.1016/j.energy.2022.125459.
- [185] F. Wulandari. *Uranium price forecast: Is uranium a good investment?* Dec. 2022. URL: <https://capital.com/uranium-price-forecast>.
- [186] Akio YAMAJI and Kiyoshi SAKO. "Shielding design to obtain compact marine reactor". In: *Journal of Nuclear Science and Technology* 31.6 (1994), pp. 510–520. DOI: 10.1080/18811248.1994.9735185.
- [187] Ritsuo Yoshioka and Motoyasu Kinoshita. "Liquid fuel, thermal neutron spectrum reactors". In: *Molten Salt Reactors and Thorium Energy* (2017), pp. 281–373. DOI: 10.1016/b978-0-08-101126-3.00011-7.



Nuclear reactors

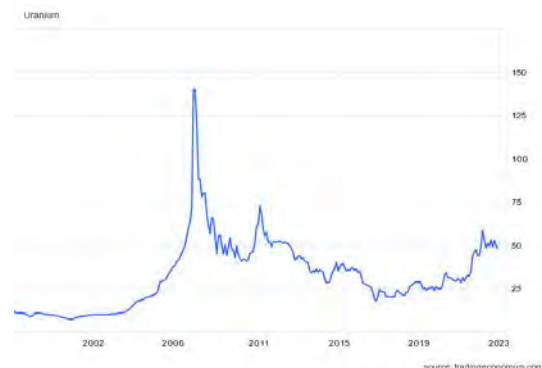
A.1. Nuclear fuel costs

A.1.1. Fuel costs

A study conducted in 2009 looked at spot prices for SWU between 1989-2009 and it showed an increase of 50% between 1991 and 2008. This high end price was around 160\$/kg and decreased a lot after Fukushima up until 2018 where a slight increase in SWU can be observed which can be explained by the start of the energy crisis as SWU is highly influenced by the electricity price. The varying price of SWU is depicted on figure A.1a. When this graph is compared to the Uranium cost per kg it can be seen that both unities follow the same trend which is explained by demand and supply and the same short-time events like the Fukushima meltdown or the war in Ukraine [143].



(a) SWU value in \$/SWU up until present [143]



(b) Uranium price in \$/kg [42]

Figure A.1: SWU cost and uranium cost [42] & [143]

A.1.2. Fuel cost calculation

Full breakdown of the fuel costs is shown below where a paper by Tsoulfanidas [169] is used to carry out the calculation. The boxes marked in yellow are variables that can be changed. The example given here is for an enrichment level of 5% with median values of 2020 for the raw material price of uranium and the SWU for producing one kilogram of 5% enriched uranium. All other values depicted in tables 1.5 and 1.6 are calculated in a similar matter.

Feed Factor		eq Tsoulfanidas ch 3.5	Cost breakdown 2020 MED	
Enrichment level (xp)	5		U3O8 [\$/kgU]	91
Tails assay (xw)	0,2	percentage of U235 in tails	Conversion [\$/kgU]	16
Feed assay (xf)	0,711	amount of U235 in U3O8	Enrichment [SWU]	80
feed factor	9,393346		fuel fabrication [\$/kg%U]	300
Number of kg enriched U required	1		FILL IN	
Total feed factor	9,393346			
SWU			COST	
Seperation potentials			U3O8	854,7945
V(xp)	2,649995		conversion	150,2935
V(xw)	6,187756		enrichment	708,0691
V(xf)	4,868883		fuel fabrication	300
SWU	8,850864		Total price per kg enriched U3O8	2013,157
Total SWU	8,850864			

Figure A.2: Full nuclear fuel cost calculation for 5% enriched Uranium

A.1.3. Sizing & weight estimation

A.1.3.1 reactor vessel

Using the height and diameter the volume was calculated in order to find a relation between power and density of the reactor vessel which is represented on figure A.3a. When a stable trend line for the density was found this relation is used to calculate the volume again. By using the relation between diameter and height of the reactor vessel which is depicted on figure A.3b it was possible to also calculate the height and diameter in a generic way.

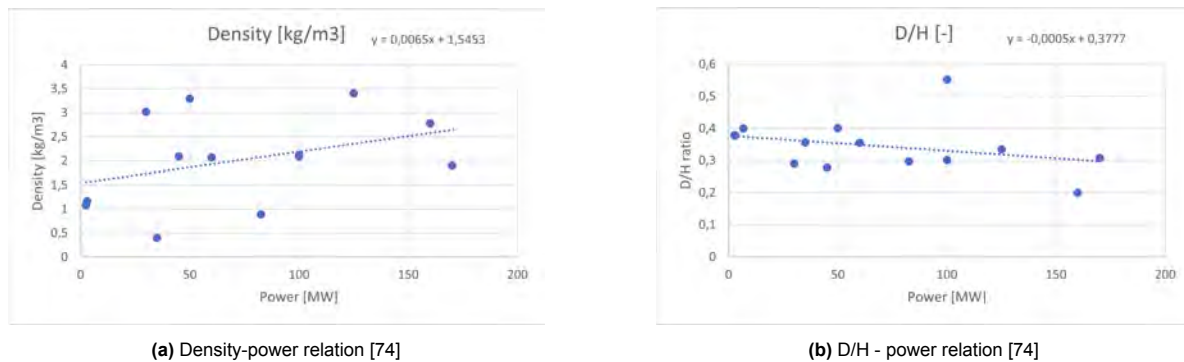


Figure A.3: Trend lines constructed with data from [74]

B

Relation speed & income

B.1. Capital cost

According to Stopford [159] capital costs are subdivided in three forms when the cashflow of a shipping company is concerned. In the first place there is the new build price of the vessel that is payed to the shipyard, secondly the possible mortgage needs to be paid on a monthly basis to banks or investors and last there is the amount of money received after sale of the vessel. For the purpose of this report only the first two will be taken into account. A study carried out by the OECD made a comparison between capital cost and increasing number of TEU based on Clarksons Research Services Limited and their own assumptions. The result is seen on figure B.1 where the the cost per TEU is also expressed per year.

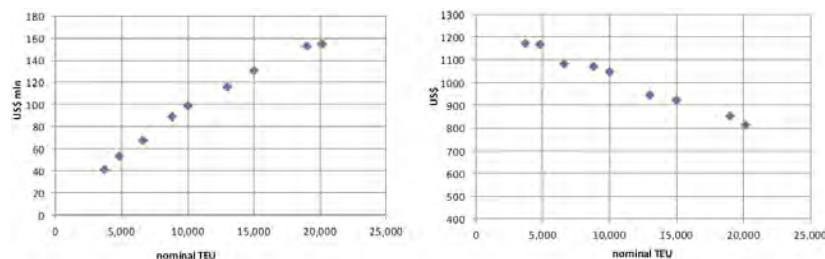


Figure B.1: Total capital cost and cost per TEU for increasing vessel size [125]

Despite the increasing total capital cost it can be seen that the capital cost per TEU diminishes for larger vessel sizes which is also beneficial for nuclear propulsion because of the large capital cost of the reactor as seen in the previous chapter. This phenomena is called economy of scale which refers to a decreasing cost per unit when the total cost increases with the total cost here being the capital cost. The same trend was seen in a study by Murray which gave as reasoning the increased efficiency in ship design because ships with larger capacities are built with the same ratio's as smaller versions plus more effectiveness in modern shipbuilding techniques. His result can be seen on Figure B.2 [117].

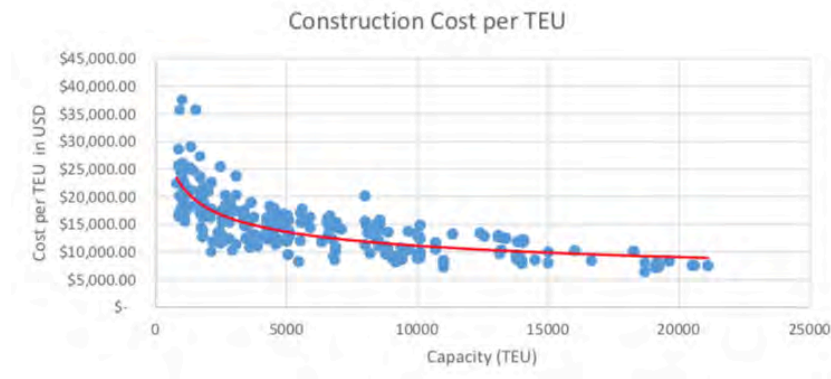


Figure B.2: Construction cost per TEU for increasing vessel size [117]

An important factor that needs to be considered to full-fill this decrease in cost is utilization. This is vital because the unit capital cost will only decrease if the number of shipped containers increases [149]. This economy of scale only takes into account the days spend at sea and not time spend in port or terminals. According to Jansson & Shneersson the economies of scale at sea result in diseconomies at the ports thus there should be a trade-off between these two factors. The trade-off will then result in an optimal ship size depending on the vessel costs per TEU and the handling costs per TEU [85].

It should not be disregarded that vessel prizes are also significantly influenced by world economy, raw material price and the number of vessels ordered in one batch[149]. These influences are the same for the joint construction market so it could appear from figure B.3 that the cost per TEU is independent of the vessel size. Nevertheless when a more detailed analysis is made as in figure B.1 and B.2 it is observed that the construction cost per TEU decreases for larger vessel sizes which as said before is mainly due to economy of scale.

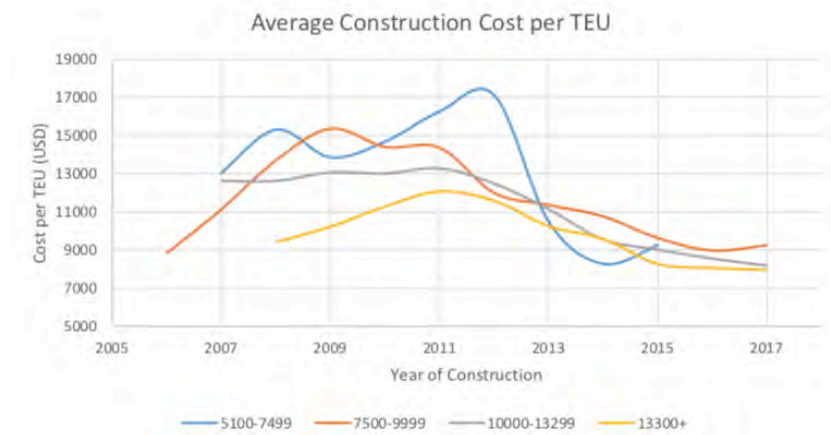


Figure B.3: Construction cost per TEU 2005-2017 [117]

As the initial filtering gave way to a container vessel with capacity 20.000 TEU+ it can be assumed from the found literature above that the capital cost per TEU will be around \$8000/TEU.

B.2. Machinery cost

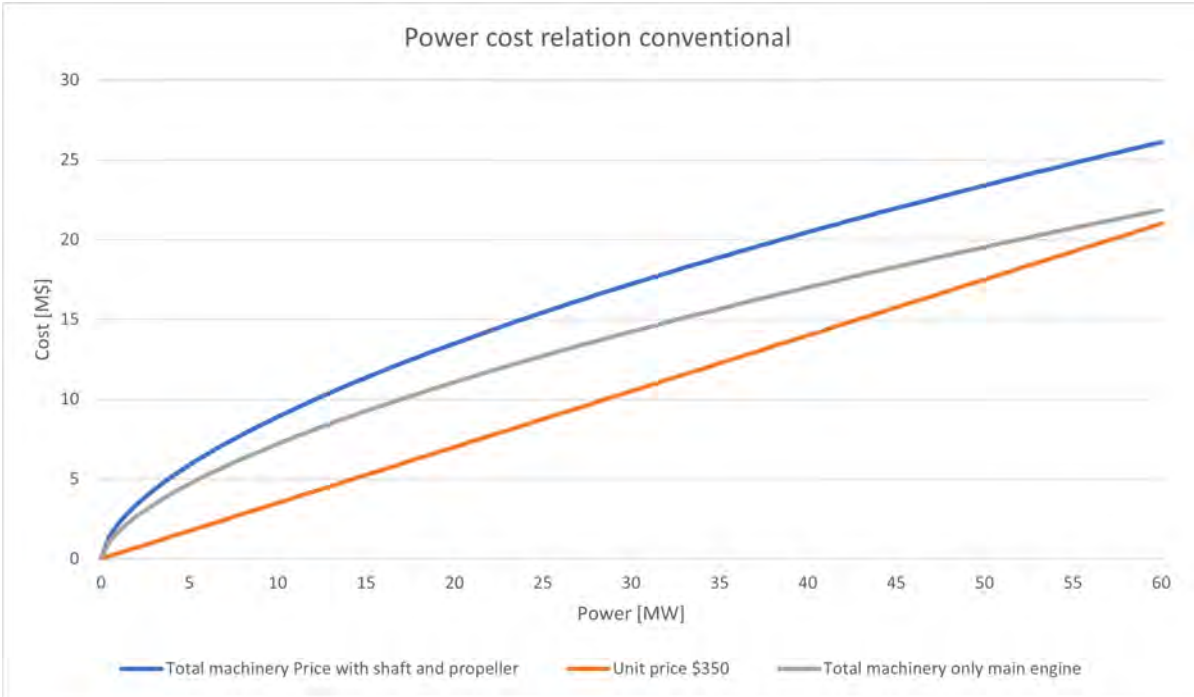


Figure B.4: Power cost relation for a conventional container ship

B.3. Operational costs

B.3.1. Freight rates

B.3.1.1 China/East Asia - Northern Europe

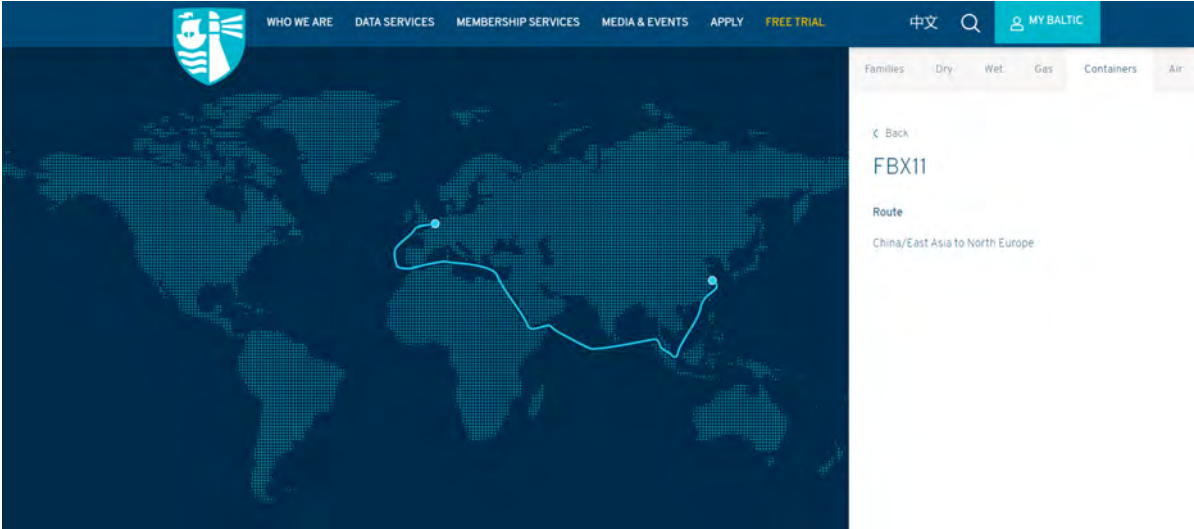


Figure B.5: FBX 11 - Route

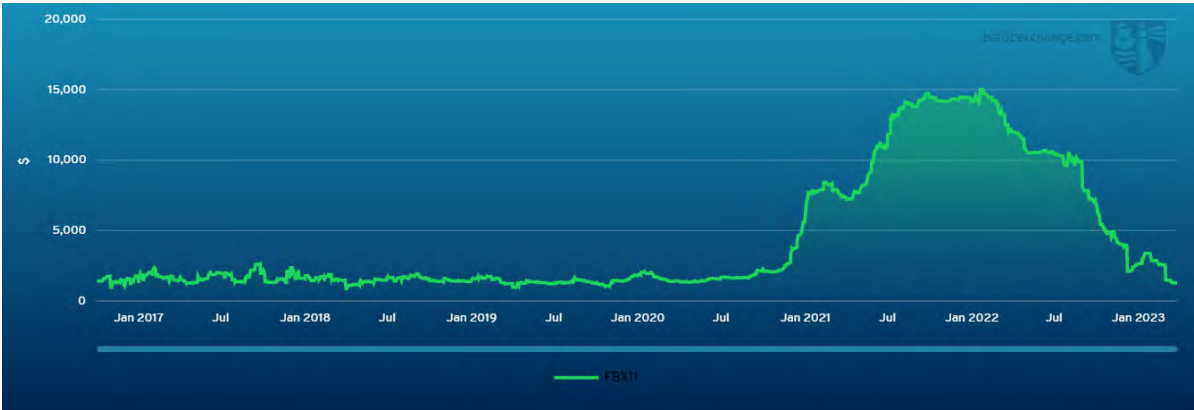


Figure B.6: FBX 11 - Freight rate

B.3.1.2 Northern Europe - China/East Asia

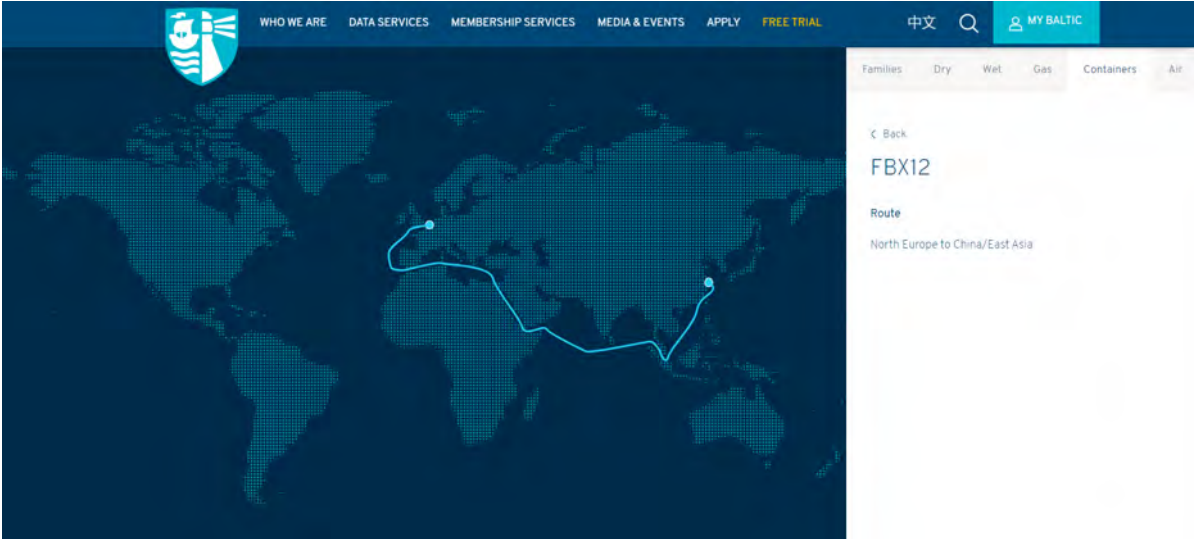


Figure B.7: FBX 12 - Route

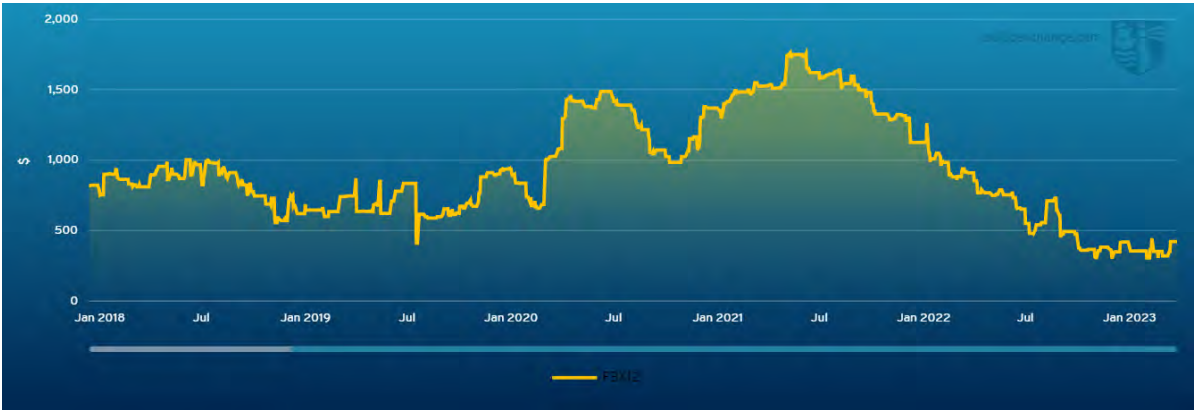


Figure B.8: FBX 12 - Freight rate

B.3.1.3 North America East coast - Northern Europe

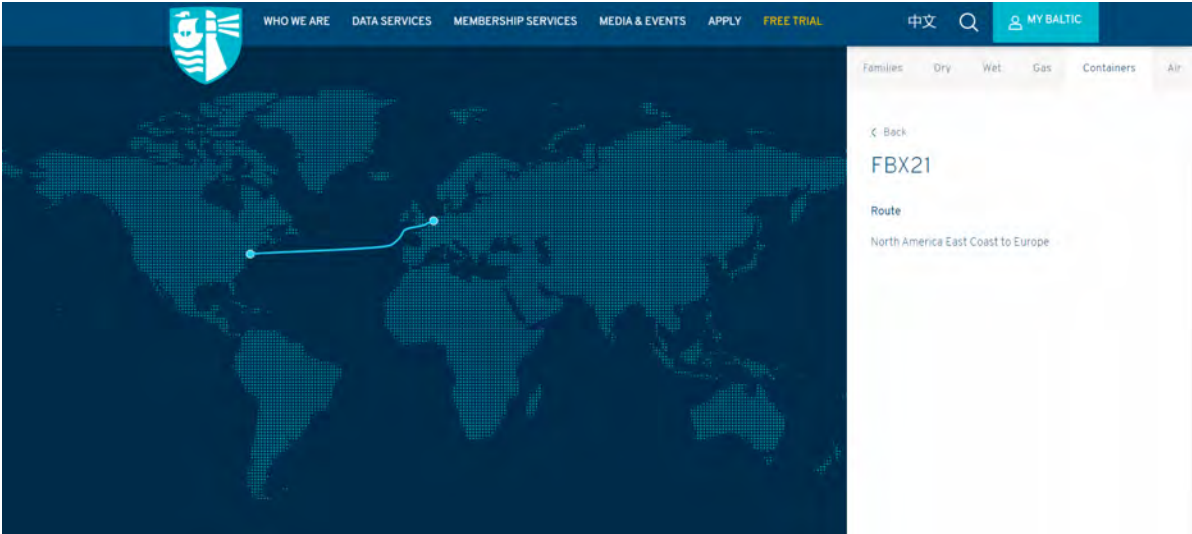


Figure B.9: FBX 21 - Route

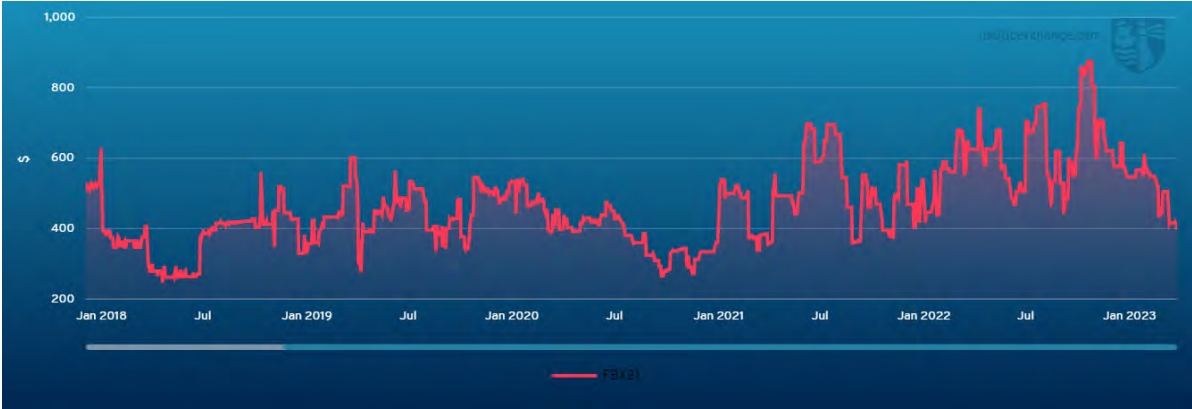


Figure B.10: FBX 21 - Freight rate

B.3.1.4 Northern Europe - North America East coast

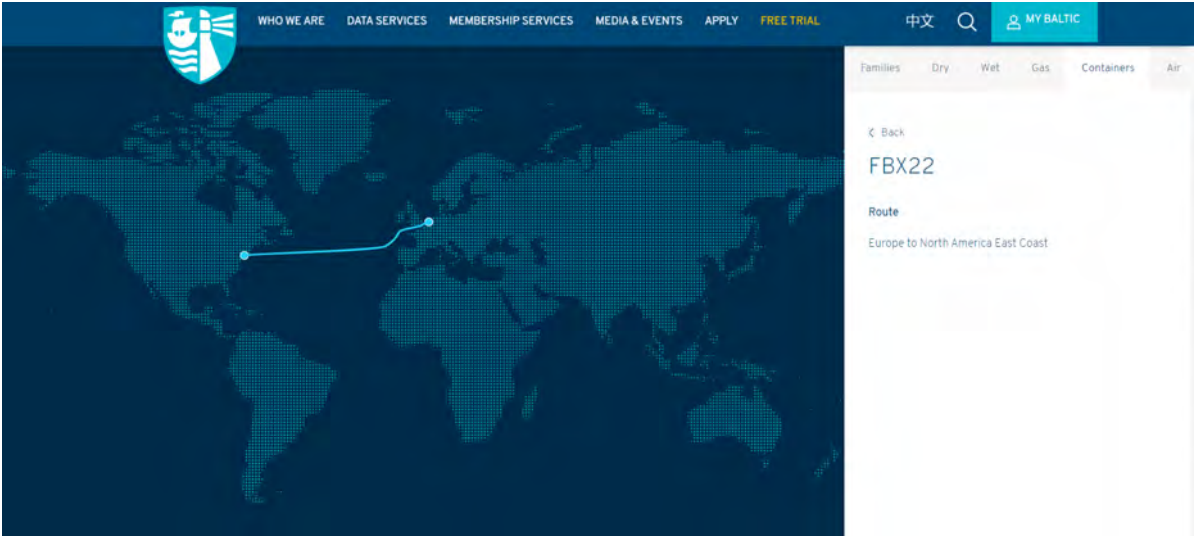


Figure B.11: FBX 22 - Route

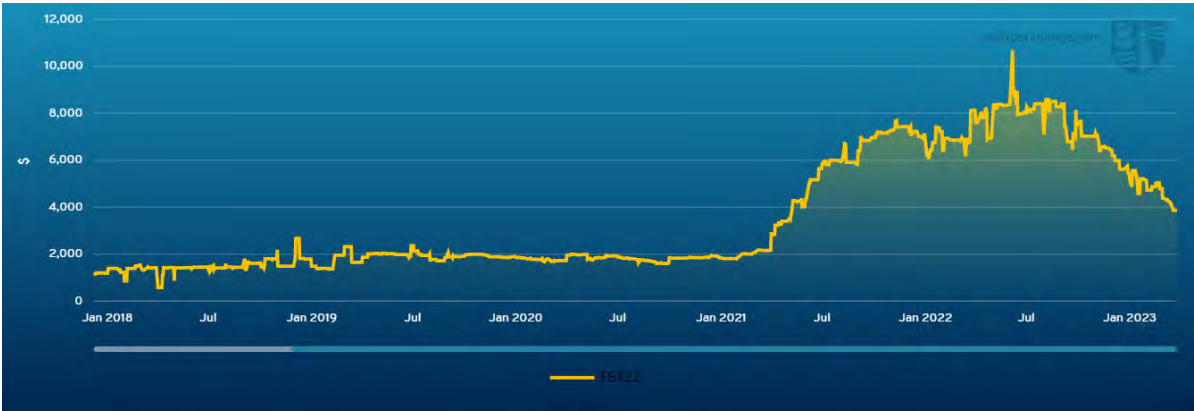


Figure B.12: FBX 22 - Freight rate

C

Propulsion line

C.1. Waterjets

$$\eta_I = \frac{4}{3 + \sqrt{1 + 2C_t}} \quad (\text{C.1})$$

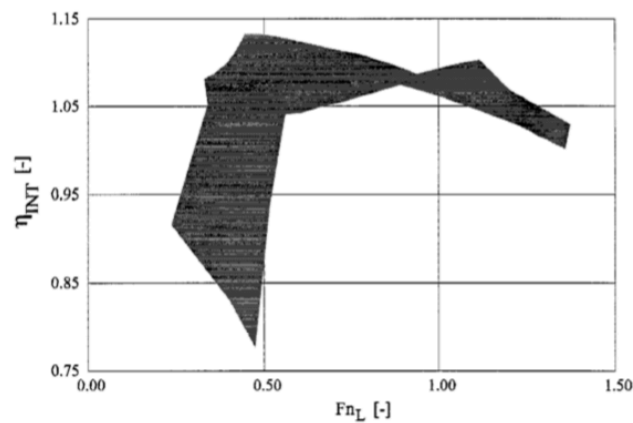


Figure C.1: Interaction efficiencies vs froude number for monohull and catamaran[163]

' Tests for this interaction efficiency were carried out for a monohull and catamaran with a L/B ratio of respectively 5 and 15 which are showed on figure C.1. The fast short monohull is very sensitive in the hump speed region and can be identified with the extreme values as 0.70 or 1.10. This can be explained by planing of the monohull. The catamaran its interaction efficiency corresponds more with the average value which lies around 0.95. Thus the interaction efficiency is more constant for larger L/B ratio's as was also confirmed by the writer of this paper T. Terwisga [131]

D

Optimal speed determination

D.1. Initial resistance estimation

In the equations below it is shown that the wetted area does not matter for the resistance estimation as this is dependent on the scaling factor which is fixed for this exercise as seen on figure D.1.

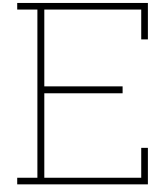
$$R_{tM} = \frac{1}{2} \times C_t \times \rho \times V_{sM}^2 \times S_m \quad (D.1)$$

$$R_{tS} = \frac{1}{2} \times C_t \times \rho \times V_{sS}^2 \times S_S = \frac{1}{2} \times C_t \times \rho \times V_{sS}^2 \times S_M \times \lambda_t^2 \quad (D.2)$$

On figure D.1 the complete initial resistance estimation is shown where the top speeds are highlighted in yellow.

Maersk B		Resistance calc maersk b		Resistance calc concept vessel		Concept vessel (froude scaling)	
TEU	4000	P_b	68,64 MW	P_ne	512,60 MW	TEU	20000
LWL	278,2 m	eta_schaft	0,99 (Assumption)	eta_s_nbl	0,89 (M,P,SB) (Assumption)	LWL	475,72 m
B	32,18 m	P_s	67,95 MW	P_sh	457,95	B	55,03 m
T	12,2 m	eta_r	1,00 (Assumption)	eta_s_TRM	0,97 (Assumption)	T	20,86 m
Vs	29,3 knots	eta_r	1,00 (Assumption)	P_r	444,30 MW	Vs	38,18 kts
Vs	15,02 m/s	eta_h	1,06 (Assumption)	eta_r	1,00 (Assumption)	Vs	15,64 m/s
Fr	0,29 -	eta_h	1,06 (Assumption)	eta_h	1,06 (Assumption)	Fr	0,29 -
Lambda_f	1,71	eta_d	0,65 (Assumption)	eta_d	0,65 (Assumption)		
		P_e	46,93 MW	P_e	305,85 MW		
		Rt	3,12 MN	Rt	15,62 MN		
		S _m	12086,00 m ²	S _e	35339,68 m ²		
		C _t	2,24E-09 -	C _t	2,235E-09 -		
Maersk B		Concept vessel					
C	Vs [kts]	P [MW]	Vs [kts]	P [MW]			
0,002756949	0	0	0,009208	0			
0,002756949	5	0	0,009208	5			
0,002756949	10	3	0,009208	10			
0,002756949	15	9	0,009208	15			
0,002756949	20	21	0,009208	20			
0,002756949	25	43	0,009208	25			
0,002756949	29,3	69	0,009208	30			
0,002756949	30	74	0,009208	35			
0,002756949	35	118	0,009208	38,183586			
0,002756949	40	176	0,009208	40			
0,002756949	45	251	0,009208	45			
0,002756949	50	345	0,009208	50			

Figure D.1: Froude scaling exercise



Optimal speed model

E.1. Analytical speed model

Analytical form of speed model:

First of all the trip time is defined as:

$$T_{\text{triptime}} = T_{\text{harbourtime}} + \frac{\text{tripdistance}}{\text{speed}} \quad (\text{E.1})$$

Where the trip distance is equal to two times the distance for port to port and the harbour time is equal to six days. Next the number of trips is defined as:

$$NoT = \frac{T_O}{T_{\text{triptime}}} \quad (\text{E.2})$$

Where T_O is the operating lifetime and is evaluated as either 25 or 50 years.

The installed power depending on speed is calculated by the following equations which is based upon the scaled up version of the Maersk B multiplied by 1,000 to get the result in kW. Which differs for the nuclear and diesel concept ship.

$$P_{ne(nuclear)} = 0.0148X^3 - 0.3275X^2 + 3.6448X - 7.2576 \quad (\text{E.3})$$

$$P_{b(diesel)} = 0.0130X^3 - 0.2867X^2 + 3.1911X - 6.3541 \quad (\text{E.4})$$

With these inputs cost functions for the CAPEX, OPEX, Voyage costs and total revenue are made.

The CAPEX cost function is constructed by following formula:

$$C_{cap} = C_{aptotal} \times P_b \quad (\text{E.5})$$

The OPEX cost function consist out of two parts being the fuel and O&M cost:

$$C_{fuel} = P_b \times SFC_{cost} \times \frac{\text{tripdistance}}{\text{Speed}} \quad (\text{E.6})$$

$$C_{O\&M} = C_{fixed} + C_{variable} = OM_{fix} \times P_b \times T_O + OM_{var} \times P_b \times T_O \quad (\text{E.7})$$

$$C_{opex} = (C_{fuel} + C_{O\&M}) \times NoT \quad (E.8)$$

Where the specific fuel consumption cost is calculated by multiplying the specific fuel consumption with the fuel unit cost. For the O&M costs a correction for the operating time should be made depending on the unit of the considered cost. For both the fuel and the variable O&M cost it is assumed that their cost in harbour and during transit in the Suez canal is equal to the power usage when sailing 8 knots. This is chosen due to the maximal speed in the Suez canal.

The total voyage cost is calculated by multiplying the port dues (p.d.), pilotage costs (p.c.), tug costs (t.c.) and suez canal dues (s.c.d.) with the number of trips as shown in following equation:

$$C_{voyage} = (p.d. + p.c. + t.c. + s.c.d) \times NoT \quad (E.9)$$

As last the total revenue is calculated using following equation:

$$Revenue = R = FEU \times \eta_{load} \times Freight_{rate} \times NoT \quad (E.10)$$

These functions are than used to determine the total income using following formula:

$$Income = R - C_{cap} - C_{opex} - C_{voyage} \quad (E.11)$$

Plotting all functions over varying speeds will give an optimal speed for a scenario with fixed inputs as depicted on the figure below.

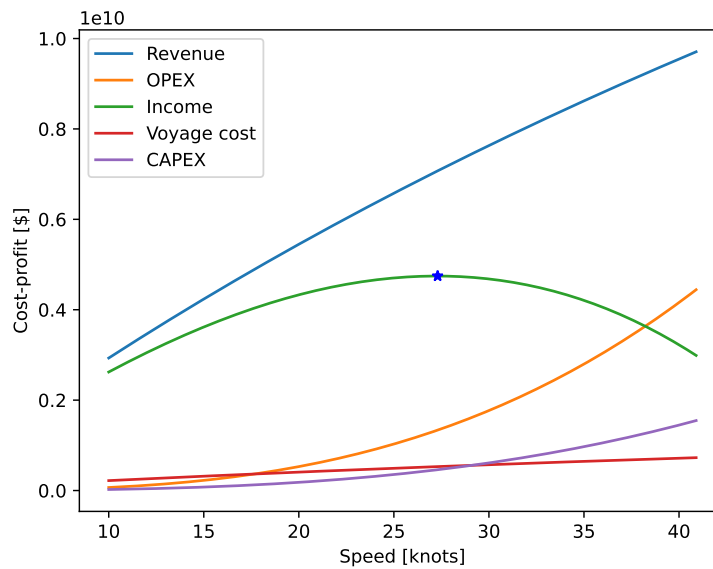


Figure E.1: Optimal speed model with only varying speed

This is the basis of the optimal speed model.

E.2. Optimal speed model plots

E.2.1. Rotterdam - New York

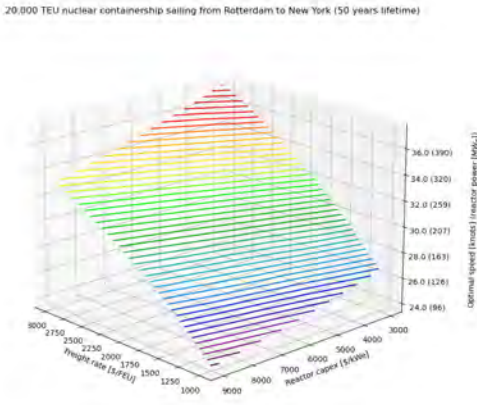


Figure E.2: Sensitivity plot Rotterdam-New York Nuclear 50 years

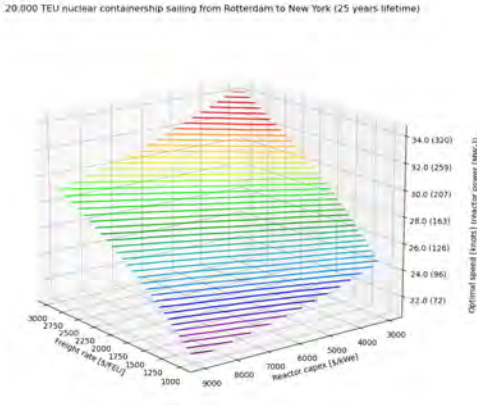


Figure E.3: Sensitivity plot Rotterdam-New York Nuclear 25 years

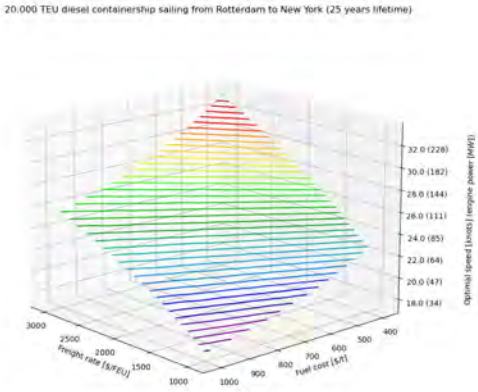


Figure E.4: Sensitivity plot Rotterdam-New York Diesel 25 years

F

Volume check

F.1. Turbine cross-section calculation

INPUT (AIR)		CALCULATION		OUTPUT NEEDED	
isotropic efficiency turbine	0.9	T2	565.69 K	power per kg/s	0.107008 MW/kg/s
isotropic efficiency compressor	0.9	T4	589.96 K	needed power	202 MW @
inlet losses	0.02	T2'	586.98 K	total air massflow	1878.365 kg/s
exhaust losses	0.01	T4'	590.87 K	turbine duct cross section factor	0.062 m ² /kg/s
Compression ratio	10			turbine duct cross section	118.337 m²
k (heat capacity ratio)	1.4	P_comp	308.51 kW		
Cp (specific heat etc pressure)	1.005 kJ/kgK	P_turbine	411.52 kW		
T1	293 K	P_total usable	107.01 kW	Measurement duct	
T3	973 K	Q_added	376.89 kW	width	7.00 m
m air	1 kg/s	total efficiency	28.24%	length	16.90 m

Figure F.1: Turbine duct cross-section calculation

F.2. Midship cross-section

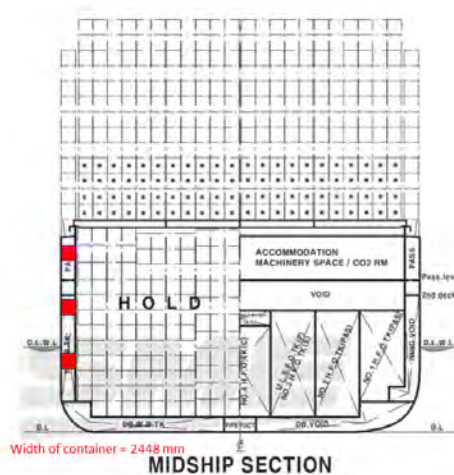


Figure F.2: Midship cross-section HMM Algeciras

F.3. Weight assessment

	MSC Gilsun (23,756 TEU)	CMA CGM JACQUES (23,112 TEU)	Nuclear concept vessel (20,000 TEU)		7,86 8,19	DWT/TEU
Design deadweight [t]						
Bunkers [t]	186800	189261	180557			
HFO (0,9 t/m ³)	12510	2287				
Diesel oil (0,85 t/m ³)	765	1348				978
LNG (0,45 t/m ³)	0	8443				
Nuclear fuel	-	-				1,725
Ballast [t] (1,025 t/m ³)	0	0				0
Crew [t]	10	10				10
Lube oil [t]	398	109				29
spares [t]	67	67				456
Fresh water [t]	84	84				84
Remaining deadweight for cargo [t]	172966	176913	159027			
t/TEU	7,28	7,65	7,95			
Daily fuel consumption [t/day] fuel oil	301,1	255,7	140			
Daily fuel consumption [t/day] gas	-	208,7	-			
Daily fuel consumption [t/day] Nuclear fuel	-	-				0,0047
Autonomy based on diesel fuel [days]	44	14	7			
Autonomy based on gas mode [days]	-	40	-			
Autonomy based on nuclear mode [days]	-	-				365

Figure F.3: Deadweight breakdown



Stability 1st iteration

G.1. Center of gravity calculation

G.1.1. Loaded Condition

This starts with the center of gravity of the lightship which is influenced by the steel structure of the vessel and the machinery room excluding the weight of fuel. The calculation of the point of gravity for the lightship is summarized in table G.1.

Component	weight [t]	LCG [m]	TCG [m]	VCG[m]	L-MOM [tm]	T-MOM [tm]	V-MOM [tm]
Steel structure	51016	180.868	0.000	21.428	9227,074	0	1,093,141
Machinery room	18,354	55.712	-0.388	20.119	1,022,541	-7,113	369,264
Total	69,370	147.754	-0.103	21.081	10,249,615	-7,113	1,462,405

Table G.1: Point of gravity determination of lightship

The center of gravity of the steel structure is calculated using the created rhino model and assuming a weight factor of 0.5 for the superstructure steel as this is assumed to be thinner steel as that of the ships hull and funnels. The center of gravity for the machinery room is determined using the general arrangement as described in the previous section. A full calculation can be found in appendix G.1.3.

Next the center of gravity for the deadweight needs to be determined. The biggest influence is the distribution of the cargo deadweight. The amount of full containers is taken as 85% to adhere to the load factor of the speed model as discussed before in section 6.2.5. The weight of a full container and empty container are respectively 9 and 2 ton. The loading arrangement of the nuclear concept vessel is depicted on figure G.1. Where a total of 20,000 containers are depicted 3,000 empty and 17,000 full.



Figure G.1: Container arrangement; red = empty (2 ton), green = full (9 ton)

The empty containers are positioned in the top tiers for the containers structural integrity and to keep the point of gravity as low as possible to enhance initial stability. The longitudinal position is chosen aft due to the aft position of the machinery room. This way the point of gravity is shifted towards the bow which will decrease the trim in this loading condition. The LCG, TCG and VCG are calculated for each bay separately and thereafter used to calculate the position of the center of gravity for the cargo deadweight. A complete calculation of all 25 bays can be found in appendix G.1.4. The remaining factors that are included in the deadweight are nuclear fuel, MDO fuel, lube oil, spares, fresh water and crew weight. These have a limited influence but are added for completeness. The center of gravity calculation of the deadweight is depicted in table G.2.

Component	weight [t]	LCG [m]	TCG [m]	VCG[m]	L-MOM [tm]	T-MOM [tm]	V-MOM [tm]
Cargo deadweight	15,9000	190.001	0.000	31.923	30,210,195	0	5,075,751
Nuclear fuel	9	76.371	0.000	19.785	687	0	178
MDO fuel	1,081	76.590	-18.210	18.029	82,794	-19,685	19,489
Lube oil	29	81.478	14.442	23.475	2363	419	681
Spares	585	80.926	18.149	24.018	47,341	10,617	14,050
Fresh water	252	80.926	22.453	24.104	20,393	5,658	6,074
Crew	10	243.127	0.000	49.263	2,431	0	493
Total	160,798	188.762	-0.042	31.796	30,352,610	-6.763	5,112,667

Table G.2: Point of gravity determination of deadweight

Using table G.1 and G.2 it is possible to determine the center of gravity location of the nuclear concept vessel which is depicted in table 6.13.

G.1.2. Ballast Condition

Component	weight [t]	LCG [m]	TCG [m]	VCG[m]	L-MOM [tm]	T-MOM [tm]	V-MOM [tm]
Cargo deadweight	0	191.498	0	31.557	0	0	0
Nuclear fuel	9	76.371	0.000	19.785	763	0	198
MDO fuel	1,081	76.590	-18.210	18.029	82,794	-19,685	19,489
Lube oil	29	81.478	14.442	23.475	2363	419	681
Spares	585	80.926	18.149	24.018	47,341	10,617	14,050
Fresh water	252	80.926	22.453	24.104	20,393	5,658	6,074
Crew	10	243.127	0.000	49.263	2,431	0	493
Ballast tanks				-			
Side SB	21,626	188.767	-28.920	18.922	4,082,171	-625,408	409,197
Side PS	21,626	188.767	28.920	18.922	4,082,171	-625,408	409,197
Bottom SB	11,546	187.483	-14.108	1.326	2,164,604	-162,885	15,310
Bottom PS	11,546	187.483	14.108	1.326	2,164,604	-162,885	15,310
Forepeak	4,055	370.573	0	14.433	1,502,637	0	58,524
Total	138,394	175.724	-0.100	16.765	24,319,044	-13,876	2,32,0163

Table G.3: Deadweight ballast condition

G.1.3. Lightship

Component	m2	LCG [m]	TCG [m]	VCG [m]	weight factor	long-Oppervlaktemoment [m3]	ver-Oppervlaktemoment [m3]
Hull	67509	182,930	0,000	18,308	1	12349421	1235955
Accommodatie	5676	243,127	0,000	49,263	0,5	689934	139796
Funnels	4006	48,032	0,000	49,265	1	197356	192416
Total	73185	180,868	0,000	21,428		13236711	1568167

Figure G.2: Steel structure center of gravity calculation

Component	weight [t]	LCG [m]	TCG [m]	VCG [m]	LONG - MOM [tm]	TRANS - MOM [tm]	VERT-MOM [tm]
Machinery room							
Nuclear island							
Reactor	4606	76,371	0,000	19,785	351765	0	91130
IHX (He working medium, helical coil based)	2425	76,275	0,000	21,420	184967	0	51944
Decay heat exchanger	4	82,383	0,000	13,484	330	0	54
Turbine island							
HEX (helical coil based)	2788	57,999	0,000	19,030	161701	0	53056
Turbine	1334	40,916	0,000	20,020	54582	0	26707
Generator	1908	27,739	0,000	19,022	52926	0	36294
Battery system							
Battery pack	238	77,082	17,634	14,852	18346	4197	3535
Emergency propulsion							
emergency genset	593	59,865	-19,072	18,178	35500	-11310	10780
fuel (MGO density of 0,860 t/m ³)	0	76,590	-18,210	18,029	0	0	0
Propulsion and consumers							
Electro motor	887	76,294	0,000	7,295	67673	0	6471
Switchboard room	3171	21,814	0,000	27,340	69172	0	86695
Gearbox	388	65,928	0,000	6,702	25580	0	2600
Total	18354	55,712	-0,388	20,119	1022541	-7113	369264

Figure G.3: Machinery room center of gravity calculation

G.1.4. Deadweight

Component	weight [t]	LCG [m]	TCG[m]	VCG[m]	LONG MOM [tm]	TRANS MOM [tm]	VERT MOM [tm]
Cargo Deadweight							
empty container	2						
Full container	9						
Bay 1 empty	0	3,770	0,000	0,000	0	0	0
Bay 1 full	918	3,770	0,000	36,946	3461	0	33916
total 1	918	3,770	0,000	36,946	3461	0	33916
Bay 2 empty	288	9,874	0,000	58,702	2844	0	16906
Bay 2 full	2682	9,874	0,000	43,367	26482	0	116310
total 2	2970	9,874	0,000	44,854	29326	0	133217
Bay 3 empty	320	23,494	0,000	58,702	7518	0	18785
Bay 3 full	2880	23,494	0,000	43,499	67663	0	125277
total 3	3200	23,494	0,000	45,019	75181	0	144062
Bay 4 empty	320	37,224	0,000	58,702	11912	0	18785
Bay 4 full	2880	37,224	0,000	43,499	107205	0	125277
total 4	3200	37,224	0,000	45,019	119117	0	144062
Bay 5 empty	192	50,948	0,000	58,702	9782	0	11271
Bay 5 full	1728	50,948	0,000	43,499	88038	0	75166
total 5	1920	50,948	0,000	45,019	97820	0	86437
Bay 6 empty	352	64,672	0,000	58,702	22765	0	20663
Bay 6 full	3168	64,672	0,000	43,499	204881	0	137805
total 6	3520	64,672	0,000	45,019	227645	0	158468
Bay 7 empty	352	78,402	0,000	58,702	27588	0	20663
Bay 7 full	3168	78,402	0,000	43,499	248378	0	137805
total 7	3520	78,402	0,000	45,019	275975	0	158468
Bay 8 empty	384	92,094	0,000	58,181	35364	0	22342
Bay 8 full on deck	3024	92,094	0,000	43,373	278492	0	131159
Bay 8 full below deck	4356	92,094	0,000	18,017	401161	0	78482
total 8	7764	92,094	0,000	29,879	715018	0	231983
Bay 9 empty	384	105,824	0,000	58,181	40636	0	22342
Bay 9 full on deck	3024	105,824	0,000	43,373	320012	0	131159
Bay 9 full below deck	4716	105,824	0,000	16,323	499066	0	76980
total 9	8124	105,824	0,000	28,370	859714	0	230480
Bay 10 empty	384	119,554	0,000	58,181	45908,736	0	22341,61843
Bay 10 full on deck	3024	119,554	0,000	43,373	361531	0	131159
Bay 10 full below deck	4716	119,554	0,000	16,323	563817	0	76980
total 10	8124	119,554	0,000	28,370	971257	0	230480
Bay 11 empty	384	133,284	0,000	58,181	51181	0	22342
Bay 11 full on deck	3024	133,284	0,000	43,373	403051	0	131159
Bay 11 full below deck	4716	133,284	0,000	16,323	628567	0	76980
total 11	8124	133,284	0,000	28,370	1082799	0	230480
Bay 12 empty	384	147,014	0,000	58,181	56453	0	22342
Bay 12 full on deck	3024	147,014	0,000	43,373	444570	0	131159
Bay 12 full below deck	4716	147,014	0,000	16,323	693318	0	76980
total 12	8124	147,014	0,000	28,370	1194342	0	230480
Bay 13 empty	384	160,744	0,000	58,181	61726	0	22342
Bay 13 full on deck	3024	160,744	0,000	43,373	486090	0	131159
Bay 13 full below deck	4716	160,744	0,000	16,323	758069	0	76980
total 13	8124	160,744	0,000	28,370	1305884	0	230480
Bay 14 empty	384	174,474	0,000	58,181	66998	0	22342
Bay 14 full on deck	3024	174,474	0,000	43,373	527609	0	131159
Bay 14 full below deck	4716	174,474	0,000	16,323	822819	0	76980
total 14	8124	174,474	0,000	28,370	1417427	0	230480
Bay 15 empty	384	188,320	0,000	58,181	72315	0	22342
Bay 15 full on deck	3024	188,320	0,000	43,373	569481	0	131159
Bay 15 full below deck	4716	188,320	0,000	16,323	888119	0	76980
total 15	8124	188,320	0,000	28,370	1529915	0	230480
Bay 16 empty	384	201,934	0,000	58,181	77543	0	22342
Bay 16 full on deck	3024	201,934	0,000	43,373	610648	0	131159
Bay 16 full below deck	4716	201,934	0,000	16,323	952321	0	76980
total 16	8124	201,934	0,000	28,370	1640512	0	230480
Bay 17 empty	384	215,664	0,000	58,181	82815	0	22342
Bay 17 full on deck	3024	215,664	0,000	43,373	652168	0	131159
Bay 17 full below deck	4698	215,664	0,000	16,323	1013189	0	76686
total 17	8106	215,664	0,000	28,397	1748172	0	230187
Bay 18 empty	336	228,956	0,000	58,886	76929	0	19786
Bay 18 full on deck	3240	228,956	0,000	43,548	741817	0	141097
Bay 18 full below deck	4626	228,954	0,000	16,323	1061177	0	75511
total 18	8202	229,203	0,000	28,821	1879923	0	236393
Bay 19 empty	0	0,000	0,000	0,000	0	0	0
Bay 19 full on deck	4320	256,854	0,000	46,911	1109609	0	202656
Bay 19 full below deck	4302	256,854	0,000	19,383	1104986	0	83386
total 19	8622	256,854	0,000	33,176	2214595	0	286041
Bay 20 empty	0	0,000	0,000	0,000	0	0	0
Bay 20 full on deck	3888	270,584	0,000	45,732	1052031	0	177804
Bay 20 full below deck	4104	270,584	0,000	19,848	1110477	0	81456
total 20	7992	270,584	0,000	32,440	2162507	0	259260
Bay 21 empty	0	0,000	0,000	0,000	0	0	0
Bay 21 full on deck	3888	284,314	0,000	45,732	1105413	0	177804
Bay 21 full below deck	3816	284,314	0,000	20,529	1084942	0	78339
total 21	7704	284,314	0,000	33,248	2190355	0	256143
Bay 22 empty	0	0,000	0,000	0,000	0	0	0
Bay 22 full on deck	3456	298,044	0,000	44,552	1030040	0	153972
Bay 22 full below deck	3492	298,044	0,000	21,260	1040770	0	74240
total 22	6948	298,044	0,000	32,846	2070810	0	228212
Bay 23 empty	0	0,000	0,000	0,000	0	0	0
Bay 23 full on deck	2772	311,774	0,000	43,081	864238	0	119421
Bay 23 full below deck	3060	311,774	0,000	21,762	954028	0	66592
total 23	5832	311,774	0,000	31,895	1818266	0	186013
Bay 24 empty	0	0,000	0,000	0,000	0	0	0
Bay 24 full on deck	2772	325,504	0,000	43,081	902297	0	119421
Bay 24 full below deck	2628	325,504	0,000	22,766	855425	0	59829
total 24	5400	325,504	0,000	33,194	1757722	0	179250
Bay 25 empty	0	0,000	0,000	0,000	0	0	0
Bay 25 full on deck	2376	339,234	0,000	42,193	806020	0	100251
Bay 25 full below deck	2088	339,234	0,000	23,804	708321	0	49703
total 25	4464	339,234	0,000	33,592	1514341	0	149954
Bay 26 empty	0	0,000	0,000	0,000	0	0	0
Bay 26 full on deck	2160	352,964	0,000	42,193	762402	0	91137
Bay 26 full below deck	1566	352,964	0,000	24,716	552632	0	38705
total 26	3726	352,935	0,000	34,848	1315034	0	129843
Total	159000	19,000	0,000	31,923	30210195	0	5075751

Figure G.4: Cargo deadweight center of gravity calculation

G.1.5. Wind silhouette

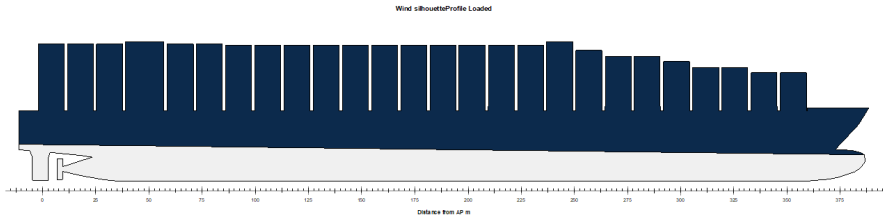


Figure G.5: Wind silhouette loaded condition

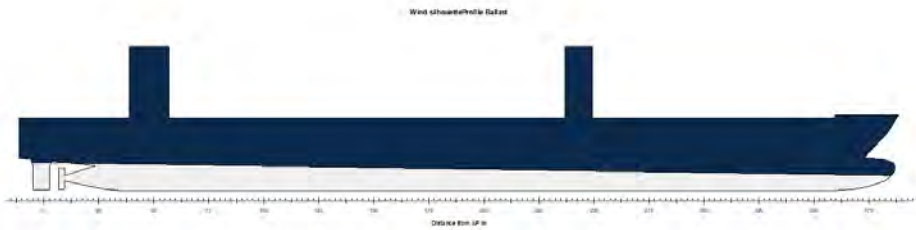


Figure G.6: Wind silhouette ballast condition

G.1.6. Ballast tank configuration

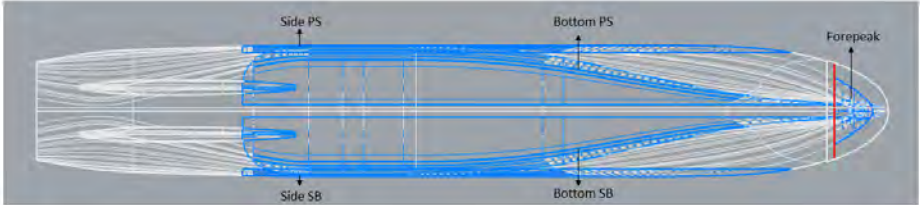
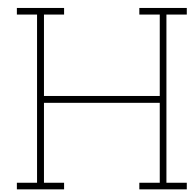


Figure G.7: Ballast tank configuration



Propulsors 1st iteration

H.1. Open water diagrams

H.1.1. Two propeller lay-out

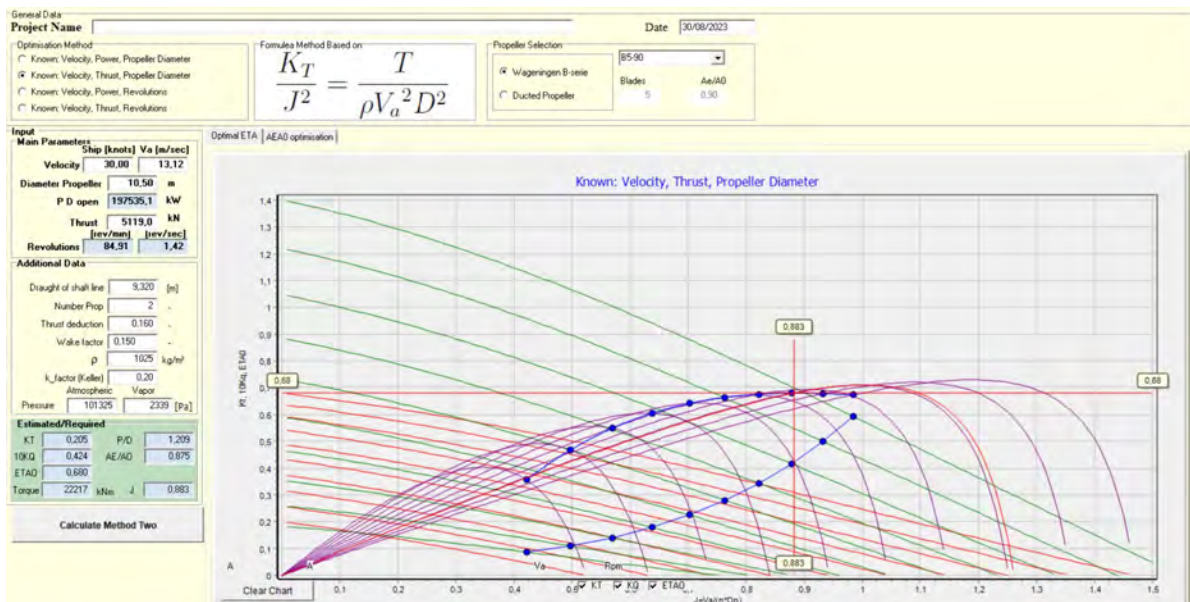


Figure H.1: Open water diagram propeller

H.1.2. Three propeller lay-out

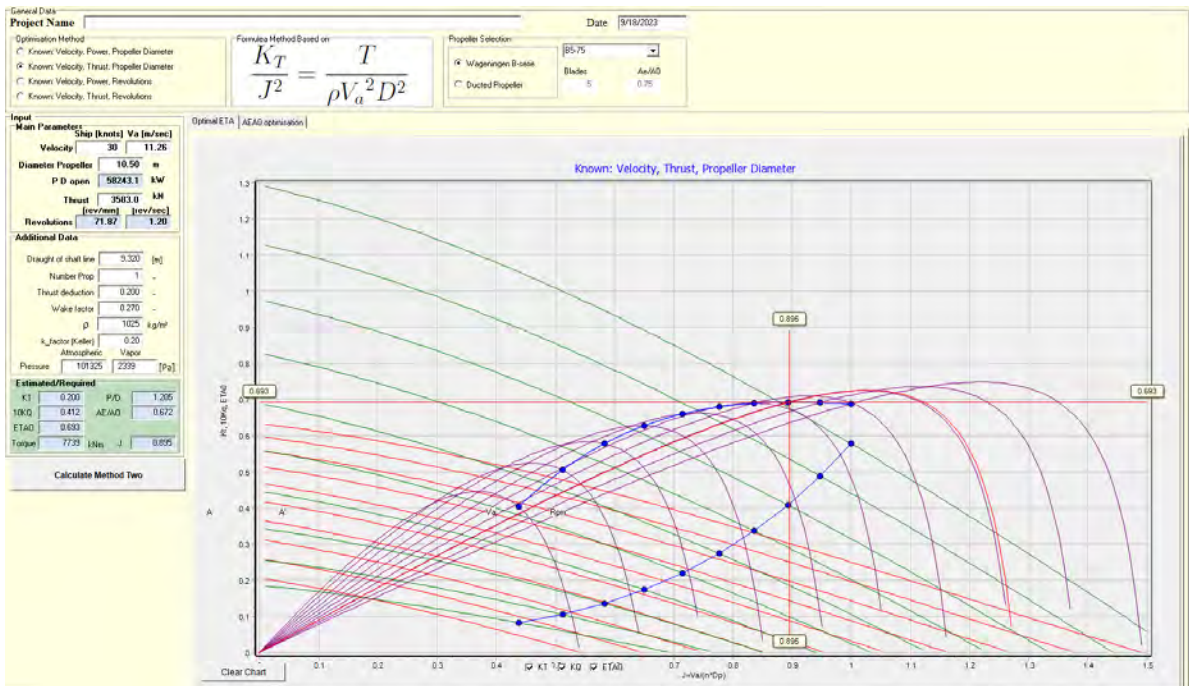


Figure H.2: Open water diagram center propeller

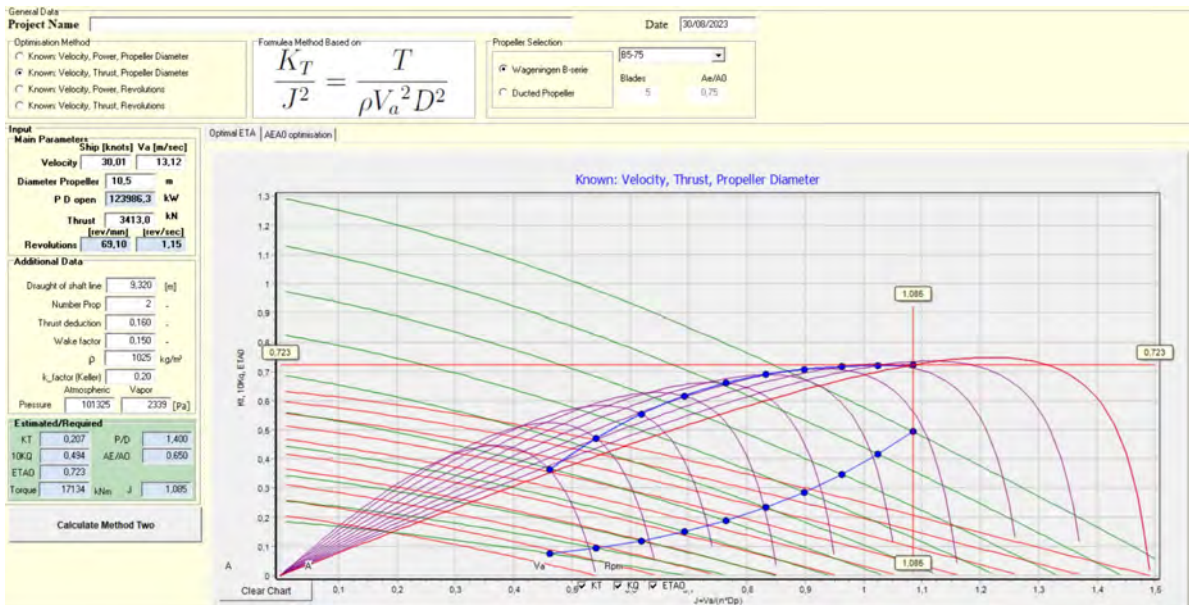


Figure H.3: Open water diagram wing propellers



General arrangement second iteration

I.1. Machinery room

Components	Volume [m ³]	weight [t]	amount [redundancy]
Reactor (spheric-cubic)	1521-2904	4509	1
IHX	-		2
(V)HTR	371	1113	
MSR	99	297	
Decay heat exchanger	-		2
(V)HTR	1	4	
MSR	1	3	
HEX	-		2
(V)HTR	427	1280	
MSR	74	223	
Open brayton turbines	-		2
<i>Turbines [set of two]</i>	1224	612	
<i>Funnel in- and outlet</i>	120 m ²	-	
Generator	471	876	2
Battery pack	391	219	1
Emergency genset	326	272	2
MGO fuel tank	1154	992	1
Switchboard room*	2550	1457	2
Electromotor outer	148	275	2
Gearbox outer	68	124	2
Electromotor inner	127	236	1
Gearbox inner	59	107	1
Total_{(V)HTR spheric}	14,425	18,083	
Total_{(V)HTR cubic}	15,809	18,083	
Total_{MSR spheric}	13,176	14,336	
Total_{MSR cubic}	14,560	14,336	

Table I.1: Volume and weight of machinery room components three propeller lay-out (*) including converters, busbars and rectifiers (210 MW_e)